List of Contributors

Professor B. Wrackmeyer, *Laboratorium für Anorganische Chemie, Universität Bayreuth, 95440 Bayreuth, Germany*

Professor H. Saito, S. Tuzi and M. Tanio, *Department of Life Science, Himeji Institute of Technology, Harima Science Garden City, Kamigori, Hyogo 678-1297, Japan*

Professor A. Naito, *Faculty of Engineering, Yokohama National University, 79-5 Tokiwadai, Yokohama 240-8501, Japan*

A. M. Gil and E. Alberti, *Department of Chemistry, University of Aveiro, 3810-193 Aveiro, Portugal*

P. S. Belton, *School of Chemical Sciences, University of East Anglia, Norwich NR4 7TJ, UK*

K. K. Laali, *Department of Chemistry, Kent State University, Kent, OH 44242, USA*

T. Okazaki, *Department of Energy and Hydrocarbon Chemistry, Kyoto University, Kyoto 606-8501, Japan*

Preface

Volume 47 of *Annual Reports on NMR* contains egregious accounts of modern applications of NMR spectroscopy in four distinct areas of scientific research. It is my very pleasant responsibility to thank all of the contributors to this volume for their considerable efforts in the production of their timely accounts. The first chapter covers progress in the Application of ^{207}Pb NMR Parameters by B. Wrackmeyer, providing an update on this area of activity which was previously reviewed in volume 22 of this series. Following this, H. Saito, S. Tuzi, M. Tanio and A. Naito review Dynamic Aspects of Membrane Proteins and Membrane-Associated Peptides as Revealed by ^{13}C NMR: Lessons from Bacteriorhodopsin as an Intact Protein. Applications of NMR to Food Science is an area of activity last visited in volume 32 of this series, and more recent developments are discussed by E. Alberti, P. S. Belton and A. M. Gil in the third chapter. The final contribution by K. K. Laali and T. Okazaki is on NMR of Persistent Carbocations from Polycyclic Aromatic Hydrocarbons.

My sincere thanks are also accorded to the production staff at Academic Press (London) for their help and kind cooperation in the realization of this volume.

Royal Society of Chemistry
Burlington House
London, UK

G. A. WEBB
November 2001

Application of ^{207}Pb NMR Parameters

BERND WRACKMEYER

Laboratorium für Anorganische Chemie der Universität Bayreuth, D-95440 Bayreuth, Germany

1. Introduction 2
2. Experimental 2
   2.1. Referencing 2
   2.2. Techniques for observing ^{207}Pb resonances 4
3. ^{207}Pb nuclear spin relaxation 6
4. Chemical shifts δ^{207}Pb 9
   4.1. General 9
   4.2. Patterns of ^{207}Pb chemical shifts 9
      4.2.1. Coordination number of lead and electronic structure 9
      4.2.2. Substituent effects and effects of cyclic structures 17
      4.2.3. Lead compounds with a formal oxidation state of less than +2 22
   4.3. Isotope-induced ^{207}Pb chemical shifts 22
5. Indirect nuclear spin–spin coupling constants $^{n}J(^{207}\mathrm{Pb,X})$ 23
   5.1. General 23
   5.2. One-bond couplings, $^{1}J(^{207}\mathrm{Pb,X})$ 23
      5.2.1. Coupling constants $^{1}J(^{207}\mathrm{Pb,}^{13}\mathrm{C})$, $^{1}J(^{207}\mathrm{Pb,}^{29}\mathrm{Si})$, $^{1}J(^{207}\mathrm{Pb,}^{119}\mathrm{Sn})$, and $^{1}J(^{207}\mathrm{Pb,}^{207}\mathrm{Pb})$ 23
      5.2.2. Coupling constants $^{1}J(^{207}\mathrm{Pb,}^{15}\mathrm{N})$, $^{1}J(^{207}\mathrm{Pb,}^{31}\mathrm{P})$, $^{1}J(^{207}\mathrm{Pb,}^{77}\mathrm{Se})$, $^{1}J(^{207}\mathrm{Pb,}^{125}\mathrm{Te})$, and $^{1}J(^{207}\mathrm{Pb,}^{19}\mathrm{F})$ 28
      5.2.3. Coupling constants $^{1}J(^{207}\mathrm{Pb,M})$, where M is a transition metal nucleus 29
   5.3. Two-bond (geminal) coupling, $^{2}J(^{207}\mathrm{Pb,X})$ 30
   5.4. Three-bond (vicinal) coupling, $^{3}J(^{207}\mathrm{Pb,X})$ 31
   5.5. Long-range coupling constants $^{n}J(^{207}\mathrm{Pb,X})$ with $n > 3$ 31
6. Conclusions 31
Acknowledgement 33
References 33

^{207}Pb NMR parameters [chemical shifts δ^{207}Pb, indirect nuclear spin–spin coupling constants $^{n}J(^{207}\mathrm{Pb,X})$, and relaxation times $T_1(^{207}\mathrm{Pb})$, $T_2(^{207}\mathrm{Pb})$] are listed and discussed with respect to the structure and dynamics of lead compounds, focusing mainly on the liquid state. Referencing of δ^{207}Pb data is described, as well as the usual experimental techniques for observing ^{207}Pb NMR signals. The importance of the chemical shift anisotropy (CSA) as a

ANNUAL REPORTS ON NMR SPECTROSCOPY
VOLUME 47 ISBN 0-12-505447-5

Copyright © 2002 Elsevier Science Ltd.
All rights of reproduction in any form reserved

relaxation mechanism at moderate to high field strengths is emphasized. Patterns of $\delta^{207}Pb$ data (range of ≈ 17 000 ppm with plumbylenes at the high frequency and plumbocenes at the low frequency end) are related to structure, substituent effects, and the lead coordination number. Contributions of relativistic effects to ^{207}Pb nuclear shielding become obvious, in particular for lead(II) compounds. Isotope-induced chemical shifts $^{n}\Delta X(^{207}Pb)$ may attract more attention in the future. Many coupling constants $^{n}J(^{207}Pb,X)$ are reported, where X stands for numerous nuclei throughout the Periodic Table. The determination of the sign of ^{n}J is demonstrated for various examples. It is shown that these signs are not always predictable, even for X = ^{13}C and n = 1, and therefore experimental evidence is required.

1. INTRODUCTION

The element lead possesses only one magnetically active isotope, ^{207}Pb, with spin $I = 1/2$, a fairly high natural abundance of 22.6%, and an appreciably high NMR receptivity (factor 11.9 when compared with ^{13}C; see Table 1 for some properties of selected spin-1/2 nuclei, and Table 2 for some quadrupolar nuclei). Thus, ^{207}Pb NMR studies of solutions can be carried out within reasonable time, whereas solid-state ^{207}Pb NMR measurements may be more cumbersome because of the large chemical shift anisotropy (see below) typical of heavy nuclei. Owing to the ever increasing performance of modern NMR spectrometers, ^{207}Pb NMR has become a valuable routine tool in many fields of lead chemistry. Furthermore, numerous more sophisticated NMR techniques,[1,2] aiming to extract more detailed information from NMR measurements of spin-1/2 nuclei, can be applied if necessary. In the last two decades, the progress in ^{207}Pb NMR has been addressed in several reviews.[3–6] The present review intends to give representative examples for the application of ^{207}Pb NMR measurements rather than a complete assessment. Paramagnetic compounds, alloys and most inorganic solids containing lead are excluded [see, for example, the leading references dealing with fluoride materials containing lead,[7,8] lead(II) oxides,[9,10] lead nitrate,[11a–d] ^{207}Pb relaxation in solid lead nitrate,[11e] perovskite-phase materials,[12,13] and lead containing zeolites[14]]. The relevant literature is covered and selected for the period from 1989 to the beginning of 2001, and only few data, reported already in a previous review,[3] will be included if necessary for comparison.

2. EXPERIMENTAL

2.1. Referencing

The commonly used external reference for ^{207}Pb chemical shifts, $\delta^{207}Pb$, was and will be in the future tetramethyllead, Me_4Pb. However, using modern NMR

spectrometers, it is more convenient to define a fixed frequency Ξ in MHz as the reference for the chemical shifts δ of those nuclei for which an internal reference cannot be generally applied. Such frequencies Ξ are given in Table 1 for ^{207}Pb and for a number of other nuclei of interest also in Tables 1 and 2. By multiplying these Ξ values with the appropriate factor, depending on the ^{1}H(Me_4Si) frequency of the individual NMR spectrometer, the exact reference frequency is obtained, and handling of potentially hazardous chemicals like Me_4Pb is not necessary. This procedure[15] guarantees precise reproducibility of δ^{207}Pb data

Table 1. NMR properties of some spin-1/2 nuclei[a]

Nucleus	N.A. (%)	R^{C} [b]	γ [10^7 rad s^{-1}T^{-1}]	Ξ (MHz)	Reference standard
^{1}H	99.985	5.67 10^3	26.7522	100.000000	$SiMe_4$, 1% in $CDCl_3$
^{207}Pb	22.6	11.9	5.6264	20.920597	$PbMe_4$ (neat)
^{13}C	1.108	1.00	6.7283	25.145020	$SiMe_4$, 1% in $CDCl_3$
^{15}N	0.37	2.19 10^{-2}	−2.7126	10.136767	$MeNO_2$ (neat)
^{19}F	100	4.73 10^3	25.1815	94.094003	$CFCl_3$ (neat)
^{29}Si	4.70	2.10	−5.3190	19.867187	$SiMe_4$ 1% in $CDCl_3$
^{31}P	100	3.77 10^2	10.8394	40.480747	H_3PO_4, 85% aq
^{57}Fe	2.19	4.25 10^{-3}	0.8687	3.237798	$Fe(CO)_5$ (neat)
^{77}Se	7.58	3.02	5.1214	19.071523	Me_2Se (neat)
^{103}Rh	100	0.180	−0.8468	3.160000	No compound
^{115}Sn	0.35	0.707	−8.8014	32.718780	$SnMe_4$ (neat)
^{117}Sn	7.61	19.9	−9.589	35.632295	$SnMe_4$ (neat)
^{119}Sn	8.58	25.7	−10.0318	37.290665	$SnMe_4$ (neat)
^{125}Te	6.99	12.8	−8.5087	31.549802	Me_2Te (neat)
^{195}Pt	33.8	19.9	5.8383	21.400000	No compound δ^{195}Pt($[PtCl_6]^{2-}$) = +4533
^{199}Hg	16.84	5.68	4.8458	17.910841	$HgMe_2$ (neat)[c]

[a] Most data taken from refs 126 to 128.
[b] Receptivity relative to that of ^{13}C in natural abundance.
[c] Ξ(^{199}Hg) = 17.870535 MHz for $Hg(ClO_4)_2$ (0.1 M in 0.1 M $HClO_4$).

Table 2. NMR properties of some quadrupolar nuclei[a]

Nucleus	N.A. (%)	Spin I	Q [10^{-28} m^2]	γ (10^7 rad s^{-1} T^{-1})	Ξ [MHz]	Reference standard
^{2}H	0.015	1	2.87 10^{-3}	4.1066	15.350609	$Si(CD_3)_4$ (D_{12}-TMS)
^{6}Li	7.42	1	−6.4 10^{-4}	3.9371	14.716106	LiCl, $D_2O \approx 9.7$ M
^{7}Li	92.58	3/2	−3.7 10^{-3}	10.3976	38.863790	LiCl, $D_2O \approx 9.7$ M
^{11}B	80.42	3/2	4.1 10^{-2}	8.5847	32.083971	F_3B–OEt_2 ($CDCl_3$)
^{14}N	99.63	1	1.67 10^{-2}	1.9338	7.226324	$MeNO_2$ (neat)
^{17}O	0.037	5/2	6.11 10^{-2}	−3.6280	13.556430	D_2O (liquid)
^{35}Cl	75.53	3/2	−8.2 10^{-2}	2.6242	9.797931	KCl, $D_2O \approx 2.2$ M
^{37}Cl	24.47	3/2	−6.5 10^{-2}	2.1844	8.155764	KCl, $D_2O \approx 2.2$ M

[a] Most data taken from refs 126 to 128.

and of course also of chemical shifts of other nuclei, and is recommended as a substitute for other less reliable referencing techniques, some of which are still proposed in various textbooks.

2.2. Techniques for observing ^{207}Pb resonances

According to the relatively high NMR sensitivity of ^{207}Pb (Table 1), ^{207}Pb NMR spectra can generally be measured readily by direct PFT single-pulse techniques by applying ^{1}H decoupling, ^{207}Pb{^{1}H}, if necessary. In most cases, the positions of ^{207}Pb NMR signals depend significantly on temperature gradients in the sample. Therefore, it is advisable to adjust the decoupling power carefully to the minimum [e.g. by using composite pulse decoupling (CPD) with the frequency offset on resonance for the respective ^{1}H nuclei] necessary for complete decoupling, and to observe conditions that keep the temperature of the sample as

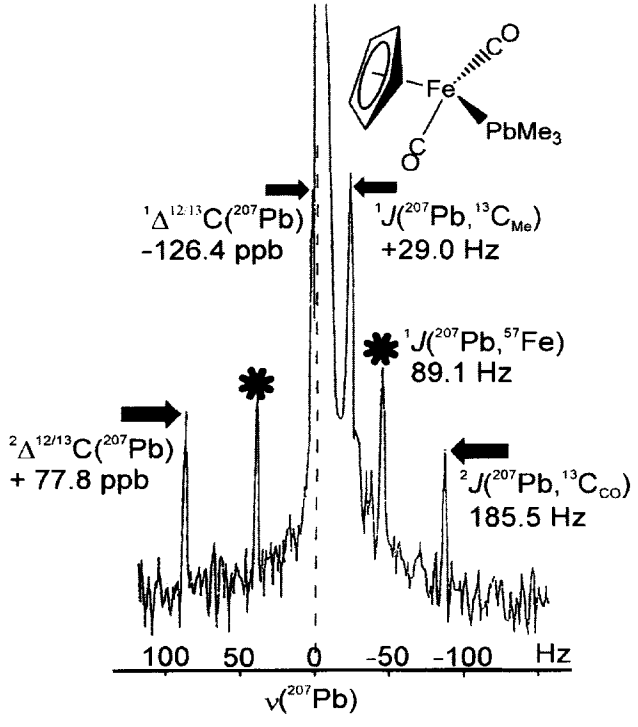

Fig. 1. 62.8 MHz ^{207}Pb NMR spectrum of (Cp)Fe(CO)$_2$–PbMe$_3$ (25 °C; ≈5% in C_6D_6), recorded by using the refocused INEPT pulse sequence with CPD ^{1}H decoupling (200 transients with a repetition time of 8 s and an acquisition time of 4 s).[94] The line width $h_{1/2}$ = 2 Hz is rather small for ^{207}Pb NMR signals and makes it possible to observe ^{57}Fe satellites and also ^{13}C satellites in order to measure accurately the isotope-induced chemical shifts $\Delta^{12/13}$C(^{207}Pb).

constant as possible. Even then it might be difficult to rule out all influences on the line widths of ^{207}Pb NMR signals arising from experimental conditions.

In principle, the application of polarization transfer pulse sequences such as INEPT [16] or DEPT [17] is straightforward in order to enhance the sensitivity of the NMR experiments, provided there is scalar ^{207}Pb-^{1}H coupling (Fig. 1). However, ^{207}Pb nuclear spin relaxation (see below) can be rather efficient, which means that the expected gain in sensitivity by polarization transfer is not always possible. As a result of fast ^{207}Pb spin relaxation, direct single-pulse ^{207}Pb{^{1}H} NMR spectra (Fig. 2) can be obtained in the same time with a similar or even better signal-to-noise ratio, when compared with polarization transfer experiments.

Indirect detection of ^{207}Pb NMR signals, in general by ^{1}H NMR, using various types of technique[1,18] (HMQC, HMBC, HSQC) is easy, and can be used to study rather dilute solutions. It is predictable that these experiments may be further improved by the application of pulsed field gradients,[2a,b] in the same way as has been shown for indirect detection of ^{119}Sn NMR signals.[18] A major advantage of indirect detection is the dramatic increase in sensitivity, considering a gain by $[\gamma(^{1}H)/\gamma(^{207}Pb)]^{3/2} = 10.37$, when compared with the INEPT experiment, and by $[\gamma(^{1}H)/\gamma(^{207}Pb)]^{5/2} = 49.3$, when compared with direct single-pulse methods.

Solid-state ^{207}Pb NMR spectra can be obtained for static samples or by MAS and CP MAS techniques,[19] and for organolead compounds CP MAS techniques are definitely preferred (see Fig. 3). The huge chemical shift anisotropy is a drawback for all techniques, although, on the other hand, this parameter contains valuable additional information.

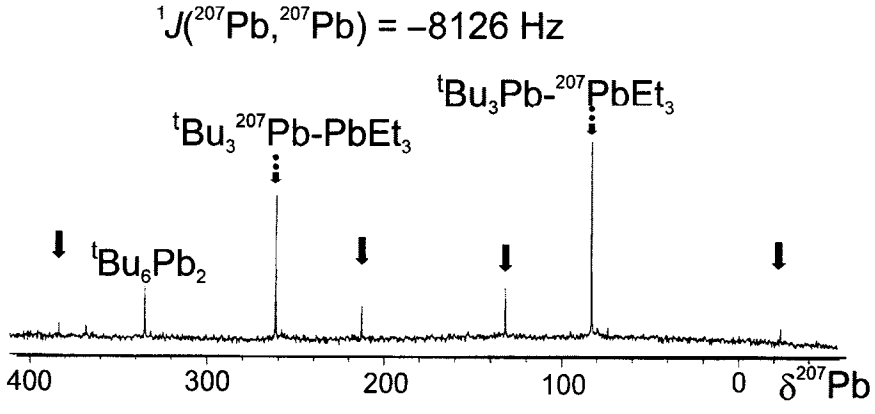

Fig. 2. 52.3 MHz ^{207}Pb{^{1}H} NMR spectrum (single-pulse technique) of a typical reaction solution obtained from the reaction of $^{t}Bu_3Pb$–Li with Et_3Pb–Cl.[76] In addition to the formation of the desired mixed diplumbane, the ^{207}Pb NMR signal of $^{t}Bu_3Pb$–Pb$^{t}Bu_3$ is also observed. The isotopomer of $^{t}Bu_3{}^{207}Pb$–$^{207}PbEt_3$, containing two ^{207}Pb nuclei, gives rise to an AB spin system with the typical distortion of intensities and positions of the inner and outer lines (marked by arrows).

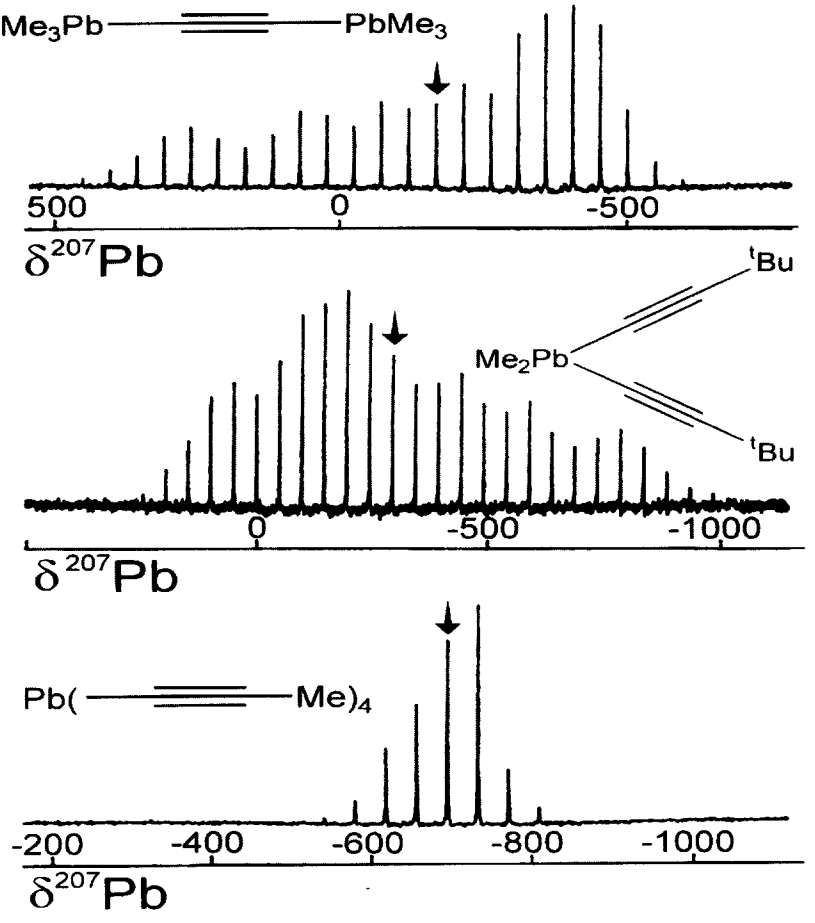

Fig. 3. 62.8 MHz solid-state ^{207}Pb CP MAS NMR spectra of 1-alkynyllead compounds as shown.[121] The spinning side bands arise from rotation of the samples (upper trace 3.4 kHz; middle trace 3.1 kHz; lower trace 2.4 kHz). The isotropic δ^{207}Pb NMR data are indicated by arrows [δ^{207}Pb (in C_6D_6)/δ^{207}Pb (solid): Me_3Pb–C≡C–$PbMe_3$: −158.6/−169.0; $Me_2Pb(C{\equiv}C{-}^tBu)_2$: −298.5/−295.0; $Pb(C{\equiv}C{-}Me)_4$: −687.5/−695.0].

3. ^{207}Pb NUCLEAR SPIN RELAXATION

In solution, contributions from the various relaxation mechanisms[20] (DD = dipole–dipole; SC = scalar; SR = spin–rotation; CSA = chemical shift anisotropy) have to be considered, and for longitudinal relaxation times $T_1(^{207}Pb)$ in particular SR and CSA are important. Using magnetic field strengths B_0 > 4.7 T, the CSA mechanism is likely to become dominant for ^{207}Pb nuclei in anisotropic surroundings. Since this mechanism becomes increasingly efficient at higher field strengths B_0 (it depends on B_0^2), the times $T_1(^{207}Pb)$ can be rather

short, and then significant broadening of the ^{207}Pb resonances ($T_1^{CSA} = 6/7T_2^{CSA}$) will be the result of spin dynamics rather than of other dynamical processes.

In ^{207}Pb or in X NMR spectra, the observation of indirect nuclear ^{207}Pb–X spin–spin coupling may be affected by fast relaxation either of the ^{207}Pb or of the X nucleus (see Fig. 4 for X = ^{11}B with moderately fast ^{11}B quadrupolar spin relaxation[21]). The broadening of ^{207}Pb satellites in X NMR spectra, recorded at high field strength B_0, may indicate highly anisotropic surroundings of the ^{207}Pb

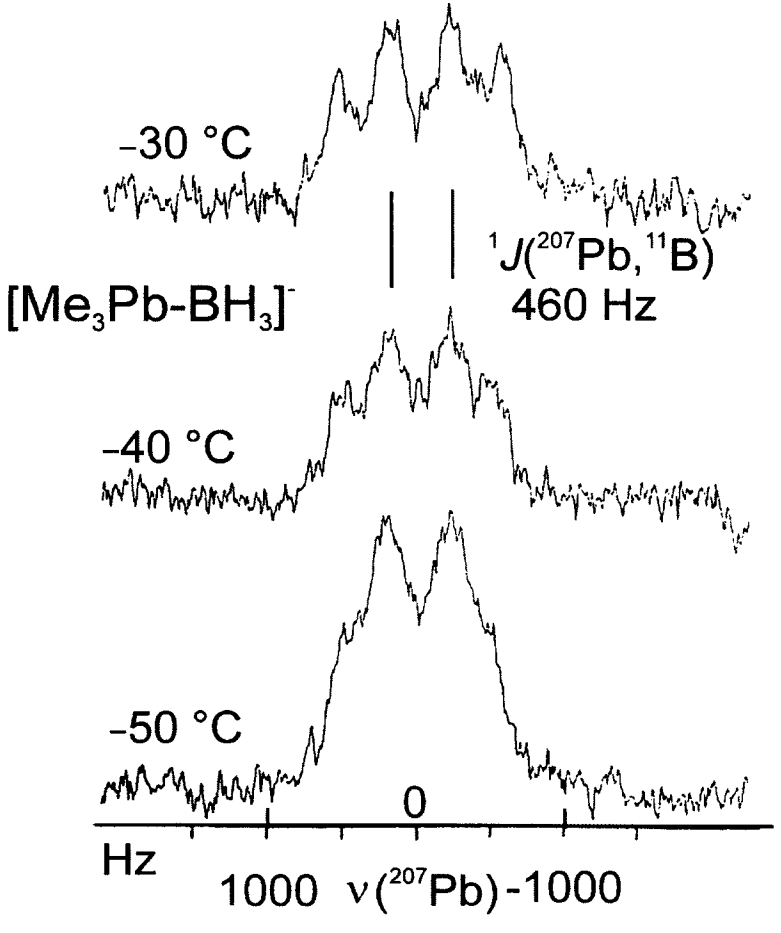

Fig. 4. 62.8 MHz ^{207}Pb{^{1}H} NMR spectrum of a solution of Li[Me$_3$Pb–BH$_3$] in tetrahydrofuran, measured at various temperatures (extensive decomposition occurs above −30 °C).[21] The signal shows splitting due to indirect nuclear ^{207}Pb–^{11}B spin–spin coupling as indicated (^{11}B: $I = 3/2$). At lower temperature, the lifetime of the ^{11}B spin states becomes increasingly shorter owing to efficient quadrupolar ^{11}B nuclear spin relaxation, and consequently the splitting of the ^{207}Pb NMR signal starts to collapse.

nuclei. If the same compounds can be studied by solid-state ^{207}Pb NMR, and the structures in solution and in the solid state are comparable, the anisotropy parameters are accessible. Fast relaxation of the X nuclei, e.g. by efficient quadrupolar interactions, leads to scalar relaxation of the second kind (T_2^{SC}),[20] and the result is broadening of the ^{207}Pb resonance signals (e.g. for X = Cl, Br, I) or, as shown in Fig. 4, residual splitting of the broadened ^{207}Pb resonance signal owing to partially relaxed ^{207}Pb–X spin–spin coupling (X = ^{11}B). Figure 5 shows the competition between scalar relaxation of the second kind [T_2^{SC}(^{207}Pb) is short owing to partially relaxed ^{207}Pb-^{14}N scalar spin–spin coupling] and CSA relaxation.

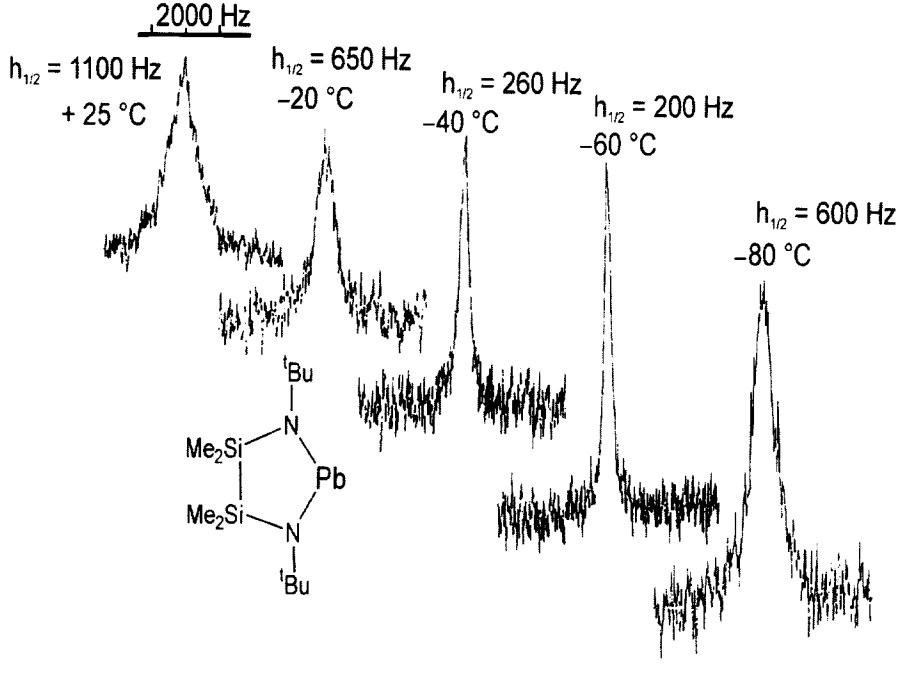

Fig. 5. 62.8 MHz ^{207}Pb{^{1}H} NMR spectra of a cyclic bis(amino)plumbylene (≈15% in [D$_8$]toluene), showing the competition between scalar relaxation of the second kind [short relaxation times T_2^{SC}(^{207}Pb) caused by partially relaxed scalar ^{207}Pb–^{14}N coupling (^{14}N: $I = 1$)] and CSA relaxation [relaxation times T_2^{CSA}(^{207}Pb) become shorter at lower temperature, owing to decreasing correlation times τ_c].[29] At lower temperatures, 'quadrupolar ^{14}N decoupling' becomes dominant (sharpening of the ^{207}Pb NMR signal), and then the CSA relaxation mechanism takes over (broadening of the ^{207}Pb NMR signal at temperatures below −70 °C).

4. CHEMICAL SHIFTS δ^{207}Pb

4.1. General

General concepts of nuclear shielding (or chemical shifts) have already been noted in previous reviews.[3,4] Theoretical approaches to the reliable calculation of ^{207}Pb nuclear shielding may soon be successful,[22] and this will help to improve our understanding of this parameter. ^{207}Pb chemical shifts cover a range of approximately 17 000 ppm, from ca +11 000 to ca –6000 with δ^{207}Pb for Me_4Pb at zero. The most deshielded ^{207}Pb nuclei are found in monomeric plumbylenes in which substituted alkyl groups are linked to lead, and the most shielded ^{207}Pb nuclei are present in plumbocene derivatives.

There are two different crudely linear correlations between δ^{207}Pb and δ^{119}Sn values for comparable lead and tin compounds. One correlation includes many Pb(IV) and Sn(IV) compounds[23,24] and Zintl anions,[25] and the straight line passes close to the origin with the coordinates δ^{207}Pb(Me_4Pb) = 0 and δ^{119}Sn(Me_4Sn) = 0 {δ^{207}Pb [lead(IV)] = 2.43 δ^{119}Sn [tin(IV)] + 34.1}, whereas the second correlation comprises pairs of lead(II) and tin(II) compounds, including plumbocenes and stannocenes {δ^{207}Pb [lead(II)] = 3.30 δ^{119}Sn [tin(II)] + 2336}. It has been suggested[26] that relativistic effects[27] related to the lone pair of electrons are responsible for the marked differences (slope and intercept) between these correlations. An increase in the coordination number in lead(II) [e.g. in dimers of bis(amino)plumbylenes,[28,29] in lead alkoxides and oxoalkoxides,[30] or in lead(II) complexes of monothiohydroxamic acid[31]] as well as in lead(IV) compounds [e.g. in the association of organolead(IV) halides and alkoxides (see previous reviews[3,4] for references)] is indicated by an increase in ^{207}Pb magnetic shielding. This behaviour is similar, although studied in a less systematic way, to that for ^{119}Sn magnetic shielding. Lead tetracarboxylates, studied by ^{207}Pb NMR both in solution and in the solid state,[32] reflect dynamic processes in solution and the coordination number 8 of the lead atoms in the solid state. The intermolecular exchange of the carboxylate ligands has been investigated by 2D ^{207}Pb exchange spectroscopy (EXSY).[32b] The impact of solid-state ^{207}Pb NMR of organolead compounds[19,33–35] is becoming increasingly important, and the comparison of isotropic δ^{207}Pb values measured in solution with those for solids (see, for example, Figs 3, 6,[36] and 7 [37]) provides an important link for structural arguments if the crystal structures have been determined.

4.2. Patterns of ^{207}Pb chemical shifts

4.2.1. Coordination number of lead and electronic structure

Most lead compounds contain lead in the formal oxidation state +2 or +4 (see ref. 38 for an example of oxidation state +1 with a lead–lead bond; and there are of

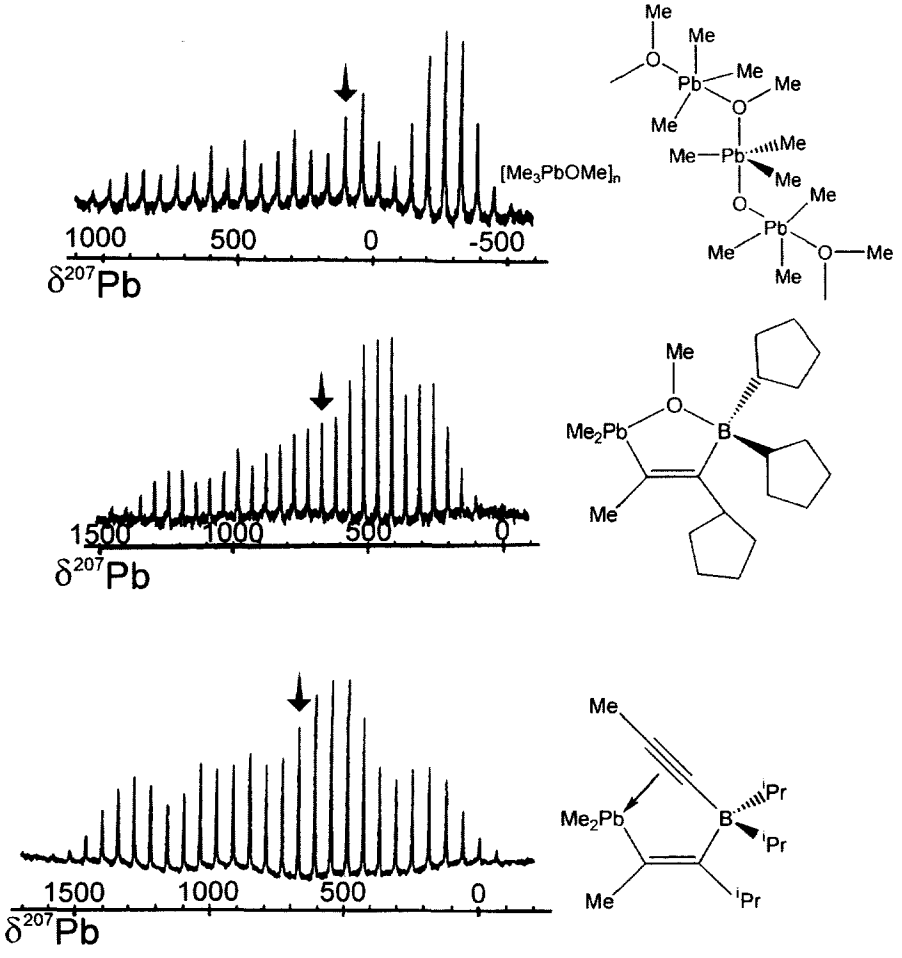

Fig. 6. 62.8 MHz solid-state ^{207}Pb NMR (CP/MAS) spectra of organolead compounds containing a bridging methoxy and a bridging alkynyl group, all of which increase the lead coordination number in the solid state as well as in solution.[36] Isotropic shifts δ^{207}Pb are indicated by arrows. The δ^{207}Pb values in solution and in solid state are as follows: Me_3PbOMe in $CDCl_3$ +307.5 (1.18 M), +379.9 (0.40 M), +391.2 (0.18 M); solid +103.8; middle trace: in C_6D_6 +661.0; solid +662.0; lower trace: in C_6D_6 +667.2; solid +670.5.

course numerous diplumbanes, in which the lead atoms have the format oxidation state +3). In the case of lead(II) compounds, the lowest ^{207}Pb nuclear shielding is observed for monomeric plumbylenes, such as **1** (in contrast to the analogous tin compound, **1** does not dimerize in solution, and in the solid state there are very weak Pb–Pb interactions) or for related compounds such as **2** [39] or **3**.[40] In the case of **4**,[41–43] the δ^{207}Pb data cover a large range, and the relationship to the aryl substituent is not obvious, except for Ar = 2,4,6-$(CF_3)_3C_6H_2$, where it

must be assumed that weak F–Pb interactions exist which lead to a considerable increase in ^{207}Pb nuclear shielding.[44] In the plumbylenes **5**[45] with metal–Pb bonds, strong deshielding with respect to diarylplumbylenes is observed, most likely because of the M–Pb bond. Now, there are several examples, for which convincing crystallographic evidence has been presented[46–48] that some plumbylenes are dimeric in the solid state. They exhibit rather long Pb–Pb bonds, indicating the absence of a Pb=Pb bond, being typical of donor–acceptor interactions. These compounds either show the ^{207}Pb resonance of a monomer in solution or ^{207}Pb NMR signal(s) could not be detected at all, which might point towards a monomer–dimer equilibrium. Similarly, the attempt failed to detect the ^{207}Pb NMR signal of the remarkable alkyne analogue ArPbPbAr [Ar = C_6H_3-2,6-(C_6H_2-2,4,6-$^iPr_3$)$_2$],[49] the unique Pb–Pb bonding of which has been the subject of a theoretical study.[50]

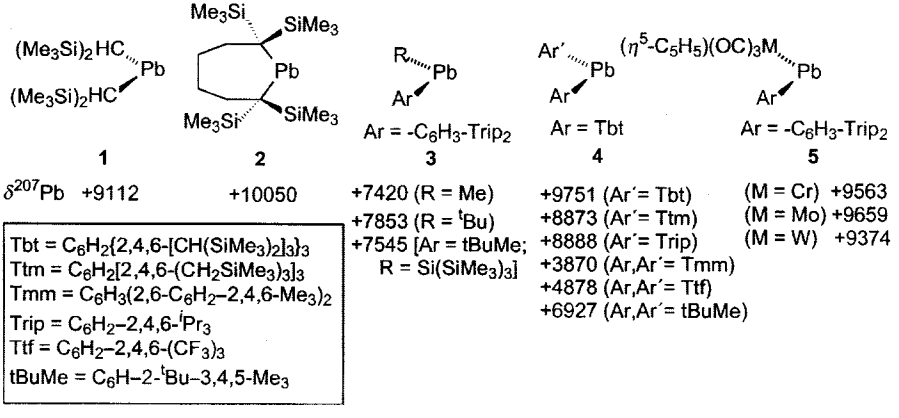

The shielding of ^{207}Pb nuclei in monomeric bis(amino)plumbylenes such as **6–8** is increased when compared with **1–5**, although it remains still fairly low. The shielding difference between these diorgano- and bis(amino)plumbylenes can be explained by considering the relative energies of electrons in the Pb–C and Pb–N σ bonds. In the bis(amino)plumbylenes, their energy is lower and, therefore, the larger energy differences between ground states and relevant excited states cause a smaller contribution to the paramagnetic shielding term. The molecular structure of **6** shows that the planes of the N($SiMe_3$)$_2$ groups are twisted by almost 90° against the PbN_2 plane. This should also apply to the N(^{t}Bu)$SiMe_3$ group in **7**, whereas in the comparable cyclic bis(amino)plumbylene **8** PbN(pp)π bonding may be considered as a result of the favourable molecular geometry. However, the δ^{207}Pb values of **7** and **8** lie in the same range, the ^{207}Pb nuclear shielding in **8** being slightly increased with respect to **7**. Therefore, potential

PbN(pp)π bonding must play a minor role (the same as SnN(pp)π bonding in the corresponding aminotin compounds), and cannot be responsible for the large increase in ^{207}Pb nuclear shielding in the amides **6–8** [26] with respect to most of the diorganoplumbylenes **1–5**.

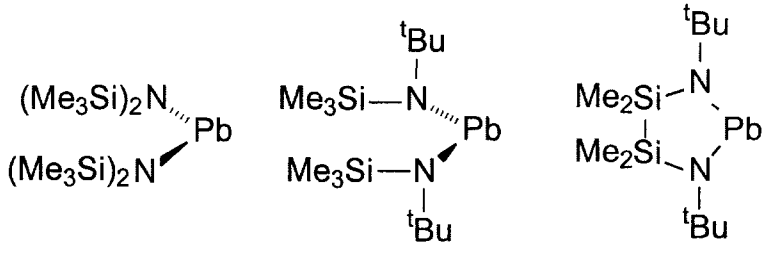

6 **7** **8**

δ^{207}Pb +4916 +5371 +4900

A carbene adduct **9** of a diarylplumbylene has been characterized in the solid state as the zwitterionic species.[51] The labile compound decomposes in solution, and the position of the ^{207}Pb resonance could not be determined.

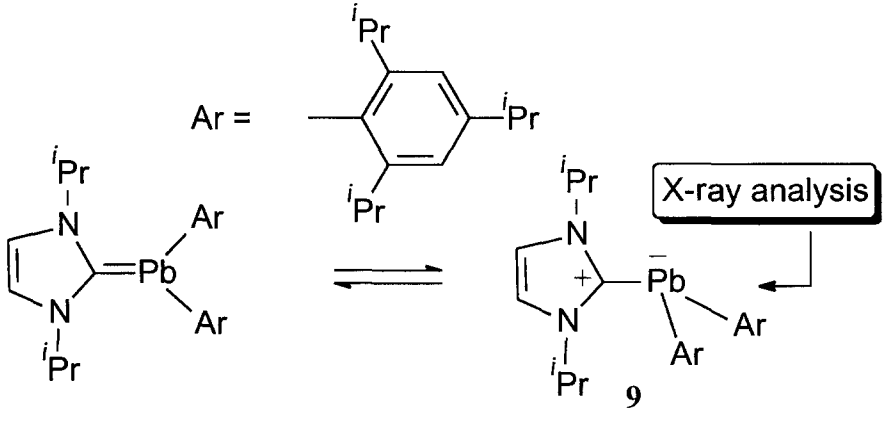

9

Similarly, only a weak carbene adduct **10** is formed with a bis(amino)plumbylene, as shown by temperature-dependent ^{207}Pb NMR spectra which change by ca 1000 ppm, when solutions are studied between 358 and 198 K.[52]

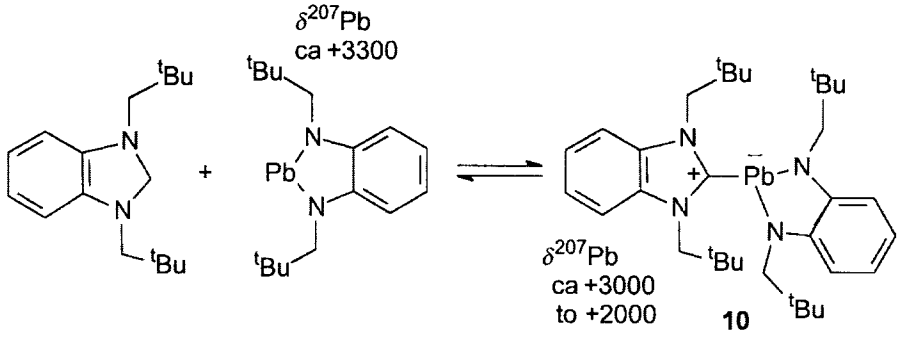

Lead in the formal oxidation state +2 has a rich coordination chemistry which, in principle, can be studied by ^{207}Pb NMR, as has been shown for solutions of lead(II) complexes with chelating ligands derived from EDTA. In this work[53] it was shown that indirect detection methods such as HMQC ^{1}H/^{207}Pb experiments[1,17] can be applied in order to study highly diluted solutions. The complex chemistry of Pb^{2+} ions in aqueous solution can be analysed using ^{207}Pb NMR by measuring the temperature and concentration dependence of the ^{207}Pb NMR signal, as has been suggested previously,[54] and been reinvestigated.[55] The lead(II)–hydroxide system has been studied by various physical methods, all of which, including ^{207}Pb NMR, were found to be useful in providing evidence for up to four mononuclear hydroxide complexes.[56]

In plumbocenes, in which lead also has the formal oxidation state +2, another extreme bonding situation is encountered. The lead atom has a formal coordination number of 10 if η^5 coordination of each cyclopentadienyl ring is assumed, and the ^{207}Pb resonances are observed at the low frequency end of the scale. Of the compounds **11** and **12**,[57] the molecular structures have been determined by X-ray analysis in the solid state, and the ^{207}Pb NMR spectra have been measured both in the solid state and in solution. Figure 7 shows a comparison of the solid-state ^{29}Si, ^{119}Sn, and ^{207}Pb NMR spectra of the bis(pentamethylcyclopentadienyl)metallocenes, Cp^*_2Si, Cp^*_2Sn, and Cp^*_2Pb respectively.[37] Differences between the isotropic shifts in solution and in the solid state are small, but significant for δ^{29}Si, and relatively small, almost negligible, for δ^{119}Sn and δ^{207}Pb. In all three cases, the crystallographic results are fully reproduced by the solid-state metal NMR spectra (in contrast to the corresponding solid-state ^{13}C NMR spectra). There is hardly any change in the δ^{207}Pb data if the cyclopentadienyl rings adopt a bent or parallel arrangement.[57] It has been pointed out[57] that the δ^{207}Pb value (−6150) given for $(Ph_5C_5)_2Pb$[58] may be wrong by ca 1000 ppm (a value of ca −5000 ppm was suggested[57]) as a result of a mistake in the assignment of the isotropic shift or by a referencing problem.

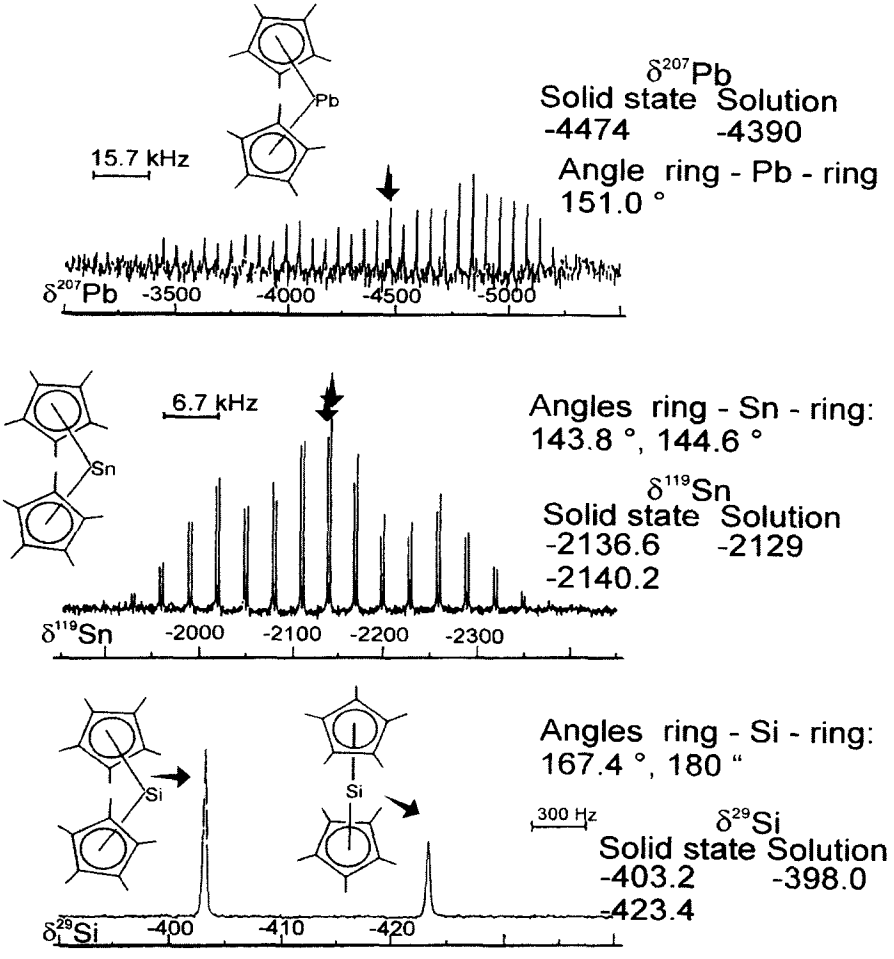

Fig. 7. 59.6 MHz, 111.9 MHz, and 62.8 MHz solid-state ^{29}Si, ^{119}Sn, and ^{207}Pb NMR spectra (CP/MAS) of the respective decamethylmetallocenes.[37] The silicon compound contains the molecules with bent and parallel arrangement of Cp* in the crystal (ratio 2:1);[122] in the tin compound two independent molecules are in the unit cell, with slightly different centroid–Sn–centroid angles;[123] the unit cell of the lead compound contains a single type of molecule.[124]

The isolobal replacement of CH by P leads to heteroplumbocenes such as the hexaphosphaplumbocene derivative $(\eta^5\text{-}P_3C_2{}^tBu_2)_2Pb$, for which the $\delta^{207}Pb$ value [−3752; $J(^{207}Pb,^{31}P)$ = 358 and 250 Hz] indicates a bonding situation similar to that of other plumbocenes.[59] Similarly, the replacement of the cyclopentadienyl anions by 1-methylboratabenzene anions leads to bis(1-methylboratabenzene)lead **13** (the tin **14** and germanium derivatives are also characterized).[60] Although the ^{207}Pb and ^{119}Sn nuclear shieldings are markedly reduced with

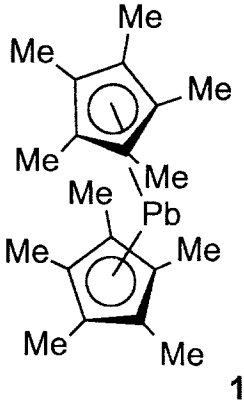

11

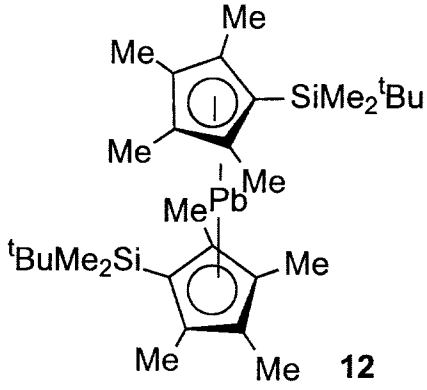

12

δ^{207}Pb -4390 -4474

-4595 (solution)
-4692 (solid state)

respect to bis(cyclopentadienyl) complexes, the metal nuclei are still well shielded, and an electronic structure comparable to group 14 metallocenes can be envisaged.

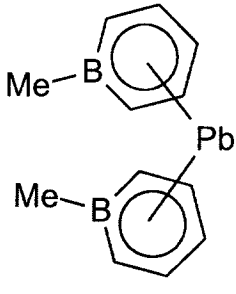

13

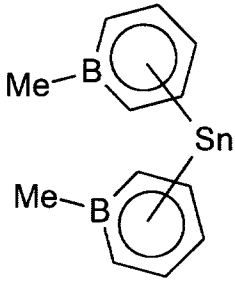

14

δ^{207}Pb -2579 δ^{119}Sn -1535

Lead(IV) compounds are known with coordination numbers 4, 5, and 6, and in some cases >6. Typically, the nuclear shielding of ^{207}Pb nuclei increases with coordination number. This is shown for coordination numbers 4 and 5 by the example given below for compound **15** and the anion **16**.[61]

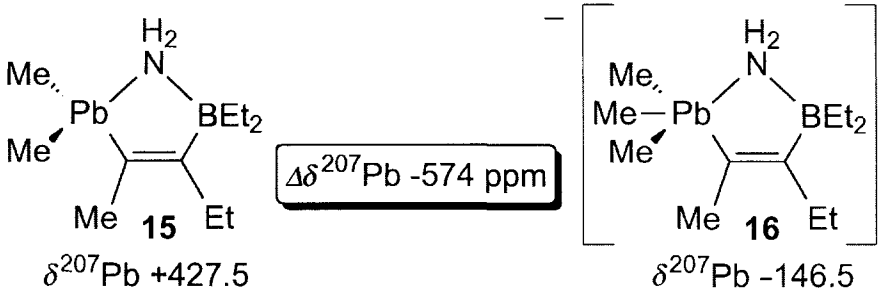

The existence of a new class of organolead(IV) compounds has been firmly established.[62] These are zwitterionic species, in which a formally positively charged lead atom is coordinated to an alkynyl group (**17**) which is part of an alkynylborate fragment. The surroundings of the lead atom by its next neighbours, two methyl and the alkenyl carbon atoms, are exactly trigonal–planar, as expected for a triorganolead cation. This coordinatively unsaturated situation is compensated for by the side-on coordination to the C≡C bond. However, the low ^{207}Pb nuclear shielding is in line with the cationic character of this fragment. The relevant structural features of the solid-state structure[62] are retained in solution, as shown by the comparison of solid- (see Fig. 6) and liquid-state ^{207}Pb NMR data.[36] Firm evidence of the existence of 'free' three-coordinate organolead cations in solution is still missing.

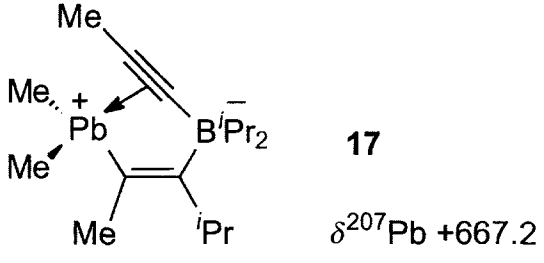

Octahedral coordination of lead by six oxygen atoms is found in iminium, Pb_3O_4, for the site of the Pb^{4+} ions, and this is reflected by the solid-state ^{207}Pb NMR spectra.[10] In contrast, the surroundings of the Pb^{2+} sites are unsymmetrical and there is a rather short Pb–Pb distance of 379 pm. The isotropic δ^{207}Pb values for Pb_3O_4 are -1091 ± 3 (Pb^{4+}) and $+804 \pm 10$ (Pb^{2+}).

The anions $[PbCl_nF_{6-n}]^{2-}$ **18–26** have been generated in MeCN, and the chemical shifts δ^{207}Pb and δ^{19}F have been measured together with the coupling constants $^1J(^{207}Pb,^{19}F)$, as shown in the following list:[63]

	δ^{207}Pb	δ^{19}F [$^2J(^{19}F,^{19}F)$ in Hz]	$^1J(^{207}Pb,^{19}F)$ [(Hz)]
18 $[PbF_6]^{2-}$	−1978.9	−103.8	3331
19 $[PbClF_5]^{2-}$	−1908.1	−97.7 (q), −72.9 (d) (62)	3086, 3722
20 *cis*-$[PbCl_2F_4]^{2-}$	−1887.6	−66.8 (t), −42.4 (t) (74)	3416, 3970
21 *trans*-$[PbCl_2F_6]^{2-}$	−1843.6	−40.9 (s)	4041
22 *fac*-$[PbCl_3F_3]^{2-}$	−1920.3	−36.2 (s)	3613
23 *mer*-$[PbCl_3F_3]^{2-}$	−1881.2	−33.7 (t), −10.4 (d) (84)	3682, 4162
24 *cis*-$[PbCl_4F_2]^{2}$	−1973.7	−3.3 (s)	3759
25 *trans*-$[PbCl_4F_2]^{2-}$	−1945.6	21.5 (s)	4236
26 $[PbCl_5F]^{2-}$	−2102.6	29.3 (s)	3790
27 $[PbCl_6]^{2}$	−2326.0	—	—

The δ^{207}Pb values of **18–27** are significantly different from δ^{207}Pb of halogenoplumbate anions $[PbX_3]^-$ (**28–30**) and $[Pb_3Br_8]^{2-}$ (**31**, **32**) which were measured in DMSO solutions.[64] The role of the solvent DMSO in coordination to lead is not fully understood, since the δ^{207}Pb values change considerably after several months. Data for freshly prepared solutions are given below:

	$[PbCl_3]^-$	$[PbBrCl_2]^-$	$[PbBr_2Cl]^-$	$[Pb_3Br_8][Ph_4P]_2$	$[Pb_3Br_8][Ph_4As]_2$
	28	**29**	**30**	**31**	**32**
δ^{207}Pb	+430	+466	+439	+323	+386

4.2.2. Substituent effects and effects of cyclic structures

The influence of various substituents on δ^{207}Pb of tetracoordinate lead(IV) compounds has been shown in previous reviews.[3,4] The slowly growing dataset available today for tetraorganolead compounds confirms the trends outlined previously. This holds for various trimethylplumbyl-substituted methanes,[65] for alkenylplumbanes,[66–73] tetraarylplumbanes,[74,75] and also for ^{207}Pb NMR data of a number of tri(*tert*-butyl)lead derivatives **33–38** with selected data given below:[76]

$^tBu_3Pb$-R	Me	Et	Pr	Bu	CH_2Ph	CH_2SiMe_3
	33	**34**	**35**	**36**	**37**	**38**
δ^{207}Pb	+101.1	+40.1	+41.1	+41.5	+7.9	+124.5
$[^1J(^{207}Pb,^{13}C_R)]$	[104.4]	[21.7]	[20.7]	[34.0]	[132.5]	[204.4]
$\{^1J(^{207}Pb,^{13}C_{tBu})\}$	{224.6}	{190.2}	{191.3}	{191.0}	{164.2}	{202.7}

The δ^{207}Pb data for Ph_3PbCF_3, $Ph_2Pb(CF_3)_2$, and $PhPb(CF_3)_3$ (−236.6, −316.0, and −515.0) have been reported without comment.[77] Together with the data for

numerous alkyllead–CF_3 compounds,[78] both series demonstrate the shielding effect on the ^{207}Pb nuclei exerted by the CF_3 group(s). The comparison of $\delta^{207}Pb$ of Ph_4Pb (−179) and $(C_6F_5)_4Pb$ [79] (−391) reveals that the C_6F_5 groups also have a shielding influence, and, as in the case of CF_3, this may arise as the result of polarization of the σ bonding framework or by weak F–Pb interactions with fluorine atoms in close spatial proximity of the lead atom.

It appears that the bond angles at the lead atom have an influence on $\delta^{207}Pb$ values (in a similar way to that demonstrated for ^{119}Sn nuclear shielding). Thus, ^{207}Pb nuclei as part of a five-membered ring are deshielded when compared with non-cyclic structures or larger rings.[24,80]

The growing availability of numerous reactive plumbylenes opens routes to new lead(IV) compounds with halogen–lead[81,82] (**39**) or chalcogen–lead bonds (**40**).[83] However, there are also new data for mesityllead bromides (**41**, **42**) [84] and trimeric diaryllead sulfides $(Ar_2PbS)_3$ (**43**),[85] prepared in the usual ways.

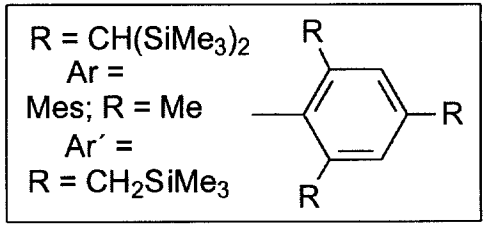

		$\delta^{207}Pb$
41	Mes_3Pb-Br	−97.0
42	Mes_2PbBr_2	−147

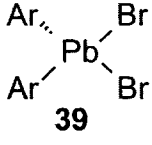

39

$\delta^{207}Pb$ −83.0

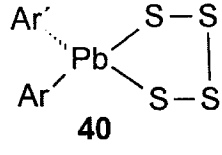

40

+313.9

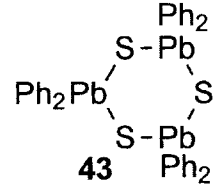

43

+172.8

Organolead–nitrogen compounds have been studied repeatedly by using ^{207}Pb NMR. This has led to ^{207}Pb NMR data of several series of compounds with triorganolead amides and diorganolead bis(amides), as shown below for some examples (**44–55**):[86–90]

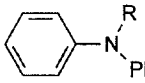

R	H **44**	Me **45**	$SiMe_3$ **46**	$PbMe_3$ **47**
δ^{207}Pb	+156.3	+226.5	+200.7	+188.7
[$^1J(^{207}Pb,^{15}N)$]	[293.4]	261.0	231.8	294.2

	$(Me_3Si)_2N-PbMe_3$ **48**	$[(Me_3Si)_2N]_2PbMe_2$ **49**	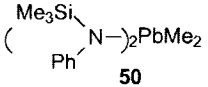 **50**	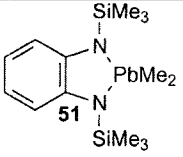 **51**
δ^{207}Pb	+171.9	+133.5	+131.7	+127.7
[$^1J(^{207}Pb,^{15}N)$]	[242.7]	[273.2]	[275.9]	[208.1]

	$^tBu_3Pb-NH_2$ **52**	$^tBu_3Pb-N(H)Ph$ **53**	$^tBu_3Pb-N(H)-SiMe_3$ **54**	$Me_3Pb-N(H)-SiMe_2{}^tBu$ **55**
δ^{207}Pb	+115.9	+44.8	+87.1	+155.2
[$^1J(^{207}Pb,^{15}N)$]	[343.2]	[450.2]	[372.0]	[249.3]

Organolead–phosphorus compounds are highly attractive from the NMR point of view, considering the presence of the spin-1/2 nuclei ^{1}H, ^{13}C, ^{31}P, and ^{207}Pb in the same molecule. This has been used in a study focusing on tris(*tert*-butyl)plumbyl phosphanes.[91] Some selected data for **56–59** are given below.

	$^tBu_3Pb-P^tBu_2$ **56**	$^tBu_3Pb-P(^tBu)NH^tBu$ **57**	$^tBu_3Pb-P(^tBu)N(Me)CH_2Ph$ **58**	$Me_3Pb-P(^tBu)N(Me)CH_2Ph$ **59**
δ^{207}Pb	+165.6	+47.0	+89.5	−99.3
$^1J(^{207}Pb,^{31}P)$]	[1951]	[1796]	[1083]	[1736]

There are further examples of compounds with Pb–Si, Pb–Ge, Pb–Sn, and Pb–Pb bonds, and the majority have been characterized by ^{207}Pb NMR.[76,92] Some selected data[76] for silylplumbanes **60–64**, a germylplumbane **65**, stannylplumbanes **66–70**, and diplumbanes **71–75** are given below. In some cases, identification and characterization of silylplumbanes proved to be difficult.[93]

$^tBu_3Pb–MR_3$	$SiMe_3$ **60**	$SiMe_2{}^tBu$ **61**	$SiMe_2Ph$ **62**	$SiPh_3$ **63**	$SiMe_2SiMe_3$ **64**	$GeMe_3$ **65**
$\delta^{207}Pb$	–47.4	–32.0	–65.1	–67.2	+18.7	+21.0
$[^1J(^{207}Pb,^{29}Si)]$	[207.6]	[102.5]	[151.4]		[57.9]	
$\{^1J(^{207}Pb,^{13}C_{tBu})\}$	{118.3}	{103.2}	{118.3}	{125.7}	{106.8}	{120.9}

$^tBu_3Pb–MR_3$	$SnMe_3$ **66**	$SnEt_3$ **67**	$SnBu_3$ **68**	Sn^tBu_3 **69**	$SnPh_3$ **70**
$\delta^{207}Pb$	+110.5	+131.7	+120.9	+158.0	+135.7
$[^1J(^{207}Pb,^{119}Sn)]$	[1637]	[2504]	[2441]	[6685]	[3581]
$\{^1J(^{207}Pb,^{13}C_{tBu})\}$	{105.2}	{88.3}	{84.6}	{92.3}	{120.9}

$^tBu_3Pb–PbR_3$	$PbMe_3$ **71**	$PbEt_3$ **72**	Pb^iPr_3 **73**	Pb^tBu_3 **74**	$Pbhex_3$ **75**
$\delta^{207}Pb$ ($^tBu_3Pb$)	+213.6	+261.2	+309.1	+335.1	+302.3
$\delta^{207}Pb$ (R_3Pb)	+0.4	+83.0	+164.8	+335.1	+75.4
$[^1J(^{207}Pb,^{207}Pb)]$	[7380]	[8126]	[9114]	[> 10000]	[9200]
$\{^1J(^{207}Pb,^{13}C_{tBu})\}$	{81.7}	{52.5}	{23.6}	{-16.4}	{34.8}

Few new examples became available for compounds with Pb–B bonds (see Fig. 4), and triorganoplumbyl lithium compounds in solution (e.g. $^tBu_3Pb–Li$ in THF at –30°C: $\delta^{207}Pb$ = +1573.8[76]) were studied. Since scalar $^{207}Pb–^7Li$ coupling was not observed in the cases of $R_3Pb–Li$ (R = Me, Et, ^tBu), the lithium cation must be solvated by THF, and the $\delta^{207}Pb$ value of $^tBu_3Pb–Li$ corresponds to the 'free' plumbyl anion.

Various transition metal complexes containing M–Pb bonds have been studied by ^{207}Pb NMR spectroscopy.[94–99] Examples are given in Fig. 8 for some iron complexes with Fe–Pb bonds (see also Fig. 1), showing that the $\delta^{207}Pb$ values cover a range of about 3500 ppm.[94]

Complexes with Mo–Pb and W–Pb bonds[96] have also been studied with respect to ^{95}Mo NMR and coupling constants $^1J(^{207}Pb,^{183}W)$. In the case of complexes with Mn–Pb bonds, there is a small shift to higher ^{207}Pb frequencies (on average) in going from solution to the solid state for $(OC)_5Mn–PbPh_3$ [97] (solution: $\delta^{207}Pb$ = 48.4; solid state with four different crystallographic sites: $\delta^{207}Pb$ = 70.1, 72.4, 105.8, 112.2). However, in the case of $[(OC)_5Mn]_2PbPh_2$, the difference in the isotropic ^{207}Pb chemical shifts is large[98] and hard to explain (solution: $\delta^{207}Pb$ = +378.3; solid state: $\delta^{207}Pb$ = 602.1). The corresponding $\delta^{119}Sn$ values differ only by 28 ppm.[98]

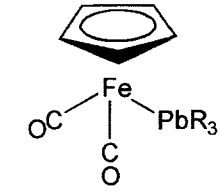

R	Me	Et	^{i}Pr	^{t}Bu	Ph
δ^{207}Pb	+243.1	+397.4	+469.8	632.1	125.1

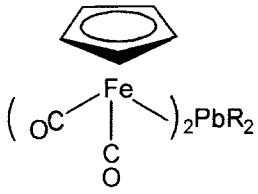

R	Me	Et
δ^{207}Pb	+692.8	+886.6

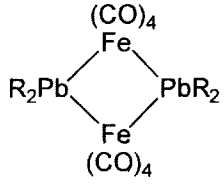

R	Me	Et	^{i}Pr
δ^{207}Pb	+293.4	+411.8	+460.9

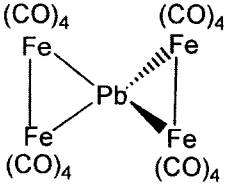

δ^{207}Pb +3586.6

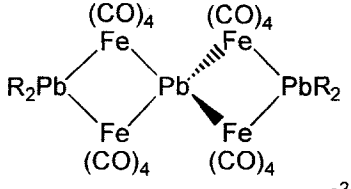

R	Me	Et	^{i}Pr
δ^{207}Pb (PbR_2)	+293.4	+411.8	+460.9
δ^{207}Pb	+ 745.3	+789.3	+825.4
[$^{2}J(^{207}Pb,^{207}Pb)$]	[1090]	[434]	[377]

Fig. 8. ^{207}Pb NMR parameters of some iron complexes with Fe–Pb bonds [all data are taken from ref. 94 except for $(Cp)Fe(CO)_2$–$PbPh_3$ [95]]. Note the extreme shift of the complex $Pb[Fe(CO)_4]_4$, in which it can be assumed that multicentre Fe–Pb–Fe bonding describes the bonding situation.

Unfortunately, ^{207}Pb NMR spectra of transition metal–lead complexes have not always been recorded, although ^{119}Sn NMR spectra of analogous tin compounds have been measured. No reason has been given why ^{207}Pb NMR data could not be obtained (e.g. in (Schiff-base) divalent group 14 element species $[(Salen)M]_nM'(CO)_{6-n}$ (n = 1, 2; M = Ge, Sn, Pb; M′ = Cr, W).[100] The same situation is found for [Salen]Sn(II) and [Salen]Pb(II) derivatives.[101]

4.2.3. Lead compounds with a formal oxidation state of less than +2

The ^{207}Pb nuclei in the highly fluxional Zintl anions of the type $[Sn_{9-n}Pb_n]^{4-}$ are well shielded (δ^{207}Pb values range from around –2667 to around –4185).[102a] The trends in ^{207}Pb and ^{119}Sn nuclear shielding are analogous in the cluster anions $[Pb_{9-n}Sn_n]^{4-}$ with n = 0 to 9. This is also true for the *closo*-cluster anions $[1\text{-}M(CO)_3(\eta^4\text{-}E_9)]^{4-}$ (M = Cr, Mo, W; E = Sn, Pb) which are rigid or less fluxional.[102b]

The extremely low ^{119}Sn nuclear shielding observed in transition metal complexes that contain trigonal–planar coordinated tin atoms in the formal oxidation state –2 (**76**)[103] finds its parallel in the ^{207}Pb deshielding in **77**.[104] This deshielding can be traced to the presence of an energetically low lying π^* LUMO available for B_0 induced charge circulation by which the paramagnetic contribution to magnetic shielding increases. Interestingly, the δ^{119}Sn / δ^{207}Pb data pair follows more the relationship for tin(IV) and lead(IV) compounds rather than the one for tin(II) and lead(II) compounds.

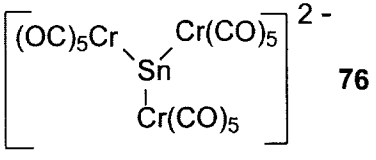

76

δ^{119}Sn +3924

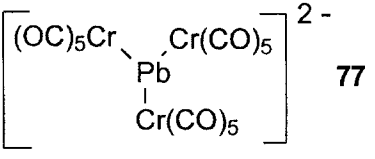

77

δ^{207}Pb +7885

An example with a Pb–Pb bond in a lead(I) compound[38] has already been addressed (see also Fig. 12).

4.3. Isotope-induced ^{207}Pb chemical shifts

Secondary isotope effects on ^{207}Pb chemical shifts may be quite large and can be readily detected from satellites in ^{207}Pb NMR spectra. Owing to the instability of lead hydrides, $^1\Delta^{1/2}$H(^{207}Pb) values have not been determined. However, a few data have been collected for $^1\Delta^{12/13}$C(^{207}Pb) (see also Fig. 1).[105] These data show the same trends as the corresponding data $^1\Delta^{12/13}$C(^{119}Sn), and the effects are more pronounced, as expected for the larger range of ^{207}Pb chemical shifts and the greater sensitivity of ^{207}Pb–^{13}C scalar coupling to polarizing effects. It should be noted that the expected shifts of the ^{207}Pb NMR signals to lower frequency for the heavy isotopomer is not observed in all cases. In addition to vibrational effects, responsible for isotope-induced chemical shifts, there is also a strong contribution arising from electronic effects.[106] Electronic effects will be reflected in particular by correlations of isotope-induced chemical shifts $^n\Delta$X(^{207}Pb) with the magnitude of the respective coupling constants ^nJ(^{207}Pb,X) (e.g. X = $^{12/13}$C).

However, so far a systematic determination of $^{n}\Delta^{12/13}$C(^{207}Pb) values has not been carried out.

The application of HEED extended pulse sequences makes it possible to determine $^{1}\Delta^{14/15}$N(^{207}Pb) values at natural abundance of the nuclei,[86,107] and it is hoped that by application of this technique a larger set of these data for lead–nitrogen compounds will become available in the future.

5. INDIRECT NUCLEAR SPIN–SPIN COUPLING CONSTANTS ^{n}J(^{207}Pb,X)

5.1. General

Previous reviews contain compilations of coupling constants ^{n}J(^{207}Pb,X), and the theoretical concepts have been summarized.[3–5] Since the gyromagnetic ratio γ(^{207}Pb) >0, the values ^{n}J(^{207}Pb,X) possess the same sign as the reduced coupling constants ^{n}K(^{207}Pb,X) if γ(X) >0 (e.g. X = ^{13}C), in contrast to the other group 14 spin-1/2 nuclei ^{119}Sn or ^{29}Si with negative γ(^{119}Sn) and γ(^{29}Si). In many cases, the signs of coupling constants ^{n}J(^{207}Pb,X) have to be determined experimentally, since predictions are much less reliable when compared with ^{n}J(^{119}Sn,X) or ^{n}J(^{29}Si,X). This is due to the polarizability and weakness of bonds between lead and other elements, and also to relativistic effects[108] which become more pronounced with the very heavy nuclei.

The most convenient techniques for the determination of coupling signs involving ^{119}Sn have been reviewed,[109] and the analogous techniques can be applied in the case of ^{207}Pb. Numerous coupling constants are already listed in previous reviews.[3–5] Therefore, this section will deal mainly with some results that have been published in the last decade.

5.2. One bond couplings, ^{1}J(^{207}Pb,X)

5.2.1. Coupling constants ^{1}J(^{207}Pb,^{13}C), ^{1}J(^{207}Pb,^{29}Si), ^{1}J(^{207}Pb,^{119}Sn), and ^{1}J(^{207}Pb,^{207}Pb)

All coupling constants ^{1}J(^{207}Pb,^{13}C) in tetraorganolead compounds are positive except for ^{1}J(^{207}Pb,^{13}C≡) in many 1-alkynyl(triorgano)lead derivatives, where a negative sign was proposed originally because of the solvent dependence,[110] and later on this was confirmed by 2D ^{13}C/^{1}H HETCOR experiments (Fig. 9).[111]

A roughly linear correlation exists for numerous values of ^{1}J(^{207}Pb,^{13}C) and ^{1}J(^{119}Sn,^{13}C) for comparable compounds.[112] However, a change in the sign of ^{1}J(^{207}Pb,^{13}C) is more likely than in the case of ^{1}J(^{119}Sn,^{13}C) in organotin compounds. An example for opposite signs of ^{1}J(^{207}Pb,^{13}C$_{Me}$) in the same molecule is given in Fig. 10.

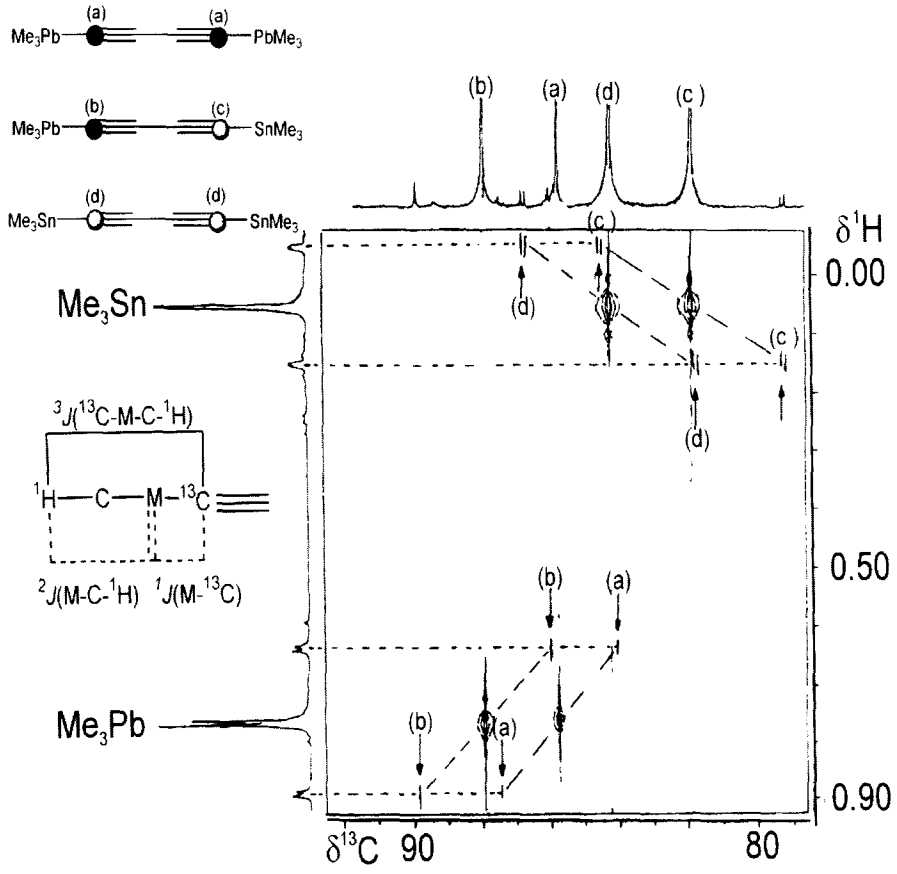

Fig. 9. Contour plot of the 75.5 MHz 2D $^{13}C/^{1}H$ HETCOR experiment [based on $^{3}J(\equiv^{13}C,M,C,^{1}H)$] of a mixture of trimethylstannyl- and trimethylplumbyl-buta-1,3-diynes.[111] The $^{13}C(M–C\equiv)$ resonances (a,b,c,d) are observed selectively, and the tilt of the cross peaks of the satellites[125] allows for the comparison of coupling signs. ^{13}C and ^{1}H are the active spins (connected by a solid line in the formula fragment) and ^{207}Pb or $^{117/119}Sn$ is the respective passive spin, and the signs of the reduced coupling constants $^{2}K(M,^{1}H_{Me})$ (known to be <0) and $^{1}K(M,^{13}C\equiv)$ are compared. A positive tilt indicates like signs and a negative tilt indicates opposite signs. Therefore, it follows that $^{1}K(^{207}Pb,^{13}C\equiv)$ and also $^{1}J(^{207}Pb,^{13}C\equiv) <0$, whereas $^{1}K(^{119}Sn,^{13}C\equiv) >0$ [$^{1}J(^{119}Sn,^{13}C\equiv) <0$ since $\gamma(^{119}Sn) <0$].

The sign of $^{1}J(^{207}Pb,^{13}C)$ in $^{t}Bu_3Pb$ derivatives can also change easily. In two different phosphanyl derivatives a positive or a negative sign follows from the 2D $^{13}C/^{1}H$ HETCOR experiments shown in Fig. 11. The sign of $^{3}J(^{207}Pb,^{1}H)$ was found to be positive in each case.[76]

In silylplumbanes, the sign of $^{1}K(^{207}Pb,^{29}Si)$ is positive,[21,76] whereas $^{1}K(^{207}Pb,^{119}Sn)$ in stannylplumbanes can be of either sign.[76]

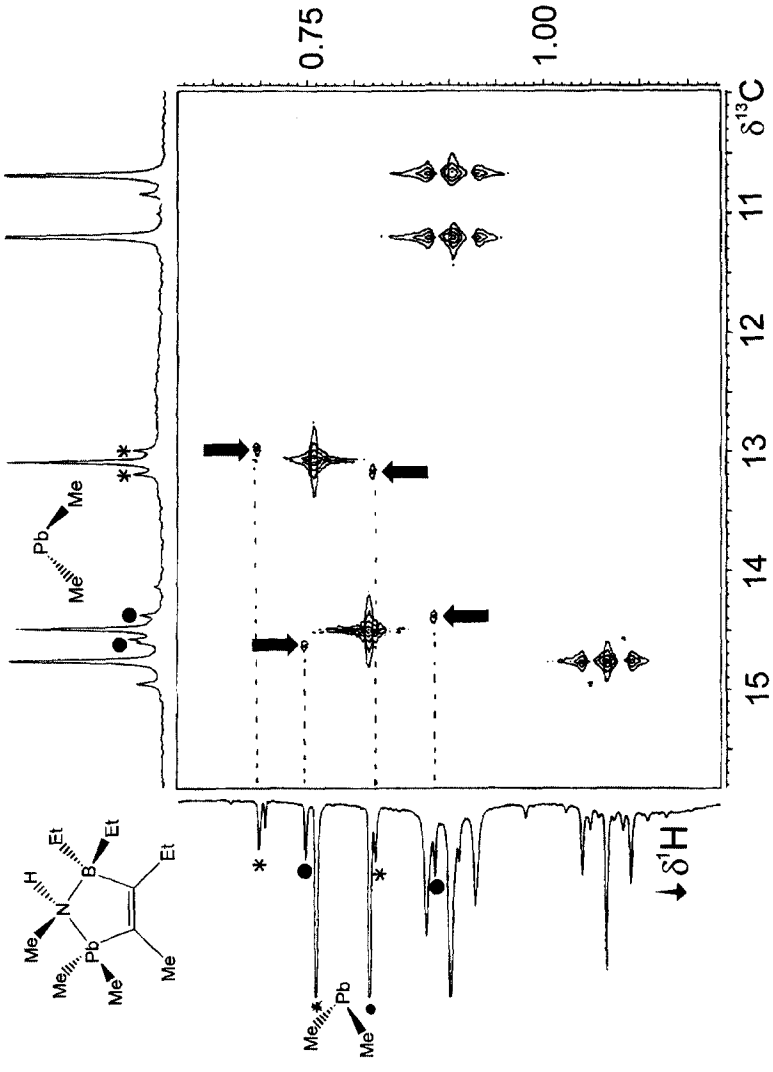

Fig. 10. Contour plot of the 75.5 MHz 2D ^{13}C/^{1}H HETCOR experiment, based on $^{1}J(^{13}C,^{1}H) = 130$ Hz. ^{207}Pb satellites of the MePb groups are indicated in the projections by filled circles and asterisks, and in the contour plot the relevant cross peaks are marked by arrows.[112] The sign of $^{2}J(^{207}Pb,^{1}H)$ (<0) does not change, whereas one of the coupling constants $^{1}J(^{207}Pb,^{13}C_{Me})$ is positive (negative tilt of the cross peaks), and the other one is negative (positive tilt of the cross peaks).

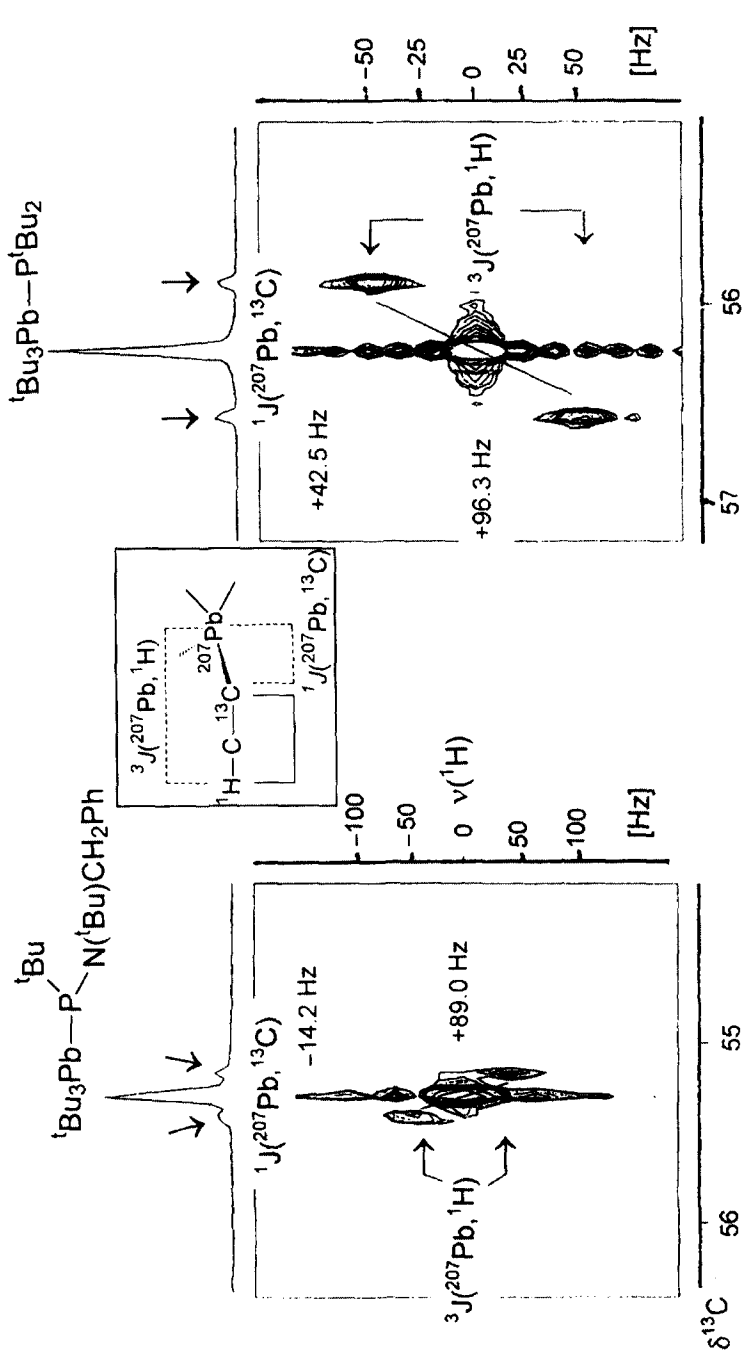

Fig. 11. Contour plots of the 2D $^{13}C/^{1}H$ HETCOR experiments of two $^{t}Bu_3Pb$ phosphanes show that the sign of $^{1}J(^{207}Pb,^{13}C)$ can be positive ($^{t}Bu_3Pb$–$P^{t}Bu_2$) or negative ($^{t}Bu_3Pb$–$P(^{t}Bu)N(^{t}Bu)CH_2Ph$), whereas there is no change in sign and hardly any change in the magnitude of $^{3}J(^{207}Pb,^{1}H)$.[76] The insert shows the path of ^{1}H–^{13}C polarization transfer (solid lines), and the coupling constants (dotted lines) which are compared with respect to their signs. A negative slope of the connection of the relevant cross peaks indicates opposite signs, and a positive slope indicates like signs.

	$Me_3Sn-PbMe_3$	$Me_3Sn-PbEt_3$	$Me_3Sn-Pb^iPr_3$	$Me_3Sn-Pb^tBu_3$
	78	**79**	**80**	**66**
$^1J(^{207}Pb,^{119}Sn)$ [Hz]	[-3570] ^{113}($^1K > 0$)	[-1398] ($^1K > 0$)	[+303] ($^1K < 0$)	[+1637] ($^1K < 0$)

In hexaalkyldiblumbanes, a positive sign of $^1K(^{207}Pb,^{207}Pb)$ has been determined for R = Me (**81**),[114] whereas for most other alkyl groups the coupling constants $^1J(^{207}Pb,^{207}Pb)$ are large and negative.[76]

	$Me_3Pb-PbMe_3$	$Et_3Pb-Pb^iPr_3$	$Me_3Pb-Pb^tBu_3$	$Et_3Pb-Pb^tBu_3$
	81	**82**	**71**	**72**
$^1J(^{207}Pb,^{207}Pb)$ [Hz]	[+290] [114]	[-6836]	[-7380]	[-8126]

The coupling constant $^1J(^{207}Pb,^{207}Pb)$ in a low-valent dilead compound is large, and the sign is most likely negative. The experimental and simulated ^{207}Pb NMR spectra are shown in Fig. 12.[38]

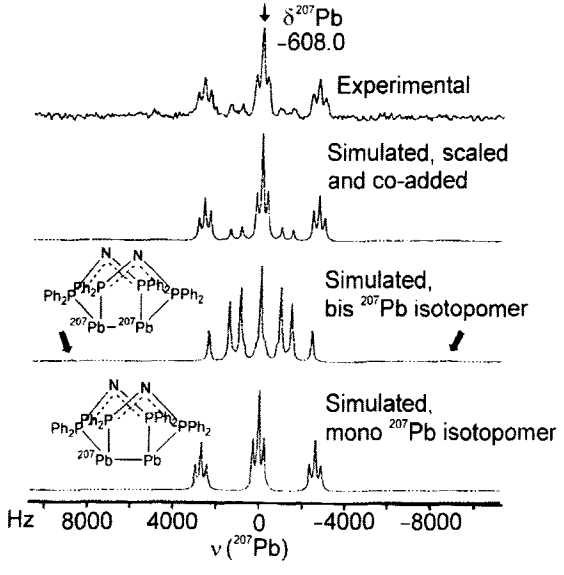

Fig. 12. 104.7 MHz ^{207}Pb{^{1}H} NMR spectra of a dimeric lead(I) compound, showing the agreement of calculated and experimental spectra.[38] The spectrum of the bis ^{207}Pb isotopomer was calculated as an AA′A″A‴XX′ spin system to give the coupling constants $^1J(^{207}Pb,^{207}Pb)$ = (–)7708 Hz, $^1J(^{207}Pb,^{31}P)$ = –2660 Hz and $^2J(^{207}Pb,^{31}P)$ = +240 Hz.

5.2.2. *Coupling constants $^1J(^{207}Pb,^{15}N)$, $^1J(^{207}Pb,^{31}P)$, $^1J(^{207}Pb,^{77}Se)$, $^1J(^{207}Pb,^{125}Te)$, and $^1J(^{207}Pb,^{19}F)$*

There are new $^1J(^{207}Pb,^{15}N)$ data (see the examples **44–55**) that confirm the trends established previously.[3] The presence of the lone pair of electrons at the nitrogen atom(s)[115] together with the polarizable Pb–N bond give large and negative contributions to the Fermi contact term (both in a non-relativistic and a relativistic model). Therefore, $^1K(^{207}Pb,^{15}N)$ values are large and negative for triorganolead amides and also for diorganolead diamides. The latter observation is in contrast to the trend observed for $^1K(^{119}Sn,^{15}N)$ for corresponding diorganotin diamides, since the Sn–N bonds become less polarizable and relativistic effects are smaller. If electropositive groups such as silyl and/or boryl groups are attached to the amide nitrogen atom, ^{14}N quadrupole-induced relaxation becomes less efficient, and therefore scalar ^{207}Pb–^{14}N coupling may be well resolved in ^{207}Pb NMR spectra, as shown in Fig. 13. In these cases, it is also worthwhile recording ^{14}N NMR spectra, since the ^{14}N NMR signals are reasonably sharp.

The sign of $^1J(^{207}Pb,^{31}P)$ is negative in all lead-phosphorus compounds (see also Fig. 12), and the recent data sets show that the magnitude of $^1J(^{207}Pb,^{31}P)$ does not change significantly with different substituents at the phosphorus atom (see **56–59**). The substitution of the methyl groups at the lead atom by *tert*-butyl groups leads to slightly more negative values of $^1J(^{207}Pb,^{31}P)$, the effect being much less pronounced than, for example, in the case of stannylplumbanes (see

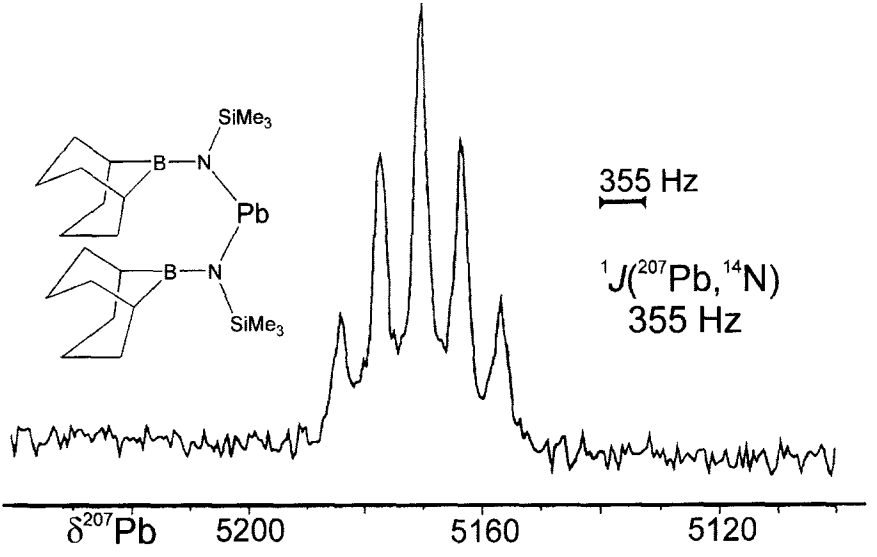

Fig. 13. 52.3 MHz $^{207}Pb\{^1H\}$ NMR spectrum (single-pulse technique) of a monomeric bis(amino)plumbylene showing the 1:2:3:2:1 pattern for scalar coupling between ^{207}Pb and two equivalent ^{14}N ($I = 1$) nuclei ($\delta^{207}Pb = +5170$).[129]

section 5.2.1.). This shows the dominant influence of the lone pair of electrons at the phosphorus atom[115] on the sign and magnitude of $^1J(^{207}Pb,^{31}P)$.

A negative sign of $^1K(^{207}Pb,^{77}Se)$ and $^1K(^{207}Pb,^{125}Te)$ is likely for all lead–selenium and lead–tellurium compounds, and this can also be assumed for $^1K(^{207}Pb,^{19}F)$ (see **18–26**). A series of dimetal trichalcogenide anions $[M_2E_3]^{2-}$ (e.g. **83–87**) has been studied by multinuclear magnetic resonance.[116,117] There is a large geminal ^{207}Pb–^{119}Sn coupling (1145 Hz) in **87**.[117]

	$[PbSe_3Pb]^{2-}$	$[PbS_2TePb]^{2-}$	$PbSSeTePb]^{2-}$	$[PbTe_3Pb]^{2-}$	$[PbSe_3Sn]^{2-}$
	83	**84**	**85**	**86**	**87**
$\delta^{207}Pb$	+3302	+3261	+3108	+1727	+3439
$[^1J(^{207}Pb,^{77}Se)]$ [Hz]	[153]		[159]		[153]
$\{^1J(^{207}Pb,^{125}Te)\}$ {Hz}		{818}	{868}		{1074}

In solid PbTe, the indirect nuclear spin–spin ^{207}Pb–^{125}Te interactions have been analysed by theoretical methods.[118]

5.2.3. *Coupling constants $^1J(^{207}Pb,M)$, where M is a transition metal nucleus*

The few data available so far are insufficient to predict all signs of $^1K(^{207}Pb,M)$. Coupling constants have been measured for M = ^{183}W (**88–92**),[96,113] M = ^{55}Mn $[Ph_3Pb–Mn(CO)_5]$: $^1J(^{207}Pb,^{55}Mn)$ = 250 ± 4, 253 ± 4, 275 ± 8 274 ± 7 Hz, and $Ph_2Pb[Mn(CO)_5]_2$: $^1J(^{207}Pb,^{55}Mn)$ = 228 ± 1 Hz; all data from solid-state ^{207}Pb NMR spectra [97,98], M = ^{57}Fe (see Fig. 1,[94] and Fig. 9 [94] for the type of complexes studied), and for M = ^{195}Pt (**93** and **94**).[99] The positive sign of $^1J(^{207}Pb,^{183}W)$ has been determined experimentally,[96] and it is likely that the sign of $^1J(^{207}Pb,^{195}Pt)$ is also positive, considering the data for comparable platinum–tin compounds.[119]

$CpW(CO)_3–PbR_3$ R = Me,	Et,	Ph;	$[CpW(CO)_3]_2PbR_2$ R = Et,	Ph
88	**89**	**90**	**91**	**92**
$\delta^{207}Pb$ -87	+25	-217	-128	-375
$[^1J(^{207}Pb,^{183}W)]$ [Hz] [+170]	[115]	[390]	[135]	[270]

	cis-[Pt(PPh$_3$)$_2$(Ph)PbPh$_3$]	*trans*-[Pt(PBu$_3$)$_2$(PbPh$_3$)$_2$
	93	**94**
δ^{207}Pb	-100	+76
[$^1J(^{207}Pb,^{195}Pt)$] [Hz]	[18380]	[14395]

5.3. Two-bond (geminal) coupling, $^2J(^{207}Pb,X)$

For X = ^{1}H, the majority of data stems from organolead compounds with coupling across a carbon atom. For intervening aliphatic carbon atoms the sign of $^2J(^{207}Pb,^1H)$ is mostly negative, although experimental evidence might be required. For methyllead and methyltin compounds, a relationship between the magnitude of $^2J(^{207}Pb,^1H)$ and $^2J(^{119}Sn,^1H)$ exists which shows that sign inversion of $^2J(^{207}Pb,^1H)$ must be considered more frequently than for $^2J(^{119}Sn,^1H)$.[112] In the case of trialkylplumbyl lithium compounds, the sign of $^2J(^{207}Pb,^1H)$ usually is positive.[21] An intervening olefinic carbon atom normally induces a positive sign of $^2J(^{207}Pb,^1H)$, and these coupling constants can become rather large, as evident in vinyllead triacetates (e.g. **96** and **97**).[120]

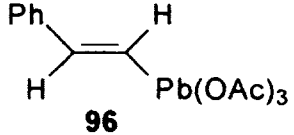

96

$^2J(^{207}Pb,^1H)$ 821.3 Hz
$^3J(^{207}Pb,^1H_{cis})$ 691.7 Hz

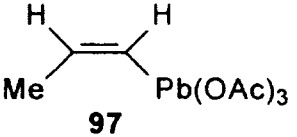

97

$^2J(^{207}Pb,^1H)$ 924.0 Hz
$^3J(^{207}Pb,^1H_{trans})$ 1668.0 Hz

There are numerous data $^2J(^{207}Pb,^{13}C)$ mostly with carbon,[36,61,66–72,74–79,84,86–88,91,94,110–112] but also with silicon,[21,76] tin,[76] lead,[76] nitrogen,[65,87,89,90] phosphorus,[91] or iron[94] as intervening atoms. Some data $^2J(^{207}Pb,^{29}Si)$ or $^2J(^{207}Pb,^{119}Sn)$ have been reported for coupling across aliphatic[65] or olefinic carbon atoms,[70–73] and also across nitrogen atoms.[29,87–90,129] The trends of most of these data follow the changes observed for corresponding values of $^2J(^{207}Pb,^1H)$.

5.4 Three-bond (vicinal) coupling, $^3J(^{207}Pb,X)$

The well-known Karplus-type dependence of the magnitude of vicinal coupling constants on the respective dihedral angle is also evident for numerous lead compounds according to values of $^3J(^{207}Pb,X)$ [X = ^{1}H (see **96** and **97**), ^{11}B,[70] ^{13}C [3]]. So far all signs determined for $^3K(^{207}Pb,X)$ are positive, with very few exceptions. If X is a quadrupolar nucleus such as ^{11}B, differential broadening of the ^{207}Pb NMR signals (as a result of partially relaxed scalar ^{207}Pb–^{11}B coupling), can be used to compare the relative magnitudes of $^3J(^{207}Pb,^{11}B)$.[70] As for geminal coupling constants involving ^{207}Pb, the major trends are the same as for the corresponding coupling constants involving ^{119}Sn.[109,130]

5.5 Long-range coupling constants $^nJ(^{207}Pb,X)$ with $n > 3$

Very often coupling between ^{207}Pb and other nuclei X across four or more bonds can be observed. The complex dependence of these parameters on structure and bonding means that their diagnostic value is still limited. As expected, such long-range couplings are fairly large and easy to observe if a π system (aryl-, benzyl, allenyl lead compounds) and/or a metal in transition metal complexes is involved. By using 2D ^{13}C/^{1}H or other X/^{1}H HETCOR experiments, the absolute signs of such long-range coupling constants can be determined. In turn, these signs can be used in further 2D experiments to determine other absolute coupling signs. Examples are a ^{13}C/^{1}H HETCOR experiment to show a negative sign of $^4J(^{207}Pb,^1H)$ in $Pb(C{\equiv}C{-}Me)_4$ (see Fig. 14),[131] and a ^{29}Si/^{1}H HETCOR experiment to show a positive sign for $^5J(^{207}Pb,^1H)$ in $Pb(C{\equiv}C{-}SiMe_3)_4$.[132] The knowledge of the sign of long-range coupling constants increases their diagnostic value.

6. CONCLUSIONS

The impact of ^{207}Pb NMR parameters, determined either by ^{207}Pb NMR or by studying the NMR spectra of other nuclei that may show satellites owing to indirect nuclear spin–spin coupling with the ^{207}Pb nucleus, is noteworthy. Although lead chemistry does not belong to the most attractive fields in chemistry, it is a fact that on the one hand lead chemicals are components of many materials with important technological applications and on the other hand, are also listed as compounds considered as being hazardous to the environment. Therefore, any useful analytical technique, including of course ^{207}Pb NMR, will have a growing influence. Clearly, ^{207}Pb NMR parameters deserve attention from all theoreticians working on relativistic effects. For the preparative working chemist, it is still a challenge to discover similarities or differences in the chemistry of one of the most heavy elements in comparison with its lighter

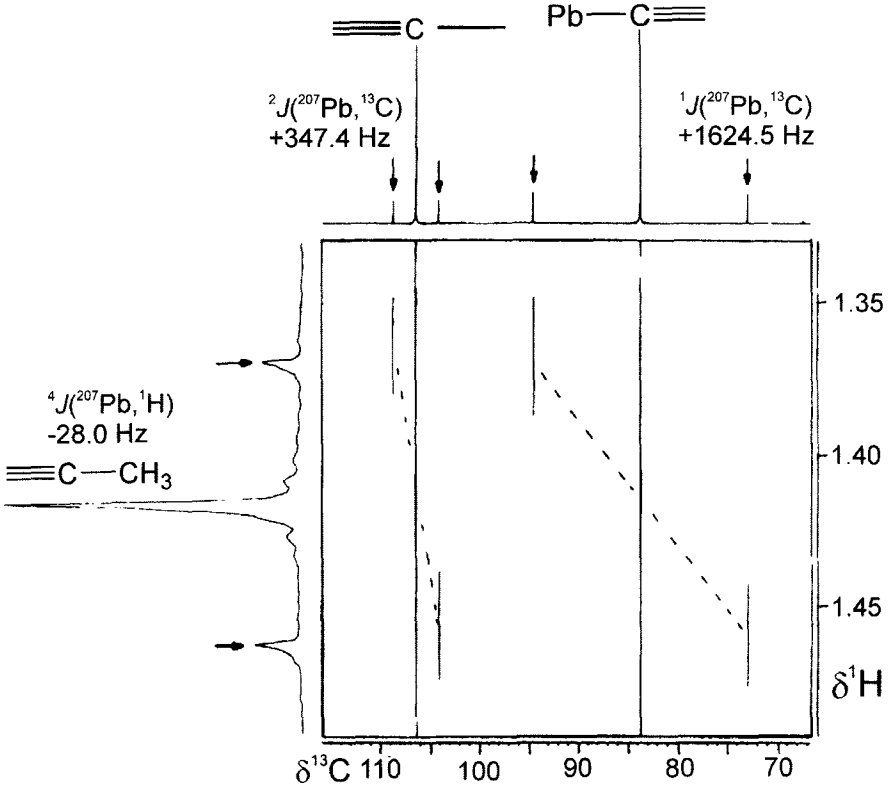

Fig. 14. Contour plot of the 125.8 MHz 2D $^{13}C/^{1}H$ HETCOR experiment for $Pb(C{\equiv}C{-}Me)_4$ in C_6D_6 (polarization transfer was based on $^{2,3}J(^{13}C,^{1}H) = 7$ Hz which gives approximately the same signal-to-noise ratio for both alkynyl ^{13}C nuclei).[131] The tilt of the pairs of cross peaks for the ^{207}Pb satellites compares the coupling signs of $^{1}J(^{207}Pb,^{13}C{\equiv})$ (>0) with $^{4}J(^{207}Pb,^{1}H)$ (<0), and of $^{2}J(^{207}Pb,{\equiv}^{13}C)$ (>0) with $^{4}J(^{207}Pb,^{1}H)$ (<0).

congeners (the bonding situation in plumbylenes is an instructive example in this respect). The powerful NMR instrumentation available nowadays, together with the inherent rather high NMR receptivity of the ^{207}Pb nucleus, makes it possible to study even fairly unstable species of lead compounds in diluted solutions. There are also interesting developments in solid-state MAS ^{207}Pb NMR spectra with regard to the analysis of complex spinning side band manifolds.[132] In these directions, we can expect some important progress in the near future. The enormous sensitivity of ^{207}Pb NMR parameters towards apparently subtle changes in the structure of a particular molecule, and the large effects exerted by various substituents, may help better to understand trends of chemical shifts and coupling constants that are not so obvious with the lighter nuclei in group 14.

ACKNOWLEDGEMENT

Support of this work by the Deutsche Forschungsgemeinschaft, Fonds der Chemischen Industrie und Volkswagen-Stiftung is gratefully acknowledged.

REFERENCES

1. S. Braun, H.-O. Kalinowski and S. Berger, in *150 and More Basic NMR Experiments, A Practical Course*, Wiley-VCH, Weinheim, Germany, 1998.
2. (a) T. Parella, *Magn. Reson. Chem.*, 1998, **36**, 467; (b) S. Berger, *Progr. NMR Spectrosc.*, 1997, **30**, 137; (c) S. Berger, T. Faecke and R. Wagner, *Magn. Reson. Chem.*, 1996, **34**, 4; (d) T. Faecke and S. Berger, *Main Group Met. Chem.*, 1994, **17**, 463.
3. B. Wrackmeyer and K. Horchler, *Annu. Rep. NMR Spectrosc.*, 1990, **22**, 249.
4. J. D. Kennedy and W. McFarlane, in *Multinuclear NMR* (ed. J. Mason), Plenum Press, New York, 1987, pp. 305–333.
5. B. Wrackmeyer, in *Encyclopedia of NMR* (eds R. K. Harris and D. M. Grant), Wiley, London, 1996, Vol. 4, pp. 2538–2548.
6. B. Wrackmeyer, in *Physical Organometallic Chemistry* (eds M. Gielen, R. Willem and B. Wrackmeyer), Wiley, Chichester, 2002, Vol. 3, in press.
7. F. Fayon, I. Farnan, C. Besseda, J. Coutures, D. Massiot and J. P. Coutures, *J. Am. Chem. Soc.*, 1997, **119**, 6837.
8. B. Bureau, G. Silly and J. Y. Buzare, *Solid State Nucl. Magn. Reson.*, 1999, **15**, 79.
9. C. Dybowski, S. P. Gabuda, S. G. Kozlova, G. Neue, D. L. Perry and V. V. Tershkik, *J. Solid State Chem.*, 2001, **157**, 220.
10. (a) S. P. Gabuda, S. G. Kozlova, V. V. Tershkik, C. Dybowski, G. Neue and D. L. Perry, *Solid State Nucl. Magn. Reson.*, 1999, **15**, 103; (b) A. M. Panich, S. D. Goren, B.-Y. Frenkel, M. Eder and G. Gritzner, *Physica C*, 2001, **356**, 129; (c) P. Gibot, S. Donze, L. Montagne and G. Palavit, *Phosphorus Res. Bull.*, 1999, **10**, 570; (d) Y.-S. Kye, S. Connolly, B. Herreros and G. S. Harbison, *Main Group Met. Chem.*, 1999, **22**, 373; (e) P. Zhao, S. Prasad, J. Huang, J. J. Fitzgerald and J. S. Shore, *J. Phys. Chem. B*, 1999, **103**, 10617.
11. (a) T. Takahasi, H. Kawashima, H. Sugisawa and T. Baba, *Solid State Nucl. Magn. Reson.*, 1999, **15**, 119; (b) Y.-S. Kye, B. Herreros and G. S. Harbison, *J. Phys. Chem. B*, 2001, **105**, 5982; (c) L. C. M. van Gorkom, J. M. Hook, M. B. Logan, J. V. Hanna and R. E. Wasylishen, *Magn. Reson. Chem.*, 1995, **33**, 791; (d) A. Bielecki and D. P. Burum, *J. Magn. Reson.*, 1995, **116**, 215; (e) J. B. Grutzner, K. W. Stuart, R. E. Wasylishen, M. D. Lumsden, C. Dybowski and P. A. Beckmann, *J. Am. Chem. Soc.*, 2001, **123**, 7094.
12. A. D. Irvin, C. D. Chandler, R. Assink and M. J. Hampden-Smith, *Inorg. Chem.*, 1994, **33**, 1005.
13. (a) D. A. Bussian and G. S. Harbison, *Solid State Commun.*, 2000, **115**, 95; (b) S. M. Komienko, I. P. Bykov, M. D. Glinchuk, V. V. Laguta and L. Jastrabik, *Ferroelectrics*, 1999, **223**, 165.
14. (a) H. G. Niessen, M. van Buskirk, C. Dybowski, D. R. Corbin, J. A. Reimer and A. T. Bell, *J. Phys. Chem. B*, 2001, **105**, 2945; (b) A. Eldevik, J. M. Hook, N. K. Singh and R. F. Howe, *Magn. Reson. Chem.*, 1999, **37**, S63.
15. W. McFarlane, *Proc. R. Soc. (Lond.) A*, 1968, **306**, 185.
16. (a) G. A. Morris and R. Freeman, *J. Am. Chem. Soc.*, 1979, **101**, 760; (b) G. A. Morris, *J. Am. Chem. Soc.*, 1980, **102**, 428; (c) G. A. Morris, *J. Magn. Reson.*, 1980, **41**, 185; (d) D. P. Burum and R. R. Ernst, *J. Magn. Reson.*, 1980, **39**, 163.
17. (a) D. T. Pegg, D. M. Doddrell, W. M. Brooks and M. R. Bendall, *J. Magn. Reson.*, 1981, **44**, 32; (b) D. T. Pegg, D. M. Doddrell and M. R. Bendall, *J. Chem. Phys.*, 1982, **77**, 2745.

18. (a) F. Kayser, M. Biesemans, M. Gielen and R. Willem, in *Physical Organometallic Chemistry – Advanced Applications of NMR to Organometallic Chemistry* (eds M. Gielen, R. Willem and B. Wrackmeyer), Wiley, London, 1996, Vol. 1, pp. 45–86; (b) J. C. Martins, M. Biesemans and R. Willem, *Progr. NMR Spectrosc.*, 2000, **36**, 271–332.
19. (a) A. Sebald, in *Physical Organometallic Chemistry – Advanced Applications of NMR to Organometallic Chemistry* (eds M. Gielen, R. Willem and B. Wrackmeyer), Wiley, London, 1996, Vol. 1, pp. 123–157; (b) A. Sebald, in *Solid-State NMR II – NMR-Basic Principles and Progress* (eds P. Diehl, E. Fluck, H. Günther, R. Kosfeld and J. Seelig), Springer, Berlin, 1994, Vol. 31, pp. 91–131.
20. A. Abragam, *The Principles of Nuclear Magnetism*, University Press, Oxford, 1961, pp. 264–353.
21. B. Wrackmeyer and K. Horchler, *Z. Naturforsch., Teil B*, 1989, **44**, 1195.
22. A. Rodriguez-Fortea, P. Alemany and T. Ziegler, *J. Phys. Chem. A*, 1999, **103**, 8288.
23. T. N. Mitchell, *J. Organomet. Chem.*, 1983, **255**, 278.
24. J. D. Kennedy, W. McFarlane and G. S. Pyne, *J. Chem. Soc., Dalton Trans.*, 1977, 2332.
25. C. Stader and B. Wrackmeyer, unpublished results.
26. B. Wrackmeyer, C. Stader and K. Horchler, *J. Magn. Reson.*, 1989, **83**, 601.
27. U. Edlund, T. Lejon, P. Pyykkö, T. Venktchalam and E. Buncel, *J. Am. Chem. Soc.*, 1987, **109**, 5982.
28. B. Wrackmeyer, K. Horchler, H. Zhou and M. Veith, *Z. Naturforsch., Teil B*, 1989, **44**, 288.
29. B. Wrackmeyer, C. Stader, K. Horchler and H. Zhou, *Inorg. Chim. Acta*, 1990, **176**, 205.
30. R. Papiernik, L. G. Hubert-Pfalzgraf and M. C. Massiani, *Polyhedron*, 1991, **14**, 1657.
31. S. Ruprecht, S. J. Franklin and K. N. Raymond, *Inorg. Chim. Acta* 1995, **235**, 185.
32. (a) J. E. H. Buston, T. D. W. Claridge, S. J. Heyes, J. L. Bretherton, M. G. Moloney and M. Stevenson, *Magn. Reson. Chem.*, 2001, **39**, 68; (b) J. E. H. Buston, T. D. W. Claridge and M. G. Moloney, *J. Chem. Soc., Perkin Trans.*, 1995, 639.
33. J. R. Ascenso, R. K. Harris and P. Granger, *J. Organomet. Chem.*, 1986, **301**, C23.
34. (a) R. K. Harris and A. Sebald, *Magn. Reson. Chem.*, 1987, **25**, 1058; (b) A. Sebald and R. K. Harris, *Organometallics*, 1990, **9**, 2096; (c) R. K. Harris and A. Sebald, *Magn. Reson. Chem.*, 1989, **27**, 81.
35. U. Behrens, A. K. Brimah, T. M. Soliman, R. D. Fischer, D. C. Apperley, N. A. Davies and R. K. Harris, *Organometallics* 1992, **11**, 1718.
36. B. Wrackmeyer, K. Horchler, A. Sebald and L. H. Merwin, *Magn. Reson. Chem.*, 1990, **28**, 465.
37. B. Wrackmeyer, A. Sebald and L. H. Merwin, *Magn. Reson. Chem.*, 1991, **29**, 260.
38. A. Winkler, W. Bauer, F. W. Heinemann, V. Garcia- Montalvo, M. Moll and J. Ellermann, *Eur. J. Inorg. Chem.*, 1998, 437.
39. D. Smith, C. Eaborn, T. Ganicz, P. B. Hitchcock, J. D. Smith and S.E. Sözerli, *Organometallics*, 1997, **16**, 5621.
40. L. Pu, B. Twamley and P. P. Power, *Organometallics*, 2000, **19**, 2874.
41. N. Kano, K. Shibata, N. Tokitoh and R. Okazaki, *Organometallics*, 1999, **18**, 2999.
42. R. S. Simons, L. Pu, M. M. Olmstead and P. P. Power, *Organometallics*, 1997, **16**, 1920.
43. M. Stürmann, M. Weidenbruch, K. W. Klinkhammer, F. Lissner and H. Marsmann, *Organometallics*, 1998, **17**, 4425.
44. S. Brooker, J.-K. Buijink and F. T. Edelmann, *Organometallics*, 1991, **10**, 25.
45. L. Pu, P. Power, I. Boltes and R. Herbst-Irmer, *Organometallics*, 2000, **19**, 352.
46. M. Stürmann, W. Saak, H. Marsmann and M. Weidenbruch, *Angew. Chem.*, 1999, 111, 145; *Angew. Chem. Int. Ed. Engl.*, 1999, **38**, 187.
47. K. W. Klinkhammer, T. F. Fässler and H. Grützmacher, *Angew. Chem.*, 1998, **110**, 114; *Angew. Chem. Int. Engl.*, 1998, **37**, 124.
48. M. Stürmann, M. Weidenbruch, K. W. Klinkhammer, F. Lissner and H. Marsmann, *Organometallics*, 1998, **17**, 4425.
49. L. Pu, B. Twamley and P. P. Power, *J. Am. Chem. Soc.*, 2000, **122**, 3524.
50. Y. Chen, M. Hartmann, M. Diedenhofen and G. Frenking, *Angew. Chem.*, 2001, **113**, 2108; *Angew. Chem. Int. Ed. Engl.*, 2001, **40**, 2051.

51. F. Stabenow, W. Saak and M. Weidenbruch, *Chem. Commun.*, 1999, 1131.
52. B. Gehrhus, P. B. Hitchcock and M. F. Lappert, *J. Chem. Soc., Dalton Trans.*, 2000, 3094.
53. E. S. Claudio, M. A. ter Horst, C. E. Forde, C. L. Stern, M. K. Zart and H. A. Godwin, *Inorg. Chem.*, 2000, **39**, 1391.
54. P. G. Harrison, M. A. Healy and A. T. Steel, *J. Chem. Soc., Dalton Trans.*, 1983, 1845.
55. N. Altounian, A. Glatfelter, S. Bai and C. Dybowski, *J. Phys. Chem. B*. 2000, **104**, 4723.
56. W. N. Perera, G. Hefter and P. M. Sipos, *Inorg. Chem.*, 2001, **40**, 3974.
57. S. P. Constantine, H. Cox, P. B. Hitchcock and G. A. Lawless, *Organometallics*, 2000, **19**, 317.
58. C. Janniak, H. Schumann, C. Stader, B. Wrackmeyer and J. J. Zuckermann, *Chem. Ber.*, 1988, **121**, 1745.
59. J. J. Durkin, M. D. Francis, P. B. Hitchcock, C. Jones and J. F. Nixon, *J. Chem. Soc., Dalton Trans.*, 1999, 4057.
60. G. E. Herberich, X. Zheng, J. Rosenplänter and U. Englert, *Organometallics*, 1999, **18**, 4747.
61. R. Köster, G. Seidel, B. Wrackmeyer, K. Horchler and D. Schlosser, *Angew. Chem.*, 1989, **101**, 945; *Angew. Chem. Int. Ed. Engl.*, 1989, **28**, 918.
62. B. Wrackmeyer, K. Horchler and R. Boese, *Angew. Chem.*, 1989, **101**, 1563; *Angew. Chem. Int. Ed. Engl.*, 1989, **28**, 1500.
63. D. Hutchinson, J. C. P. Sanders and G. J. Schrobilgen, *Eur. J. Solid State Inorg. Chem.*, 1996, **33**, 795.
64. T. M. Klapötke, B. Krumm, K. Polborn and C. M. Rienäcker, *Z. Naturforsch., Teil B*, 2000, **55**, 377.
65. B. Wrackmeyer and H. Zhou, *Spectrochim. Acta*, 1991, **47A**, 849.
66. T. N. Mitchell and W. Reimann, *Magn. Reson. Chem.*, 1987, **25**, 1019.
67. B. Wrackmeyer and K. Horchler, *Organometallics*, 1990, **9**, 1881.
68. B. Wrackmeyer and K. Wagner, *Chem. Ber.*, 1989, **122**, 857.
69. B. Wrackmeyer and K. Horchler, *Z. Naturforsch., Teil B*, 1990, **45**, 437.
70. B. Wrackmeyer and K. Horchler von Locquenghien, *Main Group Met. Chem.*, 1990, **13**, 387.
71. B. Wrackmeyer and K. Horchler, *J. Organomet. Chem.* 1990, **399**, 1.
72. B. Wrackmeyer and K. Horchler von Locquenghien, *Z. Naturforsch., Teil B*, 1991, **46**, 1207.
73. B. Wrackmeyer, K. Horchler von Locquenghien and S. Kundler, *J. Organomet. Chem.*, 1995, **503**, 289.
74. C. Schneider-Koglin, B. Mathiasch and M. Dräger, *J. Organomet. Chem.*, 1994, **469**, 25.
75. (a) M. Charisse, B. Mathiasch, M. Dräger and U. Russo, *Polyhedron*, 1995, **14**, 2429; (b) H. Stenger, B. M. Schmidt and M. Dräger, *Organometallics*, 1995, **14**, 4374.
76. M. Herberhold, V. Tröbs and B. Wrackmeyer, *J. Organomet. Chem.*, 1997, **541**, 391.
77. J. K. Galiotos and J. A. Morrison, *Organometallics*, 2000, **19**, 2603.
78. R. Eujen and A. Patorra, *J. Organomet. Chem.*, 1992, **438**, 57.
79. T. M. Klapötke, B. Krumm, M. Niemitz, K. Polborn and C. M. Rienäcker, *J. Fluor. Chem.*, 2000, **104**, 129.
80. D. C. van Beelen, Thesis, University of Leiden, The Netherlands, 1980.
81. G. Wegner, R. Berger, J. F. Raphael, A. Schier and H. Schmidbaur, *Z. Naturforsch., Teil B*, 2000, **55**, 995.
82. N. Kano, N. Tokitoh and R. Okazaki, *Organometallics*, 1997, **16**, 2748.
83. N. Tokitoh, N. Kano, K. Shibita and R. Okazaki, *Organometallics*, 1995, **14**, 3121.
84. T. M. Klapötke, J. Knizek, H. Nöth, B. Krumm and C. M. Rienäcker, *Polyhedron*, 1999, **18**, 839.
85. O. R. Flöck and M. Dräger, *Organometallics*, 1993, **12**, 4623.
86. B. Wrackmeyer, H. E. Maisel and H. Zhou, *Main Group Met. Chem.*, 1993, **16**, 475.
87. B. Wrackmeyer, G. Kehr, H. Zhou and S. Ali, *Magn. Reson. Chem.*, 1996, **34**, 921.
88. M. Herberhold, V. Tröbs, H. Zhou and B. Wrackmeyer, *Z. Naturforsch., Teil B*, 1997, **52**, 1181.
89. B. Wrackmeyer, K. Horchler and H. Zhou, *Spectrochim Acta*, 1990, **46A**, 809.
90. B. Wrackmeyer and H. Zhou, *Main Group Met. Chem.*, 1990, **13**, 99.
91. M. Herberhold, C. Köhler, V. Tröbs and B. Wrackmeyer, *Z. Naturforsch., Teil B*, 2000, **55**, 939.
92. H.-J. Koglin, K. Behrends and M. Dräger, *Organometallics*, 1994, **13**, 2733.

93. U. Englich, E. Hengge, U. Hermann, C. Marschner, K. Ruhlandt-Senge and F. Uhlig, *J. Organomet. Chem.*, 2000, **605**, 22.
94. M. Herberhold, V. Tröbs, W. Milius and B. Wrackmeyer, *Z. Naturforsch., Teil B*, 1994, **49**, 1781.
95. K. H. Pannel, J. M. Rozell, S. Cortez and R. Kapoor, *Organometallics*, 1990, **9**, 1322.
96. M. M. Kubicki, J.-Y. Le Gall, R. Kergoat and L. C. Gomes de Lima, *Can. J. Chem.*, 1987, **65**, 1292.
97. D. Christendat, I. S. Butler, D. F. R. Gilson and F. G. Morin, *Can. J. Chem.*, 1999, **77**, 1892.
98. D. Christendat, J. H. Wosnick, I. S. Butler, D. F. R. Gilson, A.-M. Lebuis and F. G. Morin, *J. Mol. Struct.*, 2001, **559**, 235.
99. S. Carr, R. Colton and D. Dakternieks, *J. Organomet. Chem.*, 1982, **240**, 143.
100. D. Agustin, G. Rima, H. Gornitzka and J. Barrau, *Eur. J. Inorg. Chem.*, 2000, 693.
101. M. C. Kuchta, J. M. Hahn and G. Parkin, *J. Chem. Soc., Dalton Trans.*, 1999, 3559.
102. (a) W. L. Wilson, R. W. Rudolph, I. L. Lohr, R. C. Taylor and P. Pyykkö, *Inorg. Chem.*, 1986, **25**, 1535. (b) J. Campbell, H. P. A. Mercier, H. Franke, D. P. Santry, D. A. Dixon and G. J. Schrobilgen, *Inorg. Chem.*, 2002, **41**, 86.
103. P. Kircher, G. Huttner and K. Heinze, *J. Organomet. Chem.*, 1998, **562**, 217.
104. P. Rutsch and G. Huttner, *Angew. Chem.*, 2000, **112**, 2187; *Angew. Chem. Int. Ed. Engl.*, 2000, **39**, 2118.
105. S. Kerschl, A. Sebald and B. Wrackmeyer, *Magn. Reson. Chem.*, 1985, **23**, 514.
106. C. J. Jameson, in *Isotopes in the Physical and Biomedical Sciences* (eds E. Buncel and J. R. Jones), Elsevier, New York, 1991, Vol. 2, pp. 1–54, and references cited therein.
107. (a) E. Kupce and B. Wrackmeyer, *Magn. Reson. Chem.*, 1991, **29**, 351; (b) E. Kupce and B. Wrackmeyer, *J. Magn. Reson.*, 1992, **97**, 568.
108. (a) P. Pyykkö and W. Wiesenfeld, *Mol. Phys.*, 1981, **43**, 557; P. Pyykkö, *J. Organomet. Chem.*, 1982, **232**, 21.
109. B. Wrackmeyer, in *Physical Organometallic Chemistry – Advanced Applications of NMR to Organometallic Chemistry* (eds M. Gielen, R. Willem and B. Wrackmeyer), Wiley, London, 1996, Vol. 1, pp. 87–122.
110. B. Wrackmeyer, *J. Magn. Reson.*, 1981, **42**, 287.
111. B. Wrackmeyer and K. Horchler, *J. Magn. Reson.*, 1990, **90**, 569.
112. B. Wrackmeyer and K. Horchler, *Magn. Reson. Chem.*, 1990, **28**, 56.
113. J. D. Kennedy, W. McFarlane and B. Wrackmeyer, *Inorg. Chem.*, 1976, **15**, 1299.
114. J. D. Kennedy and W. McFarlane, *J. Organomet. Chem.*, 1974, **80**, C47.
115. V. M. S. Gil and W. von Philipsborn, *Magn. Reson. Chem.*, 1989, **27**, 409.
116. M. Björgvinsson, J. Sawyer and G. J. Schrobilgen, *Inorg. Chem.*, 1987, **26**, 741.
117. M. Björgvinsson, H. P. A. Mercier, K. M. Mitchell, G. J. Schrobilgen and G. Strohe, *Inorg. Chem.*, 1993, **32**, 6046.
118. R. C. Patnaik, R. L. Hota and G. S. Tripathi, *Phys. Rev. B*, 1998, **58**, 3924.
119. W. McFarlane and N. H. Rees, *J. Chem. Soc., Dalton Trans.*, 1990, 3211.
120. C. J. Parkinson and M. J. Stoermer, *J. Organomet. Chem.*, 1996, **507**, 207.
121. K. Horchler, Dissertation, Universität Bayreuth, 1990.
122. P. Jutzi, U. Holtmann, D. Kanne, C. Krüger, R. Blom, R. Gleiter and I. Hyla-Kryspin, *Chem. Ber.*, 1989, **122**, 1629.
123. P. Jutzi, F. Kohl, P. Hofmann, C. Krüger and Y. H. Tsay, *Chem. Ber.*, 1980, **113**, 757.
124. J. L. Atwood, W. Hunter, A. H. Cowley, R. A. Jones and C. A. Stewart, *J. Chem. Soc., Chem. Commun.*, 1981, 925.
125. A. Bax and R. Freeman, *J. Magn. Reson.*, 1981, **45**, 177.
126. R. K. Harris, in *Encyclopedia of NMR* (eds D. M. Grant and R. K. Harris), Wiley, Chichester, 1996, Vol. 5, pp. 3301–3314.
127. R. K. Harris, in *NMR and the Periodic Table* (eds R. K. Harris and B. E. Mann), Academic Press, London, 1978, pp. 5–7.
128. J. Mason, in *Multinuclear NMR* (ed. J. Mason), Plenum Press, New York, 1987, pp. 625–629.
129. B. Wrackmeyer and J. Weidinger, *Z. Naturforsch., Teil B*, 1997, **52**, 947.

130. B. Wrackmeyer, *Annu. Rep. NMR Spectrosc.*, 1999, **38**, 203.
131. B. Wrackmeyer, K. Horchler von Locquenghien, E. Kupce and A. Sebald, *Magn. Reson. Chem.*, 1993, **31**, 45.
132. B. Wrackmeyer, G. Kehr, D. Wettinger and W. Milius, *Main Group Met. Chem.*, 1994, **16**, 445.
133. F. G. Vogt, J. M. Gibson, D. J. Aurentz, K. T. Mueller and A. L. Benesi, *J. Magn. Reson.*, 2000, **143**, 153.

Dynamic Aspects of Membrane Proteins and Membrane-Associated Peptides as Revealed by ^{13}C NMR: Lessons from Bacteriorhodopsin as an *Intact* Protein

HAZIME SAITÔ,[1] SATORU TUZI,[1] MICHIKAZU TANIO,[1] and AKIRA NAITO[2]

[1]*Department of Life Science, Himeji Institute of Technology, Harima Science Garden City, Kouto 3-Chome, Kamigori, Hyogo 678-1297, Japan*
[2]*Faculty of Engineering, Yokohama National University, 79-5 Tokiwadai, Yokohama, Japan 240-8501*

1. Introduction 41
2. NMR characteristics of membrane proteins 42
3. Bacteriorhodopsin 44
4. ^{13}C-Labeled proteins and peptides 48
   4.1. Large-scale preparation 48
   4.2. Multiple ^{13}C labeling 50
5. Assignment of ^{13}C NMR peaks 52
   5.1. Regiospecific assignment of peaks 52
   5.2. Conformation-dependent ^{13}C chemical shifts 56
   5.3. Site-directed mutagenesis and proteolysis for site-specific assignment of peaks 59
6. NMR parameters for detection of protein dynamics 63
   6.1. Dynamics-dependent ^{13}C chemical shifts 63
   6.2. Dynamics-dependent suppression of peaks 67
   6.3. Relaxation parameters 72
7. Surface structure and dynamics of bacteriorhodopsin 76
   7.1. Surface structure 76
   7.2. Effect of cations 79
   7.3. Hydration and dynamics 81
8. Transmembrane peptides as a component of bacteriorhodopsin 86
9. Local conformational change associated with proton pumping 90
10. Other protein systems 93
   10.1. Unoriented systems 93
   10.2. Oriented systems 95
11. Concluding remarks and perspectives 101
Acknowledgements 102
References 103

ANNUAL REPORTS ON NMR SPECTROSCOPY
VOLUME 47 ISBN 0-12-505447-5

Copyright © 2002 Elsevier Science Ltd.
All rights of reproduction in any form reserved

It is demonstrated here that a general feature of membrane proteins, with emphasis on revealing their dynamic aspects, is now available from extensive ^{13}C NMR studies on bacteriorhodopsin (bR) as a typical membrane protein and a variety of site-directed mutants at ambient temperature. For this purpose, ^{13}C NMR signals from ^{13}C-labeled proteins from single amino acid residues were initially regiospecifically assigned on the basis of the conformation-dependent ^{13}C chemical shifts, and then site-specifically assigned with reference to the data of site-directed mutants. Dynamic aspects of bR were obtained by means of relaxation parameters such as the carbon spin–lattice relaxation time, T_1^C and spin–spin relaxation times under the condition of proton decoupling and magic angle spinning, T_2^C, and dynamics-dependent suppression of peaks sensitive to motions of 10^{-4} s and 10^{-5} s which interfere with the frequency of magic angle spinning and proton decoupling respectively. The resulting picture of the membrane protein is not rigid, as anticipated from the structure of 2D crystals of the hexagonal assembly, but a dynamically heterogeneous structure arising from a variety of local fluctuations with a frequency range of 10^2–10^8 Hz. Consequently, it is advisable to examine the ^{13}C NMR spectra of ^{13}C-labeled bR, in which the extent of peak suppression is less pronounced, by selecting either [1-^{13}C]Ala, Val or [3-^{13}C]Ala, depending upon the timescale of the motions involved. However, the presence of molecular motions relevant to this timescale is inherently unavoidable since they are a characteristic feature of intact membrane proteins. The presence of low-frequency, anisotropic motion was further characterized by the dynamics-dependent displacement of ^{13}C peaks of Ala C_β of [3-^{13}C]Ala-labeled bR or its fragment.

NOTATION

One-letter description of amino acid residues

A	Ala
C	Cys
D	Asp
E	Glu
F	Phe
G	Gly
I	Ile
K	Lys
L	Leu
M	Met
N	Asn
P	Pro
Q	Gln
R	Arg
W	Trp
Y	Tyr

1. INTRODUCTION

Determination of the three-dimensional structures of a variety of biological molecules such as proteins, biologically active peptides, nucleic acids, carbohydrates, etc., is very important in gaining insight into their biological functions together with its application to various fields including drug discovery. Currently, X-ray crystallography or multidimensional NMR spectroscopy have proved to be the most favorable standard approaches to globular proteins for this purpose, usually problems associated with crystallization or line-broadenings of NMR signals owing to increased molecular mass of proteins are not serious. These approaches, however, turned out to be insufficient for a variety of membrane proteins which constitute one-third of the information of an expressed genome of *Mycoplasma genitalium*, the smallest known genome of any free-living organism,[1] because large-scale expression, secondary folding, and subsequent crystallization as membrane proteins are not easy when compared with those of globular proteins. From the biological point of view, it is emphasized that membrane proteins play crucial roles in maintaining various activities of cells such as the transport of appropriate molecules into or out of the cell, catalysis of chemical reaction, receiving and transducing chemical signals from the cell environment, and maintaining the cell structure.[2]

In fact, the polypeptide chains in integral membrane proteins are known to traverse the membrane once or several times, usually as α-helices (Fig. 1) but in some instance as β-strands, depending upon their own specific function,[2,3]

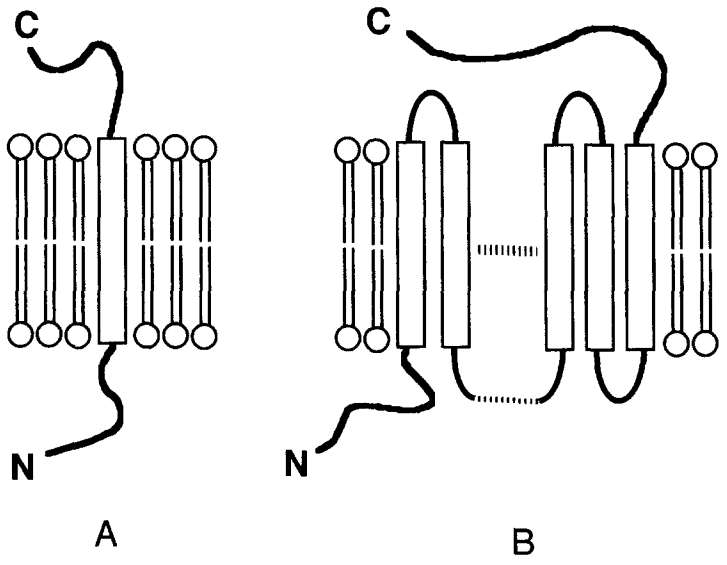

Fig. 1. Illustrative examples of membrane proteins. Single-span (A) and multiply spanned membrane proteins (B).

although the hydrophilic segment protruding from the surface of any membrane protein whose hydrophobic polypeptide chain traverses only once can be treated as a globular protein if the hydrophobic region is cleaved by a proteolytic enzyme. In such a situation, enormous line broadening of NMR signals could be expected from the assembly of the protein itself, the molecular mass of which is of the order of 100 kDa or more, its oligomerized form rather than the monomer, and surrounding lipids varying between 25 and 75% of the total mass, which renders a solution NMR study on such proteins practically impossible, as long as these proteins remain in natural biomembranes or lipid bilayers. This situation applies also to a number of membrane-associated peptides which take a disordered conformation owing to a smaller molecular mass if they remain as a single molecule in aqueous media but their secondary forms are supposed to be changed to an 'active' form once they are bound to receptor molecules as membrane proteins.

2. NMR CHARACTERISTICS OF MEMBRANE PROTEINS

It is for this reason that the high-resolution solid-state NMR approach can be sought as a complementary means to be able to study the conformation and dynamics of a variety of membrane proteins and membrane-associated peptides. This kind of approach is based on a view that spectral resolution is not any more determined by prolonged correlation times arising from increased effective molecular mass so far discussed as in solution NMR, as far as appropriate isotope enrichment either by ^{13}C or ^{15}N in order to improve spectral *sensitivity* and *selectivity* of particular residues is feasible. To this end, the following methods for a variety of membrane proteins or membrane-associated peptides have been utilized for a study by high-resolution solid-state NMR: (1) three-dimensional (3D) microcrystals; (2) fully hydrated pellets of two-dimensional (2D) crystals; (3) lyophilized preparations; (4) detergent-solubilized preparation; (5) oriented samples, etc. The first 3D structure of bacteriorhodopsin (bR) as a membrane protein was determined at 7 Å resolution by cryoelectron microscopy on naturally occurring 2D crystals as purple membrane, instead of 3D crystals by X-ray diffraction.[4] In contrast, crystallization as 3D crystals has been extremely difficult: 3D crystallization proceeds with solubilization of membrane proteins by detergent, followed by the formation of a crystalline lattice owing to molecular association on the surface of hydrophobic residues or on the hydrophobic surface of the detergent covering a hydrophilic surface. It seems to be impractical to attempt to use a single crystal of a membrane protein for NMR study in view of the 'size' of crystals currently available (of the order of a micron), even if more detailed information about the 3D structure could be potentially available from such a sample.

It is essential to prepare appropriately ^{13}C- or ^{15}N-labeled proteins in order to achieve better spectral resolution, as manifested by ^{13}C NMR spectra of 2D

crystals of [3-^{13}C]Ala-labeled bR [5] as compared with those of an unlabeled 3D crystal of cytochrome *c* oxidase.[6] Further, more detailed information on 3D structures can be obtained by careful analysis of anisotropic nuclear spin interactions such as chemical shifts and dipolar and quadrupolar interactions, if any type of oriented samples such as spontaneously aligned metalloprotein[7] or fibrous virus,[8] peptides incorporated into bicelles,[9,10] elongated liposomes,[11] and mechanically aligned bilayer samples sandwiched between glass plates[12,13] are available. This kind of approach, however, is inevitably limited to smaller peptide fragments rather than whole proteins by taking into account the manner of sample preparation. In addition, it is also taken into account that the conformation and dynamics of incorporated proteins and peptides are substantially modified by going from the fully hydrated state corresponding to the physiological condition to the low hydration condition corresponding to mechanical alignment, as encountered in our recent study on bacteriorhodopsin and melittin[11] to be discussed later. Furthermore, the oriented system is not always suitable for study of the more flexible portions such as interhelical loops (see Fig. 1) which play biologically important roles such as molecular recognition and subsequent transduction of external signals.

The utilization of unoriented samples for whole membrane proteins such as bR, either in the form of fully hydrated pellets or lyophilized preparations, is therefore inevitable. It turned out, however, that irreversible conformational changes were encountered during the lyophilization process, as manifested by the enormously increased line widths of the ^{13}C NMR spectra of [3-^{13}C]Ala-bR.[14] It should also be cautioned that the conformational features of polypeptide chains could be substantially modified from those of the native state when they are solubilized in detergent micelles as an alternative means with reference to the ^{13}C NMR spectra of intact preparations.[15,16] It is also stressed that the 3D structures of membrane proteins[17–27] so far revealed by cryoelectron microscope or X-ray diffraction studies, performed at lower temperatures to prevent radiation damage, provide one rigid and static picture as anticipated from crystalline samples. In particular, the 3D structures of bR so far studied exhibit either missing or quite different structures at the surface areas, although they are alike in the transmembrane helices.[16–27] These considerations strongly prompted us to develop a suitable means of analyzing whole membrane proteins, especially at the physiological temperature. Our solid-state NMR studies presented in this article, however, reveal that bR as a typical membrane protein is not rigid as anticipated but rather flexible, undergoing various kinds of molecular motions with correlation times of the order of 10^{-2}–10^{-8} s, depending upon the site under consideration. It is more plausible that flexibility of such protein backbones arises from interactions with surrounding lipid chains of the liquid crystalline phase[28–30] at ambient temperature which seems to be essential for biological function.

It is emphasized that bR in a purple membrane (PM) is an ideal model system to gain insight into various aspects of membrane proteins, because bR can be

considered also as a prototype of G-protein coupled receptors (GPCRs) in view of their similarity in the seven transmembrane α-helical arrangement in the membrane, and it is an exceptionally easy protein for handling, including large-scale preparations of ^{13}C-labeled proteins. More importantly, bR in PM is the *sole, intact, naturally occurring*, 2D crystal of hexagonal assembly which has been extensively studied by both diffraction and solid-state NMR. In contrast, other membrane proteins so far studied are in the form of their peptide fragments embedded in lipid bilayers, detergent-solubilized preparation, or lyophilized preparations. In such systems, no experimental proofs have been available to show to what extent native structures are retained in such systems, unless the ^{13}C NMR spectra of intact proteins or protein complexes can be obtained as reference data as in the case of bR. In fact, it turns out that no intact structures are retained for such preparations, on the basis of a comparative study on bR systems. Other studies without emphasis on dynamic aspects have been reviewed elsewhere.[31–40]

3. BACTERIORHODOPSIN

Bacteriorhodopsin is the sole membrane protein of seven α-helical transmembrane chains present in the purple membrane of *Halobacterium salinarum*. This is active as a light-driven proton pump through the photoisomerization of retinal (Fig. 2) from the all-*trans*, 15-*anti* to the 13-*cis*, 15-*anti* form covalently linked to Lys^{216} (helix G) of a single-chain polypeptide of 248 amino acid

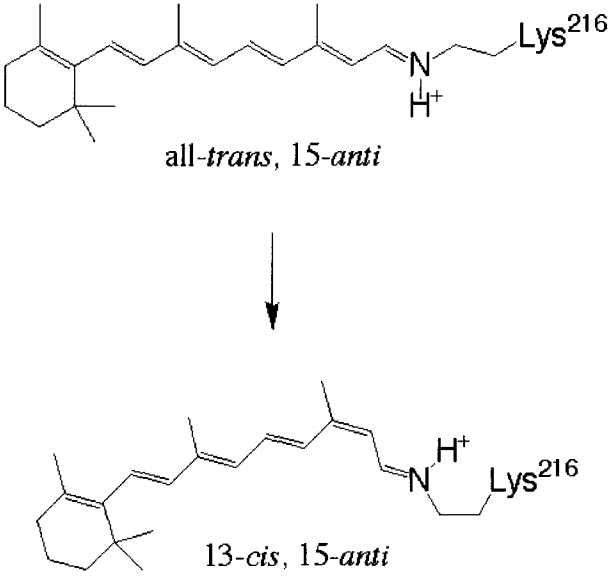

Fig. 2. Photo-illuminated isomerization of retinal in bacteriorhodopsin.

residues (26 kDa) through a protonated Schiff base.[41–44] This molecule in the membrane is known to form hexagonal arrays[45] leading to a 2D crystal lattice through oligomerization to the trimeric form (Fig. 3A),[45a] rather than the monomeric form, known as the purple membrane. Its 3D structure is now available at various degrees of resolution from a cryoelectron microscopy study on a 2D crystal and X-ray diffraction studies on 3D crystals[18–27] based on a novel crystallization concept using the lipidic cubic phase[46] or vesicle fusion[47] (Fig. 3B). It is notable that several residues from the surface are missing when compared with a schematic representation of secondary structure based on such studies, as illustrated in Fig. 4. On the basis of a comparative study of these data as well as their own atomic force microscopic (AFM) observations, Heymann *et al.* and Muller *et al.* claimed that the surface structure of the 3D crystals is

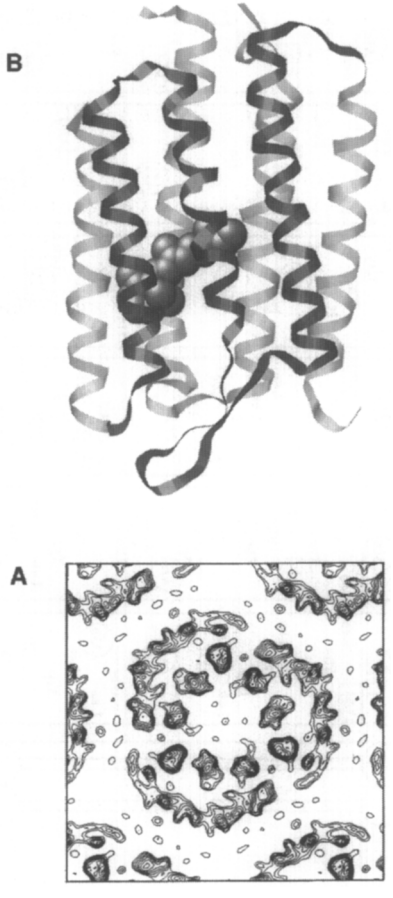

Fig. 3. Three-dimensional structure of bacteriorhodopsin from 1.5 Å resolution as determined by X-ray diffraction[25] (B) and a top view of hexagonal packing (A).[45a] Reproduced with permission from Academic Press Ltd.

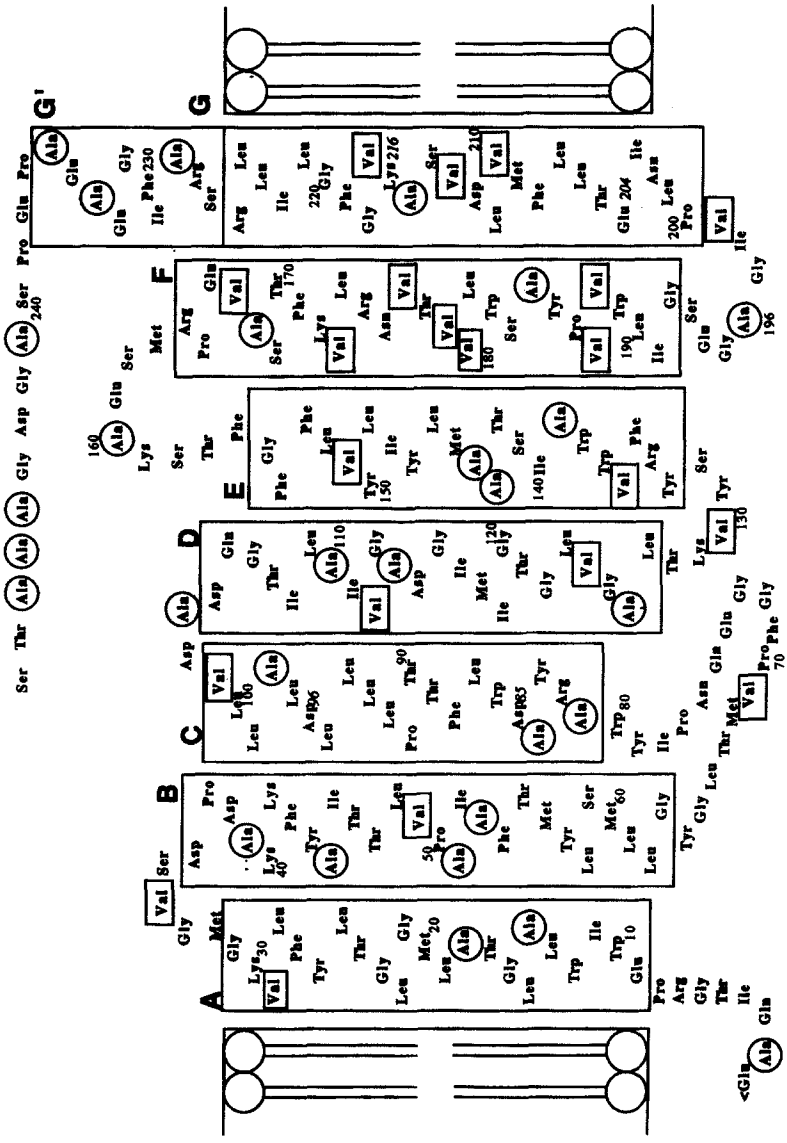

Fig. 4. Schematic representation of the secondary structure of bacteriorhodopsin. All Ala and Val residues labeled by [^{13}C]alanine and [1-^{13}C]valine indicated by the circles and boxes respectively.

substantially modified by crystallographic contacts and may not represent the true conformational state *in vivo*.[48,49] Such a structure from 2D crystals is also modified by freezing and interaction with the cryoprotectant.[49] It is therefore emphasized that both ^{13}C NMR and AFM approaches are able to probe the physiologically relevant intact surface structure of bR at ambient temperature, although the former approach alone is able to study the dynamic features as well as a more detailed conformation of atomic resolution if individual ^{13}C NMR signals are properly assigned to respective residues.

Photoisomerization of retinal from the all-*trans* to the 13-*cis* form leads to a cyclic photoreaction with intermediates, bR, K, L, M, N, and O, which are subsequently formed before recovery of the initial state, as schematically illustrated, with the absorption wavelength in the suffix (Fig. 5), together with their individual lifetimes.[50,51] The first proton transfer in the photocycle of the all-*trans*, 15-*anti* isomer is from the retinal Schiff base to Asp 85 at the central part of the protein. Then, a proton is released from the proton release complex (PRC) consisting of Glu 204, 194 and a bound water molecule at the extracellular surface, as illustrated by arrow A. This is followed by reprotonation of

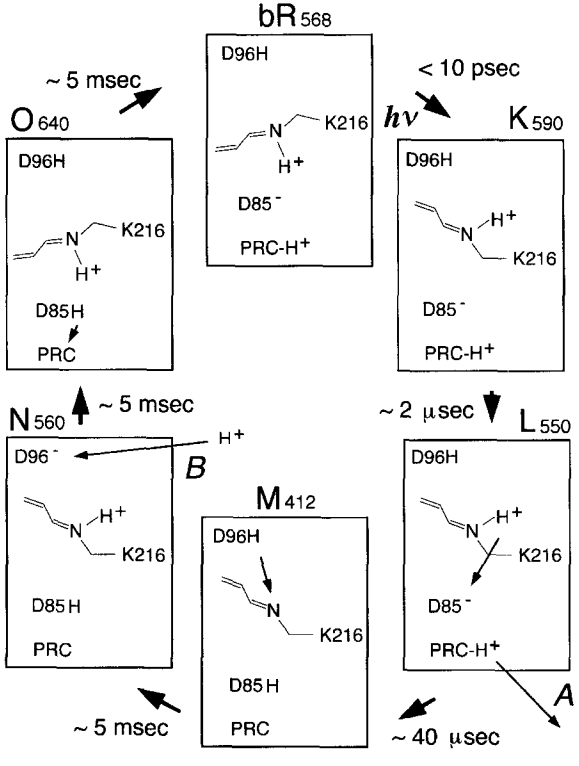

Fig. 5. Photoreaction cycles of bacteriorhodopsin. Photointermediates, the absorption wavelength, lifetime, protonation state, and stereochemical representation of a Schiff base.

the Schiff base from Asp 96 near the cytoplasmic surface in the M to N transition, as indicated by arrow B in Fig. 5. Asp 96 is reprotonated from the cytoplasmic surface during the lifetime of N. The retinal reisomerizes to the all-*trans* form in the N to O transition. These states can be distinguished over picosecond to millisecond time ranges, and a series of the cycle is completed in less than 10 ms. The accessibility change in the retinal Schiff base from the extracellular to the cytoplasmic side, which plays an important role for the reprotonation switch, is facilitated by the global conformational changes in the protein backbones and side chains, as manifested by observation of the projection map of electron or neutron diffraction and X-ray diffraction.[52]

The orientation of such retinylidene chromophore of bR can be determined by means of ^{2}H solid-state NMR spectra[28–30] if uniaxially highly oriented samples are available as in regenerated bR with a selectively CD_3-labeled retinal at various positions of retinal dispersed on a thin glass slide.[53–57] The tilt angle of the retinal chromophore during the isomerization in the M state was also determined by this approach.[56] It is natural to expect that various kinds of conformational change in side chains, protein backbones, and bound water molecules are associated with the concomitant photoisomerization of retinal mentioned above, as revealed by X-ray diffraction[58–61] and FT IR measurements.[62] This timescale at ambient temperature, however, is too short to be examined by solid-state NMR, unless an attempt is made to trap a certain state of the photocycle at a lower temperature.[40] It is not easy, however, to gain insight into the accompanying protein dynamics at ambient temperature if such an intermediate is trapped at a lower temperature (220 or 270 K). An alternative approach to study such an intermediate at ambient temperature is to use a site-directed mutant such as D85N in which the M-like state is formed at pH 10 without photoillumination.[51,63]

4. ^{13}C-LABELED PROTEINS AND PEPTIDES

4.1. Large-scale preparation

It is essential to utilize ^{13}C- or ^{15}N-labeled proteins or peptides, instead of natural abundance, as samples to be used for solid-state NMR, in order to improve the *sensitivity* and/or *selectivity* of the amino acid residues under consideration. Such isotopically labeled bR samples needed for NMR studies are readily available from the large-scale culture of *Halobacterium salinarum* S-9 strain using synthetic media[64] in which certain unlabeled amino acids are replaced with ^{13}C-labeled amino acid species such as [3-^{13}C]Ala or [1-^{13}C]Val.[14] This is shown in the circled or boxed residues, respectively, in the schematic representation of the primary sequence of bR, taking into account the secondary folding on the basis of X-ray diffraction, in Fig. 4. Undoubtedly, selective isotope labeling in this way, although not site-directed isotope labeling, could be most favorable in

terms of achievement of the maximum sensitivity enhancement free from additional broadening due to scalar ^{13}C–^{13}C couplings. It appears that site-directed isotope labeling[65] as attempted for an FTIR experiment still falls far short of the large-scale preparation required for NMR experiments at present, although the spectral interpretation based on this technique is straightforward. Twelve ^{13}C NMR signals, including the signals from five single carbon peaks, can be resolved from the [3-^{13}C]Ala-labeled bR among 29 Ala residues in bR under the condition of excess hydration (pelleted preparation), as illustrated in Fig. 6 recorded by both the CP-MAS (cross polarization-magic angle spinning)[66,67] and DD-MAS (single-pulse, dipolar decoupled magic angle spinning) methods. This better spectral resolution was made possible by increasing the sampling time of the free induction decay from 25 to 50 ms,[5,68,69] although only seven peaks were resolved from the same sample by using the sampling time of 25 ms conventionally taken. Initially, however, only four signals were resolved when a lyophilized preparation instead of the pelleted sample was used for the ^{13}C NMR measurement.[14]

Expression of the bacteriorhod-opsin and its site-directed mutants is also feasible in *E. coli*, and their product, in a denatured form, is isolated in an organic

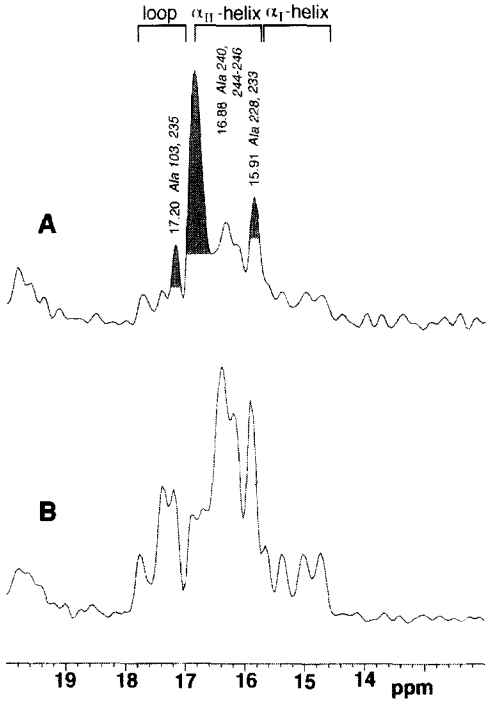

Fig. 6. Comparison of ^{13}C CP-MAS and DD-MAS NMR spectra of [3-^{13}C]Ala-labeled bacteriorhodopsin: A, DD-MAS NMR spectrum; B, CP-MAS NMR spectrum. The ^{13}C NMR signals from the C terminal residues are in gray.[5]

solvent containing chloroform, methanol, water, and triethylamine and further purified by ion-exchange chromatography.[70] These proteins are reconstituted in synthetic phospholipids such as dimyristoylphosphatidylcoline (DMPC) together with the addition of retinal. It is not guaranteed, however, to be able to form the hexagonal lattice essential for observation by ^{13}C CP-MAS NMR under this condition. Instead, it is recommended to utilize *Halobacterium* as the expression system as follows: bop gene encoding wild-type bR was subcloned into the pALTER-I vector (PROMEGA). A modified mutant bop gene including point mutation is then constructed by the Altered Sites II *in vitro* mutagenesis system (PROMEGA) and subcloned into shuttle vector pxLNor-R. Finally, *H. salinarum* strain L-33 was transformed by the above shuttle vector in the presence of Novobiocin.[71] A variety of site-directed mutants prepared in this way can be treated in a similar manner to the wild type.

It should be borne in mind that a ^{13}C-labeled signal is not always straightforwardly ascribed to the intended amino acid residue because of a plausible isotope scrambling into other amino acid residues as well as lipid molecules through biosynthetic pathways, as pointed out by Engelhard *et al.* for [4-^{13}C]Asp labeling.[72] It turns out, however, that scrambling of incorporated [3-^{13}C]Ala residues into other amino acid residues can be neglected, as proved by examination of solution NMR data on the solubilized protein in CF_3COOH solution.[14]

4.2. Multiple ^{13}C labeling

It appears that this kind of selective isotope labeling starting from the individual ^{13}C-labeled amino acid residues is too laborious and expensive when compared with the current trend of uniform isotope labeling starting from ^{13}C-labeled glucose, acetic acid, etc., or $^{15}NH_4Cl$, as commonly used for current solution NMR study. For solid-state NMR study, a uniformly ^{13}C,^{15}N-labeled α-spectrin SH3 domain (62 residue protein) was recently prepared by the addition of 2 g uniformly ^{13}C-labeled glucose and 1 g $^{15}NH_4Cl$ to an *E. coli* expression system constructed by plasmid encoding of this region from a chicken brain.[73] It was shown that the resolved ^{13}C and ^{15}N peaks of residues 7–61 of the SH3 domain, precipitated by an ammonium salt, were obtained by a suitable combination of heteronuclear and homonuclear 2D NMR techniques, and their signals were sequentially assigned on the basis of 2D MAS ^{15}N–^{13}C and ^{13}C–^{13}C dipolar correlation spectroscopy at 17.6 T, utilizing a band-selective polarization transfer under DREAM[74] (BASE-DREAM), proton-driven spin diffusion (PDSD),[75] radio-frequency-driven dipolar recoupling (RFDR),[76] and band-selective SPECIFIC-CP[77] transfer, etc. The signals of the N- and C-terminal residues 1–6 and 62, respectively, outside the domain boundaries are not detected by the MAS spectra. In addition, signals from the Tyr side chains of Y13 and Y15 and the side chain of K39 are missing owing to their flexibility. Dipolar correlation spectroscopy has been applied to rigid molecular systems

such as a ^{13}C-labeled retinal chromophore of bR[78] or reconstituted photosynthetic reaction centers of *Rhodobacter sphaeroides* R26 containing uniformly ^{13}C-labeled biosynthetically labeled pheophytin *a*.[79]

This approach, however, turned out to be not always straightforwardly applied to the polypeptides in membrane proteins. In fact, it was shown that the detection of 40% of the transmembrane segments of LH2 light-harvesting complex of frozen detergent-solubilized solution is feasible at low temperature (−30 °C) if a high-field NMR measurement, taken at 750 MHz is used.[80] This kind of sequential assignment essential for the system of uniformly labeled samples might be hampered by inherent molecular motions still present in the frozen detergent solubilized solution. In this connection, it is noteworthy that spectral resolution desperately deteriorates for samples of multiple ^{13}C labeling, as manifested by the ^{13}C NMR spectra of [1,2,3-$^{13}C_5$]Ala-labeled bR in Fig. 7.[81] The spectral resolution of the CP-MAS NMR spectra is extremely poor, although the well-resolved signals are visible from the corresponding DD-MAS NMR spectra of the carbonyl region. This is mainly caused by the presence of additionally split signals due to indirect spin–spin coupling and more seriously caused by shortened spin–spin relaxation times due to the increased number of relaxation pathways

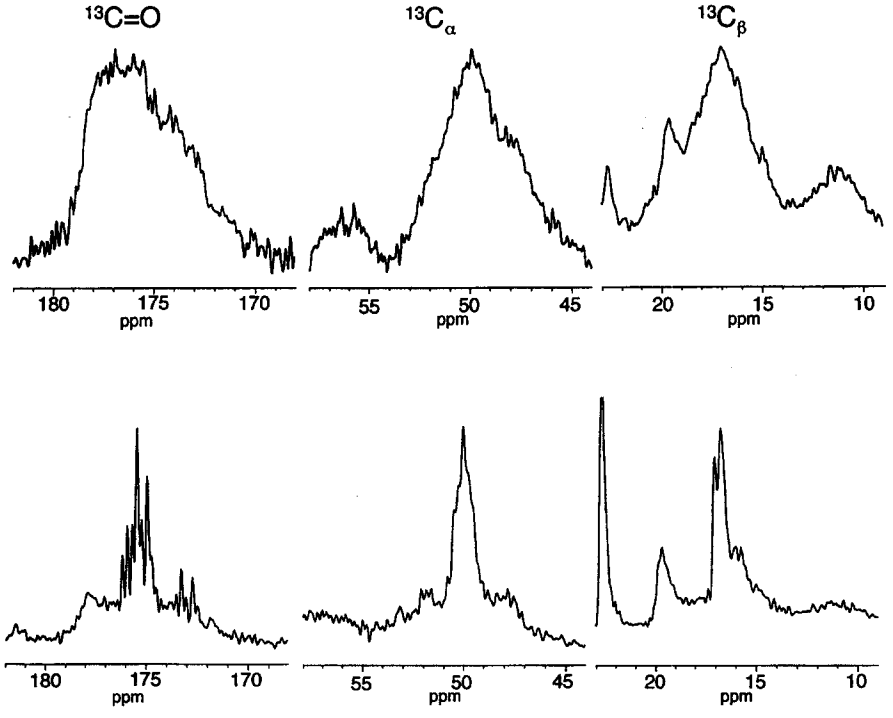

Fig. 7. ^{13}C CP-MAS NMR (upper traces) and DD-MAS NMR spectra (lower traces) of $^{13}C=O$, C_α and C_β carbons from [1,2,3-$^{13}C_3$]Ala-labeled bacteriorhodopsin.[81] Reproduced with permission from the Japanese Biochemical Society.

through a number of ^{13}C–^{13}C homonuclear dipolar interactions and scalar J-couplings in the CP-MAS NMR experiment, etc.[81] In contrast to the cases of rigid crystalline proteins, therefore, it is stressed that this kind of molecular flexibility is an inherent characteristic for a variety of membrane proteins in relation to biological functions. It is advised from this point of view that ^{13}C labeling of the single site is more favorable than the multiple labeling for membrane proteins, although handling is too laborious and time consuming.

To avoid complication from extensively labeled amino acids from either [1-^{13}C]glucose or [2-^{13}C]glycerol, Hong and Jakes utilized growth media supplemented with unlabeled amino acid products of the citric acid cycle in order to obtain simplified ^{13}C NMR spectra of the colicin Ia channel domain.[81a]

5. ASSIGNMENT OF ^{13}C NMR PEAKS

Several types of ^{13}C-labeled bR utilizing [3-^{13}C]-,[5,14] [2-^{13}C]-[81] and [1-^{13}C]Ala,[81,82] [1-^{13}C]-Val,[5] Leu,[14] Gly,[81] [4-^{13}C]-,[83] [3-^{13}C]- [83] and [1-^{13}C]Pro,[84] [4-^{13}C]Asp,[68,80,85,86] and [11-^{13}C]Trp[85] have been examined so far by ^{13}C CP-MAS and DD-MAS NMR methods. ^{13}C NMR studies on these preparations provide a convenient means of examining the local conformations and dynamics of bR and their changes during photocycles, if any, as viewed from the site of the ^{13}C-labeled amino acid residues. First, these ^{13}C NMR signals need to be sufficiently resolved and unequivocally assigned to individual residues of interest. Surprisingly, it turns out that the available information based on these probes is not always the same among [3-^{13}C]-, [2-^{13}C]-, and [1-^{13}C]Ala-bR, in contrast, for instance, to our expectation based on the conformation-dependent displacement of peaks from static molecules. This is because the resulting responses are different among the above-mentioned probe nuclei, depending upon their differential responses to the *dynamics-dependent* displacement of the ^{13}C chemical shifts and suppression of peaks which are characteristic of a variety of membrane proteins, although the spectral response depending upon the *conformation-dependent* displacement of ^{13}C chemical shifts is characteristic of static protein conformations. This is why the optimum choice of the ^{13}C NMR probe nuclei suitable for individual situations is essential. In particular, [3-^{13}C]Ala labeling turns out to be the most suitable probe, better than [2-^{13}C] or [1-^{13}C]Ala labeling, because of the least possibility of isotope scrambling to another amino acid residue, overlapping signals with those of natural abundance molecules[14] and *dynamics-dependent* suppression of NMR peaks.

5.1. Regiospecific assignment of peaks

As already pointed out, the three intense signals marked by gray in the ^{13}C DD-MAS NMR spectrum of [3-^{13}C]Ala-bR are suppressed in the corresponding

CP-MAS NMR spectrum (Fig. 6), although the spectral features of the rest are unchanged. This observation is expected, because the spin–lattice relaxation times, T_1, of the C_β signals are of the order of 0.5 s [81] which is short enough for the complete recovery of the magnetization when compared with the repetition time of the signal acquisition (4 s). The partly suppressed peaks at 17.20 ppm (Ala 235 and 103), 16.88 ppm (Ala 84, 240, 244–246), and 15.91 ppm (Ala 228, 233) (Fig. 6), are from the Ala residues in the C terminal α-helix neighboring the Pro residue (Ala 235), the C terminal tail participating in the random coil (Ala 240, 244–246), and the C terminal α-helix (Ala 228, 233), respectively, protruding from the transmembrane surface. Obviously, these selectively suppressed peaks from the CP-MAS NMR spectrum arose from time averaging of dipolar interactions due to the acquisition of very rapid or almost isotropic motions of the order of 10^{-8} s at the residues of the C terminal end. Therefore, comparison of the DD-MAS and CP-MAS NMR spectra provides the most convenient means of distinguishing the freely fluctuating C terminal or N terminal tail from the transmembrane α-helix and the interhelical loops.[5] The regiospecific assignment of the latter ^{13}C signals can be conveniently shown as the transmembrane α_I, α_{II}-helices and loops flanked by the peak position of the random coil at 16.88 ppm, in view of the conformation-dependent displacement of the ^{13}C chemical shifts from the homopolypeptides, to be described in the next section.

In contrast, the ^{13}C spin–lattice relaxation times of the C_α and C=O signals from the transmembrane α-helices and loops are substantially longer (10–20 s) [81] than the repetition time of 4–8 s conventionally used for recording DD-MAS NMR spectra. As a result, recording the ^{13}C DD-MAS NMR study on the [1-^{13}C] or [2-^{13}C]amino acid-labeled bR is suitable for locating signals from the C or N terminal residues, whereas the CP-MAS NMR approach is suitable for detecting the ^{13}C NMR signals from the transmembrane α-helices and interhelical loops. Consequently, quite different spectral features can be obtained from the ^{13}C DD-MAS (A) and CP-MAS NMR (B) spectra of [1-^{13}C]Ala-bR, as illustrated in Fig. 8. There appears, however, to be no ^{13}C NMR signal from the loop region, because the two signals located at the loop region are unequivocally ascribed to the Ala 235 next to the Pro in the C terminal α-helix and the random coil peak at the C terminal end.[81] This situation arose from the fact that the ^{13}C signal from the loop region is completely suppressed from the spectral region owing to failure of the attempted peak narrowing by the magic angle spinning (MAS) as a result of interference of an incoherent motional frequency of the order of 10^4 Hz with the coherent magic angle spinning,[87] although this timescale is not sufficient to suppress the ^{13}C NMR signals of [3-^{13}C]Ala-bR, as confirmed by counting the number of individual carbon numbers in the deconvoluted spectra.[68] In the latter, peaks can be suppressed by motions of 10^{-5} s interfered with by the proton decoupling frequency. This situation, however, is worsened when the ^{13}C NMR spectra of [2-^{13}C]Ala-labeled wild-type bR are recorded at ambient temperature, as illustrated in Fig. 9. It appears that many ^{13}C NMR signals from the transmembrane α-helices are also suppressed by interference of the motional

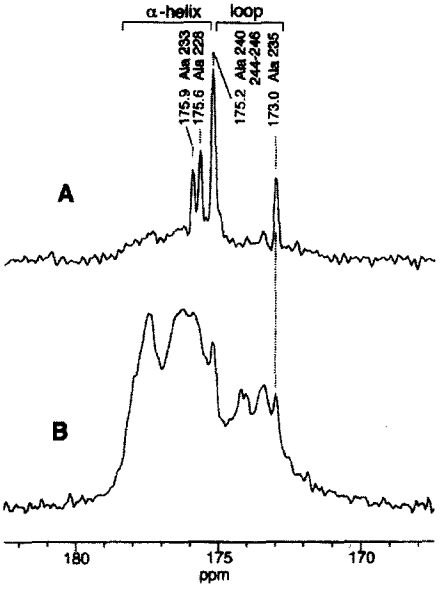

Fig. 8. ^{13}C DD-MAS (upper trace) and CP-MAS (lower trace) of [1-^{13}C]Ala-labeled bacteriorhodopsin.[81] Reproduced with permission from the Japanese Biochemical Society.

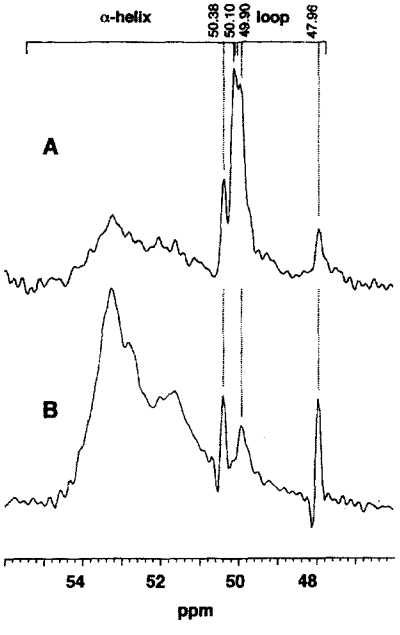

Fig. 9. ^{13}C DD-MAS (A) and CP-MAS (B) NMR spectra of [2-^{13}C]Ala-labeled bacteriorhodopsin.[81] ^{13}C NMR signals resonating at the loop region are from Ala residues in the C terminal α-helix, because those from the loop are completely suppressed.[81] Reproduced with permission from the Japanese Biochemical Society.

frequency with the magic angle spinning, as manifested by broadened ^{13}C signals in addition to the completely suppressed peaks from the loop region. This kind of fluctuation results in broadened ^{13}C signals of both the loops and transmembrane helices owing to sufficiently decreased spin–spin relaxation times under the magic angle spinning, as described later. This argument will be given in more detail in section 6.2. It is noteworthy that the intense peaks occurring in the region marked by the loop are ascribed to the Ala residues located at the C terminal α-helices and C terminal end.

Nevertheless, it is also notable that the ^{13}C NMR signals of Val 69 (B–C loop) and 199 (F–G loop), based on the assignment of peaks using enzymatic cleavage and V199A mutant respectively (to be described later), are clearly visible and can be utilized as a very convenient diagnostic probe to examine a plausible change in the conformation and dynamics in the extracellular loops (Fig. 10). This may be partly caused by modified loop dynamics due to the presence of the Pro residue neighboring these Val residues which alters the frequency of the loop

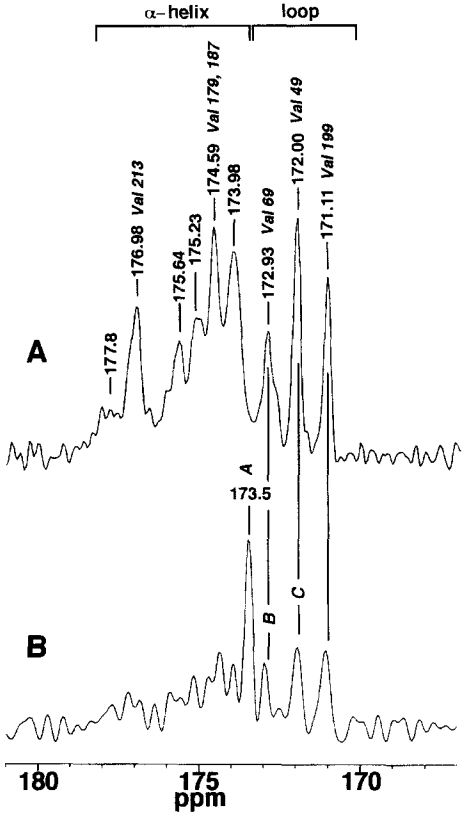

Fig. 10. ^{13}C CP-MAS (A) and DD-MAS (B) NMR spectra of [1-^{13}C]Val-labeled bR.[98] The assigned peaks, Val 179, 187, and 213, are from Arakawa *et al.*[88]

motion such that it escapes from the interference with the frequency of magic angle spinning as encountered for [1-^{13}C] and [2-^{13}C]Ala-labeled bR, as demonstrated in Figs 7 and 8. Moreover, it appears that the three peaks visible in the DD-MAS NMR spectrum (peaks A, B and C) can be tentatively ascribed to the remaining three Val residues, Val 34 (A–B loop), 101 (C–D loop), and 130 (D–E loop) respectively. In particular, peaks B and C are located underneath those of Val 69 and Val 49 respectively.[88] The fact that the Val 49 signal is located in the peak area of the loop is due to the so-called Proline effect.[89] Furthermore, it is noted that the ^{13}C NMR peaks of the three Pro residues are already assigned among seven well-resolved signals of [1-^{13}C]Pro-bR.[84]

5.2. Conformation-dependent ^{13}C chemical shifts

As excellent reference data exist for certain amino acid residues of particular conformations, it is very convenient to utilize the compiled data of the conformation-dependent displacements of ^{13}C chemical shifts so far studied for a variety of polypeptides taking different conformations, as summarized in Table 1. In fact, it is shown that the ^{13}C chemical shifts of the backbone C_α and C=O as well as the side-chain C_β signals of peptides and proteins are significantly displaced (up to 8 ppm), depending on their particular local secondary structure such as α-helix or β-sheet form, as defined by the set of torsion angles of the peptide unit, ϕ and φ, and the manner of hydrogen bonding (for [1-^{13}C]amino acid residues), irrespective of there being a variety of neighboring amino acid residues.[90–92] In particular, it has been demonstrated that the C_α and C=O ^{13}C chemical shifts of the respective amino acid residues in the right-handed α-helix form are displaced to high frequency by 3.5–8.0 ppm with respect to those of the β-sheet form, while the C_β signals of the respective amino acid residues taking the α-helix (α_I-helix) form are displaced to low frequency by 3.4–5.2 ppm with respect to those of the β-sheet form. The conformation-dependent ^{13}C chemical shifts thus compiled have proved not to be dependent upon the particular peptide sequence, except for the one followed by Pro.[89] Therefore, it has been shown that the transferability of these parameters from the particular residues from the simple model system to more complicated proteins is excellent and can be applied to any type of protein,[90–92] so long as the amino acid residues under consideration are static as in silk fibroin,[93] collagen,[94] and synthetic transmembrane peptides of bR.[16]

In contrast, such peaks could be significantly displaced to high frequency when an alternative type of α-helix (α_{II}-helix) is present in which the amide plane might be tilted from the helical axis as previously proposed by Krimm and Dwivedi[95] as the major form of transmembrane α-helix present in bR on the basis of an anomalously high frequency of the amide I band. The characteristic peak position of the ^{13}C chemical shifts of the α_{II}-helix can be defined, taken similarly to the infrared spectra by using $(Ala)_n$ dissolved in hexafluoroisopropanol (HFIP) solution,[96] as demonstrated in Table 2, together with the ^{13}C chemical shifts of

Table 1. ^{13}C chemical shifts characteristic of the α-helix and β-sheet forms (ppm from TNS)[92]

Amino acid residues in polypeptides	C-α			C-β			C=O		
	α-Helix	β-Sheet	Δ[a]	α-Helix	β-Sheet	Δ[a]	α-Helix	β-Sheet	Δ[a]
Ala	52.4	48.2	4.2	14.9	19.9	−5.0	176.4	171.8	4.6
	52.3	48.7	3.6	14.8	20.0	−5.2	176.2	171.6	4.6
	52.8	49.3	3.5	15.5	20.3	−4.8	176.8	172.2	4.6
Leu	55.7	50.5	5.2	39.5	43.3	3.8	175.7	170.5	5.2
	55.8	51.2	4.6	43.7[b]	39.6	(4.1)	175.8	171.3	4.5
Glu(OBzl)	56.4	51.2	5.2	25.6	29.0	−3.4	175.6	171.0	4.6
	56.8	51.1	5.7	25.9	29.7	−3.8	175.4	172.2	3.2
Asp(OBzl)	53.4	49.2	4.2	33.8	38.1	−4.3	174.9	169.8	5.1
	53.6[c]			34.2[c]			174.9		
Val	65.5	58.4	7.1	28.7	32.4	−3.7	174.9	171.8	3.1
		58.2			32.4			171.5	
Ile	63.9	57.8	6.1	34.8	39.4	−4.6	174.9	172.7	2.2
		57.1			33.1			171.0	
Lys[d]	57.4			29.9			176.5		
Lys(Z)	57.6	51.4	6.2	29.3	28.5	−0.8	175.7	170.4	5.3
Arg[d]	57.1			28.9			176.8		
Phe	61.3	53.2	8.1	35.0	39.3	−4.3	175.2	169.0	6.2
Met	57.2	52.2	5.0	30.2	34.8	−4.6	175.1	170.6	4.5
Gly		43.2						168.4	
		44.3						169.2	
							171.6[e]	168.5	3.1

[a] Difference in the ^{13}C chemical shifts of the α-helix form relative to those of the β-sheet form.
[b] This assignment should be reversed.
[c] Erroneously assigned to the left-handed α-helix.
[d] Data taken from neutral aqueous solution.
[e] Averaged values from the data of polypeptides containing ^{13}C-labeled glycine residues.

Table 2. Conformation-dependent ^{13}C chemical shifts of Ala residues (ppm from TMS)

	α_I-helix (α_R-helix)[a]	α_{II}-Helix[a]	α_L-Helix[a]	β-Sheet[a]	Collagen[a]	Silk I[a]	Random coil[a,b]
C_α	52.4	53.2	49.1	48.2	48.3	50.5	
C_β	14.9	15.8	14.9	19.9	17.6	16.6	16.9
C=O	176.4	178.4	172.9	171.8	173.1	177.1	

[a] Ref. 92.
[b] Ref. 81.

the other forms including the random coil form.[69,90] The ^{13}C chemical shift of the Ala C_β taking a turned structure located at the loop region should occur at higher frequency than the peak at 16.88 ppm of the random coil,[81] consistent with the experimental finding described above.

It should be pointed out here that the aforementioned argument about the two types of α-helice, the α_I and α_{II} forms, based on their conformation-dependent displacement of ^{13}C NMR signals, is restricted to an assumed *static* picture of these forms. However, a view of the dynamic equilibrium is implicitly taken into account for the interpretation of the ^{13}C chemical shifts of the loop and random coil forms. It seems, therefore, to be more realistic to discuss the conformation and dynamics of more flexible membrane proteins in terms of the new concept of the *dynamics-dependent* displacement of ^{13}C NMR peaks, to be discussed in Section 6.1.

5.3. Site-directed mutagenesis and proteolysis for site-specific assignment of peaks

Undoubtedly, the site-specific assignment of ^{13}C NMR signals to individual amino acid residues is crucially important in order to go further into a variety of applications of this approach in relation to the structure–function relationship of membrane proteins. The first step to this end is to locate the reduced peak from the site-directed mutant which lacks the amino acid residue of interest as compared with the wild type. For instance, the Ala C_β NMR signals of Ala 196 and 126 of [3-^{13}C]Ala-bR (Fig. 11) are straightforwardly assigned to the peaks whose intensities are lost in the site-directed mutants A196G and A126G respectively, because no additional spectral change was noted by introduction of this sort of site-directed mutagenesis.[5] The difference spectra between the [3-^{13}C]Ala-labeled wild type and A53G or A53V mutants were also very useful in the assignment of the Ala 53 signal, even though this particular peak is not identified as a single peak because of overlap with other unassigned peaks.[68] In a similar manner, the ^{13}C C=O signals of Val 199 (F–G loop) and 49 (B helix) are straightforwardly identified on the basis of a comparison of the ^{13}C CP-MAS NMR spectra of [1-^{13}C]Val-labeled V199A[5] and V49A,[97] respectively, with those of the wild type (Fig. 10). Further experiments utilizing V179M, 213A, V187L, V217A, and V101A were recently successfully performed to assign the respective ^{13}C NMR peaks of [1-^{13}C]Val-bR.[88]

In many instances, however, a more complicated spectral pattern can arise owing to induced local conformational change caused by site-directed mutagenesis, as in A103C and A39V.[98] Even in such situations, this approach is still effective, as far as such accompanied conformational changes remain local and their sites can be identified. This type of peak assignment is made easier if resulting superimposed signals from other residues can be preferentially removed. If such perturbed signals are due to a residue located near a site to

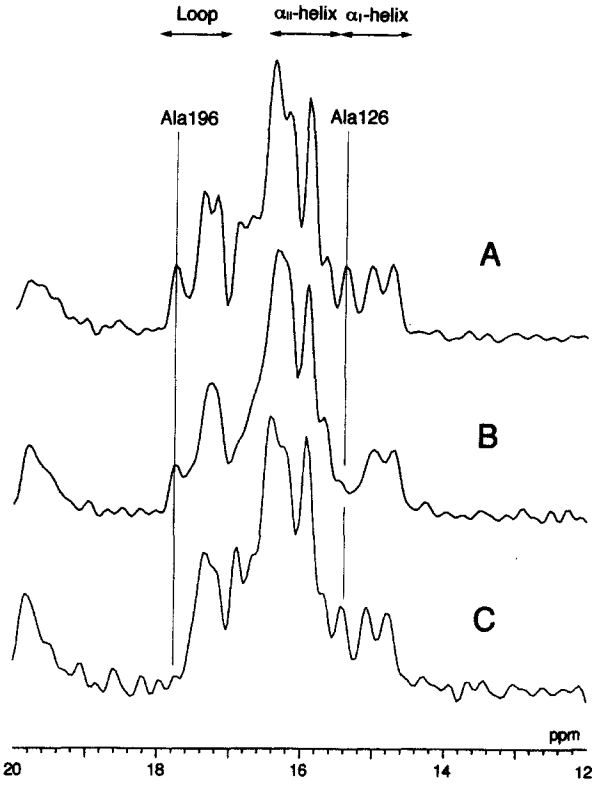

Fig. 11. Comparison of the ^{13}C CP-MAS NMR spectra of [3-^{13}C]Ala-labeled bacteriorhodopsin (A) and A126G (B) and A196G mutants (C).[5] Reproduced with permission from the Biophysical Society.

which the Mn^{2+} ion can bind,[99] the resulting accelerated transverse relaxation times due to the presence of the Mn^{2+} ions result in substantial line broadening.[100] The upper bound of the interatomic distances between the ^{13}C nuclei in bR and the Mn^{2+} ion bound to the hydrophilic surface to cause suppressed peaks by the presence of Mn^{2+} was estimated as 8.7 Å. This results in peak broadening to 100 Hz,[99] according to the Solomon–Bloembergen equation.[100,101] This analysis is consistent with the experimental finding. As a result, the Ala C_β signals of Ala 51, 53, 81, 84, and 215 around the extracellular half of the proton channel and Ala 184 located at the kink in the F helix were successfully assigned on the basis of the ^{13}C NMR spectra of bR in the presence of the Mn^{2+} ion and site-directed replacement of Ala by Gly or Val residues.[99] As demonstrated in Fig. 12A, the peak from the difference spectrum at 16.20 ppm is unequivocally ascribed to the C_β signal of Ala 215, free from the contribution of signals from other Ala residues located at the cytoplasmic surface in the presence of the Mn^{2+} ion. In a similar manner, the signal at 16.52 ppm is assigned to the C_β signal of Ala 81, although the accompanied dispersion signals arise from local conformational

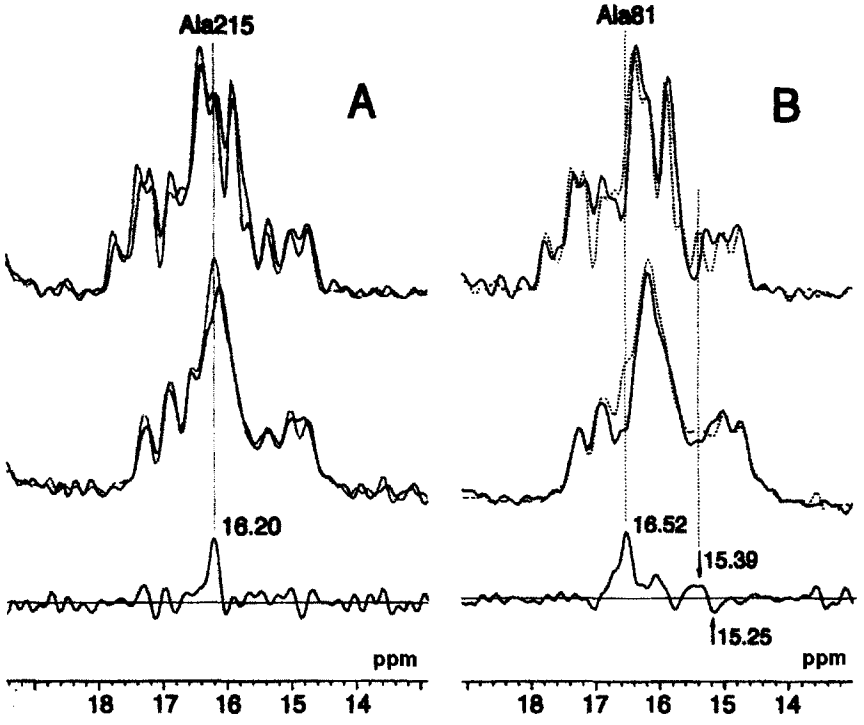

Fig. 12. ^{13}C CP-MAS NMR spectra of [3-^{13}C]Ala-labeled A215G (A) and A81G (B) in the absence (top solid traces) and presence (middle solid traces) of an Mn^{2+} ion. The corresponding spectra of [3-^{13}C]Ala-labeled wild-type bR are superimposed on the top and middle traces as dotted traces. Difference spectra between the wild-type and mutant bRs in the presence of Mn^{2+} are shown in the bottom traces.[99] Reproduced with permission from the Biophysical Society.

changes in the transmembrane α-helix, induced by replacement of Ala 81 (Fig. 12B). In particular, the pair of dispersion signals at 15.39 ppm (positive peak) and 15.25 ppm (negative peak) are ascribed to the low-frequency displacement of the Ala 126 signal owing to the accompanied local conformational change in A81G.[99]

In contrast, it is cautioned that this approach cannot be utilized if any single mutation at a certain key position would result in global conformational change as encountered for the ^{13}C CP-MAS (left) and DD-MAS (right) NMR spectra of [3-^{13}C]Ala-labeled D85N mutant (solid trace) with reference to those of the wild type (dotted trace) illustrated in Fig. 13. Furthermore, this type of approach is not feasible when the ^{13}C NMR signals under consideration are suppressed in the wild type as encountered for the C=O and C_α ^{13}C NMR signals of [1-^{13}C] (Fig. 8) or [2-^{13}C]Ala-labeled bR (Fig. 9) respectively. An illustrative example of this problem is given in Fig. 14 as an attempt to locate the Ala 196 signal of [1-^{13}C]-Ala-bR,[102] in which ^{13}C signals of Ala 196 are absent for both the wild type and

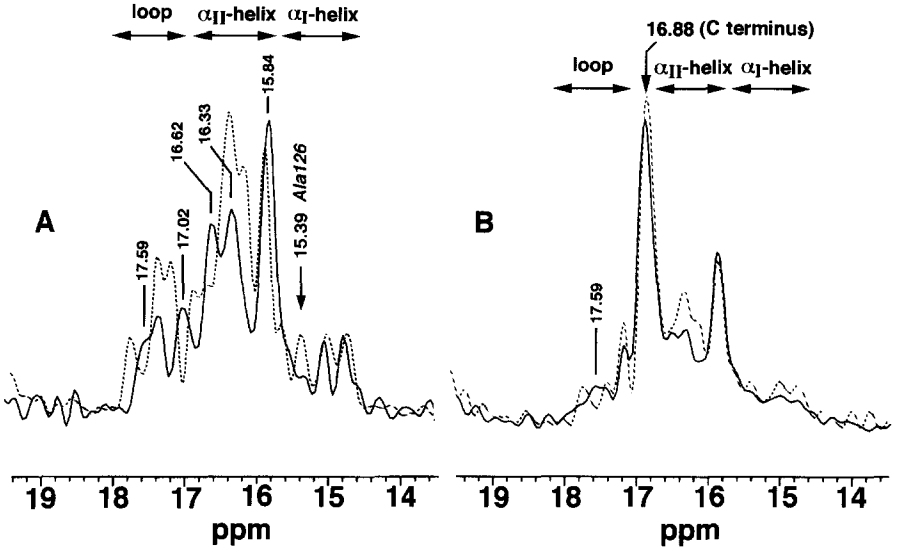

Fig. 13. Comparison of ^{13}C CP-MAS NMR (left) and DD-MAS NMR spectra (right) of D85N mutant (black traces) and wild type (dotted traces).[153] Reproduced with permission from the Biophysical Society.

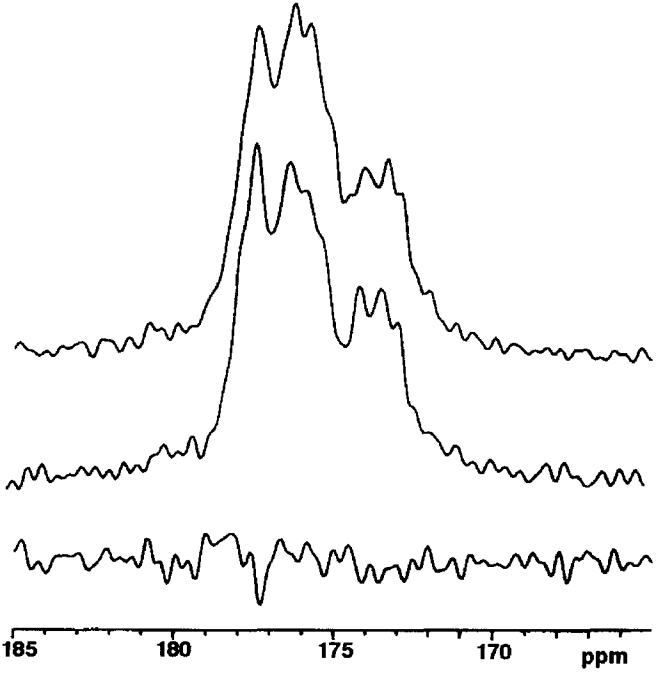

Fig. 14. Comparison of [1-^{13}C]Ala-labeled bacteriorhodopsin (A) and A196G (B), and their difference spectra.

the A196G mutant. This arises from the acquisition of motional flexibility, with a correlation time of 10^{-4} s, owing to the location of the carbons at the interfacial area between the loop and transmembrane helices.

It is shown that the comparative ^{13}C NMR observation of successively cleaved C terminal residues of [3-^{13}C]Ala-labeled bR by carboxypeptidase A and papain is an effective means of locating the ^{13}C NMR signals from Ala 245–248 and Ala 228 and 233 respectively.[81,82,103,104] Strictly speaking, the resulting ^{13}C NMR spectrum obtained from DD-MAS is not exactly the same as the CP-MAS NMR spectrum, because removal of the C terminal α-helix results in a conformational change in the cytoplasmic loops owing to disruption of the cytoplasmic surface complex consisting of the C–D and E–F loops and the C terminal α-helix.[104,105] It was also demonstrated that the induced spectral change from the single to doublet peaks caused by a cleavage of the B–C loop by chymotrypsin may be utilized as a means of locating the ^{13}C NMR signals of Val 69 in the B–C loop of [1-^{13}C]Val-labeled bR.[97]

Here, it may be worthwhile to list the assigned ^{13}C NMR signals of [3-^{13}C]Ala- and [1-^{13}C]Val-labeled bR so far obtained (Table 3) for the sake of convenience for further discussion.

6. NMR PARAMETERS FOR DETECTION OF PROTEIN DYNAMICS

6.1. Dynamics-dependent ^{13}C chemical shifts

It is noteworthy that the ^{13}C NMR peaks of α-helices (including α_I and α_{II} helices) in bR listed in Table 3 are widely spread with respect to the expected values based on the conformation-dependent displacement of peaks as summarized in Tables 1 and 2. As to the static picture of the α_{II}-helix, the direction and magnitude of the observed high-frequency displacement of the peaks are consistent with those predicted on the basis of a theoretical evaluation of ^{13}C chemical shifts for the Ala C_β carbon from the ^{13}C chemical shift contour maps based on N-acetyl-N′-methyl-L-Ala-amide [106,107] and the proposed changes in the torsion angles, together with the Ramachandran energy contour map. Nevertheless, this type of static picture seems to be insufficient for interpreting the observed ^{13}C chemical shift data both in intact bR (Table 3) and in its transmembrane peptides incorporated into the lipid bilayer, as is described below in more detail. Instead, an alternative interpretation based on the *dynamics-dependent* displacement of the ^{13}C chemical shifts through their sequence dependence is more practical, in addition to the *conformation-dependent* ^{13}C chemical shifts discussed in the previous section.

Here, it is worthwhile to demonstrate an illustrative example of how the ^{13}C NMR chemical shifts of the [3-^{13}C] and [1-^{13}C]Ala- and Val-labeled transmembrane peptides of bR are displaced to high frequency in the lipid bilayer, depending upon their positions in the peptide sequence with respect to those of

Table 3. Assigned ^{13}C NMR signals of [3-^{13}C]Ala- and [1-^{13}C]Val-labeled bR

[3-^{13}C]Ala (refs 69 and 104)		
Resolved ^{13}C signals (ppm)	Unresolved (ppm)	Ala
17.78		196
17.56		103[a]
17.37		160[b]
	17.27	184
17.20		235, 103[c]
16.88		84, 240, 244–246
16.71		
16.38		39, 168
	16.52	81
16.20		215
	16.14	53
15.92		51
15.91–15.67[d]		228, 233
15.38		
15.02		126
14.74		

[1-^{13}C]Val	
Resolved ^{13}C signals (ppm)	Val
177.0	213
175.6	
175.0	
174.6	179, 187
174.0	
173.5[e]	
172.9	69
172.0	49
171.1	199

[a] This peak is displaced to low frequency when bR is recorded at 10 mM NaCl.
[b] This peak is displaced in the range 17.36–17.15 ppm depending upon a variety of environmental factors.
[c] At 10 mM NaCl.
[d] This peak is displaced to low frequency when the temperature is lowered to −10 °C.
[e] Visible only by DD-MAS NMR spectra.

the solid or helix-promoting solvent (Table 4).[16] The interpretation of such sequence-dependent displacement of the ^{13}C chemical shifts of the transmembrane peptides in a lipid bilayer is not easy in terms of the current view of the *conformation-dependent* displacement of the ^{13}C chemical shifts, as compared with the observations in the solid and solution states. It is emphasized that this kind of displacement of a ^{13}C chemical shift is in parallel with that observed in purple membrane. The observed distribution of the chemical shifts seems to deviate greatly from their expected peak positions from the distribution of the torsion angles determined, at lower temperature, by X-ray diffraction.[25]

Table 4. ^{13}C chemical shifts of transmembrane peptides in solids and DMPC bilayer as compared with those of bR (ppm)[16]

			Transmembrane peptides							
				Solid from HFIP solution		Solid from DMSO solution	In DMPC bilayer		bR[c]	
Residue		Sample	Sequence	CH_3	C=O	CH_3	CH_3	C=O	CH_3	C=O
Ala	2								16.9	
	14	**1**	A(6–42)	15.2	176.5	20.2	15.8 (0.6)	176.7 (0.2)	16.4 (1.2)	176.0 (–0.5)
	18	**3**	A(6–35)	15.0		20.5	15.7 (0.7)			
	39	**6**	B(36–71)	15.7			16.9 (1.0)[a]		16.4 (0.7)	
	51	**6**	B(36–71)	15.4	177.5	19.9	16.2 (0.8)	178.2 (0.7)	15.9 (0.5)	
	53	**8**	B(36–71)	15.3	176.6		15.7 (0.4)	176.7 (0.1)	16.1 (0.8)	177.9 (1.3)
	84	**9**	C(72–107)		176.1			175.2[b] (–0.9)	16.9	
	98	**9**	C(72–107)	15.3			15.6 (0.3)			
	114	**10**	D(102–131)	15.2		20.9	16.3 (1.1)			
	139	**11**	E(128–166)		176.3			176.5 (0.2)		
	160	**11**	E(128–166)	15.4			16.9 (1.5)[a]			
	184								n.d.[d]	177.7
Val	49	**7**	B(36–71)		172.3			172.9 (0.6)		172.3 (0)

[a] Protruded from the surface taking random coil form due to cleavage of nearby loops.
[b] Residue either taking random coil or undergoing large amplitude motion.
[c] Assignment summarized in refs 69 and 104.
[d] Not detected owing to interference with proton decoupling frequency.

For instance, the Ala C_β signal of Ala 84 resonates at the peak position of the random coil conformation (Table 3), although this peak was detected by CP-MAS NMR spectra originating from residues undergoing anisotropic fluctuation. Therefore, it is more likely that this peak accidentally overlaps with the peak of the random coil at 16.88 ppm or is in chemical exchange with the lowermost end of the peak position of the α-helices and the random coil forms with a rate constant of the order of $10–10^2$ Hz.[16] Furthermore, the peak position of Ala 184 in helix F appears at 17.27 ppm which is at an unexpectedly high frequency for a carbon signal belonging to an α-helix.[99]

Accordingly, it seems to be more realistic to interpret the variation in the ^{13}C NMR chemical shifts of membrane proteins in terms of the *dynamics-dependent* displacement of peaks as a novel means of probing the dynamic aspect of membrane proteins. Therefore, the transmembrane α_{II}-helix could be ascribed to a residue whose time-averaged deviation of torsion angles at ambient temperature differs from that of static ones at low temperatures, arising from the presence of a low-frequency motion associated with a local anisotropic fluctuation.[16] It is interesting, however, to note that the estimated proportion of the α_{II}-helix on the basis of the carbonyl ^{13}C chemical shift is much smaller when compared with that observed for the Ala C_β, as in the case of Ala 14, 53, and 139.[16] To examine further whether an intrachain hydrogen bond between residues *i* and *i*+4 in the transmembrane peptide of bR is a normal or a distorted type as proposed by Krimm and Dwivedi,[95] the ^{13}C–^{15}N interatomic distance was measured for ^{15}N–H(Ala^{18})···O=^{13}C(Ala^{14}) for A(6–42) by means of rotational echo double resonance (REDOR).[108–112] The measured interatomic distance of 4.5±0.1 Å in this case[113] is exactly the same as that of a typical α-helical peptide determined by the same method.[114] This observation means that the above-mentioned α-helix as characterized by the α_{II}-helix viewed from the Ala C_β chemical shift of Ala 14 is of the normal type (α_I-helix), as judged from the carbonyl ^{13}C chemical shift and hydrogen bond length. Furthermore, it is demonstrated that the Ala C_β ^{13}C peak of Ala 228 and 233 which participate in the C terminal α-helix protruding from the cytoplasmic surface of the membrane appears at the position of the α_{II}-helix,[68,81,82,98,103] whereas the corresponding ^{13}C NMR peaks for the C_α and carbonyl carbons do not.[81] A possible reason for such specific sensitivity of the Ala C_β ^{13}C signal to the α_{II}-helix region is that the methyl group pointed towards the lipid bilayer might be much influenced by a local fluctuation of the peptide through a helix–lipid interaction, although the carbonyl groups not in direct contact with the lipids are naturally not affected. It is interesting to note, however, that the Ala residues involved in the C terminal α-helix, which is not always in direct contact with the fatty acyl chain of the lipid, behaves as an α_{II}-helix form.

Therefore, a more plausible explanation is that such an α-helical chain is subject to a low-frequency sequence-specific thermal fluctuation as viewed from the [3-^{13}C]Ala-labeled bR, although such a fluctuation is insensitive to displacement of the [1-^{13}C]Ala-labeled protein. Consistent with this view, it has been

shown that several peaks of bR that resonate at the position of the α_{II}-helix are generally displaced to high frequency by raising the temperature from −10 to 40 °C in a biphasic manner, whereas the peaks resonating in the α_{I}-helix region are not displaced. In particular, such high-frequency displacement towards the direction of the random coil form is most prominent for the C terminal α-helix (0.43 ppm).[104] In any case, it is emphasized that the existence of the *dynamics-dependent* ^{13}C chemical shift is a very valuable probe, although it is restricted to the [3-^{13}C]Ala residue, for locating the portion undergoing low-frequency, anisotropic fluctuations of the order of 10^2 Hz.

6.2. Dynamics-dependent suppression of peaks

As described above, it should be recognized that not all of the ^{13}C NMR signals of intact membrane proteins are always visible at ambient temperature. If there are isotropic or large-amplitude motions, whose correlation times are shorter than 10^{-8} s, as in the case of the C terminal end, these can be very easily identified by the selective suppression of CP-MAS NMR signals from the immobilized domains (blanked area **a**, corresponding to the high-frequency motion of 10^8 Hz) as compared with those of DD-MAS experiments which detect also the mobile domain, as demonstrated in Fig. 15. This kind of motion can be very easily detected by observation of the prolonged ^{13}C spin–lattice relaxation time determined by DD-MAS experiments, as illustrated by the horizontal bar in Fig. 15B.[69] This type of motion was first recognized at ambient temperature when the ^{13}C CP-MAS NMR signals of the C terminal residues were partially suppressed by comparison with the DD-MAS NMR spectra.[103] The latter is capable of detecting signals from the whole area of proteins in view of the relatively shorter spin–lattice relaxation time of the Ala C_β carbons, provided that there is no additional *incoherent* random motion which results in interference with peak narrowing by *coherent* proton decoupling or the magic angle spinning process.[87, 115]

Molecular motions of intermediate frequency, with correlation times of 10^{-5} s, which can interfere with the proton decoupling frequency (ca 50 kHz), can be very easily detected when certain ^{13}C NMR signals from both the DD-MAS and the CP-MAS NMR spectra of [3-^{13}C]Ala-bR are simultaneously suppressed (blanked area **b**), as illustrated in Fig. 15A. Such motion was first recognized when the ^{13}C NMR signals of the C terminus were almost completely suppressed both in the CP-MAS and DD-MAS NMR spectra, when the temperature was lowered to between −40 and −110 °C.[116] This kind of peak suppression is most pronounced at ambient temperature for the whole range of transmembrane α-helices and a part of the loop in the [3-^{13}C]Ala-labeled bleached bacterio-opsin (bO) where retinal was removed from bR (see Fig. 16), as viewed from the suppression of Ala 39, 53, and 84 (B and C helices), Ala 215 (G-helix), the E–F loop (Ala 160), and the F–G loop (Ala 196).[98] A similar type of peak suppression

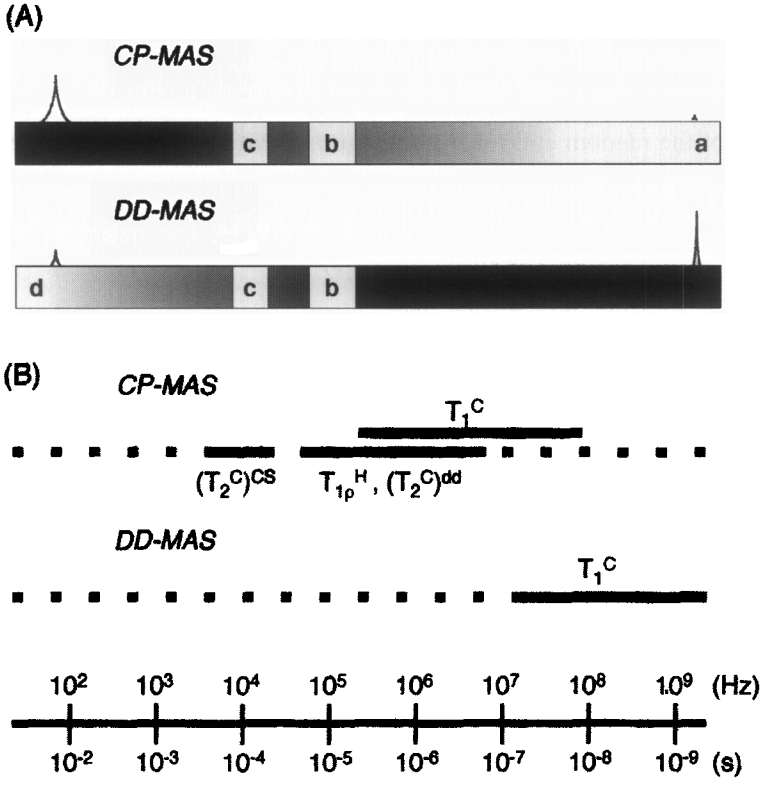

Fig. 15. Detection of several types of motion either by observation of dynamics-dependent suppressed peaks (A) or measurement of relaxation parameters (B) as a function of respective motional frequency (Hz) or its timescale or correlation times (s). NMR peak suppressed by: fast isotropic motion (**a**), interference with proton decoupling frequency (**b**), and magic angle spinning (**c**).[69] Reproduced with permission from Elsevier Science.

is distinguished in the M-like state of D85N and the D85N/D96N mutants, which is triggered by raising pH without photoillumination.[117] Such suppression of peaks is interpreted in terms of acquired intermediate motions of the protein backbones with correlation times of the order of 10^{-5} s. The electrostatic retinal–protein interaction between the positive charge of the Schiff base and the negative charge of Asp 85 in helix C, which is responsible for the protein packing and dynamics, is either completely removed, as in bO, or partly removed in the mutants by removal of retinal or neutralization of the negative charge at Asp 85 respectively. This approach can be very conveniently utilized as a *model-free determination of the correlation time* for any local fluctuation of the molecular chain, provided that the reference peak intensities without such suppression are available as in the [3-^{13}C]Ala-labeled bR of the wild type.

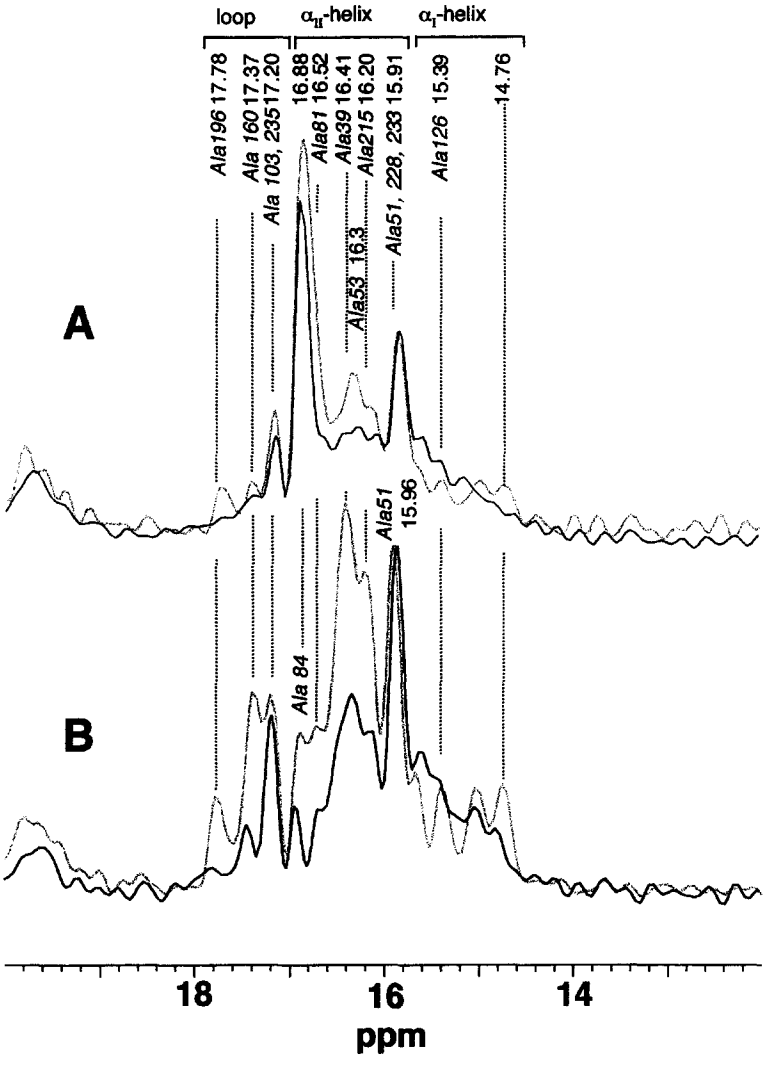

Fig. 16. ^{13}C NMR spectra of bacterio-opsin (bO) (black traces) as compared with those of bacteriorhodopsin (bR) (gray traces), recorded by the DD-MAS (A) and CP-MAS (B) NMR methods.[98] Reproduced with permission from the Japanese Biochemical Society.

As discussed in Section 5.3, the ^{13}C NMR signals of interhelical loops from either [2-^{13}C] (Fig. 9) or [1-^{13}C]Ala-labeled bR (Fig. 8) are completely suppressed, in spite of the wild-type bR examined, owing to the presence of motional fluctuation with correlation times of the order of 10^{-4} s, which can interfere with the frequency of the magic angle spinning.[98] The reason for the correlation time of 10^{-4} s instead of 10^{-5} s is that the ^{13}C NMR signals of the corresponding loop region are still visible from the [3-^{13}C]Ala-bR. Furthermore,

it is anticipated that the ^{13}C NMR peak intensities of the Ala residues of the transmembrane α-helices near the cytoplasmic and extracellular surfaces might be suppressed to some extent as long as the [1-^{13}C] or [2-^{13}C]Ala-labeled proteins are examined,[98] in spite of the use of the wild-type bR. In such a situation, the suppressed peaks can be recovered by a plausible shift in the correlation times of fluctuation from 10^{-4} to 10^{-5} s, for instance in the ^{13}C NMR spectrum of the [1-^{13}C]Ala-labeled D85N in which the backbone dynamics are substantially modified as mentioned above. Interestingly, this is the case for the ^{13}C NMR spectrum of the [1-^{13}C]Ala-labeled D85N (solid line) in comparison with that of the wild type (dotted line) recorded at ambient temperature, as illustrated in Fig. 17.[118] Obviously, it is noteworthy that the intensities of the two α-helical peaks, 175.9 and 176.5 ppm, ascribable to Ala residues at the interfacial surface, are substantially increased in D85N mutant in comparison with those of the wild type. In contrast, it appears that the peak intensities of the [1-^{13}C]Val-labeled bR are not significantly suppressed at ambient temperature.[97] Thus, it is advised that any possibility of the presence of such *dynamics-dependent* suppressed peaks should always be checked prior to any attempt at interpreting ^{13}C NMR spectra of any kind, especially when site-directed mutants are used. Surprisingly, ^{13}C

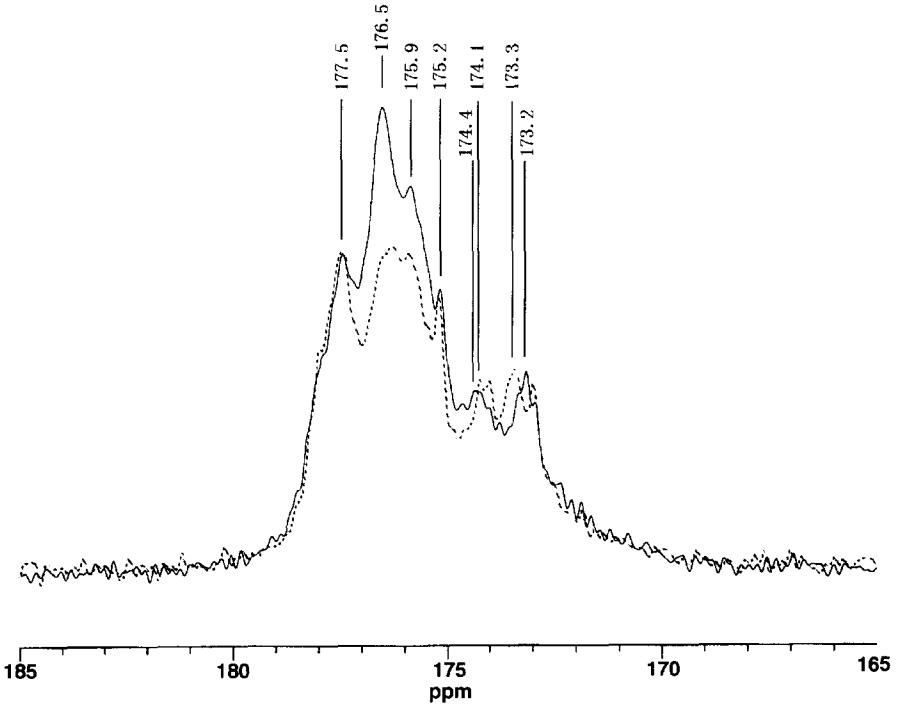

Fig. 17. Comparison of ^{13}C CP-MAS NMR spectrum of the [1-^{13}C]Ala-labeled D85N mutant (solid trace) with that of the wild type (dotted trace).

NMR signals from the transmembrane α-helices and loops of [3-^{13}C]Ala-labeled bO are substantially broadened compared with the signals of the C terminal residues, which are able to fluctuate freely, when the retinal-deficient strain E1001 is examined, as illustrated in Fig. 18.[98] This observation can be interpreted in terms of incomplete folding to the trimeric structure in the absence of retinal, which is essential for proper hexagonal packing[119,120] as seen in the native bR, leading to a shortened spin–spin relaxation time under proton decoupling. Consistent with this view, it is found that such a broadened spectral pattern is changed to the normal one of regenerated bR when retinal is added to this preparation. This finding strongly suggests that the overall protein dynamics of bR is strongly perturbed by the manner of intermolecular contact, as far as the timescale of motions defined as 10^{-4} or 10^{-5} s are concerned. In fact, we have recently found that internal motions of transmembrane α-helices of the order of 10^{-2} s in intact bR are substantially accelerated to the order of 10^{-4} s when the assembly of a trimeric structure and hexagonal lattice is perturbed by the introduction of a site-directed mutation at key positions for such interactions as in W80L and W12L, as viewed from the surprisingly reduced peak intensities of

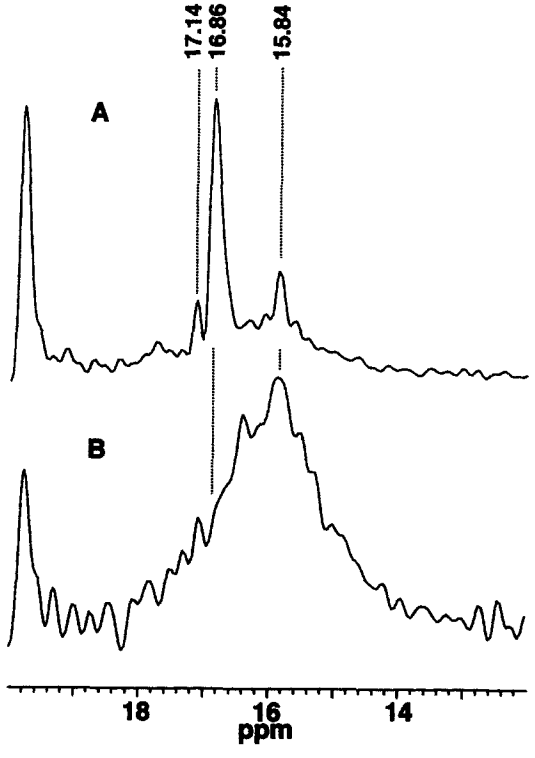

Fig. 18. ^{13}C DD-MAS (A) and CP-MAS (B) NMR spectra of [3-^{13}C]Ala-labeled bacteriopsin from the retinal-deficient E1001 strain.[98] Reproduced with permission from the Japanese Biochemical Society.

[1-^{13}C]Ala-labeled W80L and W12L by comparison with those of the bR of the wild type.[121] It is interesting to note that such flexibility of transmembrane α-helices in bR is mainly determined by the manner of the protein–protein interaction, leading to a crystal lattice. For this reason, utilization of monomeric bR at ambient temperature is obviously unfavorable for ^{13}C NMR observations as far as the [3-^{13}C]Ala-labeled proteins are concerned. It is thus advisable to examine the ^{13}C NMR spectra of ^{13}C-labeled bR, in which the extent of peak suppression is less pronounced, by selecting the source of labeling among [3-^{13}C]Ala, [1-^{13}C]Ala, or Val in order to avoid the particular timescale responsible for such dynamics-dependent suppression of peaks for any type of membrane protein. It is cautioned that this sort of dynamics-dependent suppression of peaks cannot be avoided even if measurements were made at ultrahigh field.

The observation of such suppressed peaks is not limited to membrane proteins as mentioned above but is also possible for a variety of fibrous proteins and crystalline peptides. In such cases, it is stressed that the ^{13}C NMR signals of the C_β carbons, rather than the backbone C_α and carbonyl carbons, are in many instances suppressed, depending upon the manner of crystalline packing as encountered for collagen and enkephalins.[94,122,123]

6.3. Relaxation parameters

As illustrated in Fig. 15B, more detailed characterization of molecular motions in membrane proteins is feasible by the following sets of relaxation parameters, carbon spin–lattice relaxation times, T_1^C, carbon spin–spin relaxation times under CP-MAS condition, T_2^C,[87,124,125] and proton spin–lattice relaxation times in the rotating frame, ($T_{1\rho}$H),[126] with the range of respective correlation times most suitable for detection given by the horizontal bars. As expected from the diagram in Fig. 15, the measurement of carbon spin–lattice relaxation times for [1-^{13}C]Gly- and [1-^{13}C], [2-^{13}C], and [3-^{13}C] Ala-bR is very useful for locating rather flexible portions of the membrane protein such as the N or C terminal residues protruding in the membrane surface.[68,81,97] The T_1^C values for the first three carbons, determined by CP-MAS NMR, are of the order of 20, 17–3, and 6–0.3 s respectively, whereas those determined by DD-MAS are naturally of the order of 0.3 s irrespective of the ^{13}C label. This is demonstrated in Tables 5 and 6 for [2-^{13}C]Ala- and [1-^{13}C]Gly-, Val- or Ala-labeled bR respectively.[81] This means that the shortened T_1^C values in the former are due to the C terminal α-helical portion, which is able to undergo conformational fluctuation, as compared with those of the loop regions.

Carbon spin–spin relaxation times, T_2^C, under CP-MAS conditions can provide motional information about the *individual carbon* site of interest, in contrast to the case of proton spin–lattice relaxation times in the rotating frame, $T_{1\rho}^H$, in which information on individual sites would be masked by the presence of a rapid spin–spin process. In general, the T_2^C values strongly depend on the

Table 5. ^{13}C spin–lattice relaxation times, T_1^C (s), and spin–spin relaxation times under the proton decoupling and magic angle spinning, T_2^C (ms), of [2-^{13}C]Ala-labeled bacteriorhodopsin[2]

		Transmembrane α-helix		C terminal α-helix			C terminal end
		53.2 ppm	51.2 ppm	50.37 ppm (Ala 233)	50.03 ppm (Ala 228)	47.96 ppm (Ala 235)	50.1 ppm (Ala 240, 246–248)
T_1^C	CP-MAS	5.7±1.7	9.0±0.46	0.32±0.17	1.1±0.03	0.41±0.23	
	DD-MAS			0.29±0.03	0.32±0.10	0.24±0.05	0.32±0.01
T_2^C	CP-MAS	2.8±0.53	4.5±0.17	9.4±0.98	6.8±0.05	17.3±0.9	

Table 6. ^{13}C spin–lattice relaxation times, T_1^C (s), and spin–spin relaxation times under proton decoupling and magic angle spinning, T_2^C (ms), of [1-^{13}C]Gly-, Val-, or Ala-labeled bacteriorhodopsin[2]

		Gly		Val	Ala				
		α-helix		α-helix	α-helix		α-helix/random coil	C terminus	
		172.7 ppm	171.8 ppm	174.2 ppm	177.5 ppm	176.5 ppm	175.9 ppm	175.2 ppm	173.0 ppm
T_1^C	CP-MAS	19.9±1.7	24.1±2.5	16.3±2.8	16.8±2.5			2.9±0.21	8.3±1.19
	DD-MAS		0.4±0.04				1.76±0.05	1.36±0.05	1.43±0.2
T_2^C	CP-MAS				7.2±0.67	6.8±0.67		13.3±2.8	17.1±2.8

proton decoupling frequency and are affected by interference between incoherent random motion and coherent decoupling and spinning frequencies. Therefore, the overall relaxation rate, $1/T_2^C$ can be given by[87,124,125]

$$1/T_2^C = (1/T_2^C)^S + (1/T_2^C)^M{}_{DD} + (1/T2^C)^M{}_{CS} \quad (1)$$

where $(1/T_2^C)^S$ is the transverse component due to static C–H dipolar interactions, and $(1/T_2^C)^M{}_{DD}$ and $(1/T_2^C)^M{}_{CS}$ are the transverse components due to the fluctuation of the dipolar and chemical shift interactions respectively. The latter two terms are given as a function of the correlation time, τ_c, by

$$(1/T_2^C)^M{}_{DD} = \Sigma(4\gamma_I^2\gamma_S^2h^2/15r^6)\ I(I+1)\ [\tau_c/(1+\omega_I^2\tau_c^2)] \quad (2)$$

$$(1/T_2^C)^M{}_{CS} = (\omega_0^2\delta^2\eta^2/45)\ [\tau_c/(1+4\omega_r^2\tau_c^2) + 2\tau_c/(1+\omega_r^2\tau_c^2)] \quad (3)$$

where γ_I and γ_S are the gyromagnetic ratios of the I and S nuclei respectively, r is the internuclear distance between spins I and S, ω_0 and ω_I are the carbon resonance frequency and the amplitude of the proton decoupling RF field respectively, ω_r is the rate of spinner rotation, δ is the chemical shift anisotropy, and η is the asymmetric parameter of the chemical shift tensor. Clearly, the transverse relaxation rate is dominated by modulation of either dipolar interactions or chemical shift anisotropies, if internal fluctuations cannot be ignored as in the membrane proteins. It is expected that a decoupling field of 50 kHz is sufficient to reduce the static component, and the $(1/T_2^C)^M{}_{CS}$ term will be dominant in the overall $1/T_2^C$, as far as carbonyl groups with larger chemical shift anisotropies are concerned. In addition, it is expected that the C_α carbon signal could also be affected by both the $(1/T_2^C)^M{}_{DD}$ and $(1/T_2^C)^M{}_{CS}$ terms, depending upon the frequency range of either 50 kHz (ω_I) or 4 kHz (ω_r) respectively. Typical T_2^C values obtained by such conditions are also summarized in Tables 5 and 6. Furthermore, it is notable that the ^{13}C NMR signals are extraordinarily broadened when the ^{13}C NMR spectra of fully labeled preparations, such as [1,2,3-$^{13}C_5$]Ala- bR, are recorded. This is because the broadening and splitting of peaks owing to the accelerated transverse relaxation rate, $(1/T_2^C)$, as compared with the case of single ^{13}C-labeling, causes an increase in the number of relaxation pathways through a number of ^{13}C–^{13}C homonuclear dipolar interactions and scalar J couplings respectively.

On the basis of the aforementioned measured relaxation parameters and their qualitative interpretation, together with the data of the *dynamics-dependent* suppression of peaks, it is now possible to gain insight into the regiospecific backbone dynamics of bR as schematically illustrated in Fig. 19. Obviously, the dynamic feature of the transmembrane α-helix, C terminal α-helix, and C terminal end can be readily distinguished by examination of the differential T_1^C values of [2-^{13}C]Ala-bR, although the data for the loop region are missing because of their suppressed peaks. It is noteworthy that the T_1^C values of the C terminal α-helix are one order of magnitude smaller than those of the transmembrane α-helix, reflecting its plausible internal fluctuation with correlation

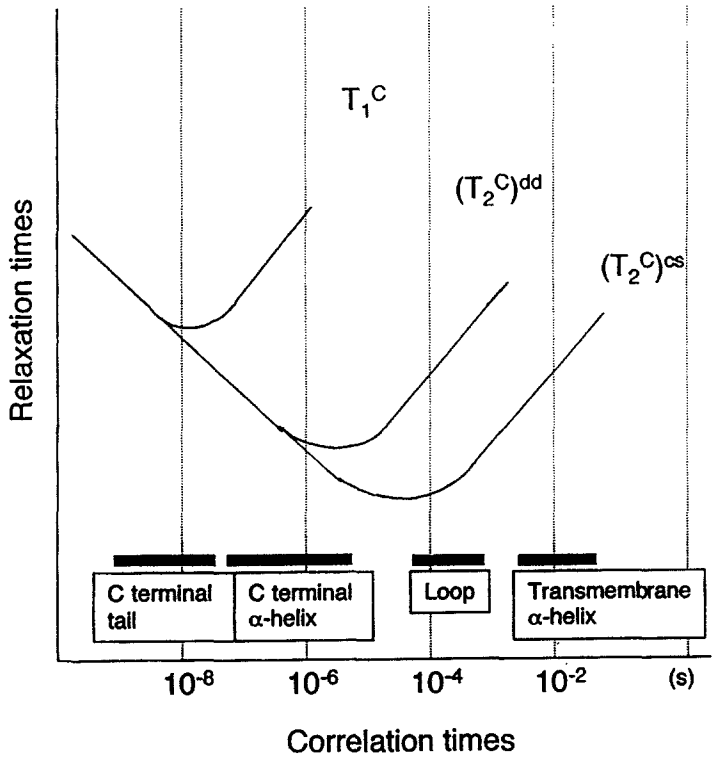

Fig. 19. Schematic representation of carbon spin–lattice relaxation time, T_1^C, and spin–spin relaxation time under CP-MAS condition, T_2^C, as a function of correlation time.

times of the order of 10^{-6} s, inferred from the diagram (Fig. 19) on the basis of the observed T_1^C and T_2^C values, compared with those of the transmembrane helix. This sort of α-helix has not been found for bR by X-ray diffraction or cryo-electron microscopy, probably because of the presence of such inherent fluctuation.[18–27] It appears that the T_2^C minimum value could be located at a correlation time of 10^{-5} or 10^{-4} s, depending on the relaxation mechanism either from the dipolar–dipolar interactions [DD, equation (2)] or chemical shift anisotropies [CS, equation (3)] respectively. As a result, the ^{13}C NMR signals from [1-^{13}C] and [2-^{13}C]Ala-bR are substantially broadened by the CS mechanism, which could be interfered with by molecular motions with correlation times of the order of 10^{-4} s. This corresponds to a magic angle spinning rate of the order of 4 kHz. This is because the chemical shift anisotropy is of the order of 3 kHz, as estimated from single crystalline alanine.[127] In fact, it was demonstrated that the ^{13}C NMR signals of transmembrane peptides labeled with the former probe are suppressed in the DMPC bilayer at ambient temperature because the rigid-body motions of the helical peptides interfere with the magic

angle spinning.[16] The absence of ^{13}C NMR peaks from the loop region of [2-^{13}C]Ala-bR indicates that the turned structure of the interhelical loop is not rigid at ambient temperature, as anticipated, but slowly fluctuates among various preferred conformations with a correlation time of the order of 10^{-4} s.

In a similar manner, the [1-^{13}C] or [2-^{13}C]Ala residues located near the surface may acquire the same degree of fluctuation by taking account of their location. The remainder of the transmembrane α-helices fluctuate with correlation time in the order of 10^{-2} s (see Section 6.1).

7. SURFACE STRUCTURE AND DYNAMICS OF BACTERIORHODOPSIN

7.1. Surface structure

Understanding the surface structure and dynamics of membrane proteins at ambient temperature is very important in view of their role in biological responses initiated either at cytoplasmic or extracellular surfaces. The surface structure of bR is still obscured, or inconsistent, among a variety of the 3D structures so far revealed by cryoelectron microscopy and X-ray diffraction studies.[18–27] This arises because it can be easily altered by a variety of intrinsic or environmental factors such as the manner of crystallization either in the 2D or 3D crystals, temperature, pH, site-directed mutagenesis or ionic strength, crystallographic contact, etc.[48,69] In addition, dynamic pictures of bR to be observed at the physiological temperature can be lost when all the 3D structures have been obtained at cryogenic temperatures. As an alternative means, fluorescence,[128,129] spin labeling,[130] heavy atom labeling,[131,132] and atomic force microscopy (AFM) techniques have been utilized to probe such structures at ambient temperature, although these techniques are not always free from plausible perturbations due to steric hindrance by the introduced probes, except for the case of AFM.[48]

^{13}C NMR studies on [3-^{13}C]Ala-labeled bR reveal that the C terminal residues, 226–235, participate in the formation of the C terminal α-helix as manifested from the peak position of 15.91 ppm with reference to the conformation-dependent ^{13}C chemical shifts.[68,69,81,82,103] The presence of the α-helix was also proved in view of the corresponding conformation-dependent displacement of peaks from [2-^{13}C] and [1-^{13}C]Ala-bR.[81] Only part of this α-helix was visible by X-ray diffraction,[25] owing to the presence of motions with correlation times of the order of 10^{-6} s, as judged from the carbon spin–lattice relaxation times, T_1^C, and spin–spin relaxation times, T_2^C, under CP-MAS conditions.[81]

This finding is consistent with the earlier hydrophobic fluorescent probe experiment by Renthal and coworkers, who claimed that the C terminal tail of bR is rigidly held at the membrane surface with motion on a timescale of 13–25 ns.[128] Engelhard and coworkers also demonstrated, on the basis of a ^{13}C NMR study of [3-^{13}C] and [4-^{13}C]Pro-labeled bR, that the first part of the C

terminus is fixed to the membrane via salt bridges between divalent cations and negative charges of the C terminus as well as by interhelical loops.[133] In this connection, Yamaguchi *et al.* examined the ^{13}C NMR spectra of [3-^{13}C]Ala-labeled bR and its mutants while varying a variety of environmental or intrinsic factors such as ionic strength, temperature, pH, truncation of the C terminal α-helix, and site-directed mutation at cytoplasmic loops.[104] For instance, increased ionic strength from 10 to 100 mM NaCl causes the high-frequency displacement of the Ala 103 signal of the C–D loop from 17.20 to 17.58 ppm and the reduced peak intensity of the C terminal α-helix at 15.89 ppm, as demonstrated in Fig. 20.[104, 105] Similar spectral changes were also noted by raising the temperature from 20 to 40 °C, decreasing the pH from 7 to 4.5, or site-directed mutagenesis, although simultaneous displacement of the Ala 160 peak of the E–F loop to lower frequencies was also noted.[105] These findings lead to the

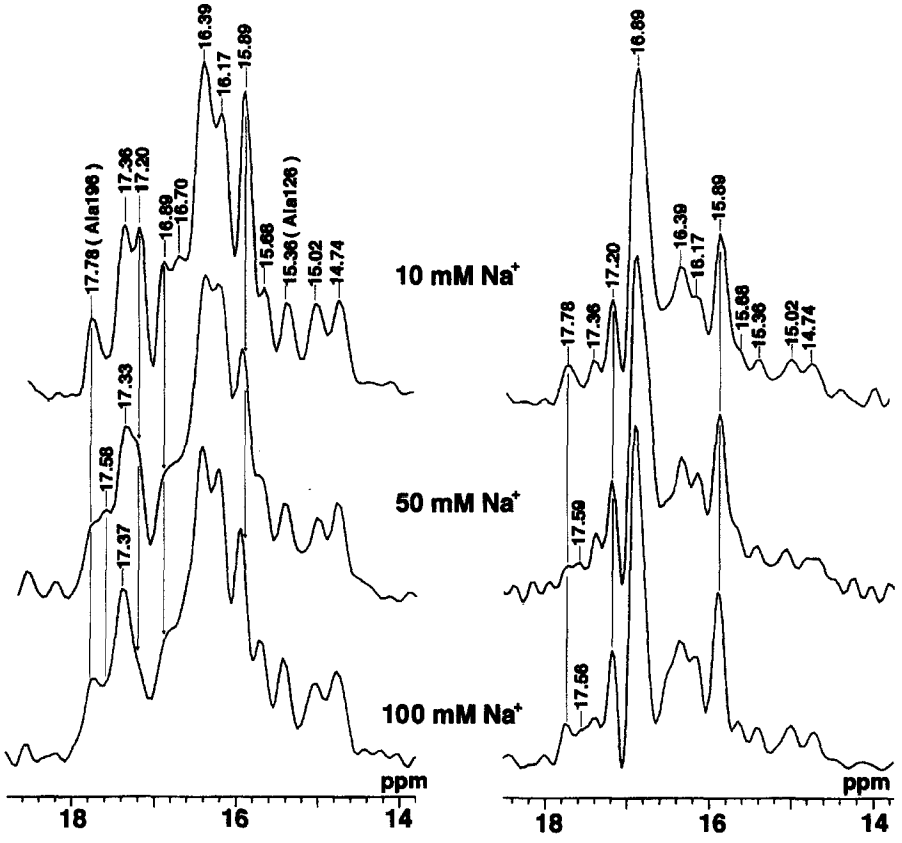

Fig. 20. ^{13}C CP-MAS (left) and DD-MAS (right) NMR spectra of [3-^{13}C]Ala-labeled bacteriorhodopsin recorded at various ionic strengths.[104] Reproduced with permission from Blackwell Science Ltd.

conclusion that the cytoplasmic loops and C terminal α-helix are not present independently but are held together to form the cytoplasmic surface complex stabilized by salt bridges and/or cation-mediated linkages of a variety of side chains, as schematically illustrated in Fig. 21.

In contrast to expectation, it should be borne in mind that no spectral resolution is improved even if the ^{13}C NMR spectra of [3-^{13}C]Ala-bR are recorded at lowered temperatures.[98, 104, 116] Instead, the ^{13}C NMR signals from the C terminal groups, including the C terminal α-helix, are completely suppressed at temperatures below −20 °C owing to a slower fluctuation motion with a correlation time of the order of 10^{-5} s which interferes with the proton decoupling frequency (Fig. 22). Furthermore, the rest of the peaks from the loops and transmembrane α-helices are substantially broadened to the extent of giving featureless peaks. This finding can be interpreted as indicating that the well-resolved ^{13}C NMR peaks of bR in a 2D crystal at ambient temperature are achieved as a result of fast chemical exchange with a rate constant of $10^2\,s^{-1}$ owing to peptide chains taking slightly different conformations with chemical shift differences of the order of 10–10^2 Hz which are observed at low temperatures.[116]

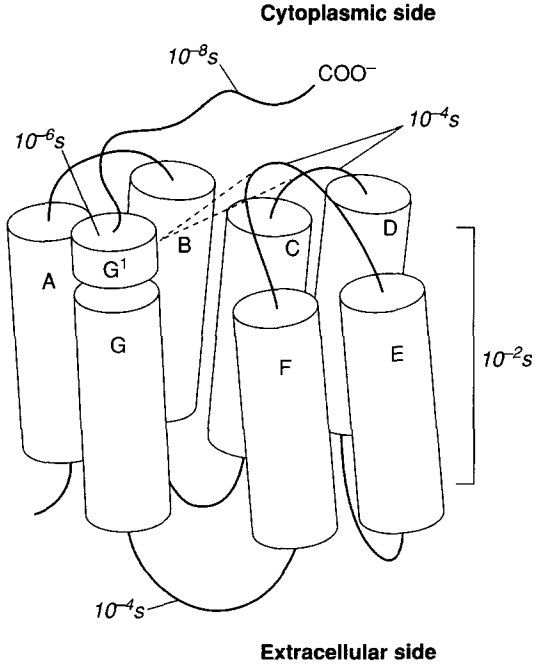

Fig. 21. Schematic representation of the location of the C terminal α-helix (helix G′ protruding from the membrane surface) and interaction with the C–D and E–F loops (indicated by the arrows).

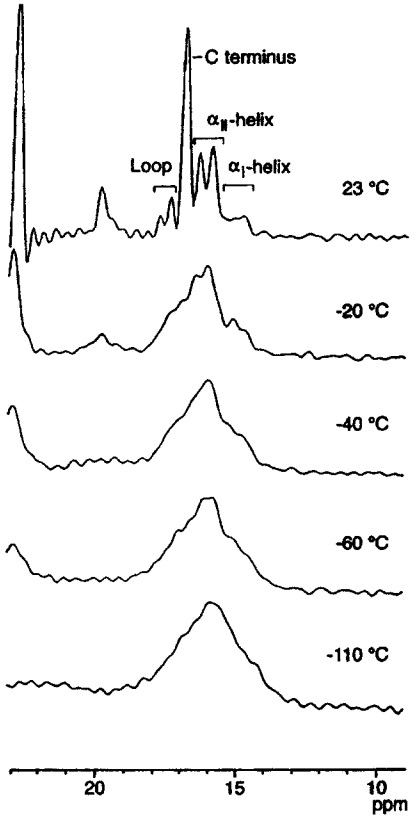

Fig. 22. Temperature-dependent change in the ^{13}C DD-MAS NMR spectra of [3-^{13}C]Ala-labeled bacteriorhodopsin. Reproduced with permission from Blackwell Science Ltd.

7.2. Effect of cations

Two kinds of experimental design are conceivable to gain insight into the problem of this complex surface: to examine the effect of (1) deionization and subsequent titration of metal cations to bR and its mutants and (2) partial neutralization of the electric charges of the amino acid residues located at the cytoplasmic side by site-directed mutagenesis. As to the former approach, it was shown that the ^{13}C NMR spectra of [3-^{13}C]Ala-bR recorded in the deionized state (pH 4) and at a lowered pH (pH 1.2) are almost the same.[5] This is consistent with the view that the removal of surface bound cations results in a lower surface pH. Furthermore, Yonebayashi *et al.* showed that the ^{13}C NMR spectra of [3-^{13}C]Ala-labeled bR and A160G are almost identical under the condition of the deionized state, in spite of their distinctly different spectral features at neutral pH.[105] This is caused by an accelerated fluctuation of the interhelical loops and

the cytoplasmic ends of the B and F helices with correlation times ranging from 10^{-4} to 10^{-5} s and at the cytoplasmic end of the B and F helices from 10^{-2} to 10^{-5} s. This is induced by the complete removal of cations from the surface, as viewed from their suppression of peaks.[105] Moreover, regenerated purple membranes prepared by the addition of 100 mM NaCl to the blue membrane yielded almost the identical spectral pattern to that of the native form. In contrast, irreversible surface structures were regenerated by the addition of Ca^{2+} up to 1 mM to the purple membrane. This means that cation binding is essential for properly maintaining their surface structures, including the above-mentioned complex surface, through binding to surface residues in a non-specific manner, although the presence of divalent cations tends to alter such surface structures in an irreversible manner, depending upon their stereochemical requirements.

In view of the highly halophilic growth condition of bR (ca 4 M NaCl), it is expected that cation binding to a lipid also plays an important role in protein dynamics through lipid–protein interactions as a result of partial electric shielding of the negatively charged groups of lipid molecules at the surface, as schematically illustrated in Fig. 23.[116] This picture was obtained by examination of the simultaneously ^{13}C-labeled peaks of the fatty acyl chain of *Halobacteria* owing to transfer from the fed [3-^{13}C]Ala which resonates at 19.0 and 22.7 ppm. The peaks are unequivocally assigned to the side and terminal methyl groups of the (3R, 7R, 11R)-15-tetramethylhexadecyl group respectively. The former and latter methyl groups are substantially suppressed at −40 and −110 °C (Fig. 22) respectively, in the presence of 10 mM NaCl, although no such spectral change is noted for bR suspended in the same buffer without salt (10 mM NaCl or

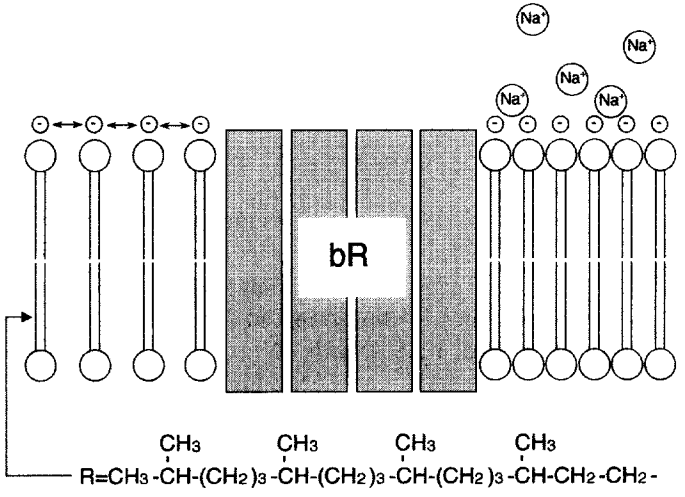

Fig. 23. Schematic representation of repulsive force among negatively charged lipid head groups (left) and the partially screened interaction by the presence of cations as represented by Na^+ ions.

$CaCl_2$). Presumably, an interaction between the acidic polar head groups of phosphatidylglycerophosphate, phosphatidylglycerol, phosphatidylglycerosulfate, and glycolipid sulfate and cations has an important effect on the specific interaction which causes neutralization of negative charge in the acidic polar head group. As a result, partially screened electrostatic interaction in the presence of cations results in the formation of a closely packed lipid organization, as manifested by the suppressed peaks of the side methyl group at –40 °C (owing to slower motion with a correlation time of 10^{-5} s), whereas loosely packed lipid molecules in the absence of cations have no such effect. This finding is consistent with the previous observations by Sternberg *et al.*,[119,120] showing that the presence of 4 M NaCl is essential for the formation of the 2D array of bR trimer, together with lipids from the purple membrane, as studied by reconstituted bilayers. Although such a high ionic strength is not practical from the NMR point of view, it is not always necessary as far as forming samples of 2D hexagonal arrays is concerned. In contrast, it was shown[134] on the basis of an ESR study of spin-labeled phospholipids and freeze-fracture electron microscopy that monomeric bR associated with 18–21 boundary lipids is formed instead of the trimeric form at temperatures above the gel-to-liquid crystalline phase transition of synthetic lipid bilayers.

It is interesting to examine how the partial neutralization of electric charge at amino acid residues located at the cytoplasmic surface modifies the manner of proton entry to the proton pump. Checover *et al.*[135,136] showed that a cluster of three carboxylates, Asp 104, Glu 161, and Glu 234, at the cytoplasmic surface acts as a strong proton attractor site, while one carboxylate, identified as Asp 36, acts as a mediator that delivers the proton to the proton-conducting channel of bR. The replacement of Asp 104 or Glu 161 with cysteine lowers the proton binding capacity of the cluster to 60% of that of the native protein. The replacement of Glu 234 with cysteine disrupts the structure of the cluster, causing the two remaining carboxylates to function as isolated residues that do not interact with each other. Interestingly, this finding is obviously consistent with the above-mentioned view of the cytoplasmic surface complex as revealed by the ^{13}C NMR studies on [3-^{13}C]Ala-labeled bR. Furthermore, it turns out that a ^{13}C NMR study on [1-^{13}C]Val-labeled related mutants, D36N, D38N, D102, D104, D102N/D104N, and E166G, shows an altered dynamic feature of the cytoplasmic surface results with respect to flexibility of the cytoplasmic surface as manifested by the enhanced helical peaks detected by the DD-MAS technique.[88]

7.3. Hydration and dynamics

It is conceivable that the dynamic features of bR are strongly related to the hydration behavior of the protein, in addition to the cation binding described above. To gain insight into this problem, Fig. 24 illustrates how the ^{13}C NMR spectra of [3-^{13}C]Ala-labeled bR vary with the regulated relative humidity (RH).

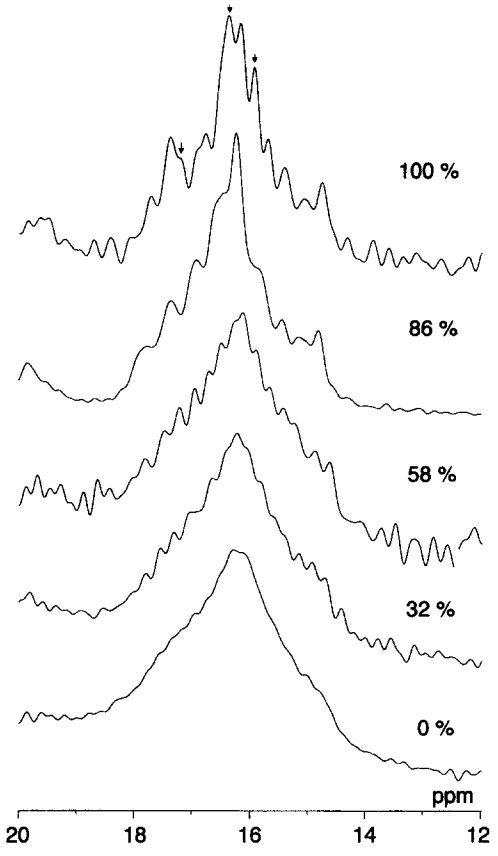

Fig. 24. Hydration-dependent spectral change in [3-^{13}C]Ala-labeled bacteriorhodopsin. Note that the three peaks marked by the arrows visible at 100% hydration are suppressed at a relative humidity lower than 86%.

These measurements were previously performed[14] utilizing lyophilized preparations which were equilibrated in an atmosphere of regulated RH values prior to measurement. It turns out that the recorded ^{13}C NMR spectra of lyophilized preparations are substantially broadened owing to irreversible conformational changes during the dehydration process.[14] It is notable that the three characteristic peaks arising from the C terminal residues (marked by the arrows) disappear from the intact pellet samples at RH <86%, as in the case of the low-temperature study below −10 °C mentioned above. Furthermore, rather featureless spectral patterns are obtained at RH <58% in spite of the intact preparation of bR, as in the ^{13}C NMR spectra recorded at lower temperatures (Fig. 24). This may be a consequence of the similarity of the data between the temperature-dependent change (Fig. 22)[116] and the dehydration/rehydration behavior of the purple

membrane (Fig. 24), studied by measurements of the lamellar spacing by neutron diffraction.[137]

Ferrand *et al.* examined the internal dynamics of bR by inelastic neutron scattering for various conditions of temperature and hydration.[138] For a normally hydrated sample, the onset of low-frequency, large-amplitude anharmonic motions occurs at about 230 K, where a dynamic transition from a low-temperature harmonic regime is observed. In a moderately dry sample, however, in which the photocyle is slowed down by several orders of magnitude, no transition is observed, and protein motions remain approximately harmonic up to room temperature. It is claimed, therefore, that the 'softness' of the membrane modulates the function of bR. As a consequence, internal water molecules buried in the proton-conducting pathways (7±1 at RH 15% by neutron diffraction[139] or 10 by X-ray diffraction[25]) have been believed to be involved in the proton translocation of bR. To clarify the behavior of such internally hydrated proteins, Gottschalk *et al.*[140] recently measured water (^{1}H, ^{2}H, ^{17}O) magnetic relaxation dispersion (MRD) of solubilized bR in micelles of the non-ionic detergent *n*-octyl-β-D-glucoside (OG), where MRD refers to the dependence of the longitudinal, R_1, and transverse, R_2, relaxation rates on the resonance frequency ω_0 as

$$R_1 = 0.2J(\omega_0) + 0.8J(2\omega_0) \tag{4}$$

$$R_2 = 0.3J(0) + 0.5J(\omega_0) + 0.2J(2\omega_0) \tag{5}$$

The spectral density function, $J(\omega_0)$, is modeled as a constant, α, plus a sum of Lorentzian terms, each characterized by an amplitude parameter, β, and a correlation time, τ_c:

$$J(\omega) = \alpha + \Sigma\beta_k\tau_{Ck}[1 + (\omega\tau_{Ck})^2]^{-1} \tag{6}$$

The frequency dependence of the water ^{2}H relaxation data of solubilized bR at 4 °C (Fig. 25) arising from biLorentzian curves were measured and the low-frequency step was studied by

$$1/\tau_c = 1/\tau_R + 1/\tau_w \tag{7}$$

where the inverse of the correlation time, τ_c, is the sum of the protein tumbling rate, $1/\tau_R$, and the water exchange rate, $1/\tau_w$. This means that the relaxation rate is dominated by the much slower isotropic modulation of the coupling brought about by protein tumbling, τ_R, and/or water exchange to the bulk (water residence time τ_w). Indeed, it is found that the relaxation rate is governed by at least seven, and probably all ten, of the crystallographically identified internal water molecules in bR, having residence times in the range 0.1–10 μs at 4 °C. It is claimed that such water exchange could be governed by a plausible conformational fluctuation with a concomitant rearrangement of the hydrogen bond network.

As discussed in Sections 6.2 and 6.3, however, there appears to be no such motion in the transmembrane helices, except for the surfaces, in the ground state

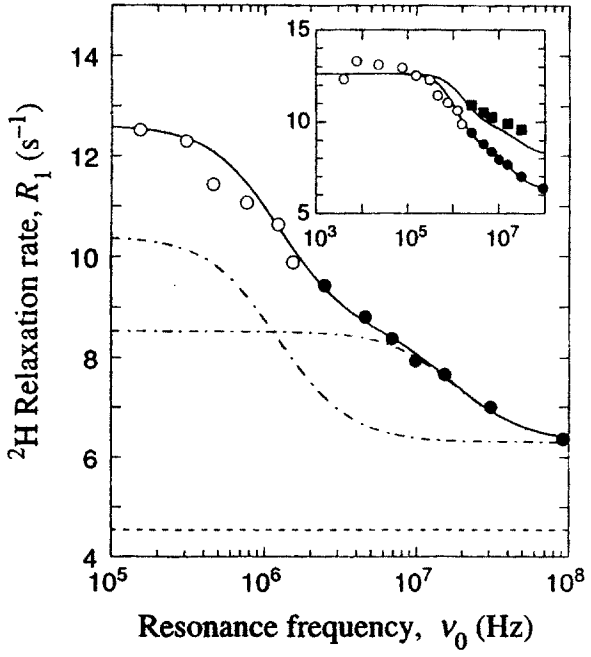

Fig. 25. Frequency dependence of the water ^{2}H longitudinal (circles) and transverse (filled squares) relaxation rates in an aqueous solution of bR solubilized in micelles of *n*-octyl-β-D-glucoside at 4°C.The broken line refers to the relaxation rate of the bulk water, while the continuous curve results from a fit to the data of a biLorentzian function as described in the text.[139] Reproduced with permission from Academic Press Ltd.

of bR. This is in contrast to the data from the solubilized preparation in OG, as manifested by the ^{13}C NMR data of [3-^{13}C]Ala-labeled bR. Nevertheless, the presence of such conformational fluctuation, corresponding to the claimed water residence time, has been located in several transmembrane α-helices viewed from the *dynamics-dependent* suppressed peaks as demonstrated for bO,[98] and several kinds of mutant such as A160G [104] and D85N taking the M-like state.[107] In particular, in addition to the apparently low-intensity peaks of the ^{13}C NMR spectra of [3-^{13}C]Ala-labeled D85N at 16.34 ppm, arising from the suppressed peaks at 16.41 ppm (including Ala 39, helix B) and 16.19 ppm (including Ala 215, helix G) at pH 7 (Fig. 13), a further reduction in the peaks at 16.62 ppm is noteworthy, due to the additionally suppressed peaks at 16.34 ppm (including Ala 53, helix B) and 15.96 ppm [Ala 51, helix B, and Ala 103, 160, and 196 (for C–D, E–F and F–G loops respectively)] upon raising the pH from 7 to 10 to deprotonate the Schiff base. Obviously, such a spectral change is caused by the acquisition of conformational fluctuation in helices B, F, and G as well as the C–D, E–F, and F–G loops with correlation times of the order of 10^{-5} s by taking the M-like state.[117]

The presence of the induced conformational change in the transmembrane α-helices by protonation of Asp 85 is more evident from the high-frequency displacement of the two arrowed ^{13}C NMR peaks, from 174.62 to 175.05 ppm and from 177.02 to 177.81 ppm in the ^{13}C NMR spectra of [1-^{13}C]Val-labeled D85N or D85N/D96N mutants at neutral pH. The latter peak displacement is due to Val 213 (helix F) participating in a strengthened hydrogen bond network (see Fig. 10) induced by modified electrostatic interactions between Asp 85 and Asp 212.[118] Interestingly, these two peaks are suppressed at pH 10, owing to the acquisition of motion with a correlation time of the order of 10^{-4} s as a result of taking the M-like state (Fig. 26).[117] Concomitantly, the Val 49 peak (helix B) is

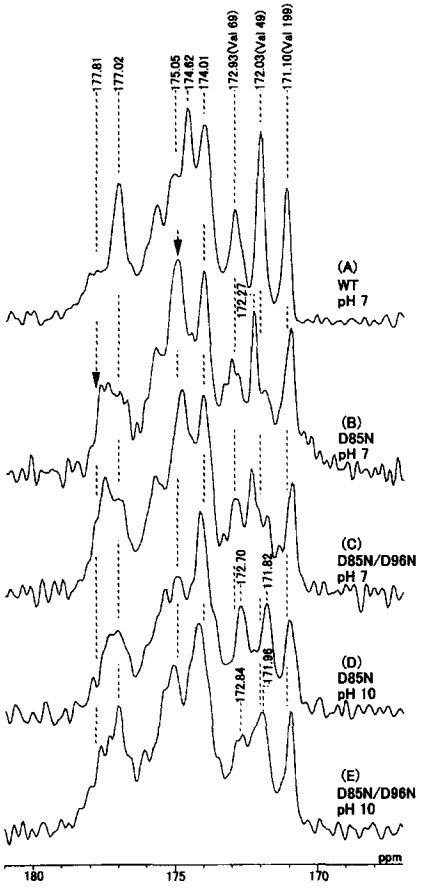

Fig. 26. ^{13}C CP-MAS NMR spectra of [1-^{13}C]Val-labeled wild type (A) and D85N (B and D) and D85N/D96N (C and E) recorded at pH 7 and 10. It is noteworthy that the arrowed peaks from the transmembrane helices are displaced to higher frequencies by protonation of Asp 85 at neutral pH and suppressed at pH 10 taking the M-like state.[117] The peak at 177.81 ppm is ascribed to Val 213.[88] Reproduced with permission from the American Chemical Society.

also suppressed at pH 10 with reference to a study of D85N/V49A mutant,[141] although this was initially claimed as the low-frequency displacement of a peak. Undoubtedly, it appears that such conformational changes as well as fluctuations are necessary, from the biological point of view, for the entry of retinal into bO to form bR (Fig. 15) or the proton translocation process in the pump activity in bR, as mentioned above.

8. TRANSMEMBRANE PEPTIDES AS A COMPONENT OF BACTERIORHODOPSIN

It is a common practice to utilize chemically synthesized transmembrane peptides instead of intractable whole membrane proteins, as a first step, to understand their folding behavior, partial 3D structure, and the consequences in relation to their biological significance. Justification of such an approach is in many instances not always straightforward, unless the subsequent results are comparable with those of the whole intact protein system. Fortunately, the present ^{13}C NMR results available from ^{13}C-labeled intact bR can serve as a very convenient reference system to examine how effectively a model approach utilizing chemically synthesized transmembrane peptides can mimic the intact system, and meaningful conclusions can be drawn.

As discussed in Section 5.2, the ^{13}C chemical shifts of the single-span transmembrane peptides so far examined are not always the same as those of intact bR.[16] This is because the displacement of the peaks differs among the peptide sequences of the transmembrane peptides and also according to the manner of the helix–helix, retinal–helix, or lipid–helix interactions which are most pronounced in intact bR. In addition, the ^{13}C DD-MAS spectra of the enzymatically cleaved [3-^{13}C]Ala-labeled C-2 fragment (1–71), consisting of helices A and B as well as the A–B loop, incorporated into a bilayer of DMPC or lipids of *Halobacterium* (Figs 27A and B respectively), are compared with the ^{13}C CP-MAS NMR spectrum of intact bR (Fig. 27C).[16] Interestingly, the highest-frequency signal of the C-2 fragment, occurring at 17.5 ppm, can be ascribed to the loop region, although no Ala residue is located in the loop of the C-2 fragment present in intact bR (see Fig. 4). In contrast, the lowest-frequency peak of the peptides spanning the lipid bilayer once is at 16.9 ppm, which is characteristic of the random coil conformation (see Table 4). Therefore, the peak at 17.5 ppm should be ascribed to an Ala residue in a newly formed loop structure as a result of the disposition of the peptide in a bilayer from the original transmembrane α-helix. The most probable candidate is Ala 39 in transmembrane peptide B, which is flanked by the hydrophilic amino acid residues Asp 38 and Lys 49 and seems to be stabilized in the aqueous phase rather than the lipid environment if the constraint to keep this residue in the lipid bilayer in intact bR is removed by the proteolytic cleavage. Furthermore, it is evident from the ^{13}C chemical shifts of [3-^{13}C]Ala-labeled transmembrane peptides **6** and **11**,

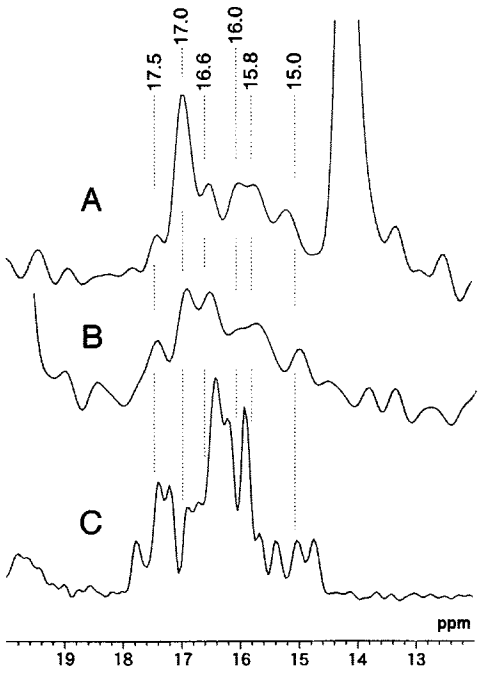

Fig. 27. ^{13}C DD-MAS NMR spectra of enzymatically cleaved [3-^{13}C]Ala-labeled C-2 fragment (1–71) incorporated into the DMPC bilayer (A) and lipids from *Halobacterium* (B) with reference to the CP-MAS NMR spectrum of intact bacteriorhodopsin.[16]

summarized in Table 4, that Ala 39 and Ala 160 take random coil conformations (16.9 ppm) as a result of protruding from the membrane surface. This occurs regardless of their original positions as transmembrane α-helix B and E–F loop respectively in intact bR. The presence of the Ala 39 originally in helix B in the aqueous phase is due to the same factor as mentioned above for the C-2 fragment. The presence of Ala 160 as a random coil is due to the cleavage at the E–F loop. Therefore, the possibility of the disposition of any transmembrane peptide in lipid bilayers that is different from the original arrangement in the intact proteins should always be taken into account when designing a new experimental protocol.

It is possible to determine the angle by which any transmembrane peptide is tilted from the bilayer normal as in the intact protein, if use is made of a spontaneously magnetically aligned lipid bilayer system, as discussed in Section 10.2. Recently, Kimura *et al.*[142] measured the ^{13}C NMR spectra of [1-^{13}C]Ala14-labeled A(6–34) incorporated into a DMPC bilayer containing dynorphin (a heptadeca-opiod peptide with very high affinity for an opioid receptor) as an essential component facilitating the spontaneous alignment of the bilayer to the applied magnetic field (dynorphin: DMPC = 1:10).[143] They found on the basis of

^{31}P NMR and ^{13}C NMR studies on the lipid structure and the ^{13}C chemical shift anisotropy of the incorporated peptide, respectively, that the transmembrane peptide A(6–34) is oriented parallel to the bilayer normal irrespective of the reorientational motion about the helical axis at temperatures above the lowered gel-to-liquid crystalline phase transition.

As briefly described in Section 6.1, an attempt was made to determine the intrachain hydrogen bond distance [N–H(Ala 18)]···O=C(Ala 14)] in the doubly [1-^{13}C]Ala 14 and [^{15}N]Ala 18-labeled transmembrane peptide A(6–42) (Fig. 28) at −30°C by a REDOR experiment.[113] For this purpose, the corrected REDOR differences are evaluated as

$$\Delta S/S_0 = (S_{\text{full echo}} - S_{\text{REDOR}})/(S_{\text{full echo}} - S_{\text{natural abundance}}) \tag{8}$$

when the full echo intensity (Fig. 29a) is superimposed upon the natural abundance peaks of the unlabeled carbonyl peak of amino acid residues other than that of the Ala 14 under consideration (Fig. 29c). This is in contrast to the ordinary REDOR difference without overlaps of signals from the peaks of natural abundance, which is defined as

$$\Delta S/S_0 = (S_{\text{full echo}} - S_{\text{REDOR}})/S_{\text{full echo}} \tag{9}$$

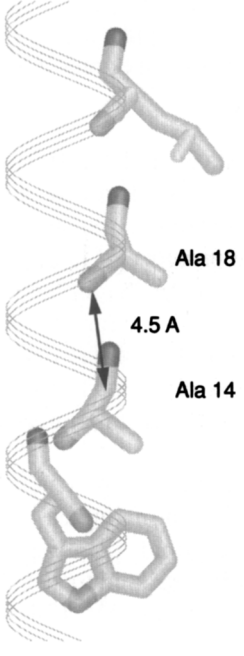

Fig. 28. Measured interatomic distance between ^{15}N-H(Ala 18)···O=^{13}C (Ala 14) by rotational echo double resonance (REDOR).[113]

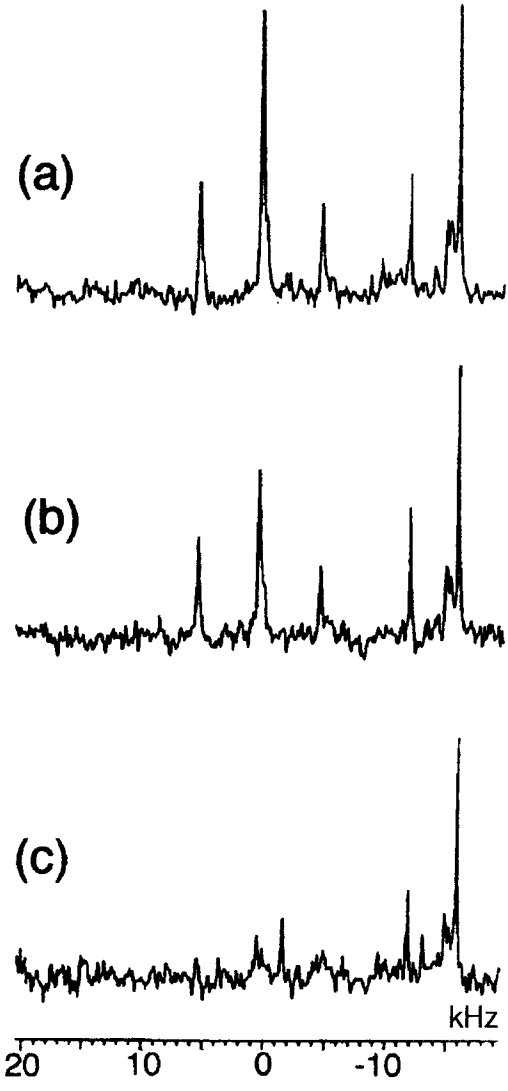

Fig. 29. ^{13}C full echo (a), REDOR (b), and natural abundance spectra (c) of a [1-^{13}C]Ala 14-labeled A(6–42) fragment of bacteriorhodopsin in the DMPC bilayer at N_cT_r of 19.2 ms, recorded at –30°C.[113] Reproduced with permission from Elsevier Science.

where, S_{REDOR}, $S_{full\ echo}$, and $S_{natural\ abundance}$ are the peak intensities of REDOR, full echo without correction of natural abundance, and full echo from natural abundance respectively. The corrected REDOR factors $\Delta S/S_0$ thus obtained are plotted against the various N_cT_r values (Fig. 30) together with the best-fit curve corresponding to a distance of 4.5±0.1 Å among the theoretically calculated REDOR factors of the C···N distance,[111] where N_c and T_r are the number of rotor

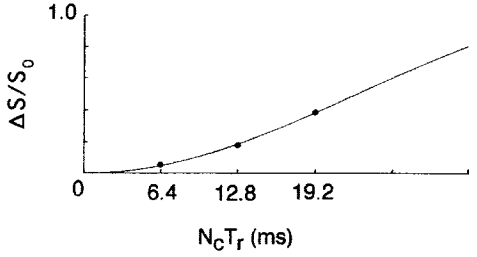

Fig. 30. Plot of the corrected REDOR factors of a [1-^{13}C]Ala 14-labeled A(6–42) fragment in the DMPC bilayer against the N_cT_r values. The experimental data are fit to the theoretical curve with r_{CN} =4.5±0.1 Å.[113] Reproduced with permission from Elsevier Science.

cycles and rotor periods, respectively.[108, 109] This helix turns out to be a normal α-helix as viewed from the similarity of the resulting distance to that of the solid state and also from the principal components of the ^{13}C chemical shift tensor, in spite of the ^{13}C NMR signal of the Ala C_β position being that of the α_{II}-helix. In the data analysis, there was no need to introduce an effective ^{13}C–^{15}N dipolar coupling as encountered for gramicidin A which undergoes fast reorientational motion in the lipid bilayer,[144] because the ^{13}C chemical shift tensor proved to be static in the DMPC bilayer even at 20 °C.[111] This technique was recently applied to measure the ^{15}N–^{13}C distance in the retinal binding pocket of [*indole*–^{15}N]Trp, [14-^{13}C]retinal-labeled, dark-adapted bR.[145]

9. LOCAL CONFORMATIONAL CHANGE ASSOCIATED WITH PROTON PUMPING

It was suggested that translocation of a proton from the cytoplasmic surface to the extracellular surface is associated with a protein conformational change.[146, 147] It has been recognized that the first proton transfer in the photocycle of bR is from the protonated Schiff base to the anionic Asp 85, in the L to M reaction. This protonation induces proton release from the proton release complex (PRC), involving Glu 194 and Glu 204,[148–152] and proton transfer from the protonated Asp 96 to the Schiff base[50] (see Fig. 5). This finding suggests that the signaling of the protonation at Asp 85 could be transmitted to both the extracellular and cytoplasmic sides through specific long-range interactions. Tanio *et al.*[97, 153] recorded the ^{13}C NMR spectra of a variety of site-directed mutants in order to clarify how such interactions could be modified by changes in electric charge or polarity in the mutants. They observed the significant displacement of the [1-^{13}C] signals from the Val 49 located at the transmembrane B helix and displacement or suppression of the [3-^{13}C]-labeled Ala 196 or [1-^{13}C]-labeled Val 199 residues located at the F–G loop in R82Q, D85N, D96N, E194Q, E194D, and E204Q mutants respectively. This finding is consistent with the expectation that such an interaction

should also exist in bR even in the unphotolyzed state, among the backbone, side chains, bound water molecules, etc. Indeed, there may be a long-range interaction between Asp 96 and the extracelluar surface through Thr 46, Val 49, Arg 82, Asp 85, Glu 194, and Glu 204 in the unphotolyzed state.

In this connection, it is notable that the Ala C_β ^{13}C NMR peak of Ala 126 is displaced to high frequency in D85N, Y83F, E194Q, E194D, and E204Q (see Fig. 11 for D85N), whereas it resonates at the normal position for D85N/R82Q and R82Q (see Fig. 31 for the former). To explain these observations, Tanio *et al.*[153] proposed the role of Arg 82 as an information mediator that transmits the effect of the protonation state of Asp 85 to the Ala 126 region of the extracellular surface. This is because the C_β of Ala 126 is in van der Waals contact with the OH of Tyr 83. This could be made possible by displacement of the side chain of Arg 82 towards Tyr 83 which is located between Arg 82 and Ala 126 (Fig. 32). Support for this view is given by the displacement of the Ala 126 signal in mutants of Asp 85, Glu 194 and Glu 204 but not in mutants of Arg 82. Indeed, reorientation of Arg 82 has been observed by X-ray diffraction studies on the M intermediate of the wild type[154] and D96N and E204Q,[155,156] in which Asp 85 is protonated and the Schiff base is deprotonated. Petkova *et al.*[157] also propose, on the basis of a ^{15}N NMR study on $[\eta_{1,2}\text{-}^{15}N_2]$-labeled bR and D85N mutant, that one arginine, probably Arg 82, is perturbed in the M intermediate trapped at −44 °C in the presence of 0.3 M guanidine chloride and D85N respectively. It should be expected that these conformational changes cause transient p*K*a changes in the protein that drives the proton transfer.

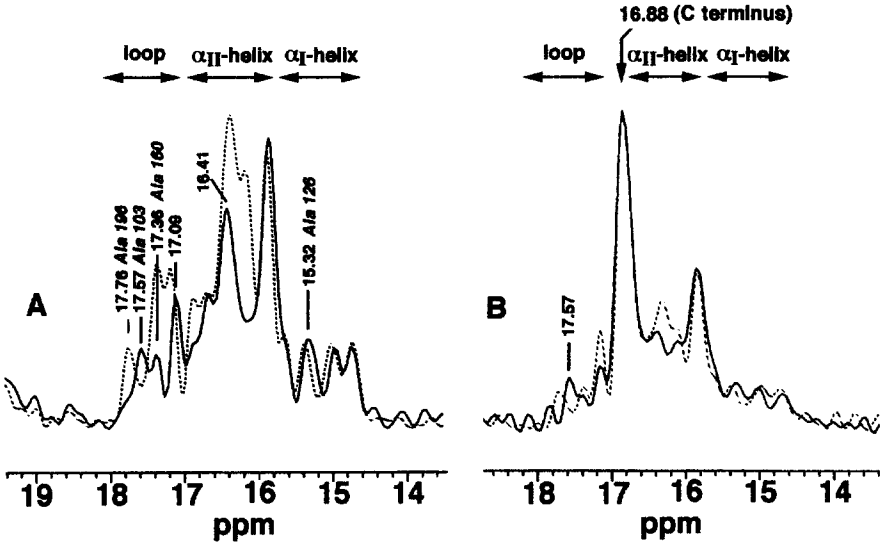

Fig. 31. ^{13}C CP-MAS (left) and DD-MAS (right) NMR spectra of the [3-^{13}C]Ala-labeled D85N/R82Q mutant at pH 7.

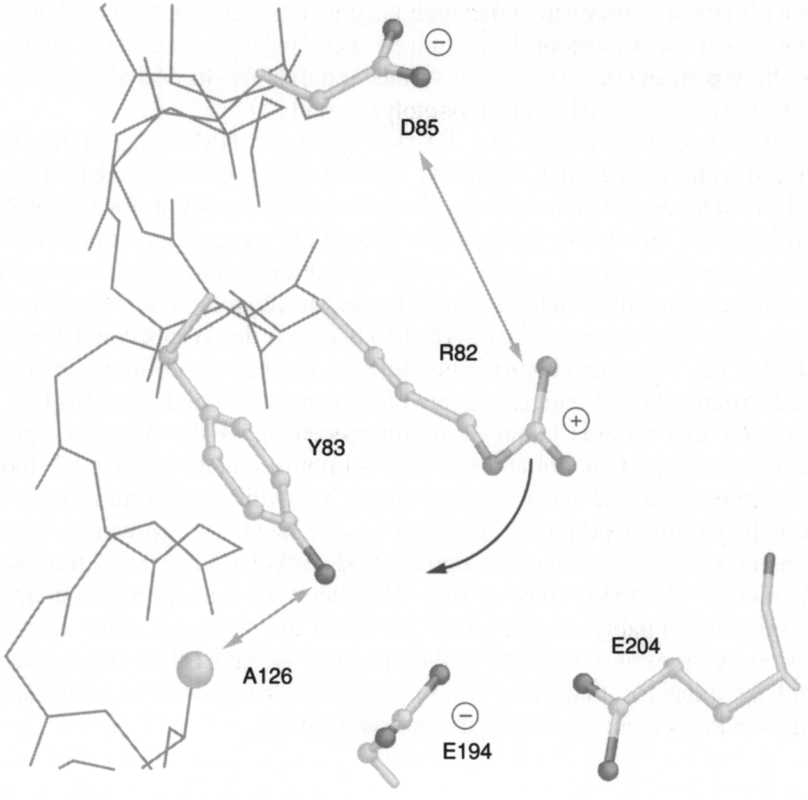

Fig. 32. Schematic representation of the displacement of the side chain of Arg 82 towards Tyr 83 owing to protonation.

It is notable that the other signal transfer in bR is found between Asp 96 and the C terminal tail.[117] The observation of the peak arising from the C terminal α-helix at 17.9 ppm from [3-^{13}C]Ala-labeled D85N at pH 10 is characteristic of the presence of the M-like state of this protein. This peak, however, disappeared from the D85N/D96N mutant at pH 10. This distinction may be ascribed to the effect of the electric charge at Asp 96 which is responsible for the proton uptake from the cytoplasmic side (see Fig. 5), because there is no such charge in the D85N/D96N mutant. This observation is consistent with the finding by Dioumaev *et al.* that the p*K*a of Asp 96 in D85N is lower than that of the wild type.[158] This result suggests that the deprotonation of Asp 96, under the protonated Asp 85 in the photocycle, is accompanied with a conformational change in the C terminal α-helix through modulation of the surface complex among the loops and the C terminal α-helix.[117]

10. OTHER PROTEIN SYSTEMS

10.1. Unoriented systems

G-protein coupled receptors (GPCRs) form the largest known family among integral membrane proteins, up to 5% of all genes encoded in the genomes of higher eukaryotes.[159] Their highly conserved topology is made up of seven transmembrane helices like bR and functions as a transducer of extracellular signals like hormones, pheromones, odorants, or light into the activation of the intracellular G-protein complex. Rhodopsin is a typical GPCR, active as a mammalian photoreceptor protein of 40 kDa covalently linked to 11-*cis* retinal through Lyls 296. Absorption of a photon by the 11-*cis* retinal causes its isomerization to all-*trans* retinal, leading to a conformational change in the protein moiety, including the cytoplasmic surface. Its 3D structure of 2.8 Å has been recently resolved by X-ray diffraction[160] and serves as an important molecular basis for the understanding of vision as well as of signal transductions for a variety of GPCRs.

Verdegem *et al.*[161] measured the C10–C20 and C11–C20 distances of a selectively ^{13}C-labeled retinylidene chromophore incorporated in bovine rhodopsin by rotational resonance experiments,[162] to examine the spatial structure of the C10–C11=C12–C13–C20 motif in the native chromophore, its 10-methyl analogue, and predischarge photoproduct metarhodopsin I. Furthermore, it was shown[163] that the ^{13}C shifts of regenerated rhodopsin with 11-Z-[8,9,10,11,12,13,14,15,19,20-$^{13}C_{10}$] retinal were recorded and sequentially assigned using 2D correlation spectroscopy and a dipolar recoupling experiment.[164,165] The chemical shift data obtained were used to measure the extent of delocalization of positive charge into the polyene. Gröbner *et al.* recorded the ^{2}H MAS NMR (MAOSS)[166] spectra of oriented regenerated bovine rhodopsin with [18-C($^{2}H_3$)]retinal stacked on glass plates both in the dark and M_1 states to determine the orientation of the methine C to methyl group vectors C5–C18, C9–C19, and C13–C20 relative to the membrane normal.[167] The two chromophore structures are consistent with the minimum energy conformation available from recent molecular orbital calculations which include extensive electron configuration interaction.[168] It is claimed that the discrepancies revealed between ^{2}H NMR and X-ray diffraction data might be caused by differences in lipid (or detergent) environment. Feng *et al.* recently determined a molecular torsion angle of the chromophore in the metarhodopsin-I photointermediate of rhodopsin by double quantum solid-state NMR.[169]

Apart from the above-mentioned studies using a ^{13}C-labeled chromophore, Eilers *et al.*[170] reported a ^{15}N and ^{13}C NMR study on regenerated bovine rhodopsin obtained from the apoprotein expressed by using suspension cultures of HEK2935 cells in defined media containing 6-^{15}N-lysine and 2-^{13}C glycine, with a yield of the protein of 1.5–1.8 mg/L^{-1}. After generation of the rhodopsin pigment by the addition of 11-*cis* retinal, the whole cell was pelleted and

solubilized with octyl-β-glucoside. For the MAS NMR experiments the labeled rhodopsin, after purification by a Sepharose column, was concentrated and reconstituted into dioleolyl phosphatidylcholine (DOPC) vesicles by dialysis. Creemers *et al.*[171] used the recombinant baculovirus Sf9 cell line (ATTC CRL-1711) to prepare 10 mg of [α,ε-^{15}N]Lys-labeled rhodopsin from two 5 L culture batches. They further reconstituted the protein into bovine retina lipids. Both groups tried to estimate the effective Schiff base counterion distance in rhodopsin on the basis of an empirical relationship between the observed ^{15}N chemical shifts of the protonated 11-*cis* retinylidene-butyl ^{15}N-imides and the inverse of the center-to-center distance squared of the crystallographic radii of N^3 and the halide counter ion.[172,173]

The resulting effective Schiff base counterion distance of greater than 4 Å is consistent with the presence of structural water in the binding site hydrogen bonded with the Schiff base nitrogen and Glu 113 counterion.[170,171] It seems to be too premature to draw any meaningful conclusion from the ^{13}C NMR spectrum of [2-^{13}C]Gly-labeled rhodopsin, because of the lack of assigned peaks based on background knowledge such as in bR.

Recently, light-induced structural changes in ^{19}F-labeled mammalian rhodopsin solubilized in detergent micelles were examined by solution ^{19}F NMR after attachment of the trifluoroethylthio (TET) CF3–CH2–S group through disulfide linkages to cysteine mutants prepared from the HEK2935 cell line containing the single cysteine opsin mutant genes.[174] On illumination, to form metarhodopsin II, low-frequency changes in chemical shifts are observed for the ^{19}F labels at positions 67 (–0.2 ppm) and 140 (–0.4 ppm) and high-frequency changes for positions 248 (+0.1 ppm) and 316 (+0.1 ppm), all of which are at the cytoplasmic surface. The solution ^{19}F nuclear Overhauser effects were used to examine the close proximity between the two ^{19}F-labeled residues at the cytoplasmic domain.[175]

The photosynthetic reaction centers (RCs) from purple bacteria such as *Rps. viridis* and *Rb spaeroides* are the first membrane proteins to be described at atomic resolution by X-ray diffraction.[2,17,176,177] The RC from *Rb spaeroides* is a transmembrane protein complex consisting of three polypeptide chains (L, M, and H) and nine cofactors [two bacteriochlorophylls $(BChl)_2$ forming the so-called special pair (P), two accessory bacteriochlorophylls, two bacteriopheophytins (P_A and P_B), two quinines (Q_A and Q_B), and one Fe^{2+} ion arranged in an almost C_2 symmetry. Solid-state NMR studies[178–184] for RCs from *Rb spaeroides* have been performed to locate the ^{13}C NMR signals of [4′-^{13}C]Tyr-enriched preparations,[178] to probe the electronic state of reconstituted cofactors of ^{13}C-enriched ubiquinone-10 [179] and pheophytin,[79] and to study the RCs by 1D or 2D CP-MAS techniques using the frozen detergent-solubilized state. Light-induced strongly polarized ^{15}N or ^{13}C NMR signals are observed from the cofactors of a natural abundance or a ^{15}N labeled sample[180–183] when forward electron transfer from the special pair P is blocked either by removal or pre-reduction of the quinone Q_A as an electron acceptor. The samples used were

dialysis precipitates against detergent-free buffer and then a water or frozen detergent-solubilized preparation. This photochemically induced dynamic nuclear polarization (photo-CIDNP)[184] experiment proved to be a very valuable means for examining information about the electron density in P in the radical pair, the spin density distribution of tetrapyrrole cofactors, and the asymmetric electronic structure of P^{+} in the primary donor.

The LH2 complex is a peripheral photosynthetic antenna pigment protein utilized to absorb light and to transfer the excited-state energy to the light-harvesting LH1 complex surrounding the RC.[2] The crystal structure of the LH2 of *Rps. acidophilia*[185] shows a ring structure of nine identical units, each containing an α and a β polypeptide, 53 and 41 respectively, which both span the membrane once as α-helices. The two polypeptides bind a total of three chlorophyll molecules and two carotenoids. The nine heterodimeric units form a hollow cylinder, with the α chains forming the inner wall and the β chains the outer wall.[2] Instead of the whole complex, Alia *et al.*[186] recorded ^{15}N and ^{13}C NMR spectra of one protomer of the [$^{13}C_6$, $^{15}N_3$]-, [π-^{15}N]-, and the [τ-^{15}N]-histidine-labeled LH2 complex solubilized in detergent at 225 K, to gain insight into the charged state of histidines and the hydrogen bonding status in this complex. Subsequently, Egorova-Zachernyuk *et al.*[187] recorded heteronuclear 2D correlation spectra of the uniformly [^{13}C, ^{15}N]-labeled LH2 complex in the frozen state of detergent-solubilized preparation. The spectral separation observed is not sufficient to draw any meaningful conclusion from their data at present. In particular, dynamic features such as for the membrane protein are unavailable from this frozen solution experiment.

Solid-state REDOR NMR distances of the serine bacterial chemotaxis receptor were measured to characterize the specific structural feature of the ligand binding site interactions in the intact, membrane bound receptor, by preparing a [^{15}N]Ser bound to a [^{13}C]Phe receptor of 60 kDa.[188] Furthermore, $^{13}C\cdots^{19}F$ distances were measured for a [1-^{13}C]cysteine and [*ring*-4-^{19}F]phenylalanine-labeled protein, which show a ligand-induced conformational change of 1.0±0.3 Å in the $\alpha 1$ and $\alpha 4$ chains.[189] It should be taken into account that there remains the possibility of conformational distortion during the process of lyophilization, even though an attempt to freeze the inherent backbone and side-chain motions leads to inevitable errors arising from REDOR measurements.

10.2. Oriented systems

Lipids can be macroscopically oriented by attaching the lipid–water dispersions on flat glass plates because the lipid orientation is achieved by mechanical shearing forces. Alternatively, lipid molecules themselves can be aligned spontaneously to the magnetic field because of their diamagnetic anisotropy. The interaction of the diamagnetic anisotropy and the magnetic field is given by

$$F = -(1/2)B_0^2\{\chi_\perp + (\chi_\parallel - \chi_\perp)\cos^2\theta\} \quad (8)$$

where F is the interaction energy and $\chi_\perp$ and $\chi_\parallel$ are the perpendicular and parallel components of the magnetic susceptibility, respectively, and θ is the angle between $\chi_\parallel$ and the magnetic field B_0. Therefore, the orientation energy of the lipid bilayer with N lipids is expressed as

$$N\Delta F = -(1/2)N\Delta\chi B_0^2 \quad (9)$$

where, $\Delta F = F(\theta=0°) - F(\theta=90°)$ and $\Delta\chi = \chi_\parallel - \chi_\perp$. If N is a small number, the orientation energy is not sufficient to align the macrodomain of the lipid bilayer, because the thermal energy, kT, tends to disturb the alignment. In the case of phospholipid bilayers, a macrodomain containing 10^6 lipid molecules can have sufficient energy for spontaneous alignment in the magnetic field.

Magnetic ordering of lipid bilayers has been reported for pure and mixed phosphatidylcholine bilayers,[190–194] including melittin–phospholipid systems.[11,195–197] Subsequently, such magnetic ordering occurs in a detergent/lipid mixture, called a bicelle,[9,10,198,199] which is shown to be oriented in a magnetic field by the negative magnetic anisotropy of the lipid acyl chain. Therefore, the acyl chain tends to orient perpendicular to the magnetic field if a large number of lipid molecules are ordered in the liquid crystalline phase possessing a sufficient degree of magnetic anisotropy to align the lipid bilayers along the magnetic field direction.

As described in Section 8, a DMPC bilayer containing a moderately high concentration of melittin (DMPC:melittin = 10:1 molar ratio) is subject to lysis and fusion at temperatures lower and higher than T_m, respectively.[11] Giant vesicles are formed at a temperature above T_m, resulting in magnetic ordering. Therefore, it is suggested that elongated bilayer vesicles in which most of the surface area of the bilayers is oriented parallel to the magnetic field are formed rather than discoidal bilayers. This is because a large magnetic anisotropy can be induced owing to the negative magnetic anisotropy of the acyl chain axes. Similar magnetic alignment, by forming elongated vesicles, is found in DMPC lipid bilayer systems containing the opioid peptide dynorphin A(1–17).[142,143] This system was further used to investigate the orientation and structure of the bR fragment incorporated into the dynorphin–DMPC bilayer system which keep the magnetic orientation.[142]

The mechanically aligned lipid bilayer system in which the acyl chain can be aligned perpendicular to the glass plate is an excellent system for study since it allows any orientation of the glass plate with respect to the magnetic field. However, this system is not suitable for fully hydrated samples (up to 50% at most), and the NMR sensitivity is inevitably low owing to the low filling factor of the glass plates in the NMR coil. Orientation of peptides bound to the magnetically aligned lipid bilayer can be examined by looking at the chemical shift anisotropy of the carbonyl carbon in the backbone in the peptide chain. In particular, when an α-helix rotates about the helical axis, it is possible to determine the orientation angle of the α-helical axis with respect to the bilayer

normal.[11] The tilt angle of the α-helix with respect to the average helical axis can be determined by comparing the anisotropic patterns of the carbonyl carbons of consecutive amino acid residues which form the α-helix with the chemical shift values of the corresponding magnetically aligned state. This relies on the fact that the angle between the consecutive peptide planes is 100° in the case of an ideal α-helix.

Similar information can be obtained by looking at the ^{15}N–^{1}H dipolar interaction of the peptide backbone. The PISEMA (Polarization Inversion Spin Exchange at the Magic Angle) experiment gives excellent resolution for the dipolar dimension in the correlation spectra between the ^{15}N chemical shift values and the ^{15}N–^{1}H dipolar interaction.[200] It is of interest to note that a characteristic circle pattern, called PISA (Polarity Index Slant Angle) wheels, is seen when an α-helix is formed in the membrane, and the shape of the wheel is sensitive to the tilting angle of the α-helix with respect to the bilayer normal.[13,200–203] By observing this PISA wheel, it is possible to know the amino acid residues involved in the α-helix even if the amino acid sequence is not known.

It is essential to consider the ^{13}C=O chemical shift tensor to evaluate the orientation of the averaged α-helical axis of peptides bound to the magnetically oriented lipid bilayer in the case where the C=O axis is parallel to the helical axis. The α-helical axis is thus defined by the polar angles α and β with respect to the principal axes of the ^{13}C=O chemical shift tensor, as shown in the top of Fig. 33. When the averaged α-helix is inclined by θ to the static magnetic field, the observed ^{13}C chemical shift value, δ_{obs}, for the rotating α-helix in the magnetically oriented state obtained from the static experiment can be given by

$$\delta_{obs} = \delta_{iso} + (1/4)(3\cos^2\theta-1)[(3\cos^2\beta-1)(\delta_{33} - \delta_{iso}) + \sin^2\beta\cos2\alpha(\delta_{11} - \delta_{22})] \quad (10)$$

When $\theta = 0°$, the α-helical axis is considered to be parallel to the static magnetic field. In that direction, δ_{obs} is denoted as $\delta_{\parallel}$ and is given by

$$\delta_{\parallel} = \delta_{iso} + (1/2)[(3\cos^2\beta - 1)(\delta_{33} - \delta_{iso}) + \sin^2\beta\cos2\alpha(\delta_{11} - \delta_{22})] \quad (11)$$

When $\theta = 90°$, the α-helix is perpendicular to the static magnetic field, and then δ_{obs} corresponds to $\delta_{\perp}$ and is expressed as

$$\delta_{\perp} = \delta_{iso} - (1/4)[(3\cos^2\beta - 1)(\delta_{33} - \delta_{iso}) + \sin^2\beta\cos2\alpha(\delta_{11} - \delta_{22})] \quad (12)$$

Using equations (11) and (12), equation (13) can be obtained:

$$\delta_{obs} = \delta_{iso} + (1/3)(3\cos^2\theta - 1)(\delta_{\parallel} - \delta_{\perp}) \quad (13)$$

This relation makes it possible to predict that the α-helix is parallel to the magnetic field when δ_{obs} is displaced to high frequency until $\delta_{\parallel}$, while the α-helix is perpendicular to the magnetic field when δ_{obs} is displaced to low frequency until $\delta_{\perp}$, as shown in Figs 33d and f respectively, for the case where $\delta_{\parallel}$ appears at a higher frequency than $\delta_{\perp}$. Generally, the orientation of the α-helical axis with respect to the lipid bilayer surface, θ, can be determined by using equation (13)

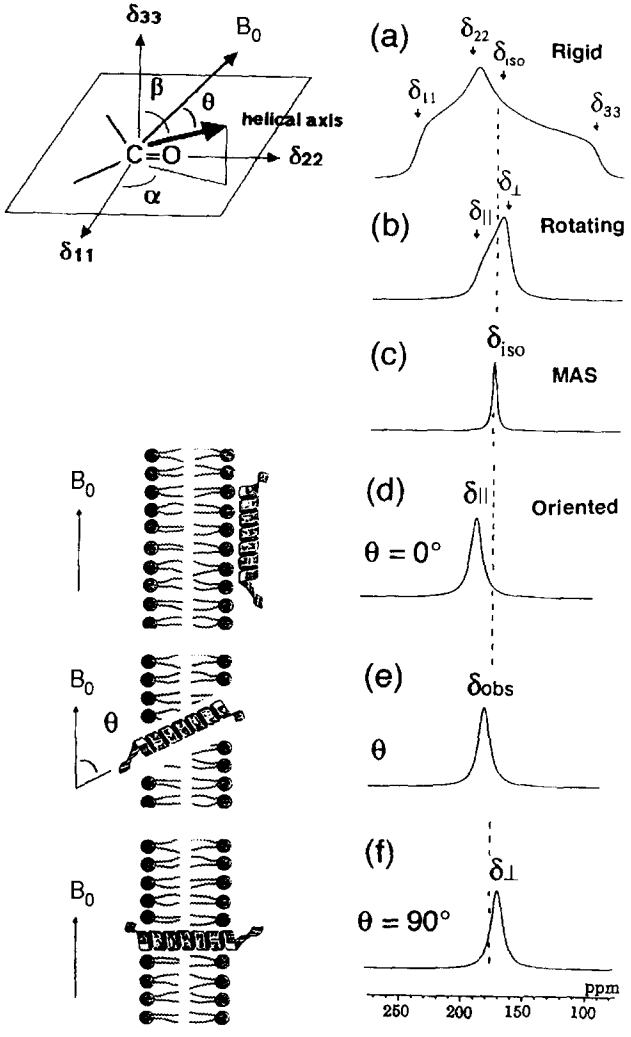

Fig. 33. Directions of the principal axes of the ^{13}C chemical shift tensor of the C=O group, helical axis, and static magnetic field, B_0, and ^{13}C NMR spectral patterns of the C=O carbons corresponding to the orientation of the α-helix with respect to the surface of the magnetically oriented lipid bilayers. Simulated spectra were calculated using δ_{11} =241 ppm, δ_{22}=189 ppm, and δ_{33}=96 ppm for the rigid case (a), rotation about the helical axis (slow MAS) (b), fast MAS (c), magnetic orientation parallel to the magnetic field (d), an angle θ with the magnetic field (e), and the direction perpendicular to the magnetic field (f).[11] Reproduced with permission from the Biophysical Society.

after the δ_{iso}, δ_{obs}, and $\delta_{\parallel}$–$\delta_{\perp}$ values are obtained from the MAS, static, and slow MAS experiment respectively.

Because the lipid bilayer is oriented with respect to the magnetic field with the bilayer surface parallel to the magnetic field and the α-helical axis of melittin

precessed about the averaged helical axis, θ reflects the direction of the averaged α-helix with respect to the surface of the lipid bilayer. Actually, the static ^{13}C chemical shift δ_{obs} of Ile^{20} C=O in the magnetically oriented state is displaced to low frequency by 4.6 ppm from the isotropic value. This makes it possible to study the average α-helical axis which is inclined by nearly 90° to the bilayer plane. The ^{13}C signal of Gly^{3} C=O is displaced to high frequency by 6.8 ppm, whereas the axially symmetrical powder pattern is reversed in shape when compared with that of Ile^{20} C=O, and hence the $\delta_{\parallel} - \delta_{\perp}$ value is negative in this case. This result leads to the conclusion that the average axis of the α-helix is inclined at 90° to the bilayer plane. Therefore, it is concluded that the transmembrane α-helices of melittin are formed in the lipid bilayer systems, and both the N and C terminal helices reorient about the average helical axis, which is parallel to the lipid bilayer normal. It is emphasized that the charged amino acid residues such as Lys^{7} in the N terminus and Lys^{21}, Arg^{22}, Lys^{23}, and Arg^{24} in the C terminus may be closely located at opposite sides of the polar head groups of lipid bilayers, although melittin forms the amphiphilic helix in the lipid bilayers. Thus, melittin turns out to form the transmembrane α-helix in the lipid bilayer, whose averaged axis is parallel to the bilayer normal.[11,204] It was also shown that the transmembrane helix is not static, but undergoes rapid rotation, namely the N and C terminal α-helical rods rotate or reorient rapidly about the average helical axis. Although the averaged direction of the α-helical axis is parallel to the bilayer normal, the local helical axis may precess about the bilayer normal by making an angle of 30 and 10° for the N and C terminal helical rods respectively, as shown in Fig. 34a. This picture clearly explains a molecular mechanism of lysis caused by melittin, as indicated by Fig. 34b.

Gramicidin A (gA), from *Bacillas brevis*, is a polypeptide of 15 amino acid residues having repeating, alternating D- and L-amino acid sequences. In lipid bilayers, the polypeptide forms a monovalent cation selective channel that is dimeric but single-stranded. The high-resolution structure of the channel monomer has been defined with 120 precise orientation constraints from solid-state NMR studies of uniformly aligned samples in bilayers.[12,205,206] It forms a single-stranded helix with a right-handed sense, with 6.5 residues per turn, and the β-strand torsion angles reported. The monomer–monomer geometry (amino terminal to amino terminal) has been characterized by solution NMR in sodium dodecyl sulfate (SDS) micelles[207] in which the monomer fold proved to be the same as in the lipid bilayers. However, the refined solid-state NMR constraints for gramicidine A in a lipid bilayer[206] are not consistent with an X-ray crystallographic structure for gramicidine having a double-stranded, right-handed helix with 7.2 residues per turn.[208]

The transmembrane portion of the M2 protein from the influenza A virus has been studied in hydrated DMPC lipid bilayers with solid-state NMR.[209] Orientational constraints are obtained from the isotopically labeled peptide samples mechanically aligned between thin glass plates. ^{15}N chemical shifts from single-site labeled samples constrain the molecular frame with respect to

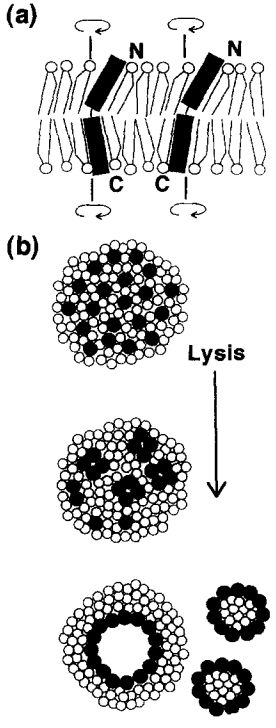

Fig. 34. (a) Schematic representation of the orientation of melittin helices bound to magnetically oriented lipid bilayers. N and C terminal helix axes make angles of 30 and 10° respectively with the average axis, which is perpendicular to the bilayer surface. Two kink angles (140 and 160°) can be taken, but they cannot be distinguished by this NMR experiment. (b) The lytic process of lipid bilayers in the presence of melittin at temperatures below T_m. ○,●, lipid and melittin molecules respectively.[11] Reproduced with permission from the Biophysical Society.

the magnetic field. When these constraints are applied to the peptides, modeled as a uniform α-helix, the tilt of the helix with respect to the bilayer normal is determined to be 33°. Furthermore, orientation about the helix axis was also determined within an error of ±30°. These results imply that the packing of this tetrameric protein is in a left-handed four-helix bundle. Only with such a large tilt angle are the hydrophilic residues aligned to the channel axis.

The structure of functional peptides corresponding to the predicted channel-lining M2 segments of the nicotinic acetylcholine receptor (AChR) and of a glutamate receptor of the NMDA subtype (NMDAR) were determined using solution NMR experiments taken on micelle samples, and solid-state NMR experiments on bilayer samples.[210] Both M2 segments form straight transmembrane α-helices with no kinks. The AChR M2 peptide inserts in the lipid bilayer at an angle of 12° relative to the bilayer normal, with a rotation about the helix long axis such that the polar residues face the N terminal side of the

membrane, which is assigned to be intracellular. A model built from these solid-state NMR data, and assuming a symmetric pentameric arrangement of M2 helices, results in a funnel-like architecture for the channel, with the wide opening on the N terminal intracellular side.

11. CONCLUDING REMARKS AND PERSPECTIVES

In general, crystalline materials, including membrane proteins as the subject of this article, are an ideal target to be studied by solid-state NMR owing to the expected narrow line widths and efficient cross-polarization dynamics. From this point of view, bacteriorhodopsin from the purple membrane is considered as an ideal, *sole*, *intact* membrane protein, which consists of naturally occurring hexagonally packed 2D crystals and belongs to the 'easy' protein family for large-scale production. This is the reason why bR has been extensively analyzed by ^{13}C NMR *at ambient temperature* to yield well-resolved ^{13}C NMR signals suitable for revealing conformation and dynamic data pertinent to its biological function. The latter aspect seems to be especially important, as viewed from the fact that solid-state NMR can be used as a complementary means to X-ray diffraction to reveal 3D structural information. Hence, we have a combination of the static picture available from X-ray diffraction data taken at low temperatures and the dynamic picture available from solid-state NMR taken at ambient temperature, which is relevant to the biological function.

As to the solid-state NMR studies targeted on membrane proteins, two types of approach have been pursued by many workers to reveal the structure and/or the dynamics of membrane proteins. Among other things, the former approach aims to analyze *whole intact* membrane proteins, ignoring all of the anisotropic interactions which make the situation complicated. This approach is based on compiled data such as the *conformation-dependent* displacement of ^{13}C chemical shifts and the *dynamics-dependent* suppression of peaks, together with comparative studies on a variety of site-directed mutants. It should be borne in mind that the problem of the dynamics-dependent suppression of peaks or line broadening cannot be overcome even if the spectra were recorded at higher field, although the frequency range could be modified depending upon the frequency of the magic angle spinning, etc. On the contrary, the latter approach aims to clarify the 3D structure by taking advantage of the solid-state NMR data arising from all of the anisotropic interactions available. However, the samples to be studied are mainly restricted to small peptide fragments rather than a whole protein system. Unfortunately, it should be taken into account that these two approaches are inevitably not compatible with each other: Detailed structural data are unavailable unless the fluctuation of the peptide chain is frozen, to prevent averaging of either the dipolar or chemical shift anisotropy interactions, either by lowering the temperature or the degree of hydration. Under such conditions, it should be borne in mind that structural data from an intrinsically

flexible surface area such as the loops and C or N terminal regions, which are biologically very important, are difficult to obtain. This is why *both* types of approach are essential as far as the final goal of a solid-state NMR study is to reveal a structure/dynamics–function relationship in order to understand the biological function.

In any case, the following more real picture of membrane proteins should be taken into account: (1) A membrane protein is not always a homogeneous, rigid system as anticipated from the 2D or 3D crystals of bR, but is a highly heterogeneous, 'soft' system undergoing conformational fluctuation with various timescales ranging from 10^{-2} to 10^{-8} s. These depend upon the domains and a variety of environmental factors such as the degree of hydration and temperature. This picture is crucially important in view of its role in the recognition and transduction of the received signals at one end of a cell from the other through conformational as well as dynamic changes in a particular polypeptide chain. (2) Both DD- and CP-MAS measurements are essential to distinguish the signals from flexible regions of fully hydrated preparations at ambient temperatures such as the C or N terminal (or loops) and the rigid portion of transmembrane helices (or loops). Local motions of wide frequency ranges are available from measurements of a variety of relaxation parameters, T_1^C, $T_{1\rho}^H$, and T_2^C. (3) The presence of *dynamics-dependent displacement of peaks* as well as *suppression of peaks*, in addition to the *conformation-dependent displacement of peaks* is particularly useful in providing a detailed picture of the underlying molecular mechanism, for example, if the ^{13}C NMR signals from [3-^{13}C]Ala- and [1-^{13}C]Ala-, Val-, or Pro-labeled bR under consideration are properly assigned in advance, mainly utilizing a variety of site-directed mutants. (4) For this purpose, several sets of isotopically labeled preparations such as [3-^{13}C]Ala-, [1-^{13}C]Val-bR should be used. This is because these two preparations exhibit different responses to the timescale of protein dynamics. (5) Regarding isotope labeling, multiple labeling should be avoided in order to prevent shortened transverse relaxation times arising from an increased number of relaxation pathways. (6) It should be taken into account that the secondary structure of a membrane protein could be distorted when solubilized in detergent micelles, depending upon the degree of lipid–protein or detergent–protein interaction as encountered for bR and its fragment.

Undoubtedly, the present approach can be extended to future studies of a variety of other membrane proteins including GPCRs.

ACKNOWLEDGEMENTS

The authors are grateful to Professor J. K. Lanyi of the University of California, Irvine, and to Professor Richard Needleman of Wayne State University for providing us with a variety of site-directed mutants and discussions through a series of cooperative works. They also wish to thank former and present students who participated in the projects cited herein: Dr S. Yamaguchi, Dr S. Kimura, Dr

K. Nishimura, and Dr M. Kamihira, K. Fukutani, Y. Shindo, T. Nagao, M. Norisada, T. Seki, K. Yokota, H. Konishi, S. Inoue, M. Okamoto, T. Mizuno, Y. Oshiro, M. Obata, K. Yonebayashi, R. Kawaminami, J. Hasegawa, S. Yokoyama, A. Kira, and T. Arakawa.

REFERENCES

1. C. M. Fraser, *et al.*, *Science*, 1995, **270**, 397C.
2. C. Branden and J. Tooze, *Introduction to Protein Structure*, 2nd edition, Garland Publishing, Inc., New York, 1998.
3. T. E. Creighton, *Proteins, Structures and Molecular Properties*, W. H. Freeman and Company, New York, 1993.
4. R. Henderson and P. N. T. Unwin, *Nature*, 1975, **257**, 28.
5. S. Tuzi, S. Yamaguchi, M. Tanio, H. Konishi, S. Inoue, A. Naito, R. Needleman, J. K. Lanyi and H. Saitô, *Biophys. J.*, 1999, **76**, 1523.
6. S. Tuzi, K. Shinzawa-Itoh, T. Erata, A. Naito, S. Yoshikawa and H. Saitô, *Eur. J. Biochem.*, 1992, **208**, 713.
7. E. Oldfield and T. M. Rothgeb, *J. Am. Chem. Soc.*, 1980, **102**, 3635.
8. T. A. Cross and S. J. Opella, *J. Am. Chem. Soc.*, 1983, **105**, 306.
9. R. S. Prosser, S. A. Hunt, J. A. DiNatale and R. R. Vold, *J. Am. Chem. Soc.*, 1996, **118**, 269.
10. C. R. Sanders and G. C. Landis, *Biochemistry*, 1995, **34**, 4030.
11. A. Naito, T. Nagao, K. Norisada, T. Mizuno, S. Tuzi and H. Saitô, *Biophys. J.*, 2000, **78**, 2405.
12. R. R. Ketchem, W. Hu and T. A. Cross, *Science*, 1993, **261**, 1457.
13. F. M. Marassi, A. Ramamoorthy and S. J. Opella, *Proc. Natl Acad. Sci. USA*, 1997, **94**, 8551.
14. S. Tuzi, A. Naito and H. Saitô, *Eur. J. Biochem.*, 1993, **218**, 837.
15. M. Tanio, S. Tuzi, S. Yamaguchi, H. Konishi, A. Naito, R. Needleman, J. K. Lanyi and H. Saitô, *Biochim. Biophys. Acta*, 1998, **1375**, 84.
16. S. Kimura, A. Naito, S. Tuzi and H. Saitô, *Biopolymers*, 2001, **58**, 78.
17. J. Deisenhofer and H. Michel, *EMBO J.*, 1989, **8**, 2149.
18. R. Henderson, J. M. Baldwin, T. A. Ceska, F. Zemlin, E. Beckman and K. H. Dowing, *J. Mol. Biol.*, 1990, **213**, 899.
19. N. Grigorieff, T. A. Ceska, K. H. Downing, J. M. Baldwin and R. Henderson, *J. Mol. Biol.*, 1996, **259**, 393.
20. Y. Kimura, D. G. Vassylyev, A. Miyazawa, A. Kidera, K. Matsushima, K. Mitsuoka, K. Murata, T. Hirai and Y. Fujiyoshi, *Nature*, 1997, **389**, 206.
21. K. Mitsuoka, T. Hirai, K. Murata, A. Miyazawa, A. Kidera, Y. Kimura and Y. Fujiyoshi, *J. Mol. Biol.*, 1999, **286**, 861.
22. E. Pebay-Peyroula, J. P. Rummel, J.P. Rosenbusch and E. M. Landau, *Science*, 1997, **277**, 1676.
23. L. Essen, R. Siegert, W. D. Lehmann and D. Oesterhelt, *Proc. Natl Acad. Sci. USA*, 1998, **95**, 11673.
24. H. Luecke, H. T. Richter and J. K. Lanyi, *Science*, 1998, **280**, 1934.
25. H. Luecke, B. Schobert, H-T. Richter, J-P. Cartailler and J. K. Lanyi, *J. Mol. Biol.*, 1999, **291**, 899.
26. H. Sato, K. Takeda, K. Tani, T. Hino, T. Okada, M. Nakasako, N. Kamiya and T. Kouyama, *Acta Crystallogr. D. Biol. Crystallogr.*, 1999, **55**, 1251.
27. H. Belrhali, P. Nollert, A. Royant, C. Menzel, J. P. Rosenbusch, E. M. Landau and E. Peybay-Peyroula, *Structure*, 1999, **7**, 909.
28. A. Seelig, *Q. Rev. Biophys.*, 1977, **10**, 353.
29. I. C. P. Smith, *Bull. Magn. Reson.*, 1981, **3**, 120.
30. J. H. Davis, *Biochim. Biophys. Acta*, 1983, **737**, 117.

31. S. J. Opella, P. L. Stuart and K. G. Valentine, *Q. Rev. Biophys.*, 1987, **19**, 7.
32. S. O. Smith and R. G. Griffin, *Annu. Rev. Phys. Chem.*, 1988, **39**, 511.
33. S. O. Smith and O. B. Peersen, *Annu. Rev. Biophys. Biomol. Struct.*, 1992, **21**, 25.
34. T. A. Cross, *Annu. Rep. NMR Spectrosc.*, 1994, **21**, 123.
35. F. M. Marassi, J. J. Gesell and S. J. Opella, *Biol. Magn. Reson.*, 1998, **16**, 121.
36. R. Fu and T. A. Cross, *Annu. Rev. Biophys. Biomol. Struct.*, 1999, **28**, 235.
37. H. J. M. de Groot, *Current Opinion Struct. Biol.*, 2000, **10**, 593.
38. B. Bechinger, *Mol. Membr. Biol.*, 2000, **17**, 135.
39. M. Engelhard and B. Bechinger, *Israel J. Chem.*, 1995, **35**, 273.
40. J. Herzfeld and B. Tounge, *Biochim. Biophys. Acta*, 2000, **1460**, 95.
41. W. Stoeckenius and R. A. Bogomolni, *Ann. Rev. Biochem.*, 1982, **51**, 587.
42. R. A. Mathies, W. Lin, J. B. Ames and W. T. Pollard, *Annu. Rev. Biophys. Biophys. Chem.*, 1991, **20**, 491.
43. J. K. Lanyi, *J. Biol. Chem.*, 1997, **272**, 31 209.
44. J. K. Lanyi, *Biochim. Biophys. Acta*, 2000, **1459**, 339.
45. E. Blaurock and W. Stoeckenius, *Nature New Biol.*, 1971, **233**, 152.
45a. J. M. Baldwin, R. Henderson, E. Beckman and F. Zemlin, *J. Mol. Biol.*, 1988, **202**, 586.
46. E. M. Landau and J. P. Rosenbusch, *Proc. Natl Acad. Sci. USA*, 1996, **93**, 14 532.
47. K. Takeda, H. Sato, T. Hino, M. Kono, K. Fukuda, I. Sakurai, T. Okada and T. Kouyama, *J. Mol. Biol.*, 1998, **283**, 463.
48. J. B. Heymann, D. J. Muller, E. M. Landau, J. P. Rosenbusch, E. Pabay-Peyroula, G. Buldt and A. Engel, *J. Struct. Biol.*, 1999, **128**, 243.
49. D. J. Muller, J. B. Heymann, F. Oesterhelt, C. Moller, H. Gaub, G. Buldt and A. Engel, *Biochim. Biophys. Acta*, 2000, **1460**, 27.
50. A. Maeda, H. Kandori, Y. Yamazaki, S. Nishimura, M. Hatanaka, Y.-S. Chon, J. Sasaki, R. Needleman and J. K. Lanyi, *J. Biochem. (Tokyo)*, 1997, **121**, 399.
51. L. S. Brown, A. K. Dioumaev, R. Needleman and J. K. Lanyi, *Biochemistry*, 1998, **37**, 3982.
52. M. Nakasako, M. Kataoka, Y. Amemiya and F. Tokunaga, *FEBS Lett.*, 1991, **292**, 73.
53. A. S. Ulrich, M. P. Heyn and A. Watts, *Biochemistry*, 1992, **31**, 10 390.
54. A. S. Ulrich, A. Watts, I. Wallat and M. P. Heyn, *Biochemistry*, 1994, **33**, 5370–5375.
55. A. S. Ulrich and A. Watts, *Solid State NMR*, 1993, **2**, 21.
56. A. S. Ulrich, I. Wallat, M. P. Heyn and A. Watts, *Nature Struct. Biol.*, 1995, 190.
57. S. Moltke, A. A. Nevzorov, N. Sakai, I. Wallat, C. Job, K. Nakanishi, M. P. Heyn and M. F. Brown, *Biochemistry*, 1998, **37**, 11 821.
58. S. Subramaniam and R. Henderson, *Biochim. Biophys. Acta*, 2000, **1460**, 157.
59. M. Kataoka and H. Kamikubo, *Biochim. Biophys. Acta*, 2000, **1460**, 166.
60. E. Pebay-Peyroula, R. Neutze and E. M. Landau, *Biochim. Biophys. Acta*, 2000, **1460**, 119.
61. H. Luecke, *Biochim. Biophys. Acta*, 2000, **1460**, 133.
62. H. Kandori, *Biochim. Biophys. Acta*, 2000, **1460**, 177.
63. M. Kataoka, H. Kamikubo, F. Tokunaga, L. S. Brown, Y. Yamazaki, A. Maeda, M. Sheves, R. Needleman and J. K. Lanyi, *J. Mol. Biol.*, 1994, **243**, 621.
64. H. Ohnishi, E. M. McCance and N. E. Gibbons, *Can. J. Microbiol.*, 1965, **11**, 365.
65. C. F. Ludlam, S. Sonar, C-P. Lee, M. Coleman, J. Herzfeld, U. L. RajBhandary and K. J. Rothschild, *Biochemistry*, 1995, **34**, 2.
66. A. Pines, M. G. Gibby and J. S. Waugh, *J. Chem. Phys.*, 1973, **59**, 569.
67. J. Schaefer and E. O. Stejskal, *J. Am. Chem. Soc.*, 1976, **98**, 101.
68. S. Tuzi, S. Yamaguchi, A. Naito, R. Needleman, J. K. Lanyi and H. Saitô, *Biochemistry*, 1996, **35**, 7520.
69. H. Saitô, S. Tuzi, S. Yamaguchi, M. Tanio and A. Naito, *Biochim. Biophys. Acta*, 2000, **1460**, 39.
70. M. S. Braiman, L. J. Stern, B. H. Chao and H. G. Khorana, *J. Biol. Chem.*, 1987, **262**, 9271.
71. R. Needleman, M. Chang, B. Ni, G. Varo, J. Fornes, S. H. White and J. K. Lanyi, *J. Biol. Chem.*, 1991, **266**, 11 478.

72. M. Engelhard, B. Hess, D. Emeis, G. Metz, W. Kreutz and F. Siebert, *Biochemistry*, 1989, **28**, 3967.
73. J. Pauli, M. Baldus, B. van Rossum, H. de Groot and H. Oschkinart, *Chembiochem.*, 2001, **2**, 272.
74. R. Verel, M. Baldus, M. Ernst and B. H. Meier, *Chem. Phys. Lett.*, 1998, **287**, 421.
75. N. Bloembergene, *Physica*, 1949, **15**, 386.
76. A. E. Bennett, H. H. Ok, R. G. Griffin and S. Vega, *J. Chem. Phys.*, 1992, **96**, 8624.
77. M. Baldus, A. T. Petkova, J. Herzfeld and R. G. Griffin, *Mol. Phys.*, 1998, **95**, 1197.
78. J. M. Griffiths, K. V. Lakshmi, A. E. Bennett, J. Raap, C. M. van der Wielen, J. Lugtenburg, J. Herzfeld and R. G. Griffin, *J. Am. Chem. Soc.*, 1994, **116**, 10178.
79. T. A. Egorova-Zachernyuk, B. van Rossum, G.-J. Boender, E. Franken, J. Ashurst, J. Raap, P. Gast, A. J. Hoff, H. Oschkinat and H. J. M. de Groot, *Biochemistry*, 1997, **36**, 7513.
80. T. A. Egorova-Zachernyuk, J. Hollander, N. Fraser, P. Gast, A. J. Hoff, R. Cogdell, H. J. M. de Groot and M. Baldus, *J. Biomol. NMR*, 2001, **19**, 243.
81. S. Yamaguchi, S. Tuzi, K. Yonebayashi, A. Naito, R. Needleman, J. K. Lanyi and H. Saitô, *J. Biochem. (Tokyo)*, 2001, **129**, 373.
81a. M. Hong and K. Jakes, *J. Biomol. NMR*, 1999, **14**, 71.
82. S. Yamaguchi, S. Tuzi, T. Seki, M. Tanio, R. Needleman, J. K. Lanyi, A. Naito and H. Saitô, *J. Biochem. (Tokyo)*, 1998, **123**, 78.
83. M. Engelhard, S. Finkler, G. Metz and F. Siebert, *Eur. J. Biochem.*, 1996, **235**, 526.
84. S. Tuzi, J. Hasegawa, R. Kawaminami, M. Tanio, A. Kira, T. Arakawa and H. Saitô, Proceedings of 40th NMR Meeting of Japan, Kyoto, 2001.
85. G. Metz, F. Siebert and M. Engelhard, *FEBS Lett.*, 1992, **303**, 237.
86. M. Engelhard, B. Hess, G. Metz, W. Kreutz, F. Siebert, J. Soppa and D. Oesterhelt, *Eur. Biophys. J.*, 1990, **18**, 17.
87. W. P. Rothwell and J. S. Waugh, *J. Chem. Phys.*, 1981, **75**, 2721.
88. T. Arakawa, M. Tanio, S. Tuzi and H. Saitô, Proceedings of 40th NMR Meeting, Kyoto, 2001.
89. D. S. Wishart, C. G. Bigam, A. Holm, R. S. Hodges and B. D. Sykes, *J. Biomol. NMR*, 1995, **5**, 67.
90. H. Saitô, *Magn. Reson. Chem.*, 1986, **24**, 835.
91. H. Saitô and I. Ando, *Annu. Rep. NMR Spectrosc.*, 1989, **21**, 209.
92. H. Saitô, S. Tuzi and A. Naito, *Annu. Rep. NMR Spectrosc.*, 1998, **36**, 79.
93. M. Ishida, T. Asakura, M. Yokoi and H. Saitô, *Macromolecules*, 1990, **23**, 88.
94. H. Saitô and M. Yokoi, *J. Biochem.* (Tokyo), 1992, **111**, 376.
95. S. Krimm and A. M. Dwivedi, *Science*, 1982, **216**, 407.
96. J. R. Parrish, Jr and E. R. Blout, *Biopolymers*, 1972, **11**, 1001.
97. M. Tanio, S. Inoue, K. Yokota, T. Seki, S. Tuzi, R. Needleman, J. K. Lanyi, A. Naito and H. Saitô, *Biophys. J.*, 1999, **77**, 431.
98. S. Yamaguchi, S. Tuzi, M. Tanio, A. Naito, J. K. Lanyi, R. Needleman and H. Saitô, *J. Biochem.* (Tokyo), 2000, **127**, 861.
99. S. Tuzi, J. Hasegawa, R. Kawaminami, A. Naito and H. Saitô, *Biophys. J.*, 2001, **81**, 425.
100. I. Solomon, *Phys. Rev.*, 1955, **99**, 559.
101. N. Bloembergen, *J. Chem. Phys.*, 1957, **27**, 572.
102. H. Konishi, BS thesis, Himeji Institute of Technology, 1998.
103. S. Tuzi, A. Naito and H. Saitô, *Biochemistry*, 1994, **33**, 15046.
104. S. Yamaguchi, K. Yonebayashi, H. Konishi, S. Tuzi, A. Naito, J. K. Lanyi, R. Needleman and H. Saitô, *Eur. J. Biochem.*, 2001, **268**, 2218.
105. K. Yonebayashi, S. Yamaguchi, S. Tuzi and H. Saitô, *J. Biochem.*, 2002, submitted.
106. I. Ando, H. Saitô, R. Tabeta and A. Shoji, *Macromolecules*, 1984, **17**, 457.
107. I. Ando, S. Kuroki, H. Kurosu, M. Uchida and T. Yamamoto, *ACS Symp. Ser.*, 1999, **732**, 24.
108. T. Gullion and J. Schaefer, *J. Magn. Reson.*, 1989, **81**, 196.
109. T. Gullion and J. Schaefer, *J. Magn. Reson.*, 1991, **92**, 439.
110. A. Naito, K. Nishimura, S. Tuzi and H. Saitô, *Chem. Phys. Lett.*, 1994, **229**, 506.
111. A. Naito, K. Nishimura, S. Kimura, M. Aida, N. Yasuoka, S. Tuzi and H. Saitô, *J. Phys. Chem.*, 1996, **100**, 14995.

112. K. Nishimura, A. Naito, S. Tuzi, H. Saitô, C. Hashimoto and M. Aida, *J. Phys. Chem. B.*, 1998, **102**, 7476.
113. S. Kimura, A. Naito, S. Tuzi and H. Saitô, *J. Mol. Struct.*, 2002, **602–603**, 25.
114. S. Kimura, A. Naito, H. Saitô, K. Ogawa and A. Shoji, *J. Mol. Struct.*, 2001, **562**, 197.
115. J. S. Waugh, in *NMR and Biochemistry* (eds S. J. Opella and P. Liu), Marcel Dekker, New York, 1979, pp. 203–210.
116. S. Tuzi, A. Naito and H. Saitô, *Eur. J. Biochem.*, 1996, **239**, 294.
117. Y. Kawase, M. Tanio, A. Kira, S. Yamaguchi, S. Tuzi, A. Naito, J. K. Lanyi, R. Needleman and H. Saitô, *Biochemistry*, 2000, **39**, 14472.
118. M. Tanio, K. Miyata, S. Tuzi and H. Saitô, Proceedings of 40th NMR Meeting, Kyoto, 2001.
119. B. Sternberg, C. L'Hosstis, C. A. Whiteway and A. Watts, *Biochim. Biophys. Acta*, 1992, **1108**, 21.
120. B. Sternberg, A. Watts and Z. Cejka, *J. Struct. Biol.*, 1993, **110**, 196.
121. T. Tsuchida, BS thesis, Himeji Institute of Technology, 2002.
122. A. Naito, M. Kamihira, S. Tuzi and H. Saitô, *J. Phys. Chem.*, 1995, **99**, 12041.
123. M. Kamihira, A. Naito, K. Nishimura, S. Tuzi and H. Saitô, *J. Phys. Chem. B.*, 1998, **102**, 2826.
124. A. Naito, A. Fukutani, M. Uitdehaag, S. Tuzi and H. Saitô, *J. Mol. Struct.*, 1998, **441**, 231.
125. D. Suwelack, W. P. Rothwell and J. S. Waugh, *J. Chem. Phys.*, 1980, **73**, 2559.
126. M. Mehring, *High Resolution NMR Spectroscopy in Solids*, Springer Verlag, New York, 1983.
127. A. Naito, S. Ganapathy, K. Akasaka and C. A. McDowell, *J. Chem. Phys.*, 1981, **74**, 3190.
128. R. Renthal, N. Dawson, J. Tuley and P. Horowitz, *Biochemistry*, 1983, **22**, 5.
129. J. Marque, K. Kinoshita, Jr., R. Govindjee, A. Ikegami, T. G. Ebrey and J. Otomo, *Biochemistry*, 1986, **25**, 5555.
130. H. J. Steinhoff, R. Mollaaghababa, C. Altenbach, K. Hideg, M. Krebs, H. G. Khorana and W. L. Hubbell, *Science*, 1994, **266**, 105.
131. W. Behrens, U. Alexiev, R. Mollaaghababa, H. G. Khorana and M. P. Heyn, *Biochemistry*, 1998, **37**, 10411.
132. M. P. Krebs, W. Behrens, R. Mollaaghababa, H. G. Khorana and M. P. Heyn, *Biochemistry*, 1993, **32**, 12830.
133. M. Engelhard, S. Finker, G. Metz and G. Siebert, *Eur. J. Biochem.*, 1996, **235**, 526.
134. P. Gale, *Biochem. Biophys. Res. Commun.*, 1993, **196**, 879.
135. S. Checover, E. Nachliel, N. A. Dencher and M. Gutman, *Biochemistry*, 1997, **36**, 13919.
136. S. Checover, Y. Marantz, E. Nachliel, M. Gutman, M. Pfeiffer, J. Tittor, D. Oesterhelt and N. A. Dencher, *Biochemistry*, 2001, **40**, 4281.
137. R. E. Lechner, J. Fitter, N. A. Dencher and T. Hauss, *J. Mol. Biol.*, 1998, **277**, 593.
138. M. Ferrand, A. J. Dianoux, W. Petry and G. Zaccai, *Proc. Natl Acad. Sci. USA*, 1993, **90**, 9668.
139. G. Papadopoulos, N. A. Dencher, G. Zaccai and G. Büldt, *J. Mol. Biol.*, 1990, **214**, 15.
140. M. Gottschalk, N. A. Dencher and B. Halle, *J. Mol. Biol.*, 2001, **311**, 605.
141. A. Kira, MS thesis, Himeji Institute of Technology, 2002.
142. S. Kimura, A. Naito, S. Tuzi and H. Saitô, *Biopolymers*, 2002, **63**, 122.
143. A. Naito, T. Nagao, M. Obata, Y. Shindo, M. Okamoto, S. Yokoyama, S. Tuzi and H. Saitô, *Biochim. Biophys. Acta.*, 2002, **1558**, 34.
144. A. W. Hing and J. Schaefer, *Biochemistry*, 1993, **32**, 7593.
145. M. Helmle, H. Patzelt, A. Ockenfels, W. Gartner, D. Oesterhelt and B. Bechinger, *Biochemistry*, 2000, **39**, 10066.
146. S. Subramaniam, M. Gerstein, D. Oesterhelt and R. Henderson, *EMBO J.*, 1993, **12**, 1.
147. H. Kamikubo, M. Kataoka, G. Varo, T. Oka, F. Tokunaga, R. Needleman and J. K. Lanyi, *Proc. Natl Acad. Sci. USA*, 1996, **93**, 1386.
148. L. S. Brown, J. Sasaki, H. Kandori, A. Maeda, R. Needleman and J. K. Lanyi, *J. Biol. Chem.*, 1995, **270**, 27122.
149. R. Govindjee, R. S. Misra, S. P. Balashov, T. G. Ebrey, R. K. Crouch and D. R. Menick, *Biophys. J.*, 1996, **71**, 1011.
150. S. P. Balashov, E. S. Imasheva, T. G. Ebrey, N. Chen, D. R. Menick and R. K. Crouch, *Biochemistry*, 1997, **36**, 8671.

151. S. P. Balashov, M. Lu, E. S. Imasheva, R. Govindjee, T. G. Ebrey, B. I. Othersen, Y. Chen, R. K. Crouch and D. R. Menick, *Biochemistry*, 1999, **38**, 2026.
152. A. K. Dioumaev, H. T. Richter, L. S. Brown, M. Tanio, S. Tuzi, H. Saitô, Y. Kimura, R. Needleman and J. K. Lanyi, *Biochemistry*, 1998, **37**, 2496.
153. M. Tanio, S. Tuzi, S. Yamaguchi, R. Kawaminami, A. Naito, R. Needleman, J. K. Lanyi and H. Saitô, *Biophys. J.*, 1999, **77**, 1577.
154. H. J. Sass, G. Buldt, R. Gessenich, D. Hehn, D. Neff, R. Schlesinger, J. Berendzen and P. Ormos, *Nature*, 2000, **406**, 649.
155. H. Leucke, B. Schobert, H. T. Richter, J. P. Cartailler and J. K. Lanyi, *Science*, 1999, **286**, 255.
156. H. Leucke, B. Schobert, J. P. Cartailler, H. T. Richter, A. Rosengarth, R. Needleman and J. K. Lanyi, *J. Mol. Biol.*, 2000, **300**, 1237.
157. A. T. Petkova, J. G. Hu, M. Bizounok, M. Simpson, R. G. Griffin and J. Herzfeld, *Biochemistry*, 1999, **38**, 1562.
158. A. K. Dioumaev, L. S. Brown, R. Needleman and J. K. Lanyi, *Biochemistry*, 1998, **37**, 9889.
159. L.-O. Essen, *Chembiochem.*, 2001, **2**, 5413.
160. K. Palczewski, T. Kumasaka, T. Hori, C. A. Behnke, H. Motoshima, B. A. Fox, I. Le Trong, D. C. Teller, T. Okada, R. E. Stenkamp, M. Yamamoto and M. Miyano, *Science*, 2000, **289**, 739.
161. P. J. E. Verdegem, P. H. M. Bovee-Geurts, W. J. de Grip, J. Lugtenburg and H. J. M. de Groot, *Biochemistry*, 1999, **38**, 11316.
162. M. H. Levitt, D. P. Raleigh, F. Creuzet and R. G. Griffin, *J. Chem. Phys.*, 1990, **92**, 6347.
163. M. A. Verhoven, A. F. L. Creemers, P. H. M. Bovee-Geurts, W. J. de Grip, J. Lugtenburg and H. J. M. de Groot, *Biochemistry*, 2001, **40**, 3282.
164. A. E. Bennet, J. H. Ok, R. G. Griffin and S. Vega, *J. Chem. Phys.*, 1992, **96**, 8624.
165. R. G. Griffin, *Nature Struct. Biol. (Suppl. S)*, 1998, **5**, 508.
166. C. Glaubitz, I. J. Burnett, G. Gröbner, A. J. Mason and A. Watts, *J. Am. Chem. Soc.*, 1999, **121**, 5787.
167. G. Gröbner, I. J. Burnett, C. Galubitz, G. Choi, A. J. Mason and A. Watts, *Nature*, 2000, **405**, 810.
168. D. Singh, B. S. Hudson, C. Middleton and R. R. Birge, *Biochemistry*, 2001, **40**, 4201.
169. X. Feng, P. J. E. Verdegem, M. Eden, D. Sandstrom, Y. K. Lee, P. H. M. Bovee-Geurts, W. J. de Grip, J. Lugtenburg, H. J. M. de Groot and M. H. Levitt, *J. Biomol. NMR*, 2000, **16**, 1.
170. M. Eilers, P. J. Reeves, W. Ying, H. G. Khorana and S. O. Smith, *Proc. Natl Acad. Sci. USA*, 1999, **96**, 487.
171. A. F. L. Creemers, C. H. W. Klaassen, P. H. M. Bovee-Geurts, R. Kelle, U. Kragl, J. Raap, W. J. de Grip, J. Lugtenburg and H. J. M. de Groot, *Biochemistry*, 1999, **38**, 7195.
172. J. G. Hu, R. G. Griffin and J. Herzfeld, *Proc. Natl Acad. Sci. USA*, 1994, **91**, 8880.
173. J. G. Hu, R. G. Griffin and J. Herzfeld, *J. Am. Chem. Soc.*, 1997, **119**, 9495.
174. J. Klein-Seetharaman, E. V. Getmanova, M. C. Loewn, P. J. Reeves and H. G. Khorana, *Proc. Natl Acad. Sci. USA*, 1999, 13744.
175. M. C. Loewen, J. Klein-Seetharaman, E. V. Getmanova, P. J. Reeves, H. Schwalbe and H. G. Khorana, *Proc. Natl Acad. Sci. USA*, 2001, **98**, 4888.
176. T. O. Yeates, H. Komiya, A. Chirino, D. C. Rees, J. P. Allen and G. Feher, *Proc. Natl Acad. Sci. USA*, 1988, **85**, 7993.
177. D. C. Rees, H. Komiya, T. O. Yeates, J. P. Allen and G. Feher, *Annu. Rev. Biochem.*, 1989, **58**, 607.
178. M. R. Fischer, H. J. M. de Groot, J. Raap, C. Winkel, A. J. Hoff and J. Lugtenburg, *Biochemistry*, 1992, **31**, 11038.
179. W. B. S. van Liemt, G. J. Boender, P. Gast, A. J. Hoff, J. Lugtenburg and H. J. M. de Groot, *Biochemistry*, 1995, **34**, 10229.
180. J. Matysik, Alia, P. Gast, H. J. van Gorkom, A. J. Hoff and H. J. M. de Groot, *Proc. Natl Acad. Sci. USA*, 2000, **97**, 9865.
181. M. G. Zysmilich and A. McDermott, *J. Am. Chem. Soc.*, 1994, **116**, 8362.
182. M. G. Zysmilich and A. McDermott, *J. Am. Chem. Soc.*, 1996, **118**, 5867.
183. M. G. Zysmilich and A. McDermott, *Proc. Natl Acad. Sci. USA*, 1996, **93**, 6857.

184. R. Kaptein, in *Introduction to Chemically Induced Magnetic Polarization* (ed. L. T. Muss), D. Reidel, Dordrecht, the Netherlands, 1977.
185. G. McDermott, S. M. Prince, A. A. Freer, A. M. Hawthornthwaite-Lawless, M. Z. Papiz, R. J. Cogdell and N. W. Isaacs, *Nature*, 1995, **374**, 517.
186. J. Alia, C. Matysik, M. Soede-Huijbregts, J. Baldus, J. Raap, P. Lugtenburg, H. Gast, J. van Gorkom, A. J. Hoff and H. J. M. de Groot, *J. Am. Chem. Soc.*, 2001, **123**, 4803.
187. T. A. Egorova-Zachernyuk, J. Hollander, N. Fraser, P. Gast, A. J. Hoff, R. Cogdell, H. J. M. de Groot and M. Baldus, *J. Biomol. NMR*, 2001, **19**, 243.
188. J. Wang, Y. S. Balazs and L. K. Thompson, *Biochemistry*, 1997, **36**, 1699.
189. O. J. Murphy III, F. A. Kovacs, E. L. Sicard and L. K. Thompson, *Biochemistry*, 2001, **40**, 1358.
190. F. Scholz and W. Helfrich, *Biophys. J.*, 1984, **45**, 589.
191. J. Seelig, F. Borle and T. A. Cross, *Biochim. Biophys. Acta*, 1985, **814**, 195.
192. J. B. Spryer, P. K. Spipada, S. K. Das Gupta, G. G. Shipley and R. G. Griffin, *Biophys. J.*, 1987, **51**, 687.
193. T. Brumm, C. Mops, C. Dolainsky, S. Bruckner and T. M. Bayerl, *Biophys. J.*, 1997, **61**, 1018.
194. X. Qin, P. A. Mirau and C. Pidgeon, *Biochim. Biophys. Acta*, 1993, **1147**, 59.
195. C. E. Dempsey and A. Watts, *Biochemistry*, 1987, **26**, 5803.
196. C. E. Dempsey and B. Sternberg, *Biochim. Biophys. Acta*, 1991, **1061**, 175.
197. T. Pott and E. J. Dufourc, *Biophys. J.*, 1995, **68**, 965.
198. C. R. Sanders and J. H. Prestegard, *Biophys. J.*, 1990, **58**, 447.
199. C. R. Sanders and J. P. Schwonek, *Biochemistry*, 1992, **31**, 8898.
200. C. H. Ho, A. Ramamoorthy and S. J. Opella, *J. Magn. Reson.*, 1994, **A109**, 270.
201. F. M. Marassi and S. J. Opella, *J. Magn. Reson.*, 2000, **144**, 150.
202. F. M. Marassi, C. Ma, J. J. Gesell and S. J. Opella, *J. Magn. Reson.*, 2000, **144**, 156.
203. J. Wang, J. Denny, C. Tian, S. Kim, Y. Mo, F. Kovacs, Z. Song, K. Nishimura, Z. Gan, R. Fu, J. R. Quine and T. A. Cross, *J. Magn. Reson.*, 2000, **144**, 162.
204. R. Smith, F. Separovic, T. J. Milne, A. Whittaker, F. M. Bennett, B. A. Cornell and A. Makriyannis, *J. Mol. Biol.*, 1994, **241**, 456.
205. R. R. Ketchem, B. Ronx and T. A. Cross, *Structure*, 1997, **5**, 1655.
206. F. Kovacs, J. Quine and T. A. Cross, *Proc. Natl Acad. Sci., USA*, 1999, **96**, 7910.
207. A. L. Lomize, V. Y. Urekhov and A. S. Arseniev, *Bioorg. Khim.*, 1992, **18**, 182.
208. R. M. Burkhart, N. Li, D. A. Langs, W. A. Pangborn and W. L. Duax, *Proc. Natl Acad. Sci. USA*, 1998, **95**, 12950.
209. I. Song, F. A. Kovacs, J. Wang, K. Denny, S. C. Shekav, J. R. Quine and T. A. Cross, *Biophys. J.*, 2000, **79**, 767.
210. S. J. Opella, F. M. Marassi, J. I. Gesell, A. P. Valente, Y. Kim, M. Oblatt-Montal and M. Montal, *Nature Structural Biology*, 1999, **6**, 374.

Applications of NMR to Food Science

E. ALBERTI,[1] P. S. BELTON,[2] and A. M. GIL[1]

[1]*Department of Chemistry, University of Aveiro, 3810-193 Aveiro, Portugal*
[2]*School of Chemical Sciences, University of East Anglia, Norwich NR4 7TJ, UK*

1. Introduction 110
2. Water in foods 111
   2.1. Location and translation of water 111
   2.2. Water/biopolymer interactions 112
   2.3. Water in microbiological systems 112
   2.4. Other applications 113
3. Biopolymers 113
   3.1. Proteins 114
   3.2. Polysaccharides 116
      3.2.1. Starch 116
      3.2.2. Other polysaccharides 119
   3.3. Plant cell walls 119
4. Analysis and authentication 122
   4.1. Stable isotope ratio determination 122
   4.2. High-resolution NMR spectroscopy 123
      4.2.1. Fruit products, vinegar, coffee, and tea 123
      4.2.2. Lipids 124
      4.2.3. Genetically modified products 126
      4.2.4. Other studies 126
   4.3. Solid-state NMR spectroscopy 127
5. Complex systems 128
   5.1. Textural measurements 128
   5.2. Fish and meat 128
   5.3. Fruit and vegetable products 129
   5.4. Other systems 130
6. New methods for food analysis 132
   6.1. Fast field cycling NMR 132
   6.2. Liquid chromatography-NMR 134
   6.3. High-resolution MAS NMR 135
   6.4. Rheological NMR 137
References 137

This report reviews the literature on the applications of NMR to food science from 1995 until March 2001. In order to be able to keep the number of

ANNUAL REPORTS ON NMR SPECTROSCOPY
VOLUME 47 ISBN 0-12-505447-5

Copyright © 2002 Elsevier Science Ltd.
All rights of reproduction in any form reserved

references to manageable proportions, the number of papers referred to has been limited to those applications where NMR plays a major role in the experimental programme. Applications where NMR is simply used as a routine structural tool have been left out. Following an introductory section, the report covers water in foods, biopolymers, analysis and authentication, complex systems, and new methods for food analysis.

1. INTRODUCTION

Since the last review in this series[1] there has been considerable activity in the area of NMR applied to food science. The programme of international conferences has continued with meetings in 1996, 1998, and 2000. The proceedings of these conferences have been published as a special edition of *Magnetic Resonance in Chemistry*[2] and as two books.[3,4] In addition, two other books have been published that deal specifically with applications of NMR to food science.[5,6] The importance of NMR in studying water properties in foods has been attested by the number of papers listed in the 6th ISOPOW Conference Proceedings.[7] NMR has also featured in a number of more general reviews which are listed in Table 1.

Table 1. A list of reviews of applications of NMR to food science

Subject	Year (Reference)
NMR in microbiology	2000 (8)
Thirty years of flavour NMR	1999 (9)
Applications of high-resolution methods to oils and fats	1998 (10)
Applications of NMR relaxometry to food products	1998 (11)
High-field solution state NMR for foods	1998 (12)
Applications of NMR to food analysis	1998 (13–15)
Analysis of food emulsions	1998 (16)
NMR applications in food – a critical appraisal	1998 (17)
NMR spectra of lipids	1998 (18)
Principles and applications of NMR to food analysis	1997 (19)
Multidimensional detection methods for separations and their application in food analysis	1996 (20)
Applications of NMR to food and agricultural analysis	1996 (21)
Magic angle spinning applied to foods	1996 (22)
NMR self-diffusion studies of emulsions	1996 (23)
Rapid water determination in foodstuffs	1995 (24)
New techniques to characterize water in foods	1995 (25)

As the number of publications continues to grow, it is increasingly difficult to cover all the literature in a single review. In order to be able to keep the number of references to manageable proportions, we have limited our selection to those applications where NMR plays a major role in the experimental programme and have left out applications where NMR is simply used as a routine structural tool.

One of the features of the past few years is how new experimental methods in NMR have arisen. These new developments, which we consider to be of wide applicability, have been collected into one section to draw the attention of the reader to them. Although some of them have so far found little direct application to food materials, we believe that they may have considerable potential for the future.

2. WATER IN FOODS

2.1. Location and translation of water

One of the major problems in food processing and storage is accurate modelling of the translation and location of water in food. Chinachoti has reviewed this with respect to storage.[26] In processes such as cooking, drying, freezing, and thawing, magnetic resonance imaging (MRI) is an ideal technique to use, but in very dry materials the technical difficulties are considerable, as short relaxation times require short radio frequency pulses and large magnetic field gradients. One way of generating the necessary gradient is to utilize the existing static gradients that occur around the outside of a high field magnet. This technique, known as stray field (STRAFI), has been used by Hopkinson and co-workers[27] to follow the ingress of water into amylose at very low water contents. The results show that the diffusion of water vapour into the sample is Fickian, but that of liquid water is type II diffusion. Type II diffusion is associated with the water having first to soften the material before it can diffuse into it. Typically, the water forms a sharp front which moves through the sample rather than the extended distribution of water seen in Fickian diffusion.

The problem of cooking and drying of pasta has been tackled by Hills and co-workers in a series of papers. The basis of their method is to exploit the radial symmetry of the sample to collect radial profiles of the water content;[28] this method has advantages in speed of acquisition and signal-to-noise ratio. In a study of pasta cooking it was shown that the diffusion behaviour of water into the sample depended on the types of wheat used in manufacture. When the amount of hard wheat in the sample was increased, the diffusion behaviour tended more to move way from Fickian towards type II behaviour.[29] In pasta drying,[30] the loss of water from the surface was shown to 'case harden' the material so that after the initial water loss a steep moisture gradient was established in which the exterior region was dry and slowed diffusion of water out of the interior.

Understanding the movement of water during the cooking of grains is an area of research that continues to attract attention because of its industrial significance and its importance to consumers. Watenabe and co-workers[31–33] have examined the changes in distribution in rice grains during cooking with a view to understanding the behaviour in domestic rice cookers. An interesting outcome of this work was the result that the endosperm cell walls seemed to have no effect on the migration of water in the system. Similar studies have also been carried out on

wheat grains.[34,35] A feature of this work is that the vapour and liquid were observed to diffuse differently into the seed. This appears to be analogous to the effects seen in amylose. However, the explanation is rather different and is due to the effects of vapour condensation heating the grain.

Other studies on the location and mobility of water have included the models of food freezing[36] and changes in the subcellular compartmentation of apple during freezing,[37] the hydration of various foods,[38] and the diffusion of water in a variety of media including fruit juice and apple tissue.[39]

2.2. Water/biopolymer interactions

The interaction of water with breads and doughs is of continuing interest. Chinachoti has published careful studies of the interactions of water with gluten using ^{2}H and ^{17}O resonances.[40,41] The effects of temperature on the water sorption of gluten in contact with an excess of liquid water have been reported.[42] It was shown that gluten is hydrophilic in its nature in that it absorbed more water on heating. Ruan and collaborators have reported on proton relaxation times in breads and doughs.[43,44]

There have been a number of papers published that are concerned with interactions of water and starch. These are listed in Table 2.

Table 2. A list of publications relating to starch/water interactions

Subject	Year (Reference)
^{17}O relaxation studies on maize starches	1998 (45)
Mobility of freezable and unfreezable water in waxy corn starch	1998 (46)
Effects of sugars on water diffusion in starch gels	1997 (47)
Restricted diffusion in freeze-dried gels	1997 (48)
Hydration of extruded maize sucrose mixtures	1996 (49)

There have been a number of other papers on the hydration of biopolymers: the effects of the degree of methylation of pectins on the proton relaxation times of water have been measured;[50] ^{17}O relaxation has been used to examine the hydration of bovine and caprine casein,[51–54] and solid-state NMR combined with atomic force microscopy has been used to examine the influence of water on the nanomechanical behaviour of cutin.[55] The effects of locust bean gum on water diffusion in sugar solutions has shown little effect,[56] and the effects of gellan gum hydrogel structure on restricted diffusion has also been considered.[57]

2.3. Water in microbiological systems

The importance of water for the growth of microbiota has always been exploited in traditional and manufactured food preservation technologies. However, the

origins of the relationship between water content and growth rate are still unclear. The problem is often to understand the local environment as experienced by the organism rather than the average environment sensed by measurements such as water activity. Hills and co-workers have explored the local environment by exploiting the sensitivity of proton NMR relaxation measurements to the details of the structure of porous systems.[58,59] By comparing the scaling laws for the behaviour of water in fast exchange between different environments, it was possible to show that NMR relaxation and electrical conductivity could be coupled and related to the amount of water in pores and at surfaces. In an extension of this, a model of water activity was used that related the overall water activity to the populations and supposed local water activities in different environments. The NMR data could then be directly related to the local water activities and to the observed bacterial growth rates. When the fast exchange regime no longer applies, porous systems exhibit multiexponential relaxation. From an analysis of the distribution of relaxation times it is possible to build up a picture of the occupation of the pores and discriminate between pore types. It was possible to show that the recovery rates of the bacteria could be related to the occupancy of the larger pores in which the local water activity was still close to unity even though the overall water activity had dropped.

Similar conclusions about the ability of NMR to predict microbial growth rates have been reached in a study of the role of water mobility on spore germination.[60] It was found that water activity measurements were a poor predictor of germination rates, whereas the rates correlated very well with the measured ^{2}H relaxation rates. This was thought to be due to the sensitivity of the relaxation rate to the local environment of the water rather than the more global sensitivity of the activity measurement. The effects of the growth of *Staphylococcus aureus*, relating to ^{17}O NMR and water activity, have also been reported.[61] The role of glassy states in spores has been considered,[62] and the effects of freeze-drying of *Lactobacillus* on the types of residual water have also been examined.[63]

2.4. Other applications

NMR as a moisture-sensing method still remains important and new devices are being developed,[64] as are new multivariate statistical approaches to data analysis.[65] NMR has been used to relate the hardness of cooked rice[66] and starch-based products[67] to water mobility and to understand more about the freezing process.[36,68]

3. BIOPOLYMERS

The area of research into food biopolymers continues to attract considerable interest. Food polymers are widely used by the food and some non-food

industries, and therefore much of the research has been directed towards a better understanding of their structure and properties.

3.1. Proteins

The use of solid-state NMR has given very useful information on the structural and dynamic properties of cereal proteins, in order to understand the origins of dough viscoelastic properties. A ^{13}C NMR study of the barley storage protein C-hordein[69] has shown that, upon hydration, the protein adopts a gel-like structure. A similar effect was observed for the wheat prolamin ω-gliadin by ^{1}H and ^{13}C solid-state NMR,[70,71] and a structural model has been proposed[72] involving the formation of freely mobile chain regions ('loops') and regions of strong interchain interaction ('trains'). Particular interest has been given to high molecular weight (HMW) subunits of wheat glutenins, thought to play an important role in conferring technological quality to wheat dough. Solid-state NMR and Fourier transform infrared (FTIR) spectroscopy have been used to follow the changes in molecular mobility and conformation upon hydration of HMW subunit 1Bx20 from durum wheat.[73] The HMW subunit 1Dx5 has been associated with good dough performance, and a ^{13}C NMR study has been carried out in order systematically to investigate the role of disulphide bonds, non-repetitive terminal domains, the length of repetitive domains, and sample heterogeneity on the structure of the hydrated protein.[74,75] The presence of disulphide bonds leads to increased molecular mobility, as do the absence of terminal domains and a smaller length of the repetitive domain. Subunit 1Dx5 was also studied by ^{1}H magic angle spinning (MAS) and by high-resolution-MAS (HR-MAS), the latter method allowing a threefold resolution improvement of the protein spectrum.[76] 2D NMR experiments revealed two different environments for glutamine residues (the most abundant amino acid), differing in chemical shift and dynamics, possibly corresponding to residues located in loops and in train sections (Fig. 1). Similar studies[75,77] have been carried out on other HMW subunits, 1Dx2, 1Dy10, and 1Dy12, which are believed to originate different technological properties to dough. Some differences were found in the behaviour of the subunits upon hydration.

The response of wheat gluten to hydration and heating has been investigated by ^{1}H MAS NMR.[78] The proteins in gluten seem to undergo reversible changes upon heating up to 65 °C and subsequent cooling, whereas residual starch and water molecules become irreversibly hindered. However, heating at higher temperatures has been shown to lead to a rigid and amorphous network. The measurement of proton rotating frame relaxation times, $T_{1\rho}$, has aided the characterization of molecular dynamics and structural homogeneity in wheat gluten upon heating.[79] ^{13}C NMR spectroscopy was used to study the effects of conventional and microwave heating on gluten/starch mixtures.[80] Few differences were found in the amino acid mobility, whereas carbohydrates

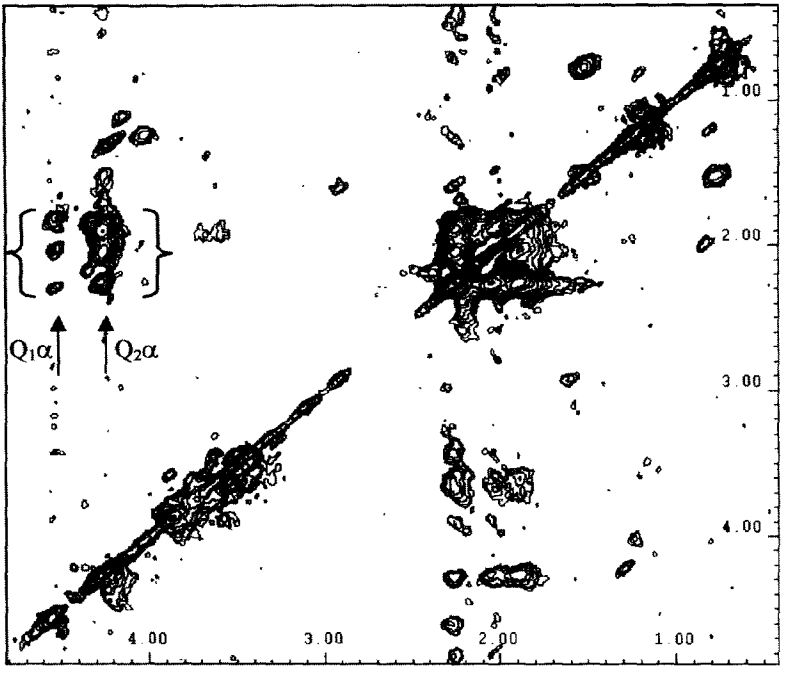

Fig. 1. Expansion of the aliphatic region of the TOCSY HR-MAS spectrum of alkylated subunit 1Dx5 hydrated with excess of D_2O. Spinning at 8 kHz. The cross-peaks of the two glutamine residues are indicated in the spectrum. Reprinted from *Biopolymers*, Vol. 58(1), E. Alberti, E. Humpfer, M. Spraul, S. M. Gilbert, A. S. Tatham, P. R. Shewry and A. M. Gil, 'A high resolution ^{1}H MAS NMR study of a high-M_r subunit of wheat glutenin', pp. 33–45, Copyright 2001, with permission from John Wiley & Sons, Inc.

appeared to be affected by the starch/water ratio and to a lesser extent by the heating method. ^{2}H and ^{17}O NMR were employed to investigate the water interactions in gluten in relation to the glass transition of gluten and the effects of temperature on the sorption of water.[40–42]

Much work has also been carried out on non-cereal plant proteins. Solid-state ^{1}H and ^{2}H NMR transverse relaxation measurements were used to investigate the effect of hydration on the plasticization of vicilin, legumin, and albumin fractions from peas.[81] Their behaviour indicated that the plasticization of the globular legume proteins is considerably less than that found before for the linear barley protein C-hordein. The effects of microbial transglutaminase treatment on soy protein samples have been studied by ^{1}H and solid-state ^{13}C NMR spectroscopy, and its relation to the glass transition temperature was examined.[82,83]

Milk proteins have also been extensively investigated by NMR. ^{17}O NMR spectroscopy has been used to study the effect of salt, temperature, and pH/pD on the hydration of bovine and caprine caseins.[51–53] Furthermore, the addition of sucrose and lactose to casein solutions was shown to lead to increased casein

hydration and reduced electrostatic repulsions.[54,84] The interactions of bovine and caprine caseins with κ-carrageenan have been studied,[85] indicating that the latter proteins may interact significantly with the polysaccharide and suggesting the formation of an electrostatic complex. The structure of κ-casein peptides was examined by high-resolution ^{1}H NMR,[86] whereas both liquid- and solid-state NMR were used to study the structure of casein micelles.[87] Solid-state ^{2}H NMR and molecular modelling were employed to study the interactions of β-casein at lipid/water interfaces. The results indicate the ability of the protein to interact with both non-charged and charged lipid phases.[88] High-resolution ^{31}P NMR was used to study the emulsifying characteristics of caseinate in model triacylglycerol-in-water emulsions.[89] More recently, the phosphorus content of milk samples has been determined by ^{31}P NMR, enabling the identification of phosphorus in the organic form and phosphorus bonded to casein as phosphoserine.[90] Solid-state ^{31}P NMR has enabled the characterization of phosphate sites in native ovine, caprine and bovine casein micelles and their caseinomacropeptides.[91]

The conformational changes in β-lactoglobulin during foaming and thermal denaturation were studied by ^{1}H NMR and ^{2}H exchange spectroscopy.[92,93] The properties of three equine whey proteins, alpha-lactoalbumin, β-lactoglobulin, and lysozyme, have been studied and compared with those of the corresponding bovine milk.[94]

Other studies included the investigation of the stabilizing effect of sorbitol on hen egg white lysozyme[95] and the use of the self-diffusion coefficient, D, to follow the solution and aggregative properties of lysozyme at different pH, temperature, and protein and salt concentrations.[96] The properties of frozen ovalbumin solutions were studied by NMR relaxation spectroscopy.[97] It is known that the functional properties of muscle proteins are affected by protein interactions with ions, and NMR was used to assess protein/water, protein/salt, and protein/protein interactions in myofibrillar protein solutions.[98] Previous X-ray and NMR studies on collagen and peptides were reviewed by Mayo[99] and, more recently, such types of system were characterized by high-resolution ^{1}H and ^{13}C NMR.[100,101] The structure, hydration state, and nature of the interactions between water and gelatin were determined by time domain NMR.[102]

An increased interest has been shown in the use of biopolymers as material for food packaging, and NMR was employed to study the physicochemical properties of plasticized corn zein films.[103] The elucidation of freezing effects in foodstuffs was approached by studying the interactions between amino acids, sugars, and alcohols at temperatures below 273 K.[104]

3.2. Polysaccharides

3.2.1. Starch

Various studies have been carried out on the gelatinization and retrogradation processes of starch. Starch gelatinization was followed by pulsed ^{1}H NMR by

means of a relative liquefying index calculated from the ratio of liquid to solid phases.[105] The gelatinization rate of rice starch was studied by observing the water diffusivity measured by pulsed field gradient (PFG) NMR methods,[106] and the water diffusivity was seen to decrease as starch gelatinization progressed. Water diffusivity reached equilibrium within 1 min at heating temperatures above 70 °C.

Proton relaxation times in the rotating frame, $T_{1\rho}$, were used to investigate the retrogradation and physical ageing of model starch systems with respect to their glass transition temperatures, T_g.[107] An interesting result is that, for materials stored below T_g, $T_{1\rho}$ increases asymptotically in time owing to physical ageing, whereas for materials stored above T_g, $T_{1\rho}$ increases owing to the development of crystallinity. The effects of water content and storage temperature on the kinetics of retrogradation of non-expanded waxy maize starch extrudates were studied by ^{1}H pulsed NMR and wide angle X-ray diffraction.[108] The increase in crystallinity was accompanied with an increase in the contribution of the solid-like component of the free induction decay (FID) and a decrease in the corresponding relaxation times. The dependence of retrogradation rate on storage temperature was modelled, as well as the effects of water on the rate of isothermal crystallization, on the glass transition, and on the melting temperature. The ^{13}C cross-polarization and magic angle spinning (CPMAS) NMR spectra of native and recrystallized starches have been improved by the analysis of the amorphous and crystalline components of the spectra and their changes with hydration.[109] The experiments show that it is possible to identify and quantify three structural phases in native A- and B-type starches: amorphous background, partially ordered interfacial, and crystalline. The role of sugars on starch retrogradation has been investigated,[110,111] and it was found that the effect depends to a great extent on sugar type and concentration, but more importantly on water content and the storage temperature at which retrogradation occurs. A comparative study by pulsed NMR and firmness measurements was carried out to investigate the staling of corn-starch gel, bread, and rice cup-cake.[112] 2D exchange NMR techniques were used to detect ultraslow motions (ms s^{-1}) in native and retrograded starch.[113] ^{2}H and ^{13}C NMR techniques were used to investigate the hydration properties and structure of raw and cooked mealy and waxy potatoes and potato starches.[114] Water in raw potato was identified as trapped, bound, or weakly bound/free water, and cooking significantly affected these three water states.

The structure of moistened starch granules was investigated by ^{13}C CPMAS, ^{13}C single-pulse excitation, and $T_{1\rho}$ measurements.[115] Study of amylose–lysophospholipid inclusion complexes suggested that three structural components are present in wheat starch: (i) highly crystalline regions formed by double helical starch chains; (ii) solid-like regions formed by lipid inclusion complexes of starch; (iii) completely amorphous regions, associated with the branching regions of amylopectin and possibly lipid-free amylose. A multinuclear NMR approach has been carried out to study in detail the microscopic distribution of water among the various subgranular compartments of three types

of native starch granule, namely maize, potato, and pea, which are representative of A-, B-, and C-type starches respectively.[116] At least three populations of water have been found to occur in starch granules: water in type B hexagonal channels or of crystallization, water in the amorphous regions, and water in semi-crystalline regions. The three populations undergo exchange on various time-scales.

Much work has been carried out to characterize the structure of starch constituents. The structure of amylopectin obtained from waxy maize was examined in dimethyl sulphoxide (DMSO) solutions, by ^{13}C NMR spectroscopy.[117] Analysis was carried out of native amylopectin, and amylopectin degraded by hydrochloric acid or bacterial alpha-amylase. Results suggested that the original branching degree of amylopectin was retained after degradation. Determination of the degree of branching and molecular weight of normal and amylopectin-type potato starch was also performed by NMR.[118] A high-resolution ^{1}H NMR spectroscopic method was evaluated for the determination of hydroxypropyl groups in commercial hydroxypropylated starches obtained from waxy maize, normal maize, wheat, and tapioca starches.[119] A proton NMR method was optimized to determine the $\alpha(1,4)/\alpha(1,6)$ ratio of starches, to select the starches with reproducible ratios, and to use the above ratio to determine amylose and amylopectin contents in starch.[120] It was found that starches from waxy maize, wheat, rice, pea, and tapioca contained highly branched amylopectin I; branched amylopectin II occurred in maize and potato; and amylopectin III was detected in high-amylose corn starches.[120] The characterization of the substituent distribution in hydroxypropylated potato amylopectin starch was also investigated.[121] The glass transition in maltodextrin was studied by measurement of proton relaxation times. Results suggested a strong relationship between glass transition and proton relaxation behaviour, indicating NMR as a powerful tool for the study of glass transition phenomena in food polymers and food such as bread, cakes, and crackers.[122, 123]

Cooking starch in the presence of amino acids may favour the occurrence of Maillard reactions, lowering the bioavailability of lysine in the diet. ^{13}C CPMAS was used to follow the effect of Maillard reactions on the bioavailability of potato starch.[124] A loss of crystallinity was found for the three samples studied: starch, amylopectin, and amylose, being more marked for amylose. A similar study on chestnut starch indicated that Maillard reactions do not influence significantly its digestibility.[125] NMR was used to characterize some Maillard reaction products extracted from model reactive mixtures such as starch–glucose–lysine [126] and lactose–lysine.[127]

Phosphorus in starch is found in different forms, mainly starch phosphate monoester, phospholipids, and inorganic phosphate. ^{31}P NMR spectroscopy was used to identify each of these forms in alpha-dextrins prepared from starches of different sources.[128] Quantitative analysis was possible in DMSO solution.

Time domain NMR was used to elucidate the molecular mechanisms involved in the plasticization and mobility in starch–sorbitol films.[129]

3.2.2. Other polysaccharides

The gellan/Mn(II) complex was studied by ^{13}C CPMAS, confirming that Mn(II) ions interact with the carboxyl groups of the D-glucuronate units. ^{1}H relaxation measurements indicated that water molecules are well coordinated to the gellan–Mn(II) ion complex in the gel state.[130] Pulsed-field gradient stimulated echo NMR was used to determine the structure of gellan gum gels formed with potassium and calcium ions.[57] ^{1}H and ^{13}C NMR spectra of gellan gum have been fully assigned, and the anomeric regions were shown to be very sensitive to the type and location of non-carbohydrate substituents.[131]

A study of maltodextrin and inulin gels was carried out by cross-relaxation spectroscopy, $T_{1\rho}$ (H) measurements, and a wideline separation experiment (WISE).[132] During ageing, the amount of immobilized polymer increases owing to the formation of crystalline regions, but it is not associated with change in molecular mobility. Different kinetics were found for maltodextrin and inulin gels.[132]

Cellulose and pectin extracts from soybean hulls and endosperm were characterized in terms of their rate of degradation in the presence of sheep rumen fluid.[133] ^{13}C CPMAS NMR was used to study the ultrastructural aspects of ultrathin cellulose microfibrils extracted from sugar beet pulp during the purification procedure. It was found that crystallinity increases as the purification proceeds. A crystallite size of 4 nm was derived from the NMR results, in good agreement with the transmission electron microscopy (TEM) observations.[134]

Pectins are widely used in the food industry as gelling agents, and their molecular structure strongly affects their rheological properties. NMR spectroscopy and statistical analysis were used to assess methyl ester distribution in native, chemically modified, and fractionated pectin solutions.[135] The conformation of the galacturonan chains in calcium pectate gels, of similar concentrations to those found in plant cell walls, was determined by ^{13}C CPMAS experiments.[136] Deuterium-labelled (methyl-*d*3) pectin was studied by solid-state ^{2}H NMR in order to monitor the dynamics of the CH_3 groups.[137] The dynamics of D-α-galacturonic acid monohydrate and its derivative methyl-α-D-galacturonic acid methyl ester monohydrate was investigated by solid-state ^{1}H NMR.[138] Three types of motion were identified, suggesting a complete picture of the spin–spin as well as the spin–lattice relaxation in both laboratory and rotating frames.

Other studies on polysaccharides are listed in Table 3.

3.3. Plant cell walls

Plant cell walls are of vital importance to the activity of cells and are also of significance to the texture of foods originating from plant sources. This type of cell wall is mostly composed of cellulose, pectin and hemicellulose, proteins,

Table 3. Additional papers on applications of NMR to polysaccharides

Subject	Year (Reference)
Characterization of β-glucans of different origin	2000 (139–141)
Application of nanoprobe NMR for structure determination of arabinoxylan oligosaccharides	2000 (142)
Assignment of ^{13}C and ^{1}H NMR spectra of pullulan and isomaltose	1995 (143)
Study of the distribution of carboxymethyl substituents in carboxymethylpullulans	2000 (144)
Structure determination of algal oligosaccharides	1999 (145)
Solid-state NMR study of interactions between guar gum and agarose	1997 (146)
Study of the structure of alginate, gum, arabic, and xanthan gum	1996 (147)
Diffusion of aqueous sugar solutions as affected by locust bean gum	1999 (56)
Quantification of the kappa/iota ratio and the lambda content in carrageenan blend by ^{13}C NMR	1996 (148)
Study of xyloglucan from apple	1999 (149); 2000 (150)
Characterization of xyloglucan polymers isolated from cyclamen seeds	1995 (151)
Characterization of potato and cork suberin	1998 (152), 2000 (153, 154)
Analysis of chitin and chitosan	1997 (155)

and polyphenols. The segmental mobility of the hydrated biopolymer network of primary plant cell walls was characterized via relaxation and anisotropy effects.[156] The molecular motions occurring in the cell walls of *Citrus* mesocarp (orange peel) and *Allium* upon hydration were characterized by means of cross-polarization kinetics and proton relaxation.[157,158] Both solid-state ^{1}H relaxation measurements and ^{13}C spectra were used to investigate rigid and flexible pectic polymers in onion cell walls.[159–161] The effect of hydration on polysaccharide mobility was also studied by WISE experiments[161] revealing spatial heterogeneity of the polysaccharide dynamics across the sample and showing at least two different motional regimes for pectin and cellulose domains. This is expressed by the narrower component that becomes observable, with hydration, on the proton wideline spectra of certain carbon sites (Fig. 2).

Changes in strawberry cell wall components upon ripening were studied by solid-state ^{13}C NMR.[162] The separation between semi-rigid (primarily polygalacturonic acid) and semi-mobile (non-cellulosic substances) domains became more distinct with ripening, whereas the ratio of non-cellulosic material (pectins and hemicellulose) to rigid cellulose decreased. The basic crystallite of strawberry cell walls appeared to be exceptionally small compared with other systems studied.[162]

The effect of a reduced polygalacturonase activity in cell walls of transgenic tomatoes was studied by ^{13}C CPMAS NMR in order to investigate the ripening

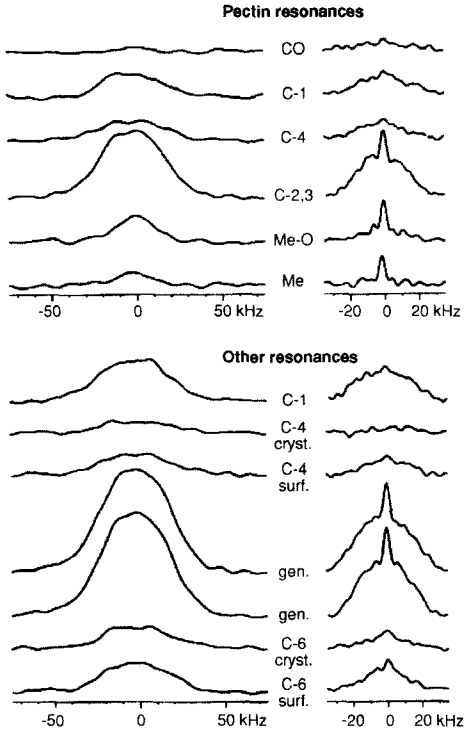

Fig. 2. Traces along the proton dimension of 2D-WISE experiments performed on 10% hydrated (left) and 35% hydrated (right) onion cell wall material. The corresponding carbon resonances are given. Proton spectral widths of 150 and 70 kHz were used for the 10 and 35% hydrated samples respectively. Reprinted from *Carbohydr. Res.*, Vol. 322(1–2), S. Hediger, L. Emsley and M. Ficher, 'Solid-state NMR characterization of hydration effects on polymer mobility in onion cell wall material', pp. 102–112, Copyright 1999, with permission from Elsevier Science.

mechanism of these fruits.[163] The results indicated that the lack of enzymatic activity reduced the softening of the cell walls, but not to the extent expected.

Investigation of cell walls in wheat bran by solid-state ^{13}C NMR showed a higher content of cutin than lignin,[164] thus it was suggested that cutin, rather than lignin, could play an important role in protecting wheat bran from microbial degradation in the rumen and in the human gut. ^{13}C CPMAS, single-pulse excitation experiments, and relaxation measurements were used to study the hydration of potato and Chinese water chestnut cell walls. It was concluded that the pectic polysaccharides experience a distribution of molecular conformations and dynamics, whereas cellulose remains as a typical rigid solid.[165] The samples were also studied by proton relaxation measurements.[166]

4. ANALYSIS AND AUTHENTICATION

The increasing need for analytical methods to establish food authenticity has led to the development of a number of approaches, many of which involve the use of NMR spectroscopy. Some texts have reviewed the generally accepted methods for quality and authenticity control.[15, 167–172]

4.1. Stable isotope ratio determination

The methods of authentication through the determination of stable isotope ratios have in recent years found a remarkably wider range of food applications. The combination of site-specific natural isotope fractionation (SNIF)-NMR with mass spectrometry methods has been the basis of the development of many applications mainly to wine, fruit juices, olive oil, and some other foods.

The democratization of wine consumption in Europe has called for the need to maintain the quality of wine produced in the European Community and to verify the wine imported from other countries. The use of ^{2}H NMR for determination of the D/H ratio in wines as a function of geographical origin has been carried out extensively in the last 10 years and has often been complemented by determination of trace element concentrations directly on the grape musts, thus circumventing the possibility of introducing agents during the vintification steps.[173–176] An on-line method for wine classification was also suggested by Fauhl and Wittkowski.[177] ^{1}H NMR spectroscopy[178] has also been used to aid determination of site-specific D/H ratios in glycerol from different wine sources, since glycerol is found in wine as a byproduct of glycolysis. The applications of the SNIF method have also been extended to spirits and brandies.[179] Since many of these studies are based on ethanol determination, a critical analysis of the accuracy of the SNIF-NMR method compared with other methods such as a time domain least-squares procedure has been carried out.[180]

NMR spectroscopy, mass spectrometry, and atomic absorption spectrometry have been combined for isotopic and trace metal analysis of fruit juices. It was shown that only four parameters – barium, rubidium, potassium, and deuterium isotope ratio performed on ethanol – were required to distinguish orange juices from Brazil, Florida, and Israel.[181] Different forms of adulteration of juices, including the addition of sugar or dilution with tap water, were also studied by ^{2}H SNIF-NMR, in some cases coupled with mass spectrometry or chemical analysis.[182–189] Isotopic methods can be applied to ingredients other than sugars present in fruit juices, e.g. organic acids, vitamins, polyols, etc. These molecules may be used as probes for detecting the addition of the same chemical species but may also provide useful internal isotopic references. A detailed methodology for measuring the natural deuterium distribution in citric acid of lemon juices by SNIF-NMR and mass spectrometry has been presented,[190, 191] using triethyl citrate (TEC) as a probe for ^{2}H NMR. The same

procedure may also integrate the determination of the ^{13}C content in sugars, citric acid, and L-malic acid.

The coupling of SNIF-NMR with stable isotope ratio analysis/mass spectrometry has been the basis of a method for detection of adulteration of maple syrup with beet, cane, or corn sugar.[192] Adulteration of mustard oil by the addition of synthetic allyl isothiocyanate, its major component, is of economic interest, and therefore a combined NMR and mass spectrometry method was developed, enabling the distinction between the natural and the synthetic compound, as well as the determination of the geographical origin of natural mustard oils.[193] Similar methods have been used for the analysis of flavourings such as vanilla flavour (vanillin and *p*-hydroxybenzaldehyde),[194,195] benzaldehyde,[196] and others.[197]

Much effort has also been employed on developing new authentication methods for olive oils. The method of determination of hydrogen isotope ratios, D/H, at specific sites in fatty acids has been used to characterize 200 oils in terms of country, region, and year of production.[198]

4.2. High-resolution NMR spectroscopy

4.2.1. Fruit products, vinegar, coffee, and tea

Proton high-field NMR has been shown to be very valuable for the analysis of low molecular weight compounds in fluid foodstuffs. Water suppression can be achieved with great efficiency, and a large dynamic range is available. Examples are applications to fruit juices,[12,199,200] vinegars,[199] and coffee.[201]

An innovative approach was applied for the differentiation of grapevine cultivars and clones, by using a set of multivariate statistical methods to 2D NMR data ($^{1}H/^{13}C$) of polyphenol extracts from grape seeds and leaves.[202] The results showed that clones are divided into three groups, according to the cultivar, and that they can be differentiated inside each cultivar. The application of multivariate analysis to the NMR spectra of foods has been extended to fruit juices.[203,204] Principal component analysis (PCA) of the ^{1}H NMR spectra of apple juices of varieties Spartan, Bramley, and Russet gave a high rate of success for their classification. The levels of malic acid and sucrose were two important variables, but variations in minor components were also found to be significant.[203] Principal component and discriminant analyses were used to discriminate between authentic and non-authentic orange juice samples.[204] The application of PCA to 1D NMR spectra of orange juice (Fig. 3) was shown to be particularly effective in the interpretation of profile differences.

Green tea has been the subject of many studies owing to its beneficial health properties, and a number of phenolic compounds have been identified.[205–207] The aluminium content in several types of tea (green, black, and oolong tea from China) was determined by ^{27}Al NMR, and the possible complexation of polyphenolic constituents with aluminium(III) was investigated.[208] An interesting

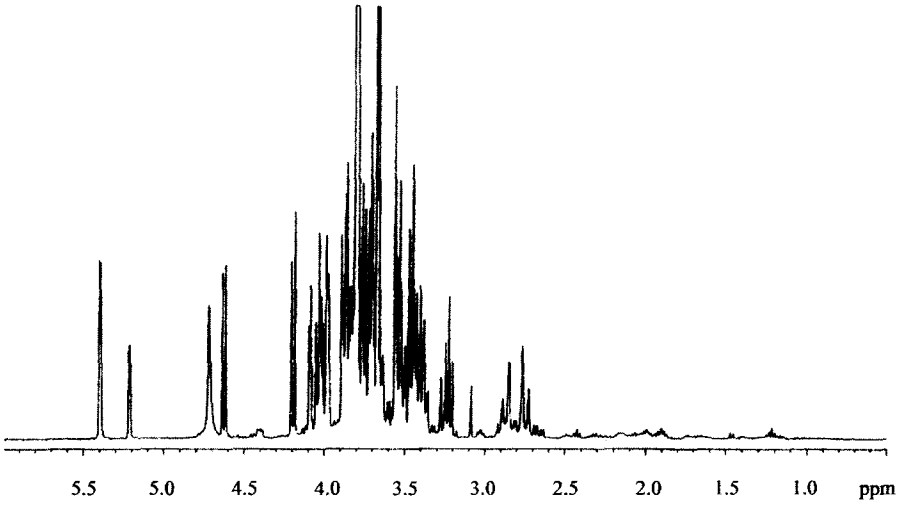

Fig. 3. Example of a typical orange juice ^{1}H NMR spectrum obtained with water peak suppression. Reprinted from *J. Agric. Food Chem.*, Vol. 44, J. T. W. E. Vogels, L. Jerwel, A. C. Tas, F. van den Berg, F. Dukel and J. van der Greef, 'Detection of adulteration in orange juices', pp. 175–180, Copyright 1996, with permission from the American Chemical Society.

study was also carried out on the possible interactions between food phenolics and aromatic flavours, using 1D and 2D NMR spectroscopy.[209]

4.2.2. Lipids

Much of the work on lipids has continued to rely on the application of conventional high-resolution methods. Many general papers are available, tackling both sampling and analysis issues (Table 4).

Olive oil has been extensively investigated in the last few years, and much work has, for instance, been applied to developing methods for discrimination of olive oil samples. High-field ^{1}H NMR spectroscopy (600 MHz) has been successfully employed to characterize olive oil, to the extent of identifying many of its minor components including many volatile compounds.[241] The same authors have then extended this work in order to discriminate oils from different varieties and from four different regions of Italy.[242] Principal component analysis showed that a good classification was obtained from the minor components such as alkenals and other volatiles. It was also noted that the effects of variety and environment are difficult to distinguish. The content of diglycerides in olive oils was determined by ^{13}C NMR and shown to relate to maturity,[243] so that sample discrimination may be done on that basis. ^{13}C NMR has been used with distortionless enhancement by polarization transfer to monitor adulterations in

Table 4. Additional NMR studies on lipids

Subject	Year (Reference)
General	
Analysis of *trans* fatty acids	1998 (210)
NMR spectra of lipids	1996 (211); 1998 (10, 18); 1999 (212, 213)
Guidelines for interpretation of ^{13}C NMR spectra	1999 (213)
Applications of high-resolution methods to oils and fats	1998 (10)
Structure determination of polyunsaturated triacylglycerols	1996 (214)
^{31}P NMR for profiling of phospholipids	1996 (215)
Vegetable oils	
Analysis of liquid oil in oilseeds	1999 (216)
Review of Italian research on the quality of extra virgin olive oil	1995 (217)
Characterization of fatty acids in olive oil and other oils	1999 (218); 1998 (219, 220)
Measurement of iodine values of vegetable oils	1998 (221)
Sampling and analysis of oilseeds	1998 (222); 1999 (216)
Influence of diglycerides on the crystallization of palm oil	1999 (223)
Analysis of conjugated linoleic acid esters	1999 (224)
Multivariate/NMR analysis of olive oil	1998 (225)
Characterization of triglycerides in olive oil and other oils	1996 (226); 1999 (227, 228)
Analysis of virgin olive oil compounds	1999 (229)
Characterization of phenolic compounds in olive oil	1998 (230); 1999 (231)
Dairy lipids	
Quantification of triglycerides and fatty acids in dairy products	1999 (232)
Oxidation effects	
Characterization of lipid oxidation by 1D and 2D NMR	1999 (233, 235); 1997 (234)
Formation of cyclic fatty acids	1998 (236)
Analysis of non-volatile components produced upon heating of fatty acid esters	1997 (237)
Oxidative stability of sesame oil	1996 (238)
Effects of hydrogenation in vegetable oils	1998 (239, 240)

olive oil and classify the samples according to variety and geographical origin.[244] Along similar lines, a method combining ^{1}H NMR and gas chromatography (GC) was employed to distinguish between pure olive oil and olive oil–hazelnut oil mixtures. It was found that linolenic acid has the highest discriminating power for the two oils.[245]

Lipid oxidation is a major problem in the food industry, and the use of NMR to assess oxidative stability has been investigated and compared with the traditional laboratory methods. In fact, a good correlation has been found between total oxidation value and ^{1}H NMR data, which establishes a rapid method for determination of oil oxidation during processing and storage.[246,247]

The interest in investigating the apparent effects of fish oils relating to lower incidences of heart disease has continued and, therefore, so have the structural studies of these types of oil. The positional distribution of $\omega 3$ fatty acids in depot fat of Atlantic salmon (*Salmon salar*), harp seal oil, and cod liver oil triacylglycerols has been investigated by ^{13}C NMR of the lipid extracts.[248] The same authors have prepared a study of the use of different NMR techniques, including imaging and MAS methods, to examine total fat content and the composition and distribution of fat in farmed fish.[249] It is shown that NMR is suitable for both *in vivo* and *in vitro* characterization of fish muscle. The oxidative deterioration of oils from marine products during storage has been examined in several studies. ^{13}C NMR has been used in tandem with GC and high-performance liquid chromatography (HPLC) to investigate the formation of hydroxy derivatives from hydroperoxides during the oxidation of methyl linoleate and mackerel oil.[250] Alterations occurring during fish canning have been the subject of some work showing that, for the lipids extracted from tuna samples and salmon white muscle, the unsaturated fatty acids located at the *sn*-2 position of the glycerol moiety are most prone to oxidative change.[251,252] Furthermore, the extent and mechanism of lipolysis seemed to be independent of the filling medium (brine or soybean oil).[251]

^{1}H and multinuclear NMR has been used to study lipid/water systems and their phase structures, touching upon crystallization and lipid translational diffusion, as these processes significantly affect the properties of foods.[253]

Additional publications are listed in Table 4.

4.2.3. Genetically modified products

Plant biotechnology holds much promise in developing quality crops requiring less inputs (such as fertilizers and pesticides) or improving certain characteristics of the food. An evaluation of these novel plants and their potential risks for environmental and health safety is, of course, of paramount importance. NMR has been applied with this purpose, in conjunction with liquid chromatography, as LC-NMR, to attempt the evaluation of the safety of genetically modified tomatoes, as an example of transgenic food crops.[254,255] In the latest work, an approach is proposed in which the chemical fingerprint of the transgenic food is compared with those of the non-transgenic food, but taking into account the effects of natural genetic and/or physiological variations. In this particular study it was found that there were minimal compositional variations between isogenic non-transgenic and transgenic lines across sites and seasons.[255]

4.2.4. Other studies

A large number of food low molecular weight components have been extracted and characterized by high-resolution NMR spectroscopy and, since the present text by no means aims at giving an extensive list of these compounds, only a few

examples are given, e.g. capsaicinoids and capsaicinoid-like substances in pepper;[256] anthocyanins in blue berries,[257] in black bean,[258] in red radish,[259] and in wine;[260] sesquiterpene hydrocarbons in distilled lime oil;[261] carotenoids,[262,263] and sapogenins in leeks;[264] phenolics in sage[265] and in oregano;[266] polyphenolics in grape pomace.[267]

The study of particular natural products characteristic of a certain food and therefore capable of being used as quality indicators has been the driving force of some work, for instance the isolation and characterization of phlorin, an orange peel marker,[268] or the isolation and characterization of resveratrol monomers found in red wine.[269] In the latter study, the evolution of *trans*- and *cis*-resveratrol, *trans*-resveratrol β-D-glucopyranoside, and *cis*-resveratrol β-D-glucopyranoside in red wine vinification was investigated. In addition, a series of oligosaccharides has been isolated from a series of different New Zealand honeys, with the aim of using the corresponding NMR and chromatographic data for fingerprinting of the samples studied.[270] The contribution of amino acids and peptides for the taste of foods has been known for many years. The Delicious Peptide is an eight-residue linear food flavour peptide responsible for the flavour of beef gravy, which has been characterized by molecular dynamics and NMR[271] in order to determine the structural origins of its characteristic flavour.

The growth of microorganisms may have an important effect on the flavour of food. An example is the lactic acid bacteria *Lactococcus lactis*, which produce mainly lactate providing a characteristic acidic flavour and contributing to the preservation of fermented food. In an innovative approach, *in situ* ^{13}C NMR was used to investigate glycolysis by an *L. lactis* strain deficient in lactate dehydrogenase.[272]

A provisional list of additives for the production of food-contact plastics has been published, anticipating an EC Directive on these additives, and their characterization by several techniques, including NMR, is described.[273] The problem of the interactions of food with packaging materials has also been addressed by a study of the migration of some food additives into packaging materials, using NMR in tandem with UV-Visible spectrophotometry.[274]

4.3. Solid-state NMR spectroscopy

In the study of complex solid and semi-solid foods, solid-state NMR becomes of valuable use. ^{13}C CPMAS NMR has been used to characterize the insoluble deposits in aromatic bitters.[275] MAS has been successfully used to characterize and quantify the oil fraction present in intact seeds, and several publications have focused on this subject, e.g. to compare the oil composition of hybrid and transgenic canola seeds.[276] In addition, the HR-MAS method has become an important new tool for the study of semi-solids such as flour doughs or intact fruits, as described in section 6.3.

5. COMPLEX SYSTEMS

5.1. Textural measurements

In the understanding and prediction of textural properties, NMR has two advantages: the sensitivity of NMR to the dynamic properties of materials on the microscopic scale and the ability of imaging non-invasively to explore changes in structure and dynamics. Indirect inference about the relationship between dynamics and texture has been drawn in an examination of the prediction of the textural properties of cooked potatoes.[277] It was shown that measurements of the decay curves from a Carr–Purcell–Meiboom–Gill (CPMG) sequence on the raw and cooked material could be related to textural properties when the data were analysed by a multivariate statistical method. The authors assign the different components observed in the CPMG sequence to different types of water in the sample. They suggest that the longer component of the two-component decay is due to water in a relatively non-restricted situation, and the faster component is due to diffusion-hindered extracellular water. However, this account of the origins of the components does not consider the major role of proton exchange in determining the relaxation rates on water. In general, without fully accounting for exchange effects it is very difficult to relate relaxation rates of water to motional states. Similar work has been carried out on bread.[278]

Imaging methods have been exploited to evaluate the internal structural changes in tomatoes during compression[279] and to explore the internal hollows in cooked rice grains.[280,281] Other applications of NMR to textural properties have been investigating the role of thickening agents on sodium binding and other taste qualities of soup.[282]

5.2. Fish and meat

The increasing importance of fish quality has been demonstrated by the number of papers devoted to this subject. Work has been reported on cod and haddock using MRI[283] and on relaxation in fresh and processed cod.[284,285] Relaxation methods have also been used to predict oil and water content in fish.[286] ^{13}C resonance has been used to select thermal processing conditions for canned fatty fish,[287] and proton spectra may be used to follow oxidation processes in mackerel muscle.[288] Metabolism may be studied at a sophisticated level: multidimensional multinuclear NMR has been employed to analyse the metabolites of crayfish.[289] In another potentially useful application of multinuclear NMR to crustaceans, Nagata and co-workers[290] have used ^{23}Na and ^{35}Cl NMR to investigate snow crabmeat. Unfortunately, the interpretation of the data is limited since the authors do not take account of the quadrupolar nature of the nuclei involved and thus attribute multiple peaks in the ^{35}Cl spectrum to chemical effects rather than the more likely residual static quadrupolar interactions.[291]

There are a number of possible methods for the instrumental testing of meat quality; comparisons of these methods with NMR have been published.[292–296] Imaging methods continue to be extensively favoured in meat science and have recently been reviewed, together with spectroscopic methods.[297] MRI has been used to estimate the mass of muscle in chickens *in vivo*[298] and more generally to image fat and muscle distribution.[299]

The process of pork brining has been studied by using ^{23}Na imaging[300] and has also been explored by observing the effects of the binding of manganese ions.[301] The use of MRI and measurement of bulk NMR properties have been compared for assessing brined pork quality, and an automated MRI system has been proposed.[302]

NMR relaxation may be a possible predictor of meat quality[303] in frozen beef and can be used on-line for the analysis of ground meats.[304] The effects of pH drop rate and chilling have been investigated using NMR relaxometry,[305] and it has been shown that the fastest pH drop rates resulted in larger extracellular volumes and the destruction of cell membranes and more tender meat. Phosphorus NMR has been used to detect differences in the post-mortem ATP turnover of normal pigs and those with malignant hypothermia,[306] and the relationship between NMR properties and warmed over flavour in meat has also been reported.[307]

5.3. Fruit and vegetable products

NMR imaging is a powerful method for the non-invasive investigation of soft tissues in fruit and vegetables; the high water contents make imaging fairly straightforward and factors such as ripeness and tissue damage appear to affect images in a clearly measurable way. A review of the application of NMR microscopy to agricultural produce has been published.[308] Comparison of MRI with X-ray methods for the quality evaluation of durian and mangosteen fruits has shown that MRI has the advantage over X-ray that it can detect the presence of water core disorder in durian fruit.[309] A similar comparison of detection of woolly breakdown in nectarines has also shown the advantages of MRI.[310] The origins of the contrast effect on fruit bruising may not only be due to changes in water content or relaxation, there may be diamagnetic susceptibility effects as well.[311]

Imaging has also been applied to the study of chilling injury in persimmon fruit,[312] to the study of growth and ripening of kiwi fruit,[313] and to the detection of pitted olives, while a conveyer belt transports the fruits through a low-field NMR magnet.[314]

Imaging is not the only way of measuring fruit quality. Relaxation time measurements can also be useful: the free induction decay signal from prunes can be analysed as containing two components that correspond to water and soluble solids. The intensity of the soluble solids signal corresponds well to those

measured by other methods.[315] A similar approach has enabled the development of a high-speed method for evaluating the maturity of avocados.[316]

The use of NMR to measure the oil content of seed is well established, but it can be extended to the simultaneous measurement of oil and moisture[317] and has been compared to near-infrared (NIR) methods.[318] MRI has been less used in the examination of seeds compared with fruits, but on the small scale it may be used to locate oil and sucrose in maize.[319]

5.4. Other systems

Breads and doughs are important commercial products, although they are still relatively poorly understood. The processes of staling and spoilage are still ones that merit further investigation. It is often held that once such a system is in a glassy state no more changes are likely. However, a study of the molecular mobility in glassy bread using a number of techniques including NMR has shown that this may not be the case.[320] The observation of a glass transition temperature did not mean that all motion had stopped, and evidence was found that even below the transition temperature textural changes could still take place. Lipids may be responsible for some of the motions detected in glassy bread, and it may be these that contribute to the instability of the system.[321] The results suggested that the lipids were in globules in the bread within which they were able to diffuse. Glass transitions have also been investigated in frozen doughs,[322] as well as the effects of DATEM esters.[323]

Chocolate makes a good NMR sample as it contains mobile and immobile phases and has a high proton density. Hall and co-workers have carried out a general survey of chocolate confectionery by MRI[324] and have visualized the migration of liquid triacylglycerol by the same method.[325] The use of NMR relaxation to assess chocolate has also been considered.[326]

Other applications of NMR to complex systems are shown in Table 5.

Table 5. Miscellaneous applications of NMR to complex systems

Application type	Year (Reference)
Temperature measurement	
New method for measuring internal temperature of meat	1999 (327)
Imaging and spectroscopy of wheat flake biscuits during cooking	1995 (328)
Pulsed field gradient study of electrical and conventional heating of carrots	1995 (329)
Temperature mapping in carrots	1995 (330)
Dairy products	
Replacement of whole milk powder with soymilk in chocolate	1999 (331)
Kinetic analysis of the crystallization of a milk fat model system	1999 (332)

Table 5. *continued*

Application type	Year (Reference)
Dairy products (*continued*)	
HPLC and NMR study of the reduction of whey permeate	1996 (333)
Characterization of cheese by statistical analysis of time domain results	1998 (334)
Direct measurement of thermal fat crystal properties	1996 (335)
NMR imaging of dairy products	1995 (336)
Acidification of pressure-treated milk	1997 (337)
Characterization of semi-solid state in milk fat	1999 (338)
Analysis of Maillard products in milk	1999 (339)
Fats and oils	
Solid fat content determination	1999 (340)
Tailoring attributes of butter fat/canola blends	1998 (341)
Restructuring butterfat through blending and chemical interesterification	1996 (342)
^{13}C NMR study of vegetable margarine	1995 (343)
Analysis of triacylglycerol composition of margarines by ^{13}C NMR	1996 (344)
Characterization of hydrogenated fats for margarine manufacturing purposes	1998 (345)
High-pressure effects on emulsified fats	1995 (346)
Determination of droplet size distributions in emulsions	1995 (347)
Emulsion formation and coalescence	1998 (348)
Identification of cocoa butter and alternative fats in chocolate	1998 (349)
Moisture and fat determination to monitor drying and coating processes of exudates	1995 (350)
Other applications	
Stability and mobility in model foods using NMR, DSC, and microbial germination	1999 (351)
High-resolution proton NMR of coffee	1999 (201)
Coffee flavourings	1998–1999 (352)
Interactions between polyphenols and aroma substances	1999 (353)
^{17}O NMR of effects of processing and storage on taro paste	1998 (354)
Structural analysis of red seaweed galactans of agar and carrageenan groups	1998 (355)
Relaxometry for determination of the reconstitutability of protein powders	1997 (356)
Pulsed NMR of rice starch during gelatinization and retrogradation	1998 (357)
^{13}C NMR of changes in metabolites of mushrooms	1997 (358)
Characterization of citrus honey by deuterium NMR	1996 (359)
Lipid protein interactions in foods	1995 (360)
Ingredient interactions	1995 (361)
Bound salt in freeze-concentrated soy sauce	1998 (362)
Phosphorus NMR of brewing yeast	1997 (363)
Preparation of epimers of tea catechins	1997 (364)
Biochemical basis of inhibition of malolactic fermentation	1997 (365)
Molecular relaxation of sucrose solutions at subzero temperatures	1995 (366)
Interaction of bile acids and barley beta glucans by CPMAS	1996 (367)
In vivo ^{13}C NMR study of adipose tissue composition	1996 (368)
In vivo measurement of the intramuscular fat content of muscle pigs	1997 (369)

6. NEW METHODS FOR FOOD ANALYSIS

6.1. Fast field cycling NMR

Many of the applications of NMR to foods use proton relaxation time measurements. The results are then interpreted qualitatively in terms of rapid or slow motions, or quantitatively using some suitable model. Typically, the data available will derive from measurements of T_1, T_2 and, occasionally, $T_{1\rho}$. Sometimes, data may be collected at one or more frequencies, but this is fairly rare and at best only tends to cover a range of from tens to hundreds of megahertz. In a complex system such as food it will not normally be the case that the motions responsible for one relaxation time will be the same as those for the other relaxation times. An example might be a protein: in the solid state, T_1 relaxation will be governed by fast side-chain motions, whereas T_2 will reflect the motion in the much slower moving backbone and the residual static interactions arising from the anisotropic motion of the side chains. Qualitatively, it is therefore difficult to make unambiguous statements about the motion in a system of this sort. The quantitative problem is considerably harder: generally, in the motional narrowing regime, the relaxation process can be described in terms of a spectral density function as follows.

$$T^{-1} = M[n_0 J(0) + n_1 J(\omega_1) + n_{1,0} J(\omega_0) + n_{2,0} J(2\omega_0)] \quad (1)$$

where $n_0 = 0$ for T_1 and $T_{1\rho}$, $n_1 = 0$ for T_2 and T_1, M is an interaction constant related to the appropriate second moment, and the terms $J(\omega)$ are the appropriate spectral density functions. In the rigid lattice regime, T_2 must be described differently[138] but may still give information about motion. Often, equation (1) is further expanded in terms of the Bloembergen–Purcell–Pound (BPP) model[370] which describes rotational motion. In foods this expansion is dubious and must be used with great caution; often, motion arises from complex biopolymer chain motions for which BPP is not appropriate. In the case of water, relaxation is governed by both diffusive and rotational motion, for which BPP theory, which is a theory of rotational motion, is incorrect.[371]

Whatever model is used, the problem with equation (1) is that it is intrinsically underdetermined since it contains the product of interaction and spectral density terms. The usual solution is to examine relaxation at different temperatures and assume a function (usually exponential) for the temperature dependence of the correlation times. This is problematic in foods, as the structure of food is typically very temperature dependent. The alternative is directly to determine the spectral density function of the material by determining T_1 over a wide range of frequencies. This may be done by using fast field cycling NMR.

A fast field cycling NMR spectrometer is similar to a normal spectrometer, with the exception that the magnetic field may be switched between different fields on the timescale of milliseconds. Further details are given elsewhere.[372] Typically, the range of frequencies covered is from about 10 kHz to 10 MHz. A simulation of the behaviour of a spin system obeying BPP theory is given in

Fig. 4. It shows typical features of a dispersion with a plateau at low frequencies (note that the scale on both axes is logarithmic).

In practice, the data from real systems are less clean cut but show the same kinds of trend. Figure 5 shows the results obtained from samples of soya 7S proteins stored under different conditions and compared with fresh material

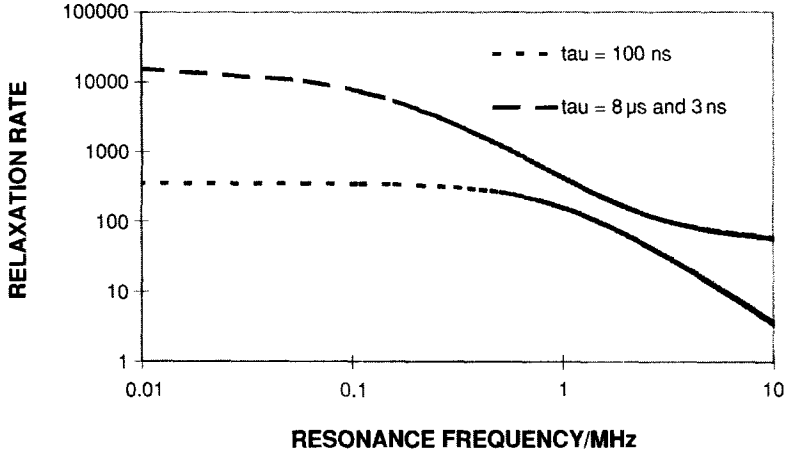

Fig. 4. Simulation of the effects of resonance frequency on relaxation rate in field cycling NMR.

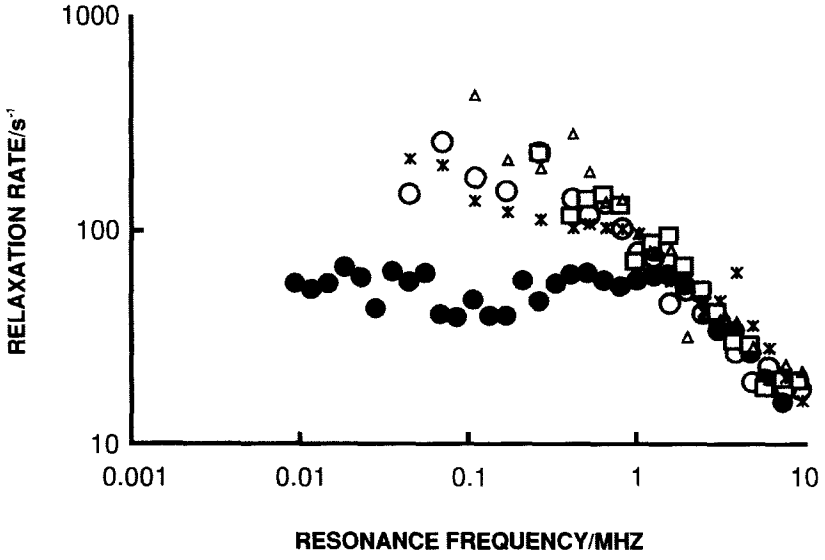

Fig. 5. Fast field cycling dispersion curve of soya 7S proteins in D_2O. The filled circles are the results from the fresh material and the other symbols are from samples stored under a variety of conditions.

(filled circles). All the stored material shows marked differences to fresh material below 1 MHz. These differences would not have been seen on an ordinary spectrometer.

The quantitative interpretation of the data for systems such as these needs some care[372] as the theoretical models seem to be ambiguous at the moment and the treatment of systems in the rigid lattice condition needs attention to the details of the spin physics if the data are not to be misinterpreted.[373] However, the use of the technique considerably extends the possibilities for the use of proton NMR in food systems and should allow a more detailed description of dynamical processes and an improvement in comparative studies. An important advantage is that the temperature dependence of the spectral density function becomes a measurable variable, thus allowing a more detailed investigation of temperature effects.

6.2. Liquid chromatography-NMR

Liquid chromatography is usually associated with the separation of very small quantities of material requiring the most sensitive detection methods. This would seem to eliminate NMR which has been conventionally regarded as an intrinsically insensitive technique. There is no denying that, generally speaking, the nuclear induction signal is small and the transition between energy levels involves low-energy quanta.

However, in spite of these limitations, there has been a revolution in the sensitivity of NMR spectrometers, which has made the detection of small signals much easier. Typically, it is now possible to work in the 100 ng region for small molecules, and LC-NMR has thus become a practical reality. In order to achieve this, new specialist hardware and software have had to be developed,[374] especially with regard to the management of the flow of material and the need to eliminate the broadening of chromatographic peaks during the measuring process by NMR. Additional improvements have been multiple solvent suppression and a high level of automation. Using these techniques, it is practical to obtain good spectra of chromatographic peaks and to store or divert the samples for further analysis. The power of NMR can thus be focused on samples that hitherto were only characterized by a limited UV spectrum and some retention time data. Typically, a single peak observed by UV may be shown to be a complex mixture by NMR. Some chemicals do not give UV active signals and may be lost altogether with a conventional sampling system.

A further sophistication is to couple the LC-NMR system with a mass spectrometer. This has two advantages. The first is that the sensitivity of the mass spectrometer is much greater than that of the NMR spectrometer, so that compounds occurring below the detection limit of NMR may be observed by mass spectrometry. The other advantage is that the combination of a 1D NMR spectrum together with a mass spectrum is often enough for unambiguous

identification of a compound. A typical LC-NMR-MS experiment will be centred on a 600 MHz spectrometer, using a magnet with a shielded magnetic field to avoid interference with the mass spectrometer magnet, and an ion trap mass spectrometer. The flow from the LC system will be managed automatically and will be split in the appropriate ratio between the NMR spectrometer and the mass spectrometer. In the mass spectrometer arm, the necessary adjustments to the solvent will be carried out, and the mass spectrum will be automatically coupled to the NMR spectrum.

So far LC-NMR and LC-NMR-MS have been typically applied to drugs and drug metabolites.[375] However, applications to natural products have been reviewed[376] and applications to leaf flavonoids reported.[377]

Chromatography methods combined with NMR have been used for the analysis of hop acids and beer bitter acids.[378,379] Supercritical fluid chromatography has been used in the analysis of ascorbigens in Brassicas, but in this case the NMR was not on line with the chromatography system.[380]

Particularly relevant for food has been the analysis of quercetin and phloretin glycosides using LC-NMR-MS.[381] In this experiment the mass spectrometer was used to monitor the outflow of the LC system for intensity at masses 301 and 273. These two masses are diagnostic for the presence of the quercetin and phloretin moieties. The NMR spectra of the corresponding fractions were then obtained, and the states of glycosylation were determined. LC-NMR has also been applied to the analysis of beer components. The signals from the sugar region of the spectrum at different retention times are shown in Fig. 6. Using this method, it has been possible to observe signals from a variety of oligosaccharides.[382]

The use of LC-NMR and LC-NMR-MS has very considerable potential in food science. It may be used in the analysis of the complex mixtures of chemicals that constitute foods. It clearly will have useful applications in human nutrition studies, where it would be possible to study the detailed metabolic history of chemicals such as antioxidants in the diet. It will also be useful in the analysis of new foods such as GM products to ensure that no unexpected metabolites are present.

6.3. High-resolution MAS NMR

MAS NMR has proved to be of great value for the study of semi-solid foodstuffs since it takes advantage of the fact that inherent molecular motion partially averages the line-broadening interactions such as dipolar interactions and chemical shift anisotropy. Residual effects like magnetic susceptibility are then weak enough to be effectively averaged out by MAS. This has been observed for intact fruits,[200] flour doughs,[78] and cereal protein doughs.[76] However, recent instrumental developments in MAS NMR equipment have enabled the use of HR-MAS NMR, leading to a significant resolution improvement in the spectra of

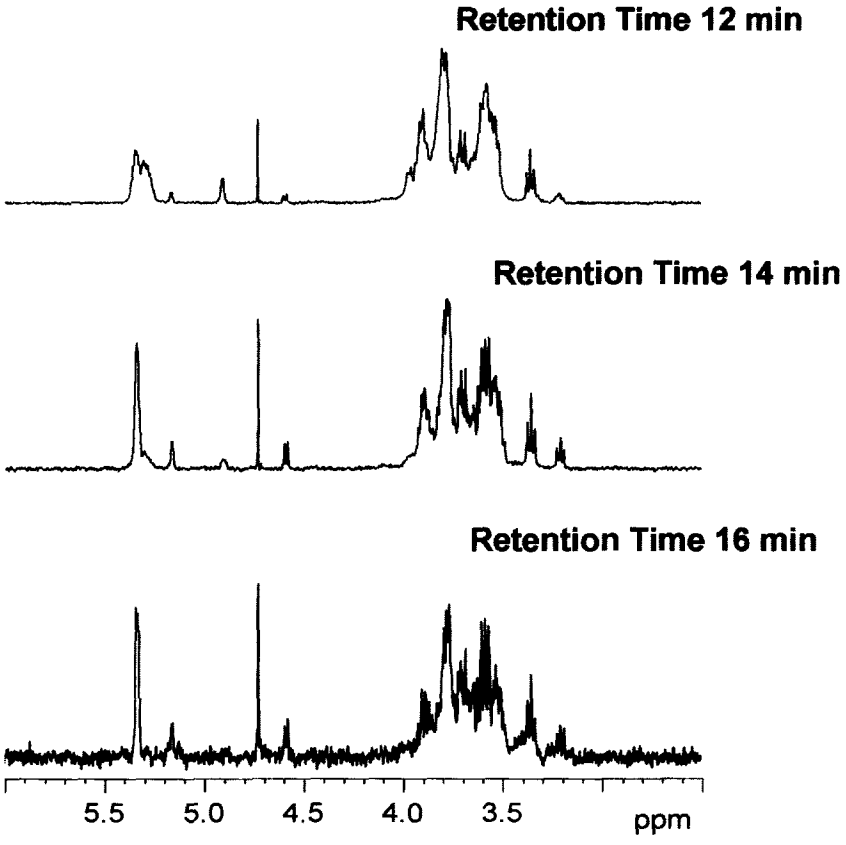

Fig. 6. ^{1}H NMR spectra of the sugar region of the LC-NMR spectrum of beer at different retention times.

semi-solid food samples and very efficient solvent suppression. Furthermore, an MAS rotor which confers a spherical geometry to the sample has been found to result in reduced magnetic susceptibility effects and, thus, spectra of enhanced resolution. HR-MAS NMR spectra of mango pulp as a function of ripening time have enabled a study of the resulting biochemical changes[200] and have shown that some components, e.g. pectins, lipids, and polyphenols, may only be studied in the intact fruit, rather than in the juice. A thorough ^{1}H HR-MAS study of durum wheat flour doughs from different regions of southern Italy has shown that a remarkable amount of compositional information may be obtained, thus avoiding any kind of sample pretreatment.[383] Preliminary multivariate analysis of the spectra suggests that samples may be distinguished according to their geographical origin. The same NMR method has also enabled 2D NMR methods to be applied to cereal protein doughs, enabling valuable structural information to be extracted.[76]

6.4. Rheological NMR

Applications of NMR methods in rheological studies on complex fluids can be broadly subdivided into two categories: (a) the use of NMR velocimetry to examine flow profiles in the various shear geometries in order to gain direct information regarding the flow curve and hence probe the non-linear, shear-dependent viscosity,[384] and (b) the use of NMR spectroscopy to gain insight regarding molecular order and dynamics under shear.[385] Both approaches have been used successfully in recent years, and a detailed review paper has been recently published on the principles and applications of rheological NMR (or rheo-NMR).[386]

Rheo-NMR methods have enormous potential in food analysis because it is very often important to follow the changes and behaviour of foods while they are subjected to some kind of stress, either during manufacturing or processing or during domestic use. A pioneering application of rheo-NMR to food materials took place in 1997 with a study of the heterogeneous shear flow in food materials.[387] Velocity profiles of foods such as tomato ketchup and egg white were recorded, reflecting the complex nature of such systems when subjected to shear forces. More recently, rheo-NMR was applied to studying the effects of shear and extensional deformations on the structure of wheat gluten.[388] The resulting changes in the ^{1}H NMR spectra of gluten suggested that hydrogen bonds are broken when stress is applied and reformed after stress cessation. The results obtained for a soft flour gluten and a hard flour gluten were compared. Since extensional stress is more relevant in dough technology, extensional studies were also carried out using a new bi-axial extension cell, offering the advantage that small (e.g. a few mg) samples may be used, and, unlike filament-stretching rheometers, there is no need for the material to adhere to the end plates.

A preliminary study was also carried out in order to follow the gel–sol and sol–gel transitions of the thermoreversible polysaccharide κ-carrageenan under shearing conditions.[389] The velocity profiles obtained at different temperatures enabled the effect of shear on the processes to be studied and an intermediate 'sol-like' transition state to be detected. ^{1}H NMR spectroscopy and T_2 measurements were recorded, showing the presence of two dynamic spin populations, possibly arising from random coil segments and helical aggregated segments.

REFERENCES

1. A. M. Gil, P. S. Belton and B. P. Hills, *Annu. Rep. NMR Spectrosc.*, 1996, **32**, 1.
2. M.-L. Martin and G. J. Martin (eds), *Magn. Reson. Chem. – Special Issue: NMR in Food Science*, John Wiley, New York, 1997, Vol. 35.
3. P. S. Belton, G. A. Webb and B. P. Hills (eds), *Advances in Magnetic Resonance in Food Science*, Royal Society of Chemistry, Cambridge, 1999.

4. G. A. Webb, P. S. Belton, A. M. Gil and I. Delgadillo (eds), *Magnetic Resonance in Food Science – A View to the Future*, Royal Society of Chemistry, Cambridge, 2001.
5. B. P. Hills, *Magnetic Resonance Imaging in Food Science*, John Wiley, New York, 1998.
6. R. R. Ruan and P. L. Chen, *Water in Foods and Biological Materials a Nuclear Magnetic Resonance Approach*, Technomic Publishers, Lancaster, Pennsylvania, 1998.
7. D. S. Reid (ed.), *The Properties of Water in Foods: ISOPOW 6, Santa Rosa, 1996*, Blackie, London, 1996.
8. J. N. Barbotin and J.-C. Portais, *NMR in Microbiology*, Horizon Scientific Press, Wymondham, Norfolk, 2000.
9. G. J. Martin and M. L. Martin, in *Flavor Chemistry: Thirty Years of Progress: Proceedings of a Symposium, Boston* (eds R. Teranishi, E. L. Wick and I. Hornstein), Kluwer Academic, New York, 1999, p. 19.
10. B. W. K. Diehl, in *Lipid Analysis in Oils and Fats* (ed. R. J. Hamilton), Blackie, London, 1998, p. 87.
11. P. Cornillon, *Seminars in Food Analysis*, 1998, **3**, 235.
12. P. S. Belton, I. Delgadillo and A. M. Gil, *Seminars in Food Analysis*, 1998, **3**, 223.
13. T. M. Eads, in *Food Analysis* (ed. S. S. Nielsen), Aspen Publishers, Gaithersburg, 1998, p. 455.
14. T. M. Eads, in *Spectral Methods in Food Analysis: Instrumentation and Applications*, Marcel Dekker, New York, 1998, p. 1.
15. I. Colquhoun and M. Lees, in *Analytical Methods of Food Authentication* (eds P. R. Ashurst and M. J. Dennis), Blackie, London, 1998, p. 36.
16. D. J. McClements, in *Food Analysis*, Aspen Publishers, Gaithersburg, 1998, p. 571.
17. S. Divakar, *J. Food Sci. Technol.*, 1998, **35**, 469.
18. M. Farines, *Oleagineux Corps Gras Lipides*, 1998, **5**, 291.
19. C. Deleanu and J. R. J. Pare, in *Instrumental Methods of Food Analysis* (eds J. R. J. Pare and J. M. R. Belanger), Elsevier, Amsterdam, 1997, p. 179.
20. M. Careri and A. Mangia, *Tren. Anal. Chem.*, 1996, **15**, 538.
21. D. N. Rutledge and D. Tome, in *Analytical Techniques for Foods and Agricultural Products* (ed. G. Linden), VCH, Cambridge, 1996, p. 249.
22. P. S. Belton and A. M. Gil, *J. Magn. Reson. Anal.*, 1996, **2**, 45.
23. O. Soderman and B. Balinov, in *Emulsions and Emulsion Stability* (ed. J. Sjoblom), Marcel Dekker, New York, 1996, p. 369.
24. H. D. Isengard, *Tren. Food Sci. Technol.*, 1995, **6**, 155.
25. P. Chinachoti, in *Food Preservation by Moisture Control: Fundamentals and Applications* (ed. G. V. Barbosa-Canovas), Technomic Publishers, Lancaster, Pennsylvania, 1995, p. 191.
26. P. Chinachoti, in *Food Storage Stability* (eds I. A. Taub and R. P Singh), CRC Press, Boca Raton, 1998, p. 245.
27. I. Hopkinson, R. A. L. Jones, S. Black, D. M. Lane and P. J. McDonald, *Carbohydr. Polym.*, 1997, **34**, 39.
28. B. P. Hills and F. Barbonneau, *Magn. Reson. Imaging*, 1994, **12**, 1065.
29. B. P. Hills, F. Barbonneau, V. M. Quantin, F. Gaudet and P. S. Belton, *J. Food Eng.*, 1996, **27**, 71.
30. B. P. Hills, J. Godward and K. M. Wright, *J. Food Eng.*, 1997, **33**, 321.
31. S. Takeuchi, M. Maeda, Y.-I. Gomi, M. Fukuoka and H. Watanabe, *J. Food Eng.*, 1997, **33**, 181.
32. S. Takeuchi, M. Maeda, Y.-I. Gomi, M. Fukuoka and H. Watanabe, *J. Food Eng.*, 1997, **33**, 281.
33. H. Watanabe, S. Takeuchi, Y.-I. Gomi and M. Fukuoka, in *Engineering and Food at ICEF 7: Proceedings of the 7th International Congress on Engineering and Food, Supplement* (ed. R. Jowitt), Sheffield Academic Press, Sheffield, 1997, p. SA5.
34. A. G. F. Stapley, P. J. Fryer and L. F. Gladden, in *Engineering and Food at ICEF 7: Proceedings of the 7th International Congress on Engineering and Food, Part 2* (ed. R. Jowitt), Sheffield Academic Press, Sheffield, 1997, p. 37.
35. A. G. F. Stapley, T. M. Hyde, L. F. Gladden and P. J. Fryer, *Int. J. Food Sci. Technol.*, 1997, **32**, 355.

36. W. L. Kerr, R. J. Kauten, M. Ozilgen, M. J. McCarthy and D. S. Reid, *J. Food Process. Eng.*, 1996, **19**, 363.
37. B. P. Hills and B. Remigereau, *Int. J. Food. Sci. Technol.*, 1997, **32**, 51.
38. S. L. Duce and L. D. Hall, *J. Food Eng.*, 1995, **26**, 251.
39. K. M. Keener, R. L. Stroshine and J. A. Nyenhuis, *Trans. ASAE*, 1997, **40**, 1633.
40. G. Cherian and P. Chinachoti, *Cereal Chem.*, 1996, **73**, 618.
41. G. Cherian and P. Chinachoti, *Cereal Chem.*, 1997, **74**, 312.
42. A. Grant, P. S. Belton, I. J. Colquhoun, M. L. Parker, J. J. Plitjer, P. R. Shewry, A. S. Tatham and N. Wellner, *Cereal Chem.*, 1999, **76**, 219.
43. P. L. Chen, Z. Long, R. R. Ruan and T. P. Labuza, *Lebensmittel-Wissenschaft und Technologie*, 1997, **30**, 178.
44. R. R. Ruan, X. Wang, P. L. Chen, R. G. Fulcher, P. Peshek and S. Chakrabarti, *Cereal Chem.*, 1999, **76**, 231.
45. N. W. H. Cheetham and L. Tao, *Carbohydr. Polym.*, 1998, **35**, 279.
46. S. Li, L. C. Dickinson and P. Chinachoti, *J. Agric. Food Chem.*, 1998, **46**, 62.
47. I. A. Farhat, E. Loisel, P. Saez, W. Derbyshire and J. M. V. Blanshard, *Int. J. Food Sci. Technol.*, 1997, **32**, 377.
48. P. Cornillon, M. J. McCarthy and D. S. Reid, *J. Texture Studies*, 1997, **28**, 421.
49. I. A. Farhat, J. R. Mitchell, J. M. V. Blanshard and W. Derbyshire, *Carbohydr. Polym.*, 1996, **30**, 219.
50. W. L. Kerr and L. Wicker, *Carbohydr. Polym.*, 2000, **42**, 133.
51. A. Mora-Gutierrez, H. M. Farrell and T. F. Kumosinski, *J. Agric. Food Chem.*, 1995, **43**, 2574.
52. A. Mora-Gutierrez, H. M. Farrell and T. F. Kumosinski, *J. Agric. Food Chem.*, 1996, **44**, 48.
53. A. Mora-Gutierrez, H. M. Farrell and T. F. Kumosinski, *J. Agric. Food Chem.*, 1996, **44**, 796.
54. A. Mora-Gutierrez, T. F. Kumosinski and H. M. Farrell, *J. Agric. Food Chem.*, 1997, **45**, 4545.
55. A. N. Round, B. Yan, S. Dang, R. Estephan, R. E. Stark and J. D. Batteas, *Biophys. J.*, 2000, **79**, 2761.
56. D. R. Martin, S. Ablett, A. Darke, R. L. Sutton and M. Sahagian, *J. Food Sci.*, 1999, **64**, 46.
57. A. Ohtsuka and T. Watanabe, *Carbohydr. Polym.*, 1996, **30**, 135.
58. B. P. Hills, C. E. Manning, Y. Ridge and T. Brocklehurst, *J. Sci. Food Agric.*, 1996, **71**, 185.
59. B. P. Hills, C. E. Manning, Y. Ridge and T. Brocklehurst, *Int. J. Food Microbiol.*, 1997, **36**, 187.
60. X. Pham, E. Vittadini, R. E. Levin and P. Chinachoti, *J. Agric. Food Chem.*, 1999, **47**, 4976.
61. J. P. Lavoie, R. G. Rabbe and P. Chinachoti, *J. Food Sci.*, 1997, **62**, 861.
62. S. Ablett, A. H. Darke, P. J. Lillford and D. R. Martin, *Int. J. Food Sci. Technol.*, 1999, **34**, 59.
63. D. Hodzic, G. Llabres, S. Zgoulli, J.-J. Gilsoul and P. Thonart, *Lebesmittel-Wissenschaft und Technologie*, 1995, **28**, 21.
64. S. I. Cho and C. H. Chung, *Trans. ASAE*, 1997, **40**, 1129.
65. A. Gerbanowski, D. N. Rutledge, M. H. Feinberg and C. J. Ducauze, *Science des Aliments*, 1997, **17**, 309.
66. R. R. Ruan, C. Zou, C. Wadhawan, B. Martinez, P. L. Chen and P. Addis, *J. Food Process. Preserv.*, 1997, **33**, 91.
67. R. R. Ruan, S. Almaer, V. T. Huang, P. Perkins, P. Chen and R. G. Fulcher, *Cereal Chem.*, 1996, **73**, 328.
68. P. Cornillon, J. Andrieu, J.-C. Duplan and M. Laurent, *J. Food Eng.*, 1995, **25**, 1.
69. A. M. Gil, K. Masui, A. Naito, A. S. Tatham, P. S. Belton and H. Saitô, *Biopolymers*, 1997, **41**, 289.
70. A. M. Gil, E. Alberti, A. S. Tatham, P. S. Belton, E. Humpfer and M. Spraul, *Magn. Reson. Chem.*, 1997, **35**, 101.
71. P. S. Belton, A. M. Gil, A. Grant, E. Alberti and A. S. Tatham, *Spectrochim. Acta A*, 1998, **54**, 955.
72. P. S. Belton, *J. Cereal Sci.*, 1999, **29**, 103.
73. P. S. Belton, I. J. Colquhoun, A. Grant and N. Wellner, *Int. J. Biol. Macromol.*, 1995, **17**, 74.

74. A. M. Gil, E. Alberti, A. Naito, K. Okuda, H. Saitô, A. S. Tatham and S. Gilbert, in *Advances in Magnetic Resonance in Food Science* (eds P. S. Belton, B. P. Hills and G. A. Webb), Royal Society of Chemistry, Cambridge, 1999, p. 126.
75. E. Alberti, S. M. Gilbert, A. S. Tatham, P. R. Shewry and A. M. Gil, *Biopolymers*, 2002, in press.
76. E. Alberti, E. Humpfer, M. Spraul, S. Gilbert, A. S. Tatham, P. R. Shewry and A. M. Gil, *Biopolymers*, 2001, **58**, 33.
77. E. Alberti, A. M. Gil, A. S. Tatham, S. Gilbert and P. T. Callaghan, in *Wheat Gluten* (eds P. R. Shewry and A. S. Tatham), Royal Society of Chemistry, Cambridge, 2001, p. 368.
78. A. M. Gil, E. Alberti and D. Santos, in *Magnetic Resonance in Food Science – A View to the Next Century* (eds G. A. Webb, P. S. Belton, A. M. Gil and I. Delgadillo), Royal Society of Chemistry, Cambridge, 2001, p. 43.
79. S. Li, L. C. Dickinson and P. Chinachoti, *Cereal Chem.*, 1996, **73**, 736.
80. S. L. Umbach, E. A. Davis and J. Gordon, *J. Cereal Sci.*, 1998, **28**, 233.
81. P. S. Belton, T. Bogracheva, Z. Cserhalmi, B. Czukor, A. Grant, N. Lambert and N. Wellner, *Food Hydrocolloids*, 1997, **11**, 485.
82. A. Mizuno, M. Mitsuiki and M. Motoki, *J. Agric. Food Chem.*, 2000, **48**, 3286.
83. A. Mizuno, M. Mitsuiki, M. Motoki, K. Ebisawa and E. I. Suzuki, *J. Agric. Food Chem.*, 2000, **48**, 3292.
84. A. Mora-Gutierrez and H. M. Farrell, *J. Agric. Food Chem.*, 2000, **48**, 3245.
85. A. Mora-Gutierrez, T. F. Kumosinski and H. M. Farrell, *J. Agric. Food Chem.*, 1998, **46**, 4987.
86. L. K. Creamer, J. E. Plowman, M. J. Liddell, M. H. Smith and J. P. Hill, *J. Dairy Sci.*, 1998, **81**, 3004.
87. L. K. Rasmussen, L. B. Johnsen, A. Tsiora, E. S. Sorensen, J. K. Thomsen, N. C. Nielsen, H. J. Jakobsen and T. E. Petersen, *Int. Dairy J.*, 1999, **9**, 215.
88. J. A. G. Arêas, M. M. Cassiano, C. Glaubitz, G. Gröbner and A. Watts, in *Magnetic Resonance in Food Science – A View to the Future* (eds G. A. Webb, P. S. Belton, A. M. Gil and I. Delgadillo), Royal Society of Chemistry, Cambridge, 2001, p. 193.
89. Y. Mine, *J. Agric. Food Chem.*, 1997, **45**, 68.
90. J. Belloque, M. A. de la Fuente and M. Ramos, *J. Dairy Sci.*, 2000, **67**, 529.
91. L. K. Rasmussen, E. S. Sorensen, T. E. Petersen, N. C. Nielsen and J. K. Thomsen, *J. Dairy Sci.*, 1997, **80**, 607.
92. J. Belloque and G. M. Smith, *J. Agric. Food Chem.*, 1998, **46**, 1805.
93. J. Belloque and G. M. Smith, *J. Dairy Sci.*, 1998, **81**, 2580.
94. S. Sugai, M. Ikeguchi and A. Shimizu, *Int. J. Food Sci. Technol.*, 1999, **34**, 437.
95. R. Wimmer, M. Olsson, M. T. Neves-Peterson, R. Hatti-Kaul, S. B. Petersen and N. Muller, *J. Biotechnol.*, 1997, **55**, 85.
96. W. S. Price, F. Tsuchiya and Y. Arata, in *Advances in Magnetic Resonance in Food Science* (eds P. S. Belton, B. P. Hills and G. A. Webb), Royal Society of Chemistry, Cambridge, 1999, p. 35.
97. N. R. Konstantinova and V. I. Lozinski, *Food Hydrocolloids*, 1997, **11**, 113.
98. I. C. Baianu, T. F. Kumosinski, A. Mora-Gutierrez, E. M. Ozu, T. S. Lioutas and P. J. Bechtel, in *Application of Polymers in Foods: Proceedings of a Symposium, Dallas, 1998* (eds H. N. Cheng, G. L. Cote and I. C. Baianu), Wiley-VCH, Weinheim, 1999, p. 225.
99. K. H. Mayo, *Biopolymers (Pept. Sci.)*, 1996, **40**, 359.
100. A. Rochdi, L. Foucat and J. P. Renou, *Food Chem.*, 2000, **69**, 295.
101. R. Consonni, L. Zetta, R. Longhi, L. Toma, G. Zanaboni and R. Tenni, *Biopolymers*, 2000, **53**, 99.
102. M. C. Vackier and D. N. Rutledge, *Food Chem.*, 1996, **57**, 287.
103. W. Wei and I. C. Baianu, in *Application of Polymers in Foods: Proceedings of a Symposium, Dallas, 1998* (eds H. N. Cheng, G. L. Cote and I. C. Baianu), Wiley-VCH, Weinheim, 1999, p. 197.
104. P. S. Belton, R. Boetzel and E. Bord, *Sciences des Aliments*, 1997, **17**, 145.
105. C. E. Mendes da Silva, C. F. Ciacco, G. E. Barberis, W. M. R. Solano and C. Rettori, *Cereal Chem.*, 1996, **73**, 297.
106. Y. Gomi, M. Fukuoka, T. Mihori and H. Watanabe, *J. Food Eng.*, 1998, **36**, 359.

107. A. L. M. Smits, F. C. Ruhnau, J. F. C. Vliegenthart and J. J. G. van-Soest, *Starke,* 1998, **50**, 478.
108. I. A. Farhat, J. M. V. Blanshard and J. R. Mitchell, *Biopolymers*, 2000, **53**, 411.
109. M. Paris, H. Bizot, J. Emery, J. Y. Buzare and A. Buleon, *Carbohydr. Polym.*, 1999, **39**, 327.
110. I. A. Farhat, J. M. V. Blanshard, M. Descamps and J. R. Mitchell, *Cereal Chem.*, 2000, **77**, 202.
111. D. Le Botlan and P. Debois, *Cereal Chem.*, 1995, **72**, 191.
112. C. C. Seow and C. H. Teo, *Starke*, 1996, **48**, 90.
113. A. S. Kulik and J. Haverkamp, *Carbohydr. Polym.*, 1997, **34**, 49.
114. I. C. Baianu, P. I. Yakubu and E. Ozu, in *Application of Polymers in Foods: Proceedings of a Symposium, Dallas, 1998* (eds H. N. Cheng, G. L. Cote and I. C. Baianu), Wiley-VCH, Weinheim, 1999, p. 187.
115. K. R. Morgan, R. H. Furneaux and N. G. Larsen, *Carbohydr. Res.*, 1995, **276**, 387.
116. H. Tang and B. P. Hills, in *Magnetic Resonance in Food Science – A view to the Next Century* (eds G. A. Webb, P. S. Belton, A. M. Gil and I. Delgadillo), Royal Society of Chemistry, Cambridge, 2001, p. 157.
117. H. Falk, R. Micura, M. Stanek and R. Wutka, *Starke*, 1996, **48**, 344.
118. G. S. Nilsson, K. E. Bergquisit, U. Nilsson and L. Gorton, *Starke*, 1996, **48**, 352.
119. A. Xu and P. A. Seib, *J. Cereal Sci.*, 1997, **25**, 17.
120. L. B. Dunn and W. J. Krueger, in *Paradigm for Successful Utilization of Renewable Resources* (eds D. J. Sessa and J. L. Willet), AOCS Press, Champaign, 1998, p. 156.
121. S. Richardson, G. S. Nilsson, K. E. Bergquist, L. Gorton and P. Mischnick, *Carbohydr. Res.*, 2000, **28**, 365.
122. R. Ruan, Z. Long, A. Song and P. Chen, *Lebensmittel-Wissenschaft und Technologie*, 1998, **31**, 516.
123. R. Ruan, Z. Long, P. Chen, V. Huang, S. Almaer and I. Taub, *J. Food Sci.*, 1999, **64**, 6.
124. L. Pizzoferrato, M. Paci and G. Rotilio, *J. Agric. Food Chem.*, 1998, **46**, 438.
125. L. Pizzoferrato, G. Rotilio and M. Paci, *J. Agric. Food Chem.*, 1999, **47**, 4060.
126. J. M. Ames, A. Arnoldi, L. Bates and M. Negroni, *J. Agric. Food Chem.*, 1997, **45**, 1256.
127. S. M. Monti, A. Ritieni, G. Graziani, G. Randazzo, L. Mannina, A. L. Segre and V. Fogliano, *J. Agric. Food Chem.*, 1999, **47**, 1506.
128. T. Kasemsuwan and J. L. Jan, *Cereal Chem.*, 1996, **73**, 702.
129. S. Gaudin, D. Lourdin, D. Le Botlan, J. L. Ilari and P. Colonna, *J. Cereal Sci.*, 1999, **29**, 273.
130. S. Kawahara, A. Yoshikawa, T. Hiraoki and A. Tsutsumi, *Carbohydr. Polym.*, 1996, **30**, 129.
131. A. J. Jay, I. J. Colquhoun, M. J. Ridout, G. J. Brownsey, V. J. Morris, A. M. Fialho, J. H. Leitao and I. Sa-Correia, *Carbohydr. Polym.*, 1998, **35**, 179.
132. J. P. M. van Duynhoven, A. S. Kulik, H. R. A. Jonker and J. Haverkamp, *Carbohydr. Polym.*, 1999, **40**, 211.
133. C. T. M. Fransen, H. van Laar, J. P. Kamerling and J. F. G. Vliegenthart, *Carbohydr. Res.*, 2000, **328**, 549.
134. L. Heux, E. Dinand and M. R. Vignon, *Carbohydr. Polym.*, 1999, **40**, 115.
135. T. G. Neiss and H. N. Cheng, in *Proceedings of a Symposium – Application of Polymers in Foods* (eds H. N. Cheng, G. L. Cote and I. C. Baianu), Wiley-VCH, Weinheim, 1999, p. 165.
136. M. C. Jarvis and D. C. Apperley, *Carbohydr. Res.*, 1995, **275**, 131.
137. M. A. K. Williams, R. D. Keenan and T. K. Halstead, *Food Hydrocolloids*, 1998, **12**, 89.
138. H. R. Tang and P. S. Belton, *Solid-State NMR*, 1998, **12**, 21.
139. W. Cui, P. J. Wood, B. Blackwell and J. Nikiforuk, *Carbohydr. Polym.*, 2000, **41**, 249.
140. L. Johansson, L. Virkki, S. Maunu, M. Lehto, P. Ekholm and P. Varo, *Carbohydr. Polym.*, 2000, **42**, 143.
141. J. P. Roubroeks, R. Andersson and P. Aman, *Carbohydr. Polym.*, 2000, **42**, 3.
142. A. Broberg, K. K. Thomsen and J. O. Duus, *Carbohydr. Res.*, 2000, **328**, 375.
143. C. Arnosti and D. J. Repeta, *Starke*, 1995, **47**, 73.
144. K. Glinel, J. P. Sauvage, H. Oulyadi and J. Huguet, *Carbohydr. Res.*, 2000, **328**, 343.
145. C. Michel, C. Benard, C. M. Llahaye, D. Formaglio, B. Kaeffer, B. Quemener, S. Berot, J. C. Yvin, H. M. Blottiere and C. Cherbut, *Science des Aliments*, 1999, **19**, 311.
146. R. B. Gracia and C. T. Andrade, *Carbohydr. Polym.*, 1997, **34**, 157.

147. D. D. McIntyre, H. Ceri and H. J. Vogel, *Starke*, 1996, **48**, 285.
148. T. Turquois, S. Acquistapace, F. Arce Vera and D. H. Welti, *Carbohydr. Polym.*, 1996, **31**, 269.
149. D. K. Watt, D. J. Brasch, D. S. Larsen and L. D. Melton, *Carbohydr. Polym.*, 1999, **39**, 165.
150. C. Picard, J. Gruza, C. Derouet, C. M. G. C. Renard, K. Mazeau, J. Koca, A. Imberty and C. H. du Penhoat, *Biopolymers*, 2000, **54**, 11.
151. I. Braccini, C. H. du Penhoat, V. Michon, R. Goldberg, M. Clochard, M. C. Jarvis, Z.-H. Huang and D. A. Gage, *Carbohydr. Res.*, 1995, **276**, 167.
152. B. Yan and R. E. Stark, *Macromolecules*, 1998, **31**, 2600.
153. B. Yan and R. E. Stark, *J. Agric. Food Chem.*, 2000, **48**, 3298.
154. M. H. Lopes, A. M. Gil, A. J. D. Silvestre and C. Pascoal-Neto, *J. Agric. Food Chem.*, 2000, **48**, 383.
155. M. Rinaudo, M. Milas and J. Desbrieres, in *Applications of Chitin and Chitosan*, Technomic Publishers, Lancaster, Pennsylvania, 1997, p. 89.
156. T. J. Foster, S. Ablett, M. C. McCann and M. J. Gidley, *Biopolymers*, 1996, **39**, 51.
157. M. C. Jarvis, K. M. Fenwick and D. C. Apperley, *Carbohydr. Res.*, 1996, **288**, 1.
158. M.-A. Ha, B. W. Evans, M. C. Jarvis, D. C. Apperley and A. M. Kenwright, *Carbohydr. Res.*, 1996, **288**, 15.
159. M.-A. Ha, B. W. Evans, D. C. Apperley and M. C. Jarvis, in *Pectins and Pectinases: Proceedings of an International Symposium, Wageningen, December 1995* (eds J. Visser and A. G. J. Voragen), Elsevier, Amsterdam, 1996, p. 561.
160. M. C. Jarvis, M.-A. Ha and R. J. Viëtor, in *Advances in Magnetic Resonance in Food Science* (eds P. S. Belton, B. P. Hills and G. A. Webb), Royal Society of Chemistry, Cambridge, 1999, p. 158.
161. S. Hediger, L. Emsley and M. Ficher, *Carbohydr. Res.*, 1999, **322**, 102.
162. T. H. Koh, L. D. Melton and R. H. Newman, *Can. J. Bot.*, 1997, **75**, 1957.
163. K. M. Fenwick, M. C. Jarvis, D. C. Apperley, G. B. Seymour and C. R. Bird, *Phytochemistry*, 1996, **42**, 301.
164. M.-A. Ha, W. G. Jardine and M. C. Jarvis, *J. Agric. Food Chem.*, 1997, **45**, 117.
165. H. Tang, P. S., Belton, A. Ng and P. Ryden, *J. Agric. Food Chem.*, 1999, **47**, 510.
166. H. Tang and P. S. Belton, in *Advances in Magnetic Resonance in Food Science* (eds P. S. Belton, B. P. Hills and G. A. Webb), Royal Society of Chemistry, Cambridge, 1999, p. 166.
167. M. J. Dennis, *Chemistry and Industry*, 1997, **24**, 997.
168. P. R. Ashurst and M. J. Dennis, *Analytical Methods of Food Authentication*, Blackie, London, 1998.
169. J. R. Jordan, *Inside Laboratory Management*, 1998, **2**, 10.
170. G. J. Martin, *Seminars in Food Analysis*, 1998, **3**, 251.
171. E. P. Mazzola, in *Spectral Methods in Food Analysis: Instrumentation and Applications* (ed. M. M. Mossoba), Marcel Dekker, New York, 1998, p. 89.
172. H. L. Schmidt, D. Weber, A. Rossmann and R. A. Werner, in *Flavor Chemistry: Thirty Years of Progress: Proceedings of a Symposium* (eds R. Teranishi, E. L. Wick and I. Hornstein), ACS Kluwer Academic/Plenum Publishers, New York, 1999, p. 55.
173. M. P. Day, B. Zhang and G. J. Martin, *J. Sci. Food Agric.*, 1995, **67**, 113.
174. G. Versini, A. Monetti and F. Reniero, in *Wine: Nutritional and Therapeutic Benefits: Proceedings of a Symposium, Chicago, August 1995*, American Chemical Society, Washington D.C., 1997, p. 113.
175. C. Fauhl, R. Wittkowski and W. Baltes, *Lebensmittechemie*, 1997, **51**, 9.
176. J. E. Giménez-Miralles, D. M. Salazar and I. Solana, *J. Agric. Food Chem.*, 1999, **47**, 2645.
177. C. Fauhl and R. Wittkowski, *Zeitschrift für Lebenmittel Untersuchung und Forschung*, 1996, **203**, 541.
178. A. Hermann, *Zeitschrift für Lebensmittel Untersuchung und Forschung*, 1999, **208**, 194.
179. G. J. Martin, L. Nicol, N. Naulet and M. L. Martin, *J. Sci. Food Agric.*, 1998, **77**, 153.
180. M. A. Cremonini, D. Tacconi, V. Clementi and C. Luchinat, *J. Agric. Food Chem.*, 1998, **46**, 3943.

181. J. B. Fournier, Y. L. Martin, F. P. Fourel, G. B. Martin and H. J. D. McManus, *Fruit Processing*, 1996, **6**, 52.
182. R. B. Taylor, in *Fruit Processing* (eds D. Arthey and P. R. Ashurst), Blackie, Glasgow, 1996, p. 1.
183. G. J. Martin and G. G. Martin, in *Methods to Detect Adulteration of Fruit Juice Beverage* (eds S. Nagy and R. L. Wade), Agscience, Auburndale, 1995, Vol. 1, p. 1.
184. G. Martin, C. Guillou and Y. L. Martin, *Fruit Processing*, 1995, **5**, 246.
185. G. G. Martin, V. Hanote, M. Lees and Y.-L. Martin, *J. AOAC Int.*, 1996, **79**, 62.
186. G. G. Martin, R. Wood and G. J. Martin, *J. AOAC Int.*, 1996, **79**, 917.
187. G. G. Martin, E. Jamin, J. Gonzales, G. Renaud, V. Hanote, P. Stober and N. Naulet, *Fruit Processing*, 1997, **7**, 344.
188. A. M. Pupin, M. J. Dennis, I. Parker, S. Kelly, T. Bigwood and M. C. F. Toledo, *J. Agric. Food Chem.*, 1998, **46**, 1369.
189. H. Forstel, *Flussiges-Obst.*, 1999, **66**, 423.
190. J. Gonzalez, E. Jamin, G. Remaud, Y.-L. Martin, G. G. Martin and M. L. Martin, *J. Agric. Food Chem.*, 1998, **46**, 2200.
191. G. G. Martin, *Fruit Processing*, 1998, **8**, 376.
192. G. G. Martin, Y.-L. Martin, N. Naulet and H. J. D. McManus, *J. Agric. Food Chem.*, 1996, **44**, 3206.
193. G. S. Remaud, Y.-L. Martin, G. G. Martin, N. Naulet and G. J. Martin, *J. Agric. Food Chem.*, 1997, **45**, 1844.
194. G. S. Remaud, Y.-L. Martin, G. G. Martin and G. J. Martin, *J. Agric. Food Chem.*, 1997, **45**, 859.
195. C. H. Manley and R. H. Potter, in *Methods to Detect Adulteration of Fruit Juice Beverage* (eds S. Nagy and R. L. Wade), Agscience, Auburndale, 1995, Vol. 1, p. 309.
196. G. Remaud, A. A. Debon, Y.-L. Martin, G. G. Martin and G. J. Martin, *J. Agric. Food Chem.*, 1997, **45**, 4042.
197. H. L. Schmidt, A. Rossmann and R. A. Werner, in *Flavourings: Production, Composition, Applications, Regulations*, Wiley-VCH, Weinheim, 1998, p. 539.
198. A. Royer, N. Naulet, F. Mabon, M. Lees and G. J. Martin, *J. Am. Oil Chem. Soc.*, 1999, **76**, 365.
199. P. S. Belton, I. Delgadillo, E. Holmes, A. Nicholls, J. K. Nicholson and M. Spraul, *J. Agric. Food Chem.*, 1996, **44**, 1483.
200. A. M. Gil, I. F. Duarte, I. Delgadillo, I. J. Colquhoun, F. Casuscelli, E. Humpfer and M. Spraul, *J. Agric. Food Chem.*, 2000, **48**, 1524.
201. M. Bosco, R. Toffanin, D. de Palo, L. Zatti and A. L. Segre, *J. Sci. Food Agric.*, 1999, **79**, 869.
202. L. Forveille, J. Vercauteren and D. N. Rutledge, *Food Chem.*, 1996, **57**, 441.
203. P. S. Belton, I. J. Colquhoun, E. K. Kemsley, I. Delgadillo, P. Roma, M. J. Dennis, M. Sharman, E. Holmes, J. K. Nicholson and M. Spraul, *Food Chem.*, 1998, **61**, 207.
204. J. T. W. E. Vogels, L. Terwel, A. C. Tas, F. van den Berg, F. Dukel and J. van der Greef, *J. Agric. Food Chem.*, 1996, **44**, 175.
205. C. Lakenbrink, U. H. Engelhardt and V. Wray, *J. Agric. Food Chem.*, 1999, **47**, 4621.
206. X. Wan, H. E. Nursten, Y. Cai, A. L. Davis, J. P. G. Wilkins and A. P. Davies, *J. Sci. Food Agric.*, 1997, **74**, 401.
207. R. Amarowicz and F. Shahidi, *Food Res. Int.*, 1996, **29**, 71.
208. D. Qi, J. Tong, Y. Sun, S. Chen and S. Luo, in *Food Flavours: Generation, Analysis and Process Influence; Proceedings of the 8th International Flavor Conference, Cos, Greece, 1994*, Elsevier, Amsterdam, 1995, p. 827.
209. D. M. Jung, J. S. De Ropp and S. E. Ebeler, *J. Agric. Food Chem.*, 2000, **48**, 407.
210. R. E. McDonald and M. M. Mossoba, in *Food Lipids: Chemistry, Nutrition and Biotechnology* (eds C.C. Akoh and D.B. Min), Marcel Dekker, New York, 1998, p. 137.
211. E. W. Hammond, *Advances in Applied Lipid Research* (ed. F. B. Padley), JAI Press, London, 1996, Vol. 2, p. 35.
212. R. J. Hamilton and J. Cast, *Spectral Properties of Lipids*, Sheffield Academic Press, Sheffield, 1999.
213. F. D. Gunstone, *Lipid Technol.*, 1999, **11**, 39.

214. M. M. Bergana and T. W. Lee, *J. Am. Oil Chem. Soc.*, 1996, **73**, 551.
215. T. Glonek and T. E. Merchant, in *Advances in Lipid Methodology* (ed. W. W. Christie), Oily Press, Ayr, 1996, Vol. 3, p. 37.
216. M. J. T. Reany, N. J. Tyler and K. Brown, *J. Am. Oil Chem. Soc.*, 1999, **76**, 859.
217. U. Pallotta, *Italian J. Food Sci., Special Issue: in Memory of Prof. C. Cantarelli*, 1995, p. 158.
218. P. Scano, M. Casu, A. Lai, G. Saba, M. A. Dessi, M. Deiana, F. P. Corongiu and G. Bandino, *Lipids*, 1999, **34**, 757.
219. Y. Miyake and K. Yokomizo, *J. Jap. Oil. Chem. Soc.*, 1998, **47**, 179.
220. Y. Miyake, K. Yokomizo and N. Matsuzaki, *J. Am. Oil Chem. Soc.*, 1998, **75**, 1091.
221. Y. Miyake, K. Yokomizo and N. Matsuzaki, *J. Am. Oil Chem. Soc.*, 1998, **75**, 15.
222. *Official Methods and Recommended Practices of the AOCS*, 5th edition, AOCS, Champaign, 1998.
223. W. L. Siew and W. L. Ng, *J. Sci. Food Agric.*, 1999, **79**, 722.
224. M. S. F., Lie Ken Jie, M. K. Pasha and M. S. Alam, in *Advances in Conjugated Linoleic Acid Research* (eds M. P. Yurawecz, M. M. Mossoba, J. K. G. Kramer, M. W. Pariza and G. J. M. P. Nelson), AOCS Press, Champaign, 1999, p. 152.
225. A. Jones, A. D. Shaw, G. J. Salter, G. Bianchi and D. B. Kell, in *Lipid Analysis in Oils and Fats* (ed. R. J. Hamilton), Blackie, London, 1998, p. 317.
226. G. Vlahov and C. S. Angelo, *Fett-(Lipid)*, 1996, **98**, 203.
227. G. Vlahov, C. Schiavone and N. Simone, *Fett-(Lipid)*, 1999, **101**, 146.
228. W. W. Christie, *Ind. Crops Prod.*, 1999, **10**, 73.
229. M. Tsimidou, *Seminars in Food Analysis*, 1999, **4**, 13.
230. M. Tsimidou, *Italian J. Food Sci.*, 1998, 10, 99.
231. M. Brenes, A. Garcia, P. Garcia, J. Rios and A. Garrido, *J. Agric. Food Chem.*, 1999, **47**, 3535.
232. L. E. Garcia Ayuso and M. D. Luque de Castro, *Seminars in Food Analysis*, 1999, **4**, 38.
233. C. J. L. Silwood and M. Grootveld, *Lipids*, 1999, **34**, 741.
234. N. Gladovic, L. Zupancic Kraly and J. Plavec, *J. Chromatogr.*, 1997, **767**, 63.
235. S. P. J. Namal Senanayake and F. Shahidi, *J. Food Lipids*, 1999, **6**, 195.
236. G. Dobson, in *Lipid Analysis in Oils and Fats* (ed. R. J. Hamilton), Blackie, London, 1998, p. 136.
237. S. L. Hansen, W. J. Kruger, L. B. Dunn and W. E. Artz, *J. Agric. Food Chem.*, 1997, **45**, 4730.
238. H. A. Abou Gharbia, F. Shahidi, A. A. Y. Shehata and M. M. Youssef, *J. Food Lipids*, 1996, **3**, 59.
239. Y. Miyake and K. Yokomizo, *J. Am. Oil. Chem. Soc.*, 1998, **75**, 801.
240. Y. Miyake, K. Yokomizo and N. Matsuzaki, *J. Jap. Oil Chem. Soc.*, 1998, **47**, 333.
241. R. Sacchi, M. Patumi, G. Fontanazza, P. Barone, P. Fiordiponti, L. Mannina, E. Rossi and A. L. Segre, *J. Am. Oil Chem. Soc.*, 1996, **73**, 747.
242. R. Sacchi, L. Mannina, P. Fiordiponti, P. Barone, L. Paolillo, M. Patumi and A. L. Segre, *J. Agric. Food Chem.*, 1998, **46**, 3947.
243. G. Viahov, *J. Am. Oil Chem. Soc.*, 1996, **73**, 1201.
244. G. Vlahov, A. D. Shaw and D. B. Kell, *J. Am. Oil Chem. Soc.*, 1999, **76**, 1223.
245. L. Mannina, M. Patumi, P. Fiordiponti, M. C. Emanuele and A. L. Segre, *Italian J. Food Sci.*, 1999, **11**, 139.
246. U. N. Wanasundara, F. Shahidi and C. R. Jablonski, *Food Chem.*, 1995, **52**, 249.
247. F. Shahidi and U. N. Wanasundara, in *Natural Antioxidants: Chemistry, Health Effects and Applications* (ed. F. Shahidi), AOCS Press, Champaign, 1997, p. 397.
248. M. Aursand, L. Jørgensen and H. Grasdalen, *J. Am. Oil Chem. Soc.*, 1995, **72**, 293.
249. M. Aursand, I. Gribbestad, T. Skjetne, H. Grasdalen and L. Jørgensen, in *Seafood from Producer to Consumer: Integrated Approach to Quality; Proceedings of the International Seafood Conference, Noordwijkerhout, November 1995* (ed. J. B. Luten), Elsevier, Amsterdam, 1997, p. 367.
250. S. Saeed and N. K. Howell, *J. Am. Oil Chem. Soc.*, 1999, **76**, 391.
251. I. Medina, R. Sacchi and S. P. Aubourg, *J. Sci. Food Agric.*, 1995, **69**, 445.
252. I. Medina, R. Sacchi, I. Giudicianni and S. Aubourg, *J. Am. Oil Chem. Soc.*, 1998, **75**, 147.

253. G. Lindblom, in *Advances in Lipid Methodology* (ed. W.W. Christie), Oily Press Ltd., Ayr, 1996, Vol. 3, p. 134.
254. H. A. Kuiper and M. Y. Noordam, *Voedingsmiddelentechnologie*, 1998, **31**, 11.
255. H. P. J. M. Noteborn, A. Lommen, R. C. van der Jagt and J. M. Weseman, *J. Biotechnol.*, 2000, **77**, 103.
256. K. Kobata, T. Todo, S. Yazawa and T. Watanabe, *J. Agric. Food Chem.*, 1998, **46**, 1695.
257. L. Cabrita, N. A. Froystein and O. M. Andersen, *Food Chem.*, 2000, **69**, 33.
258. G. R. Takeoka, L. T. Dao, G. H. Full, R. Y. Wong, L. A. Harden, R. H. Edwards and J. D. J. Berrios, *J. Agric. Food Chem.*, 1997, **45**, 3395.
259. M. M. Guisti, H. Ghanadan and R. E. Wrolstad, *J. Agric. Food Chem.*, 1998, **46**, 4858.
260. J. Bakker and C. F. Timberlake, *J. Agric. Food Chem.*, 1997, **45**, 35.
261. W. Feger, H. Brandauer and M. Ziegler, *J. Essent. Oil Res.*, 1999, **11**, 556.
262. A. Z. Mercandante, A. Steck and H. Pfander, *J. Agric. Food Chem.*, 1999, **47**, 145.
263. G. Britton, in *Natural Food Colorants* (eds G. A. F. Hendry and J. D. Houghton), 2nd edition, Blackie, Glasgow, 1996, p. 197.
264. E. Fattorusso, V. Lanzotti and O. Tagliatela Scafati, *J. Agric. Food Chem.*, 1998, **46**, 4904.
265. M. Wang, J. Li, M. Rangarajan, Y. Shao, E. J. La Voie, C. T. Huang and C. T. Ho, *J. Agric. Food Chem.*, 1998, **46**, 4869.
266. I. P. Gerothanassis, V. Exarchou, V. Lagouri, A. Troganis and M. Tsimidou, *J. Agric. Food Chem.*, 1998, **46**, 4185.
267. Y. Lu and L. Y. Foo, *Food Chem.*, 1999, **65**, 1.
268. L. M.-M. Louche, E. M. Gaydou, and J.-C. Lesage, *J. Agric. Food Chem.*, 1998, **46**, 4193.
269. F. Mattivi, F. Reniero and S. Korhammer, *J. Agric. Food Chem.*, 1995, **43**, 1820.
270. K. Astwood, B. Lee and M. Manley-Harris, *J. Agric. Food Chem.*, 1998, **46**, 4958.
271. R. J. Cutts, B. J. Howlin, F. Mulhollanh and G. A. Webb, *J. Agric. Food Chem.*, 1996, **44**, 1409.
272. A. R. Neves, A. Ramos and H. Santos, in *Magnetic Resonance in Food Science – A View to the Next Century* (eds G. A. Webb, P. S. Belton, A. M. Gil and I. Delgadillo), Royal Society of Chemistry, Cambridge, 2001, p. 75.
273. B. van Lierop, L. Castle, A. Feigenbaum, K. Ehlert and A. Boenke, *Food Add. Contam.*, 1998, **15**, 855.
274. P. Metois, D. Scholler, J. Bouquant and A. Feigenbaum, *Food Add. Contam.*, 1998, **15**, 100.
275. H. H. F. Refsgaard, K. Schaumburg and L. H. Skibsted, *Zeitschrift für Lebensmittel Untersuchung und Forschung*, 1996, **203**, 287.
276. W. C. Hutton, J. R. Garbow and T. R. Hayes, *Lipids*, 1999, **34**, 1339.
277. A. K. Thybo, I. E. Bechmann, M. Martens and S. B. Engleson, *Lebensmittel-Wissenschaft und Technologie*, 2000, **33**, 103.
278. S. B. Engelsen, M. K. Jensen, H. T. Pedersen, L. Norgaard and L. Munck, *J. Cereal Sci.*, 2001, **33**, 59.
279. J. J. Gonzalez, K. L. McCarthy and M. J. McCarthy, *J. Texture Studies*, 1998, **29**, 537.
280. A. K. Horigane, H. Toyashima, H. Hemmi, W. M. H. G. Engelaar, A. Okubo and T. Nagata, *J. Food Sci.*, 1999, **64**, 1.
281. M. Suzuki, A. K. Horigane, H. Toyoshima, X. Yan, H. Okadome and T. Nagata, *J. Food Sci.*, 1999, **64**, 1027.
282. T. R. Rosett, S. L. Kendragen, Y. Gao, S. J. Schmidt and B. P. Klein, *J. Food Sci.*, 1996, **61**, 1099.
283. N. Howell, Y. Shavila, M. Grootveld and S. Williams, *J. Sci. Food Agric.*, 1996, **72**, 49.
284. P. Lambelet, F. Renevey, C. Kaabi and A. Raemy, *J. Agric. Food Chem.*, 1995, **43**, 1462.
285. C. Steen and P. Lambelet, *J. Sci. Food Agric.*, 1997, **75**, 268.
286. S. M. Jepsen, H. T. Pedersen and S. B. Engelsen, *J. Sci. Food Agric.*, 1999, **79**, 1793.
287. I. Medina, R. Sacchi and S. Auborg, *Eur. Food Res. Technol.*, 2000, **210**, 176.
288. F. Shahidi and S. A. Spurvey, *J. Food Lipids*, 1996, **3**, 13.
289. M. J. Gradwell, T. W. M. Fan and A. N. Lane, *Anal. Biochem.*, 1998, **263**, 139.
290. T. Nagata, Y. Chuda, X. Yan, M. Suzuki and K. Kawasaki, *J. Sci. Food Agric.*, 2000, **80**, 1151.
291. P. S. Belton, K. J. Packer and T. E. Southon, *J. Sci. Food Agric.*, 1987, **41**, 267.

292. W. Hartfiel, *Fleischwirtschaft*, 1996, **76**, 1131.
293. S. D. M. Jones, *Quality and Grading of Carcasses of Meat Animal*, CRC Press, Boca Raton, 1995, p. 215.
294. R. Geers, C. Decanniere, H. Ville, P. Van- Hecke and L. Bosschaerts, *Meat Sci.*, 1995, **40**, 373.
295. H. C. Bertram, H. J. Andersen and A. H. Karlsson, *Meat Sci.*, 2001, **57**, 125.
296. J. Brondrum, L. Munck, P. Henckel, A. Karlsson, E. Tornberg and S. B. Engelsen, *Meat Sci.*, 2000, **55**, 177.
297. E. W. Laurent, J. M. Bonny and J. P. Renou, *Food Chem.*, 2000, **69**, 419.
298. N. D. Scollan, L. J. Caston, Z. Liu, A. K. Zubair, S. Leeson and B. W. McBride, *Br. Poultry Sci.*, 1998, **39**, 221.
299. J. M. Tingle, J. M. Pope, P. A. Baumgartner and V. Sarafis, *Int. J. Food Sci Technol.*, 1995, **30**, 437.
300. T. M. Guiheneuf, S. J. Gibbs and L. D. Hall, *J. Food Eng.*, 1997, **31**, 457.
301. T. M. Guiheneuf, S. L. Duce, S. J. Gibbs and L. D. Hall, *Int. J. Food Sci. Technol.*, 1995, **30**, 447.
302. T. M. Guiheneuf, J. J. Tessier, N. J. Herrod and L. D. Hall, *J. Sci. Food Agric.*, 1996, **71**, 163.
303. M. M. Farouk and J. E. Swan, *Meat Sci.*, 1998, **49**, 233.
304. T. Isaksson, B. N. Nilsen, G. Torgersen, R. P. Hammond and K. I. Hildrum, *Meat Sci.*, 1996, **43**, 245.
305. E. Tornberg, M. Wahlgren, J. Brondrum and S. B. Englesen, *Food Chem.*, 2000, **69**, 407.
306. B. Moesgaard, B. Quistorff, V. G. Christensen, I. Therkelsen and P. F. Jorgensen, *Meat Sci.*, 1995, **39**, 43.
307. J. Brondum, D. V. Byrne, L. S. Bak, G. Bertelsen and S. B. Engelsen, *Meat Sci.*, 2000, **54**, 83.
308. B. A. Goodman and S. M. Glidewell, *Microscopy and Analysis*, 1995, **50**, 7.
309. T. Yantarasri, J. Sornsrivichai and P. Chen, in *Postharvest '96: Proceedings of the International Conference, Taupo, August, 1996* (ed. R. L. Bieleski), ISHS, Leuven, 1998, p. 97.
310. L. Sonego, R. Ben-Arie, J. Raynal and J. C. Pech, *Postharvest Biol. Technol.*, 1995, **5**, 187.
311. M. J. McCarthy, B. Zion, P. Chen, S. Ablett, A. H. Darke and P. J. Lillford, *J. Sci Food Agric.*, 1995, **67**, 13.
312. C. J. Clark and J. S. MacFall, *Postharvest Biol. Technol.*, 1996, **9**, 97.
313. C. J. Clark, L. N. Drummond and J. S. MacFall, *J. Sci. Food Agric.*, 1998, **78**, 349.
314. B. Zion, S. M. Kim, M. J. McCarthy and P. Chen, *J. Sci. Food Agric.*, 1997, **75**, 496.
315. B. Zion, P. Chen and M. J. McCarthy, *J. Sci. Food Agric.*, 1995, **67**, 423.
316. P. Chen, M. J. McCarthy, S.-M. Kim and B. Zion, *Trans. ASAE*, 1996, **39**, 2205.
317. J. Warmsley, *Lipid Technol.*, 1998, **10**, 135.
318. B. Perez-Vich, L. Velasco and J. M. Fernandez-Martinez, *J. Am. Oil Chem. Soc.*, 1998, **75**, 547.
319. M. Koizumi, N. Ishida and H. Kano, *Biosci. Biotechnol. Biochem.*, 1995, **59**, 2321.
320. G. Roudaut, M. Maglione, D. Van-Dusschoten and M. le Mestre, *Cereal Chem.*, 1999, **76**, 70.
321. G. Roudaut, D. Van Dusschoten, H. Van As, M. A. Hemminga and M. le Mestre, *J. Cereal Sci.*, 1998, **28**, 147.
322. J. Rasanen, J. M. V. Blanshard, J. R. Mitchell, W. Derbyshire and K. Autio, *J. Cereal Sci.*, 1998, **28**, 1.
323. P. Kohler, *Getreide Mehl und Brot*, 1999, **53**, 224.
324. M. E. Miquel and L. D. Hall, *Lebensmittel-Wissenschaft und Technologie*, 1998, **31**, 93.
325. T. M. Guiheneuf, P. J. Couzens, H. J. Willie and L. D. Hall, *J. Sci. Food Agric.*, 1997, **73**, 265.
326. G. Ziegleder, I. Scwingshandl and I. Brulheide, *Susswaren Technik und Wirtschaft*, 1998, **42**, 30.
327. J. H. Walton and M. J. McCarthy, *J. Food Process. Eng.*, 1999, **22**, 319.
328. S. L. Duce, S. Ablett, A. H. Darke, J. Pickles, J. Hart and L. D. Hall, *Cereal Chem.*, 1995, **72**, 105.
329. A. G. F. Stapley, J. A. Sousa-Goncalves, M. P. Hollowand, L. F. Gladden and P. F. Fryer, *Int. J. Food Sci. Technol.*, 1995, **30**, 639.
330. G. J. Hulbert, J. B. Litchfield and S. J. Schmidt, *J. Food Sci.*, 1995, **60**, 780.
331. M. C. Jorge, I. Rodriguez, J. L. Rodriguez and C. Beltran, *Alimentaria*, 1999, **36**, 49.
332. M. L. Herrera, M. de Leon Gatti and R. W. Hartel, *Food Res. Int.*, 1999, **32**, 289.
333. M. Hu, M. J. Kurth, Y. L. Hsieh and J. M. Krotchta, *J. Agric. Food Chem.*, 1996, **44**, 3757.

334. M. C. Vackier, S. Lacombe and D. N. Rutledge, *Seminars in Food Analysis,* 1998, **3**, 267.
335. B. Breitschuh and E. J. Windhab, *J. Am. Oil Chem. Soc.,* 1996, **44**, 1603.
336. S. L. Duce, M. H. G. Amin, M. A. Horsefield, M. Tyszka and L. D. Hall, *Int. Dairy J.,* 1995, **5**, 311.
337. M. H. Famelart, F. Gaucheron, F. Mariette, Y. Le Graet, K. Raulot and E. Boyaval, *Int. Dairy J.,* 1997, **7**, 325.
338. D. Le Botlan, L. Ougerram, L. Smart and L. Pugh, *J. Am. Oil Chem. Soc.,* 1999, **76**, 255.
339. F. Morales and A. Arnoldi, *Food Chem.,* 1999, **67**, 185.
340. V. K. S. Shukla, G. J. Goudappel, M. C. M. Gribnau and J. Van Duynhoven, *INFORM 10*, 1999, 479.
341. D. Rousseau and A. G. Marangoni, *J. Agric. Food Chem.,* 1998, **46**, 2375.
342. D. Rousseau, K. Forestiere, A. R. Hill and A. G. Marangoni, *J. Am. Oil Chem. Soc.,* 1996, **73**, 963.
343. R. Sacchi, F. Addeo, S. S. Musso, L. Paolillo and I. Giudicianni, *Italian J. Food Sci.*, 1995, **7**, 27.
344. M. S. F. Lie Ken Jie, C. C. Lam, M. K. Pasha, K. L. Stefenov and I. Marekov, *J. Am. Oil Chem. Soc.*, 1996, **73**, 1011.
345. R. Grimaldi, R. T. Nassu, L. A. Guaraldo-Goncalves and R. N. Cavaletti-Moreira, *Grasas y Aceites*, 1998, **49**, 1.
346. W. Buchheim, M. Schutt and E. Frede, in *High Pressure Bioscience and Biotechnology: Proceedings of an International Conference, Kyoto, November 1995*, Elsevier, Amsterdam, 1997, p. 331.
347. M. M. W. Mooren, M. C. M. Gribnau and M. A. Voorbach, in *Characterisation of Foods: Emerging Methods* (ed. A. G. Goankar), Elsevier, Amsterdam, 1995, p. 151.
348. H. Y. Lee, M. J. McCarthy and S. R. Dungan, *J. Am. Oil Chem. Soc.,* 1998, **75**, 463.
349. M. Lipp, *Lipid Technol.*, 1998, **10**, 65.
350. A. Davenel and P. Marchal, *Int. J. Food Sci. Technol.*, 1995, **30**, 655.
351. Y. Kou, P. F. Molitor and S. J. Schmidt, *J. Food Sci.*, 1999, **64**, 950.
352. J. Lenoir, D. Guermonprez and L. Marion, *Aromes, Ingredients, Additifs*, 1998–1999, **19**, 54.
353. C. Dufour and C. L. Bayonove, *J. Agric. Food Chem.*, 1999, **47**, 678.
354. H. M. Lai, S. T. Jeng and C. Y. Li, *Lebensmittel-Wissenschaft und Technolgie*, 1998, **31**, 57.
355. I. A. Usov, *Food Hydrocolloids*, 1998, **12**, 301.
356. A. Davenel, P. Schuck and P. Marchal, *Milchwissenschaft*, 1997, **52**, 35.
357. K. Katsuta, in *Gums and Stabilisers For the Food Industry: Proceedings of the 9th Conference, Wrexham, July 1997* (eds P. A. Williams and G. O. Phillips), Royal Society of Chemistry, Cambridge, 1998, p. 59.
358. H. W. C. Donker and A. S. Braaksma, *Postharvest Biol. Technol.,* 1997, **10**, 127.
359. P. Lindner, E. Bermann and B. Gamarnik, *J. Agric. Food Chem.*, 1996, **44**, 139.
360. M. Le Meste and S. Davidou, in *Ingredient Interactions: Effects on Food Quality* (ed. A. G. Goankar), Marcel Dekker, New York, 1995, p. 235.
361. A. Kilara, in *Ingredient Interactions: Effects on Food Quality* (ed. A. G. Goankar), Marcel Dekker, New York, 1995, p. 1.
362. M. Watanabe, S. Tanabe, K. Furihata and A. Okubo, *Biosci. Biotechnol. Biochem.,* 1998, **62**, 1422.
363. S. Furukubo, T. Matsumoto, H. Yomo, N. Fukui, T. Ashikari and Y. Kakimi, in *Proceedings of the 26th Congress, Maastricht, 1997*, IRL Press, Oxford, 1997, p. 423.
364. R. Seto, H. Nakamura, F. Nanjo and Y. Hara, *Biosci. Biotechnol. Biochem.,* 1997, **61**, 1434.
365. M. Miranda, A. Ramos, M. Viega Da Cunha, M. C. Lauriero-Dias and H. Santos, *J. Bacteriol.,* 1997, **179**, 5347.
366. M. Sahagian and H. D. Goff, *Food Res. Int.,* 1995, **28**, 1.
367. R. K. Bowles, K. R. Morgan, R. H. Furneaux and G. D. Coles, *Carbohydr. Polym.*, 1996, **29**, 7.
368. E. L. Thomas, G. Frost, M. L. Barnard, D. J. Bryant, S. D. Taylor-Robinson, J. Simbrunner, G. A. Coutts, M. Burl, S. R. Bloom, K. D. Sales and J. D. Bell, *Lipids,* 1996, **31**, 145.
369. H. Ville, G. Rombouts, P. van-Hecke, S. Perremans, G. Maes, G. Spincemaille and R. Geers, *J. Animal Sci.*, 1997, **75**, 2942.

370. N. Bloembergen, E. M. Purcell and R. V. Pound, *Phys. Rev.*, 1948, **73**, 679.
371. P. S. Belton, *Comments Food Agric. Chem.*, 1990, **2**, 179.
372. P. S. Belton and Y. Wang, in *Magnetic Resonance in Food Science – A View to the Future* (eds G. A. Webb, P. S. Belton, A. M. Gil and I. Delgadillo), Royal Society of Chemistry, Cambridge, 2001, p. 145.
373. Y. Wang and P. S. Belton, *Chem. Phys. Lett.*, 2000, **325**, 33.
374. M. Spraul, U. Braumann, M. Godejohann and M. Hoffmann, in *Magnetic Resonance in Food Science – A View to the Next Century* (eds G. A. Webb, P. S. Belton, A. M. Gil and I. Delgadillo), Royal Society of Chemistry, Cambridge, 2001, p. 54.
375. J. C Lindon, J. K. Nicholson and I. D. Wilson, *J. Chromatogr. B*, 2000, **748**, 233.
376. S. C. Bobzin, S. Yang and T. P. Kasten, *J. Chromatogr. B*, 2000, **748**, 259.
377. W. Vilegas, J. H. Y. Vilegas, M. Dachler, T. Glaser and K. Albert, *Phytochem. Anal.*, 2000, **11**, 317.
378. J. A. de-Koning, A. C. Hogenboom, T. Lacker, S. Strohschein, K. Albert and U. A. Brinkman, *J. Chromatogr. A*, 1998, **813**, 55.
379. K. Pusecker, K. Albert and E. Bayer, *J. Chromatogr. A*, 1999, **836**, 245.
380. S. Buskov, L. B. Hansen, C. E. Olsen, J. C. Sorensen and H. Sorensen, *J. Agric. Food Chem.*, 2000, **48**, 2693.
381. A. Lommen, M. Godejohann, P. C. H. Venema, D. C. A Hollman and M. Spraul, *Anal. Chem.*, 2000, **72**, 1793.
382. I. F. Duarte, M. Godejohann, M. Spraul and A. M. Gil, Unpublished results, 2002.
383. A. Sacco, I. N. Bolsi, R. Massini, M. Spraul, E. Humpfer and S. Ghelli, *J. Agric. Food Chem.*, 1998, **46**, 4242.
384. Y. Xia and P. T. Callaghan, *Macromolecules*, 1991, **24**, 4777.
385. A. I. Nakatani, M. D. Polliks and E. T. Samulski, *Macromolecules*, 1990, **23**, 2686.
386. P. T. Callaghan, *Rep. Prog. Phys.*, 1999, **62**, 1.
387. M. M. Britton and P. T. Callaghan, *Magn. Reson. Chem.*, 1997, **35**, S37.
388. P. T. Callaghan and A. M. Gil, *Rheological Acta*, 1999, **38**, 528.
389. P. T. Callaghan and A. M. Gil, in *Magnetic Resonance in Food Science – A View to the Next Century* (eds G. A. Webb, P. S. Belton, A. M. Gil and I. Delgadillo), Royal Society of Chemistry, Cambridge, 2001, p. 29.

NMR of Persistent Carbocations from Polycyclic Aromatic Hydrocarbons (PAHs)

KENNETH K. LAALI[1] and TAKAO OKAZAKI[2]

[1] *Department of Chemistry, Kent State University, Kent, OH 44242, USA*
[2] *Department of Energy and Hydrocarbon Chemistry, Kyoto University, Kyoto 606-8501, Japan*

1. Background 150
2. Motivation 150
3. Significance of PAH carbocations 151
4. Note on superacid media as NMR solvents 151
5. Compilation of the NMR data for carbocations derived from various classes of PAHs 151
   5.1. Naphthalenium ions (Figs 1 and 2) 152
   5.2. Anthracenium ions (Fig. 3) 152
   5.3. Phenanthrenium cations (Figs 4–10) 152
   5.4. Cyclopenta[a]phenanthrenium ions (Figs 11–16) 156
   5.5. Pyrenium cations (Figs 17–34) 159
   5.6. Benzopyrenium and dibenzopyrenium cations (Figs 35 and 36) 175
   5.7. Benzanthracenium cations and carboxonium ions, and representative α-anthracenium-substituted cations (Figs 37 and 38) 175
   5.8. Dibenzoanthracenium cations (Fig. 39) 175
   5.9. Chrysenium cations and carboxonium ions (Figs 40–43) 175
   5.10. Benzo[c]phenanthrene and benzo[g]chrysene cations (Figs 44 and 45) 177
   5.11. Hexahelicenium cations (Fig. 46) 187
   5.12. Carbocations from nitro- and nitroso-PAHs (Figs 47–49) 187
   5.13. Carbocations from methylene-bridged PAHs (Figs 50–52) 187
   5.14. Carbocations from fluoranthene-PAHs (Fig. 53) 189
Acknowledgements 189
References 213

The available NMR data for persistent carbocations derived from various classes of PAHs are compiled and their key features are highlighted and compared. The review covers PAH arenium ions, PAH carboxonium ions and α-PAH-substituted carbocations. Charge delocalization mode and substituent effects are evaluated on the basis of the $\Delta\delta^{13}C$ values.

ANNUAL REPORTS ON NMR SPECTROSCOPY
VOLUME 47 ISBN 0-12-505447-5

Copyright © 2002 Elsevier Science Ltd.
All rights of reproduction in any form reserved

1. BACKGROUND

Pioneering and ground-breaking studies by G. A. Olah from the 1960s onwards enabled the direct NMR observation of carbocations and heterocations under stable ion conditions in superacid media.[1–3] With modern NMR as an indispensable tool, during the course of the ensuing four decades, stable cation chemistry proliferated and matured into a highly fertile research area that made significant contributions to the development of modern experimental and theoretical physical organic chemistry. Over 30 years of stable ion chemistry has created a wealth of NMR-based structural, dynamics, conformational, and reactivity pattern data on numerous classes of carbocations and heterocations, whose NMR spectral data are embedded in a huge literature in the form of research articles, reviews, and monographs.[4] In a relative sense, reviews devoted entirely to compiling NMR data on a group or a large class of carbocations that could be used by researchers as a reference source for comparative purposes are rare.

2. MOTIVATION

Despite the undeniable impact that NMR has had on progress in carbocation chemistry, it seemed to us surprising that there were no previous reviews in *Annual Reports on NMR Spectroscopy* that were entirely devoted to providing, under a certain umbrella, some of the NMR characteristics of certain classes of carbocations. Volume 14 (a comprehensive collection of ^{19}F NMR data by V. Wray) contains ^{19}F data for representative fluorinated carbocations. In volume 15, in a chapter on isotope effects on nuclear shielding (by P. E. Hansen), examples of deuterium isotope effects in classical and non-classical carbocations were included. However, there has not been a previous review entirely devoted to compiling NMR data on a large class or group of carbocations for comparative purposes.

Since 1991, we have been actively studying stable carbocations derived from various classes of PAHs. During this period, a large number of systems have been studied and considerable NMR data have been accumulated (references are given in the course of discussion and in the figures).

The data enable charge delocalization mode, substituent effects, and in relevant cases conformational aspects to be addressed and compared (a review article[5] in *Chemical Reviews* in 1996 included short highlights and comparisons of the NMR characteristic of the PAH carbocations available at that time). Our interest in charge delocalization mapping as a function of structure is to create a carbocation-based structure/reactivity database for comparison with biological activity data on the mutagenicity and DNA-binding potency of PAHs. Our motivation to prepare a compilation for *Annual Reports on NMR Spectroscopy* was the realization that there is a need to create a single source on PAH carbocations that can be used for comparative purposes by researchers working on various aspects of carbocation chemistry.

3. SIGNIFICANCE OF PAH CARBOCATIONS

Carbocations derived from PAHs represent models for their biological activation via oxidative pathways leading to PAH epoxides, dihydrodiols, and diol epoxides.[6–10] Depending on the structure of the PAH, the epoxide ring opening step could gain significant carbocation character. Stable ion studies by NMR allow the site(s) of electrophilic attack to be determined, and $\Delta\delta^{13}C$ values provide insight into their charge delocalization modes which help narrow down potential sites for nucleophile attachment in a subsequent (biologically crucial) step.

4. NOTE ON SUPERACID MEDIA AS NMR SOLVENTS

Superacid media allow quantitative conversion either by protonation or by ionization of suitable precursors under mild conditions at low temperatures, while low-nucleophilicity cosolvents (typically, SO_2, SO_2ClF, and SO_2F_2) reduce the viscosity of the superacid solution, thus greatly reducing NMR line broadening while at the same time providing a low-nucleophilicity medium in which carbocations remain persistent. The choice of the protic or Lewis superacid or combinations thereof is usually dictated by the basicity of the substrate and the relative stability of the carbocation to be formed. The choice of the cosolvent is dictated by the temperature range necessary for a complete NMR study (with SO_2 being most limiting), and the relative electrophilicity of the carbocation to be generated (the relative nucleophilicity order is $SO_2 > SO_2ClF > SO_2F_2$).[11] The system FSO_3H/SO_2ClF is the most widely used medium for carbocation and heterocation generation via protonation. The generation of carbocations from less basic, more electron-deficient, precursors is usually accomplished in $FSO_3H.SbF_5$ mixtures (typically 4:1 and if necessary 1:1), and typically utilizing SO_2ClF or SO_2ClF/SO_2F_2 mixtures as the cosolvent.

5. COMPILATION OF THE NMR DATA FOR CARBOCATIONS DERIVED FROM VARIOUS CLASSES OF PAHs

NOTATION

a, b, c, d, and e denote interchangeable assignments within a cation

* means one of the two or both δ values were derived from chemical shifts that were interchangeable

n.o. means not observed

dark circles are roughly proportional to the magnitude of $\Delta\delta^{13}C$ values.

5.1. Naphthalenium ions (Figs 1 and 2, pp. 153–155)

Stable naphthalenium ions were first reported by Olah *et al.* in 1973.[12] Figure 1 summarizes the reported ^{1}H (and ^{19}F) NMR data. Notable features are long-range couplings observed in methylnaphthalenium cations and the significant fluoronium ion character in the case of 1-fluoro- and 2-fluoronaphthalenium ions, resulting in significant fluorine deshielding. At the NMR temperature used, the methoxynaphthalenium cation exists as an equilibrium mixture of two conformations, and the reported ^{1}H NMR data are for an averaged carboxonium ion. Using early ^{13}C NMR, Olah *et al.* reported the first example.[12] This is included in Fig. 1 for historic significance. Positive charge is strongly localized *ortho/para* to the protonation site.

Extensive studies of naphthalenium cations were later reported by Lammertsma and Cerfontain.[13,14] Figure 2 summarizes the ^{1}H NMR data and $\Delta\delta^{13}C$ values for a series of isomeric monomethyl-, dimethyl- , trimethyl-, and tetramethylnaphthalenium, as well as for hexahydropyrenium mono- and dications. Methyl groups exert strong directive and charge-stabilizing effects. The hexahydropyrenium dication shows dramatic charge localization in the *ortho* positions. *Ipso* protonation is observed with 1,4,5-trimethyl and 1,2,3,4-tetramethyl derivatives.

5.2. Anthracenium ions (Fig. 3, p. 156)

A series of substituted anthracenium monocations were generated by van der Griendt and Cerfontain (only proton data are available).[15] A noteworthy feature is the anisotropic shielding of methyl in *ipso*-protonated ethyl-substituted carbocations. A similar effect is seen in one of the methyl groups for the *ipso*-protonated isopropyl derivative.

5.3. Phenanthrenium cations (Figs 4–10, pp. 157–163)

NMR data are available for a series of methylated phenanthrenium cations (a persistent parent phenanthrenium ion has not been observed) (Fig. 4).[16,17] The site of attack is strongly controlled by the stabilizing effect of the methyl groups. The presence of methyl at C-1 or C-3 directs the attack to the bay region (C-4). Charge delocalization is mainly confined to the ring undergoing attack, with limited delocalization into the other rings (Fig. 5). Borodkin *et al.*[18] have reported NMR data for dynamic phenanthrenium ions undergoing degenerate methyl shift (Fig. 6). In higher-acidity superacids, alkylphenanthrenes are diprotonated (Fig. 7).[16,17] The ring protons in the dications are noticeably more deshielded. Symmetrical dialkylphenanthrenes give symmetrical dications.

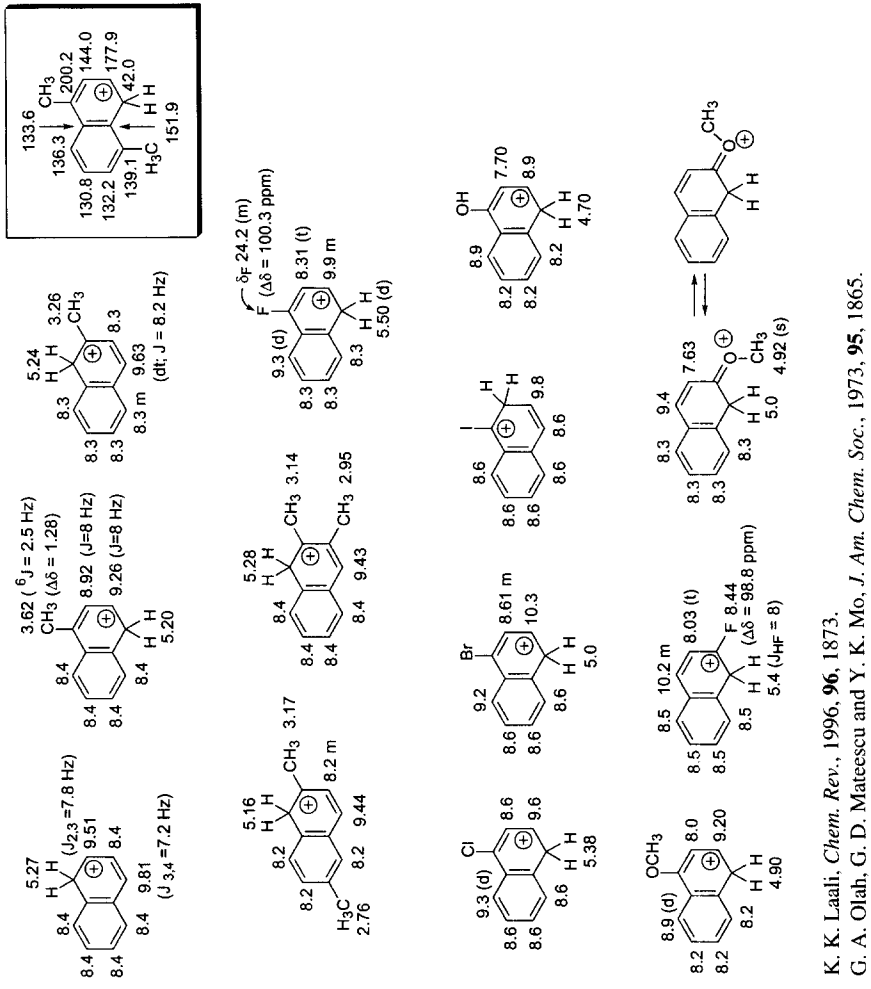

K. K. Laali, *Chem. Rev.*, 1996, **96**, 1873.
G. A. Olah, G. D. Mateescu and Y. K. Mo, *J. Am. Chem. Soc.*, 1973, **95**, 1865.

Fig. 1. Compilation of ^{1}H (^{19}F and ^{13}C) NMR data for naphthalenium ions.

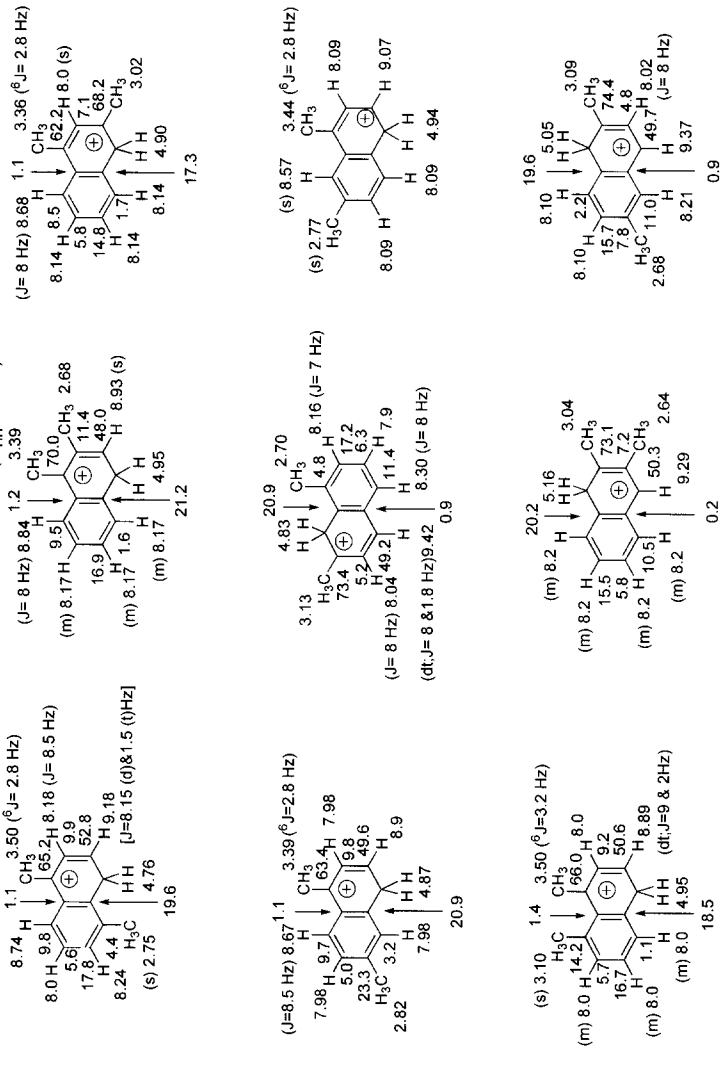

K. K. Laali, *Chem. Rev.*, 1996, **96**, 1873.
K. Lammertsma and H. Cerfontain, *J. Am. Chem. Soc.*, 1979, **101**, 3618.
K. Lammertsma, *J. Am. Chem. Soc.*, 1981, **103**, 2062.

Fig. 2. Compilation of ^{1}H NMR and $\Delta\delta^{13}$C values for alkylated naphthalenium ions.

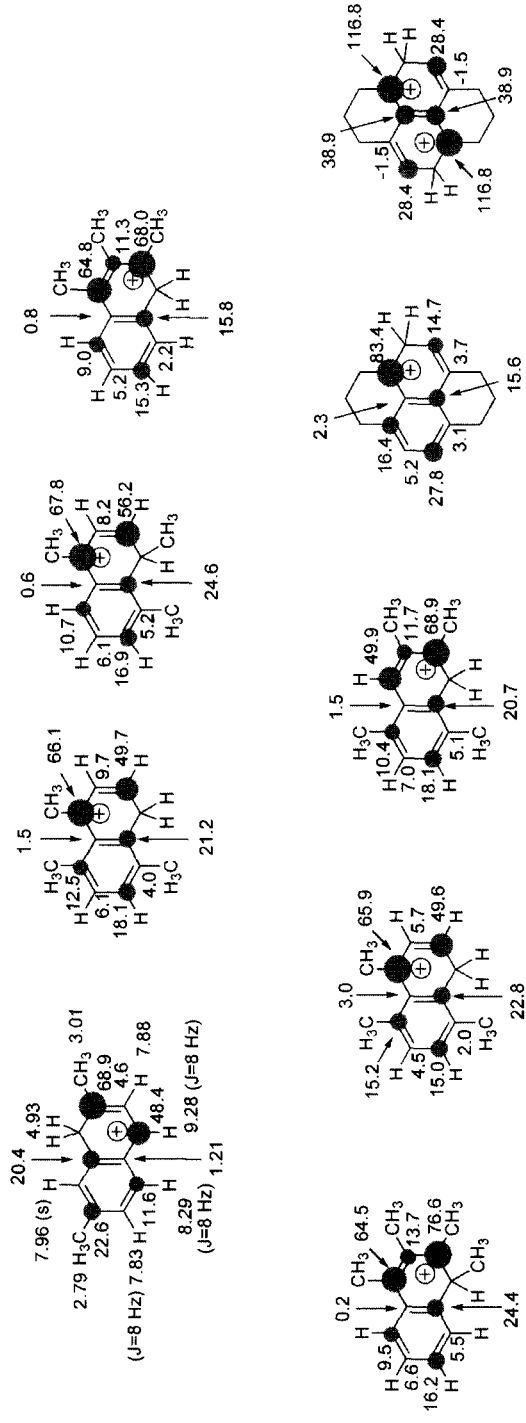

Fig. 2. (*continued*).

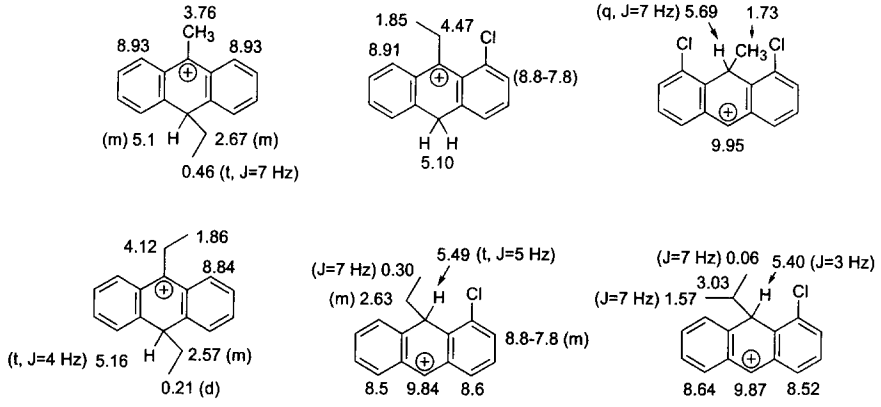

K. K. Laali, *Chem. Rev.*, 1996, **96**, 1873.
F. van de Griendt and H. Cerfontain, *Tetrahedron*, 1979, **34**, 2563.

Fig. 3. ^{1}H NMR chemical shifts for persistent 9-alkylanthracenium ions.

Charge delocalization in the dications is quite extensive (Fig. 8) and involves adjacent ring carbons in some cases.

Figure 9 is a summary of the NMR data for a series of regioisomeric α-phenanthrene-substituted tertiary carbocations that were generated from their alcohols.[19,20] Based on the $\Delta\delta$ values (Fig. 9), it is concluded that positive charge delocalization (p–π overlap) is most effective from the *meso* positions (C-9/C-10) and least effective from C-2. The presence of a α-CF_3 group destabilizes the carbocation and increases electron demand. Regioisomeric acetylphenanthrenes are CO protonated to give carboxonium ions (Fig. 10).[19] The *C*OH$^+$ chemical shift is consistent with the carboxonium character, resulting in limited delocalization into the PAH. Nevertheless, the pattern of delocalization is similar to that of α-carbocations.

5.4. Cyclopenta[a]phenanthrene ions (Figs 11–16, pp. 164–171)

Detailed NMR data are available for an extensive series of cylopenta[a]phenanthrenium cations and carboxonium ions (Figs 11 and 12).[21,22] Several examples of carboxonium–arenium dications have also been reported (Figs 13 and 14).[21] The alkyl and alkoxy substituents control the site of protonation. Protonation sites are *ortho/para* to the substituents. With methoxy and methyl groups in the bay region, ring fluorosulfonation occurs on raising temperature and/or prolonged reaction times. NMR data are also available for representative dimer dications having methoxy groups in the bay region. NMR data and charge delocalization mapping (Figs 15 and 16),[22] in comparison with the correspond-

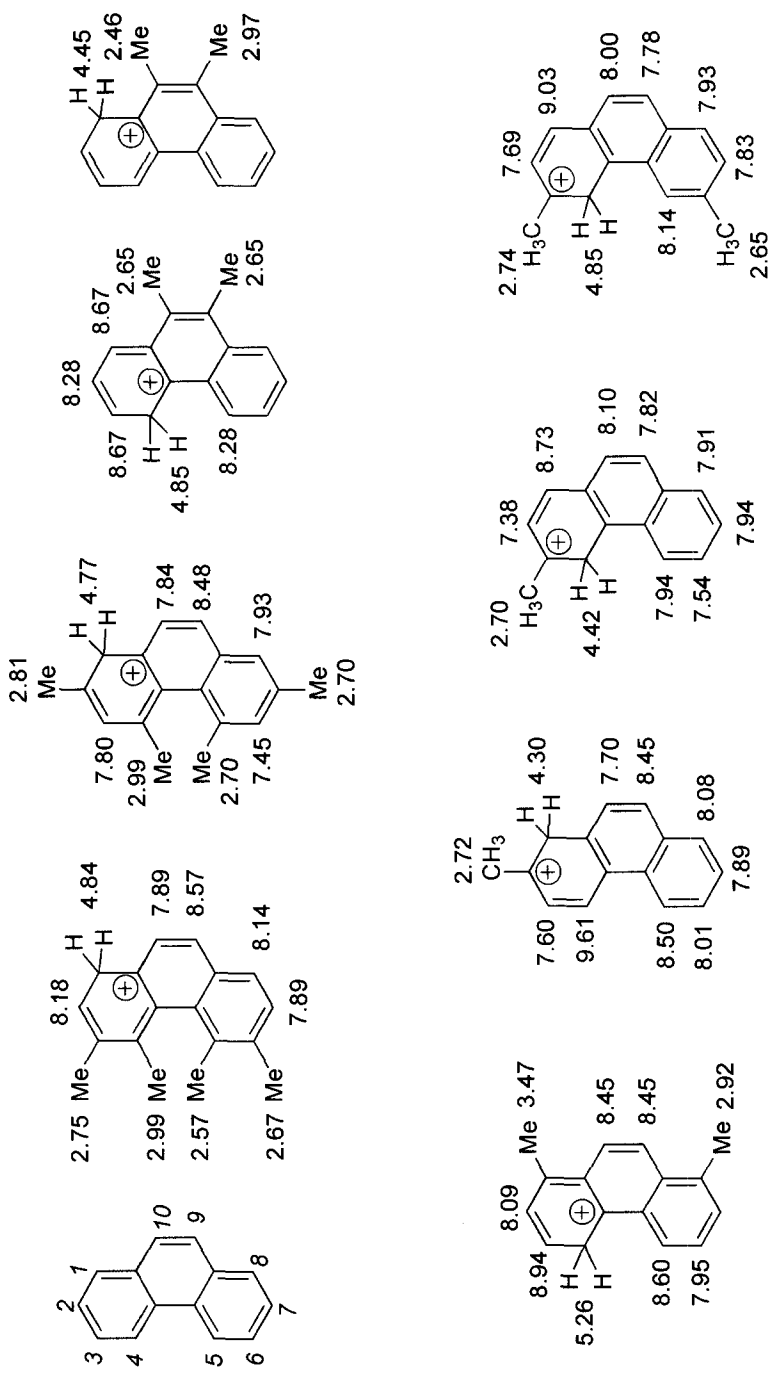

K. K. Laali, *Chem. Rev.*, 1996, **96**, 1873.
K. Laali and H. Cerfontain, *J. Org. Chem.*, 1983, **48**, 1092.
K. K. Laali, S. Hollenstein and P. E. Hansen, *J. Chem. Soc., Perkin Trans. II*, 1997, 2207.

Fig. 4. ^{1}H NMR data for methylphenanthrenium ions.

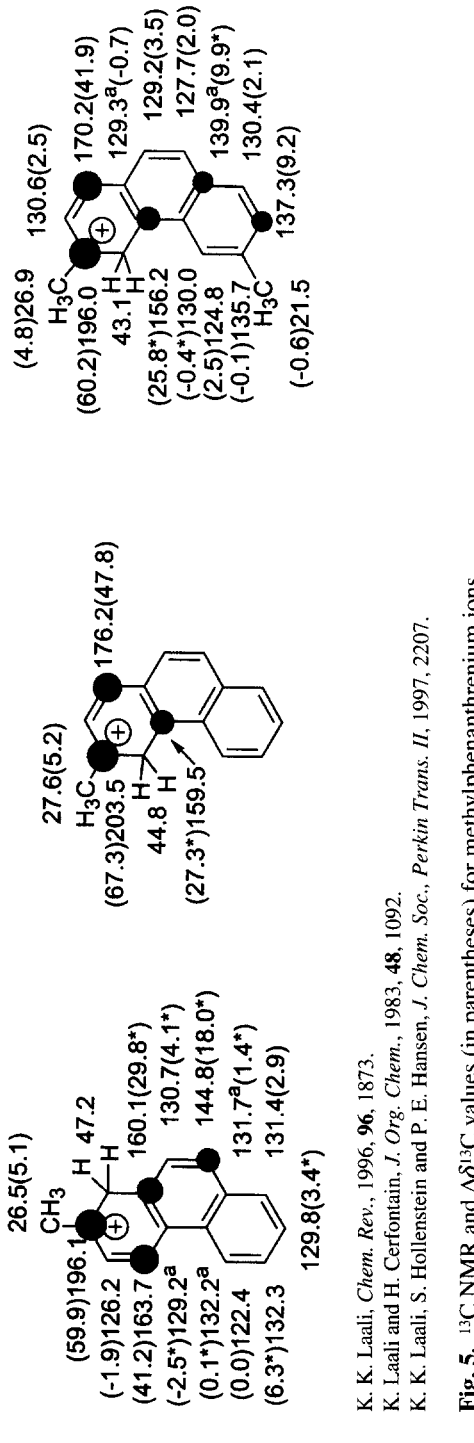

K. K. Laali, *Chem. Rev.*, 1996, **96**, 1873.
K. Laali and H. Cerfontain, *J. Org. Chem.*, 1983, **48**, 1092.
K. K. Laali, S. Hollenstein and P. E. Hansen, *J. Chem. Soc., Perkin Trans. II*, 1997, 2207.

Fig. 5. ^{13}C NMR and $\Delta\delta^{13}$C values (in parentheses) for methylphenanthrenium ions.

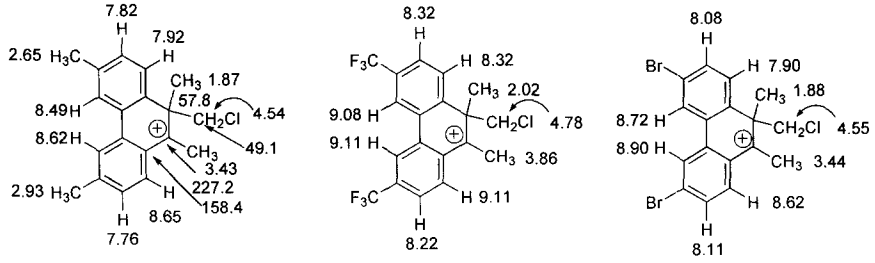

K. K. Laali, *Chem. Rev.*, 1996, **96**, 1873.
G. I. Borodkin, M. M. Shakirov and V. G. Shubin, *J. Org. Chem. USSR*, 1990, **26**, 2254.

Fig. 6. ^{1}H NMR data for dynamic phenanthrenium ions (some key ^{13}C values are also shown).

ing monomeric monocations, suggest that there is little interaction between the two PAH carbocations in the dimer dications.

5.5. Pyrenium cations (Figs 17–34, pp. 172–192)

Detailed NMR data are available for an extensive set of pyrenium cations. Proton NMR data for protonation and sulfinylation monocations are gathered in Figs 17 and 18.[23–25] Sulfinylation cations are obtained when SO_2 is used in place of SO_2ClF. Consistent with the computed relative arenium ion energies, there is a strong tendency for attack at an α-position. *Ipso* attack occurs when the α-positions are substituted. Limited examples of pyrenium cations of $\alpha\beta$-attack are available (these are formed indirectly via alkyl/cycloalkyl rearrangement). The $CH(SO_2H)$ in the sulfinylation σ-complexes is noticeably more deshielded than the CH_2 in protonated cations. The $-SO_2H$ proton is most deshielded. Among the ring protons, remote α-protons and two of the $\alpha\beta$-protons are most deshielded. Figure 19 summarizes the range of ^{1}H $\Delta\delta$ values for pyrenium ions of protonation and sulfinylation.[23] The ^{13}C NMR data and the $\Delta\delta$ values are gathered in Fig. 20 for representative pyrenium monocations.[24,25] Figure 21 focuses attention on the charge delocalization mode (deduced from $\Delta\delta^{13}$C values).

NMR data for persistent fluoropyrenium cations (including their hexahydro and tetrahydro derivatives) are gathered in Figs 22–24.[26] Fluoropyrenium cations exhibit interesting long-range C/F couplings (not shown to avoid overcrowding). Variation in the C/F couplings, changes in the ^{13}C shifts relative to non-fluorinated analogs, and the $\Delta\delta^{19}$F values are consistent with significant fluorine back-bonding. Fluorine at C-2 has a strong directive stabilizing effect. The $\Delta\delta^{13}$C and $\Delta\delta^{19}$F values are summarized in Fig. 24 and indicate uniform charge alternation and delocalization throughout the system.

Detailed NMR data are available for a series of regioisomeric α-pyrene-substituted secondary and tertiary carbocations (Figs 25 and 26)[27] as well as for

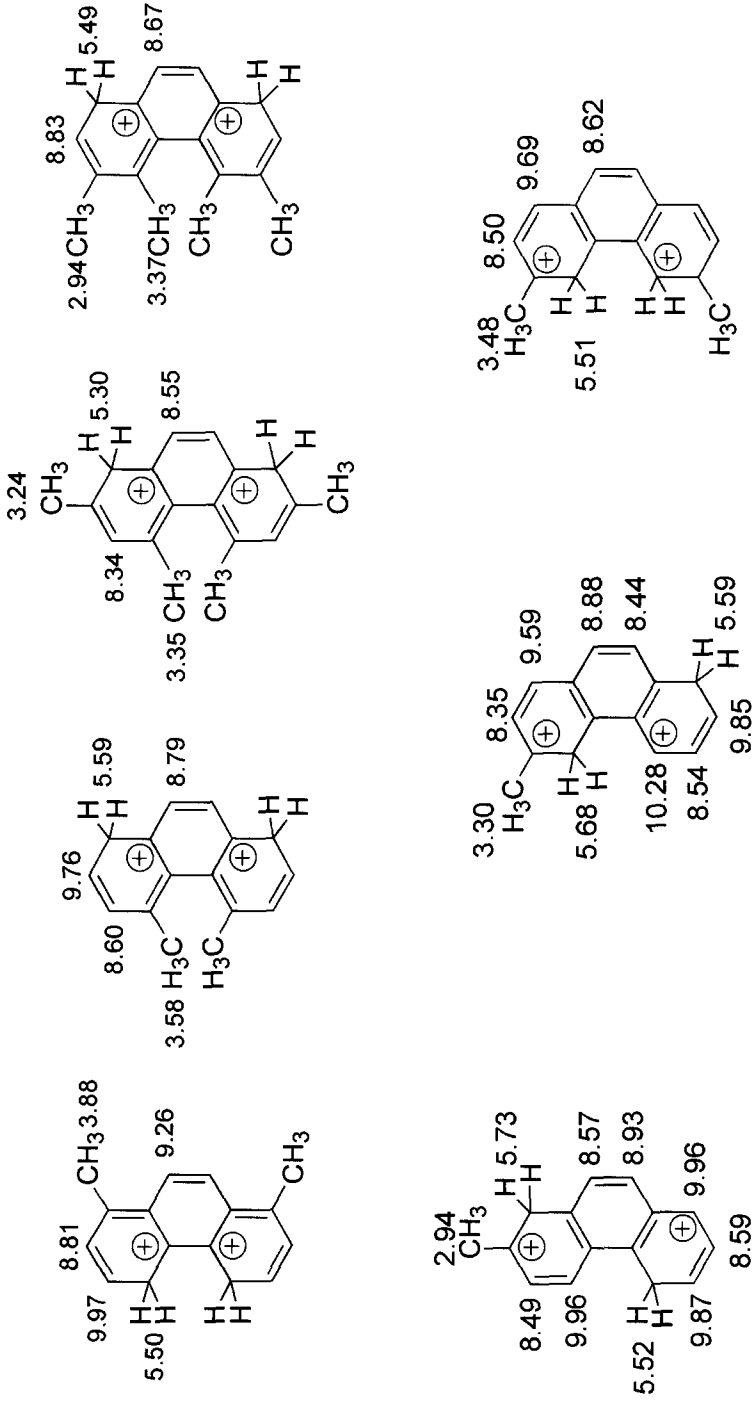

K. K. Laali, *Chem. Rev.*, 1996, **96**, 1873.
K. Laali and H. Cerfontain, *J. Org. Chem.*, 1983, **48**, 1092.
K. K. Laali, S. Hollenstein and P. E. Hansen, *J. Chem. Soc., Perkin Trans. II*, 1997, 2207.

Fig. 7. ^{1}H NMR data for methylphenanthrenium dications.

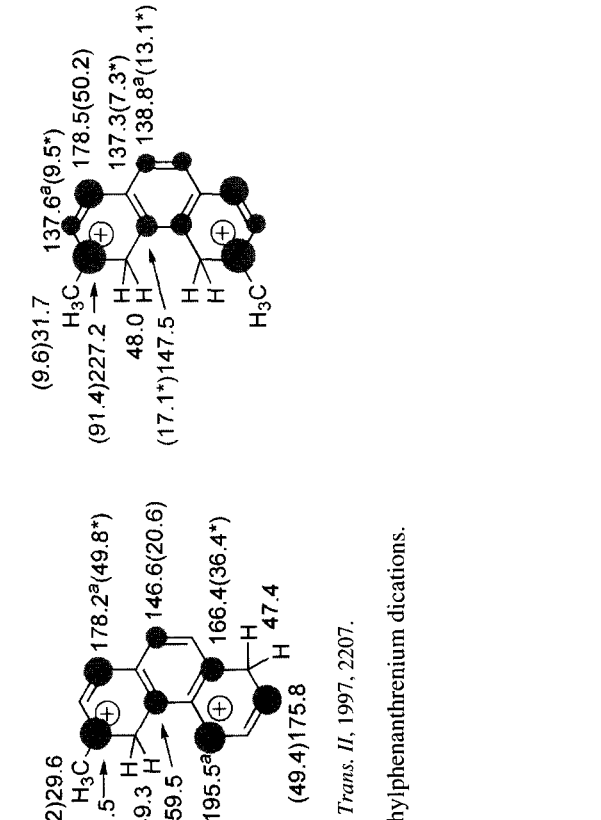

K. K. Laali, S. Hollenstein and P. E. Hansen, *J. Chem. Soc., Perkin Trans. II*, 1997, 2207.

Fig. 8. ^{13}C NMR and $\Delta\delta^{13}C$ values (in parentheses) for methylphenanthrenium dications.

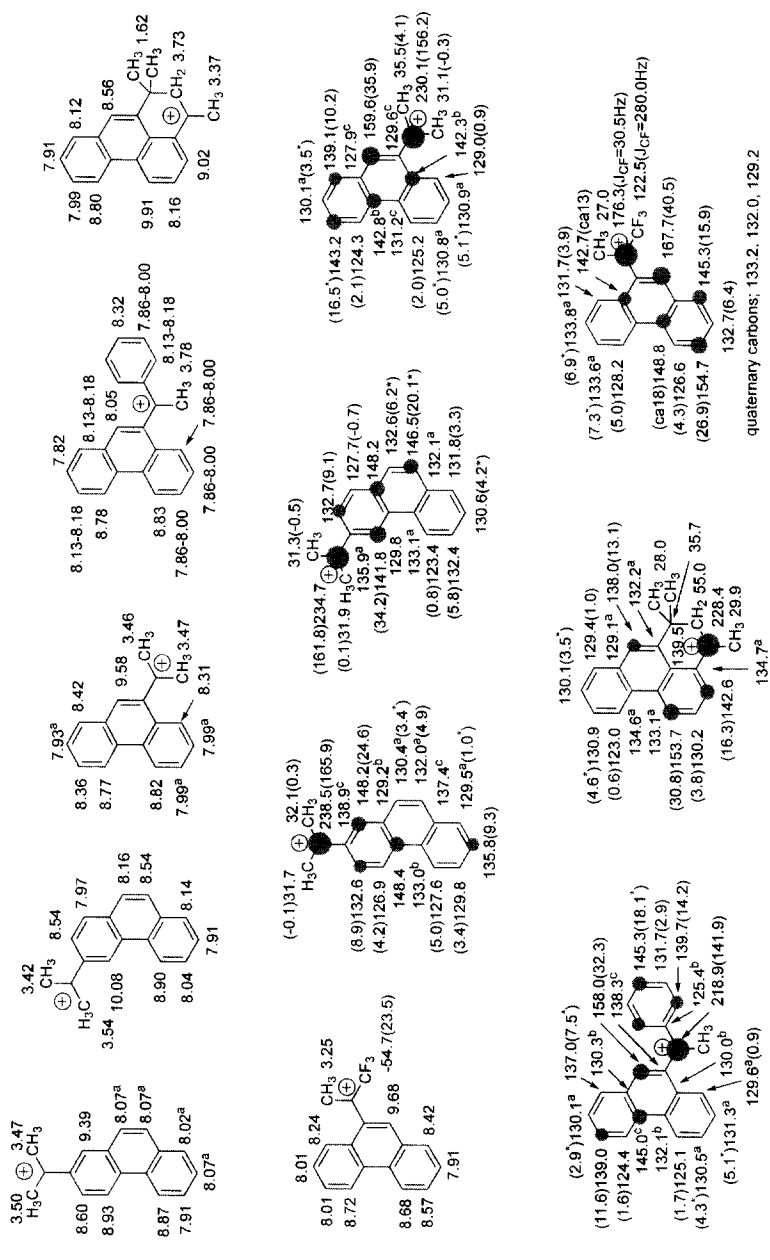

K. K. Laali and S. Hollenstein, *J. Chem. Soc., Perkin Trans. II*, 1998, 897.
S. Hollenstein and K. K. Laali, *Chem. Commun.*, 1997, 2145.

Fig. 9. ^{1}H and ^{13}C NMR chemical shifts for α-substituted phenanthrenium ions ($\Delta\delta^{13}C$ in parentheses).

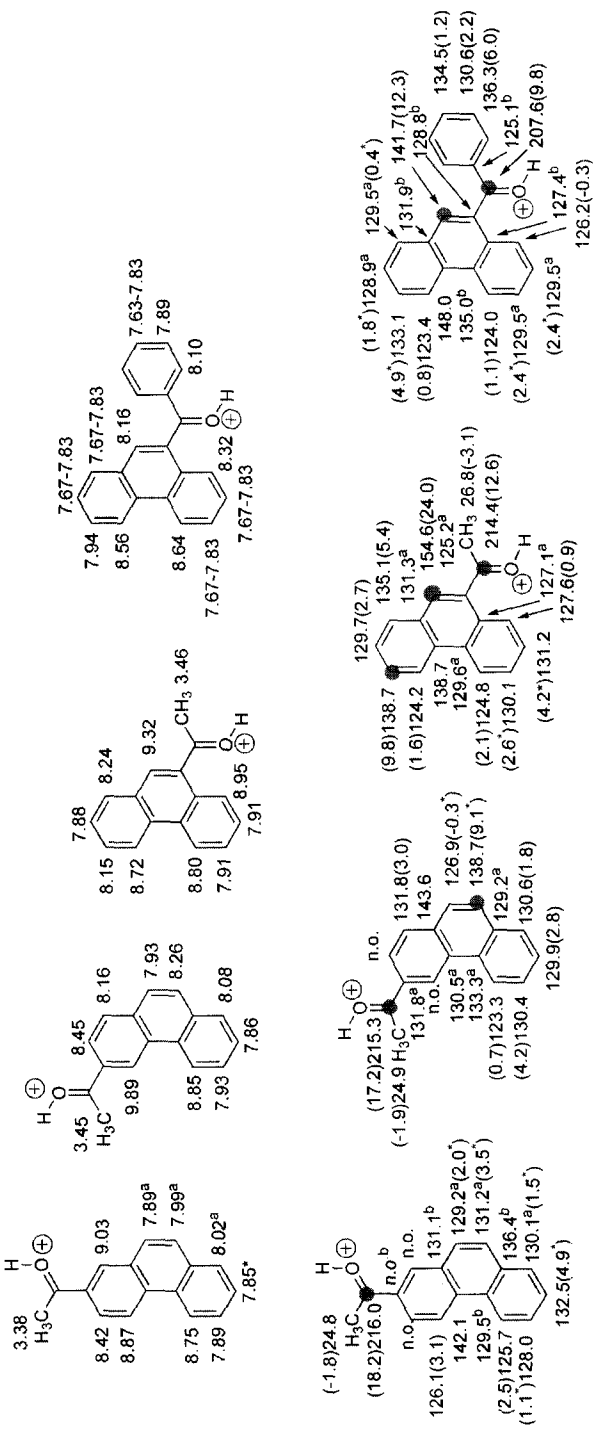

K. K. Laali and S. Hollenstein, *J. Chem. Soc., Perkin Trans. II*, 1998, 897.

Fig. 10. ^{1}H and ^{13}C NMR data for carboxonium ions from phenanthrene derivatives ($\Delta\delta^{13}C$ in parentheses).

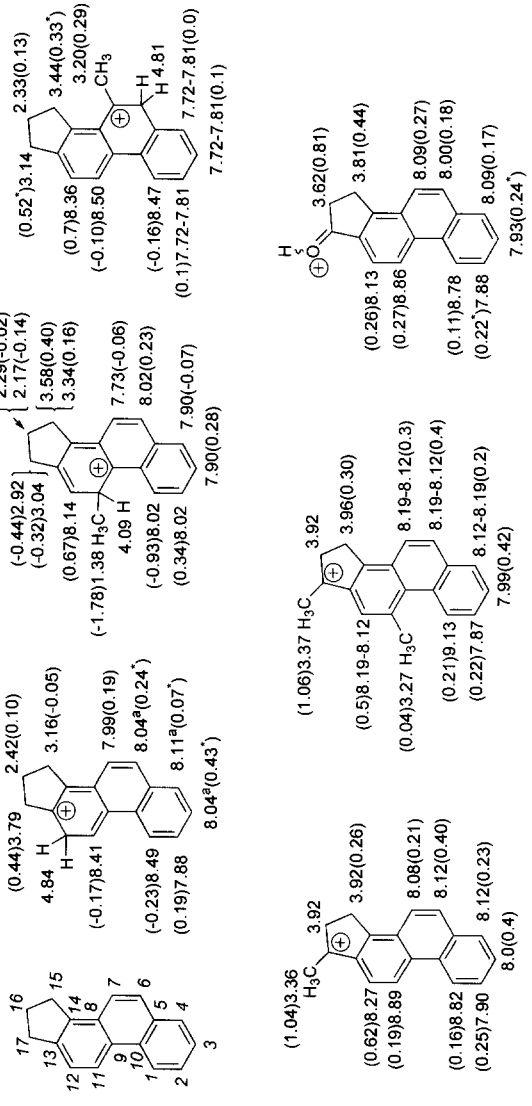

Fig. 11. ^{1}H NMR for carbocations from cyclopenta[a]phenanthrene derivatives ($\Delta\delta^1$H in parentheses).

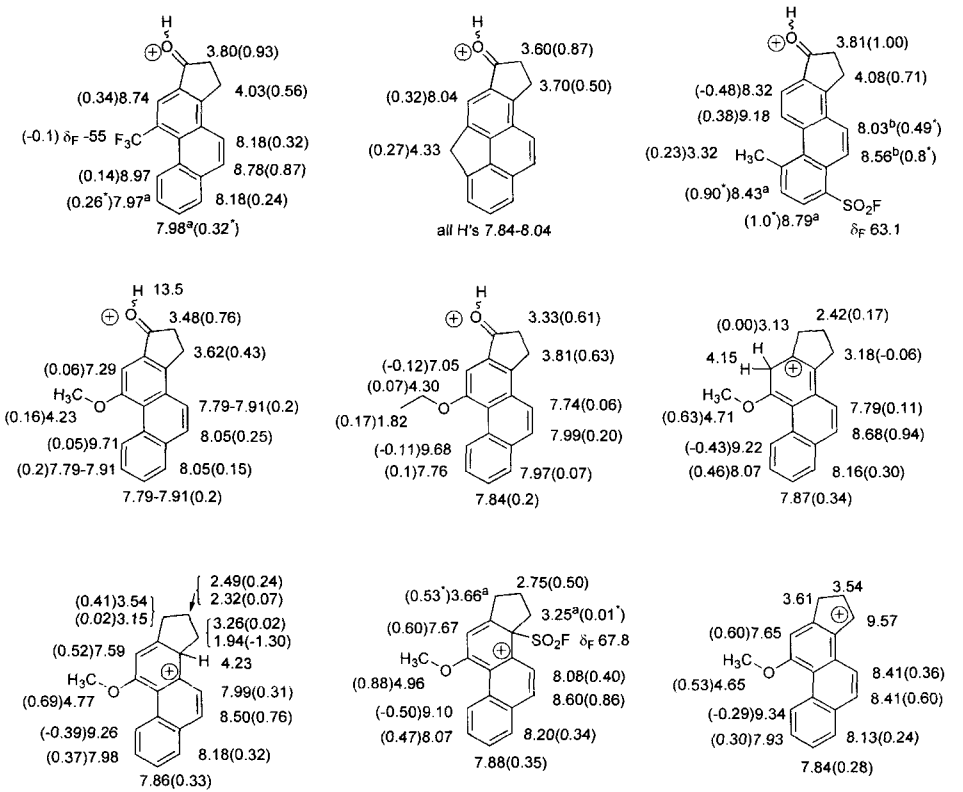

K. K. Laali, S. Hollenstein, S. E. Galembeck and M. M. Coombs, *J. Chem. Soc., Perkin Trans. II*, 2000, 211.
K. K. Laali, T. Okazaki and M. M. Coombs, *J. Org. Chem.*, 2000, **65**, 7399.

Fig. 11. (*continued*).

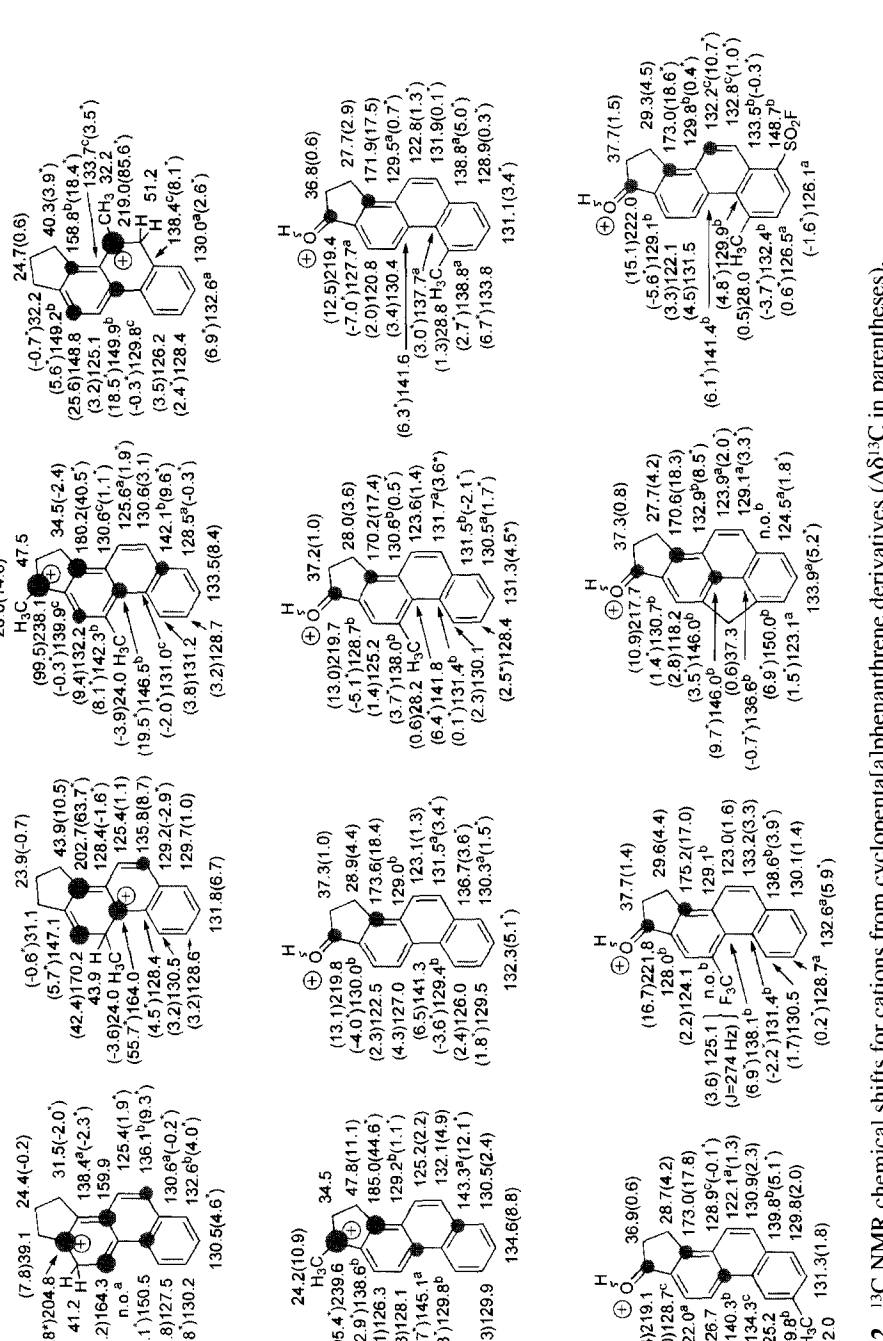

Fig. 12. ^{13}C NMR chemical shifts for cations from cyclopenta[a]phenanthrene derivatives ($\Delta\delta^{13}C$ in parentheses).

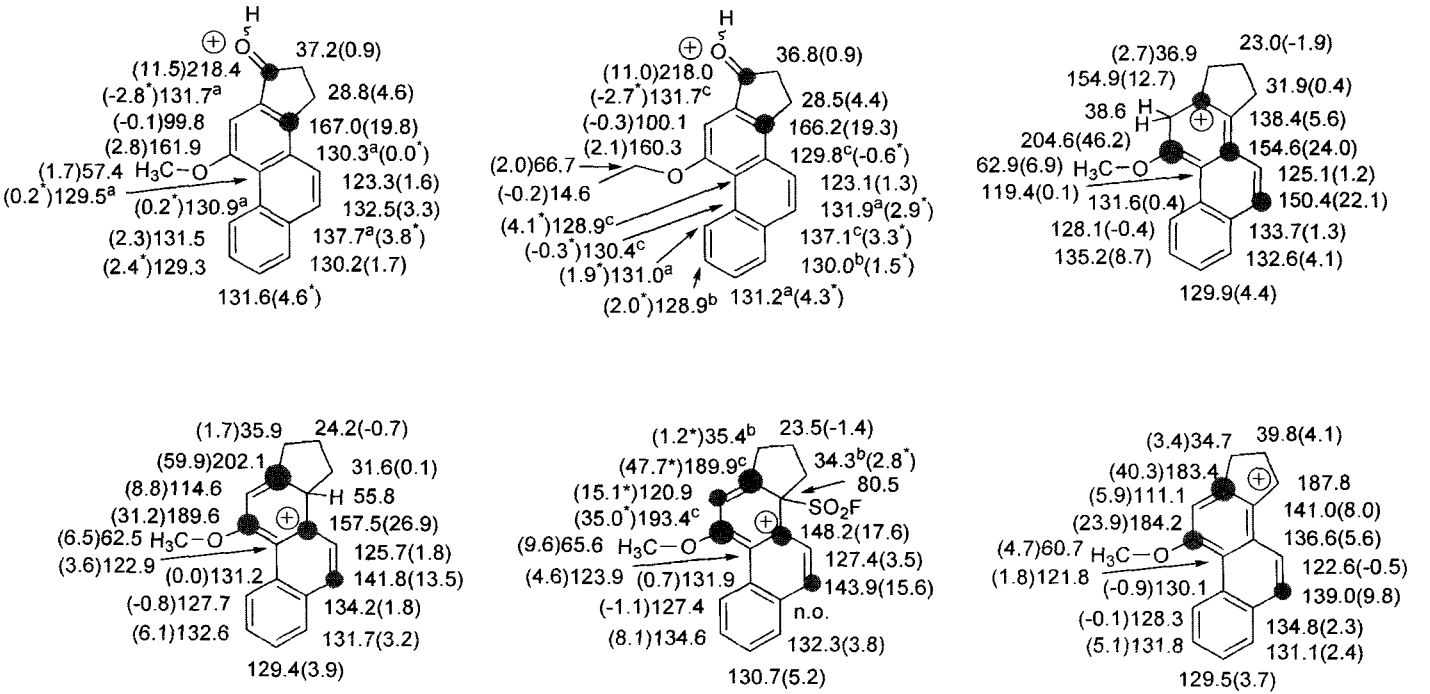

K. K. Laali, S. Hollenstein, S. E. Galembeck and M. M. Coombs, *J. Chem. Soc., Perkin Trans. II*, 2000, 211.
K. K. Laali, T. Okazaki and M. M. Coombs, *J. Org. Chem.*, 2000, **65**, 7399.

Fig. 12. (*continued*).

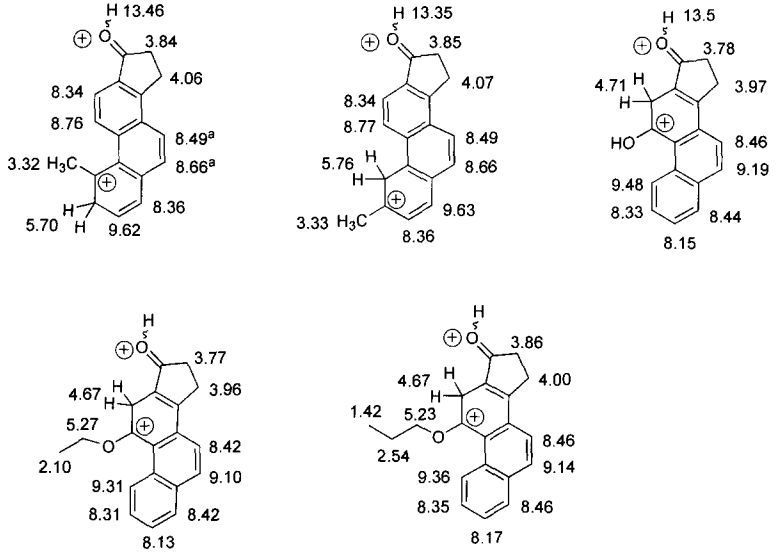

K. K. Laali, S. Hollenstein, S. E. Galembeck and M. M. Coombs, *J. Chem. Soc., Perkin Trans. II*, 2000, 211.

Fig. 13. ^{1}H NMR chemical shifts for dications from cyclopenta[a]phenanthrene derivatives ($\Delta\delta^1$H in parentheses).

a series of pyrenium–carboxonium dications (Figs 27 and 28)[28] and several dicarboxonium dications (Figs 29 and 30).[28] In α-pyrene-substituted carbocations, positive charge is most effectively delocalized from the α-position and least effectively from the β-position. The MeCO*H*$^+$ resonance in the carboxonium ion is in the 14–15 ppm range. The conformation(s) of the carboxonium group(s) were deduced on the basis of NOED spectra. In the pyrenium–carboxonium dications, ring protonation occurs at α-positions and positive charge is delocalized over the periphery. The resulting pattern is similar to the charge delocalization mode in 1-pyrenyl cations.

NMR data for regioisomeric pyrenyl-α-CF_3-substituted carbocations are gathered in Figs 31 and 32.[29] Carbocation destabilization increases π-participation and pyrenium ion character. This is reflected in larger $\Delta\delta$ values and the significant double-bond character which shields the carbocation. Because charge delocalization from the β-position is poor, CF_3-substitution can exert maximal destabilization. Thus, the alcohol precursor is not ionized; instead, protonation occurs at a remote α-position.

Figure 33 summarizes the NMR data for dihydropyrenium (ethanophenanthrenium) mono- and dications.[25] The charge delocalization mode in the symmetrical dications is noteworthy. The pattern differs from that in parent pyrenium cation and its 2,7-di-*tert*-butyl-substituted derivatives.

Protonation of cyclobutene-fused pyrene leads to a mixture of two α-protonated monocations. Only ^{1}H NMR data are available (Fig. 34).[30]

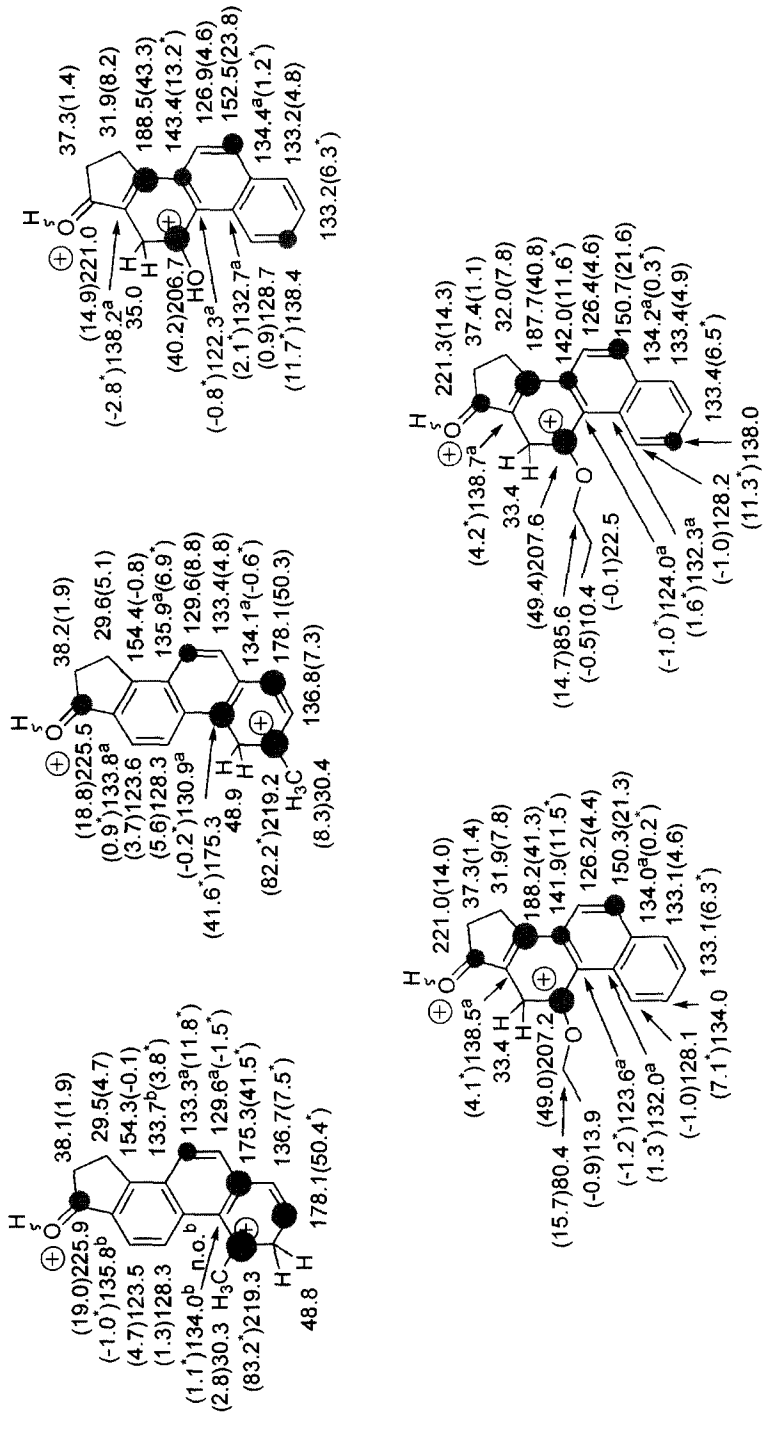

K. K. Laali, S. Hollenstein, S. E. Galembeck and M. M. Coombs, *J. Chem. Soc., Perkin Trans. II*, 2000, 211.

Fig. 14. ^{13}C NMR chemical shifts for dications from cyclopenta[a]phenanthrene derivatives ($\Delta\delta^{13}C$ in parentheses).

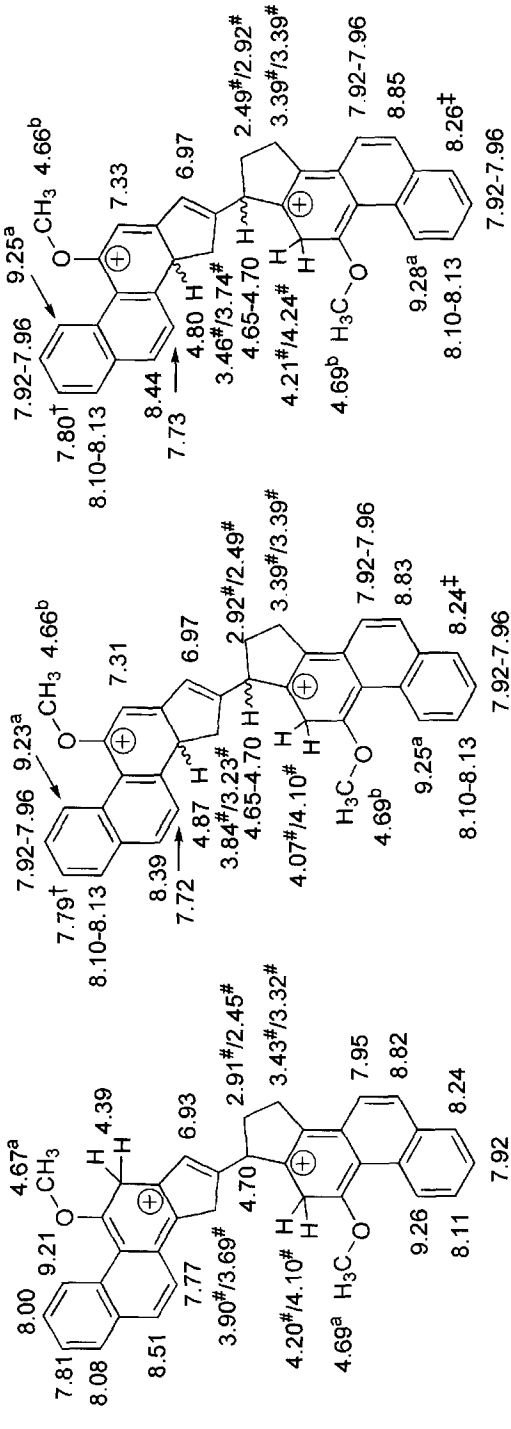

K. K. Laali, T. Okazaki and M. M. Coombs, *J. Org. Chem.*, 2000, **65**, 7399.

Fig. 15. ^{1}H chemical shifts for dications from cyclopenta[a]phenanthrene derivatives. † and ‡ denote interchangeable assignments within the two cations. # means that specific assignments of the diastereotropic protons in the five-membered rings are unknown.

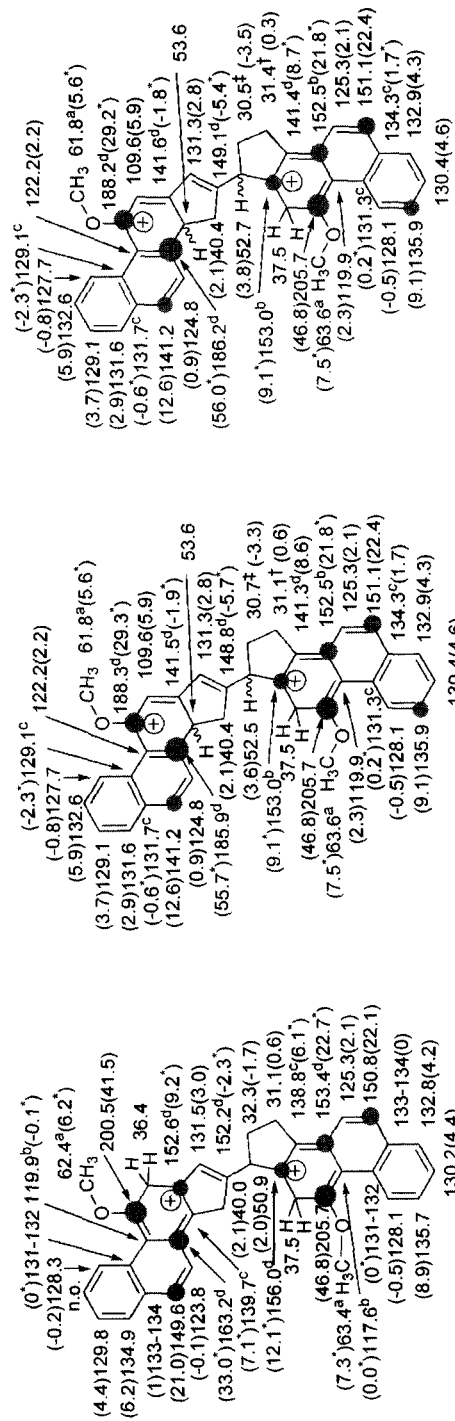

K. K. Laali, T. Okazaki and M. M. Coombs, *J. Org. Chem.*, 2000, **65**, 7399.

Fig. 16. ^{13}C NMR chemical shifts for dications from cyclopenta[a]phenanthrene derivatives ($\Delta\delta^{13}C$ in parentheses). † and ‡ denote interchangeable assignments within the two cations.

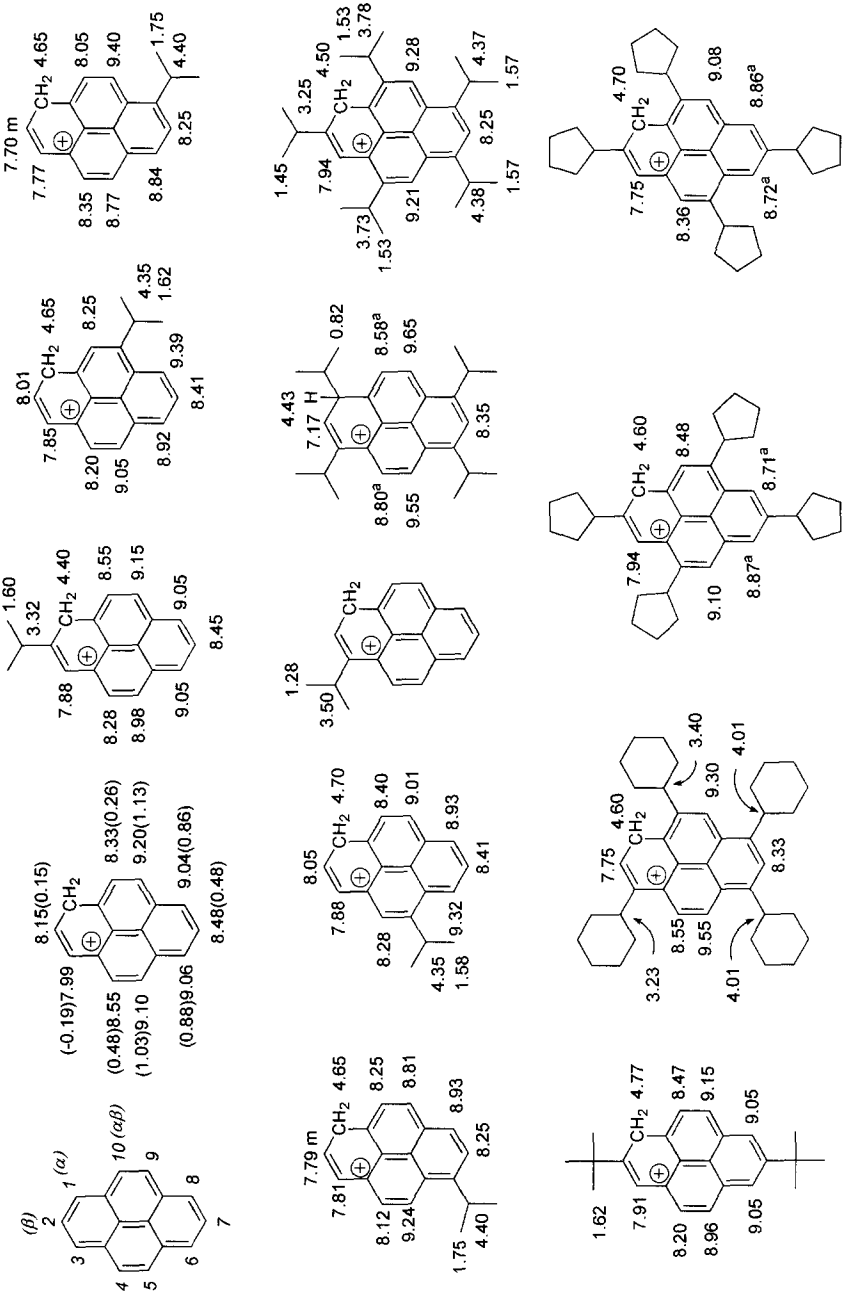

Fig. 17. ^{1}H NMR assignments for alkyl(cycloalkyl)pyrenium ions (partial $\Delta\delta^1$H values in parentheses).

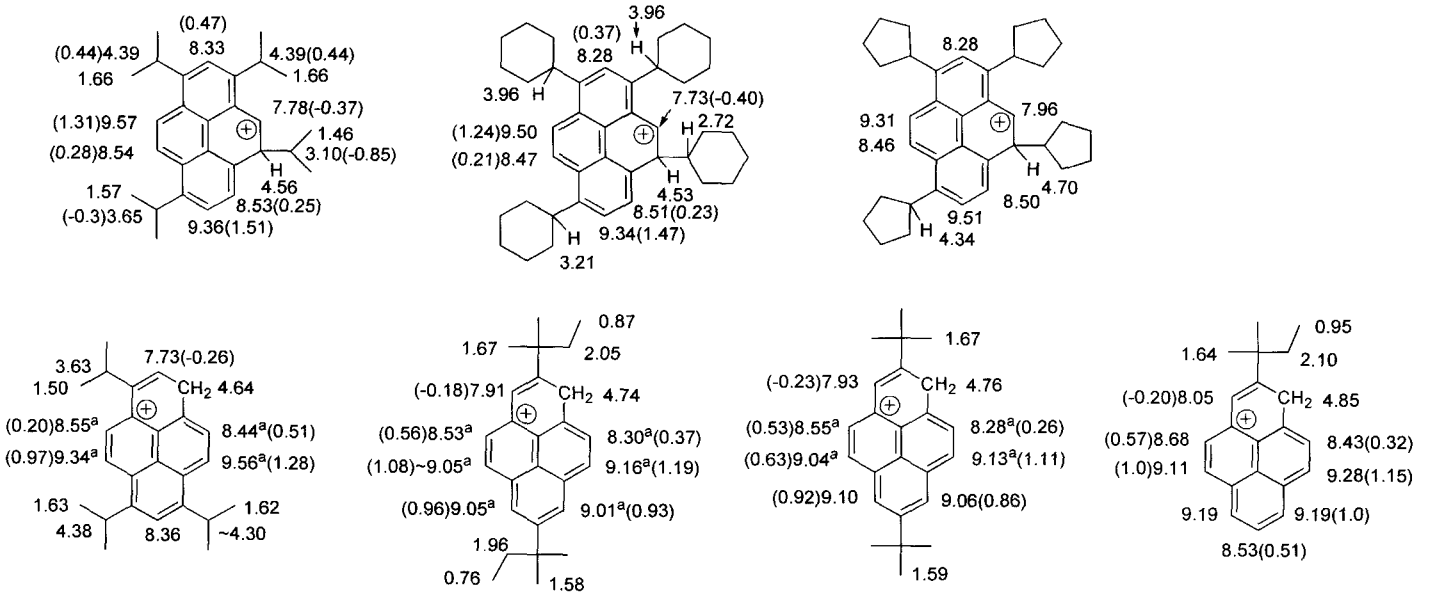

K. K. Laali, *Chem. Rev.*, 1996, **96**, 1873.
K. K. Laali and P. E. Hansen, *J. Org. Chem.*, 1991, **56**, 6795.
K. K. Laali and P. E. Hansen, *J. Chem. Soc., Perkin Trans. II*, 1994, 2249.
K. K. Laali and P. E. Hansen, *Res. Chem. Intermed.*, 1996, **22**, 737.

Fig. 17. (*continued*).

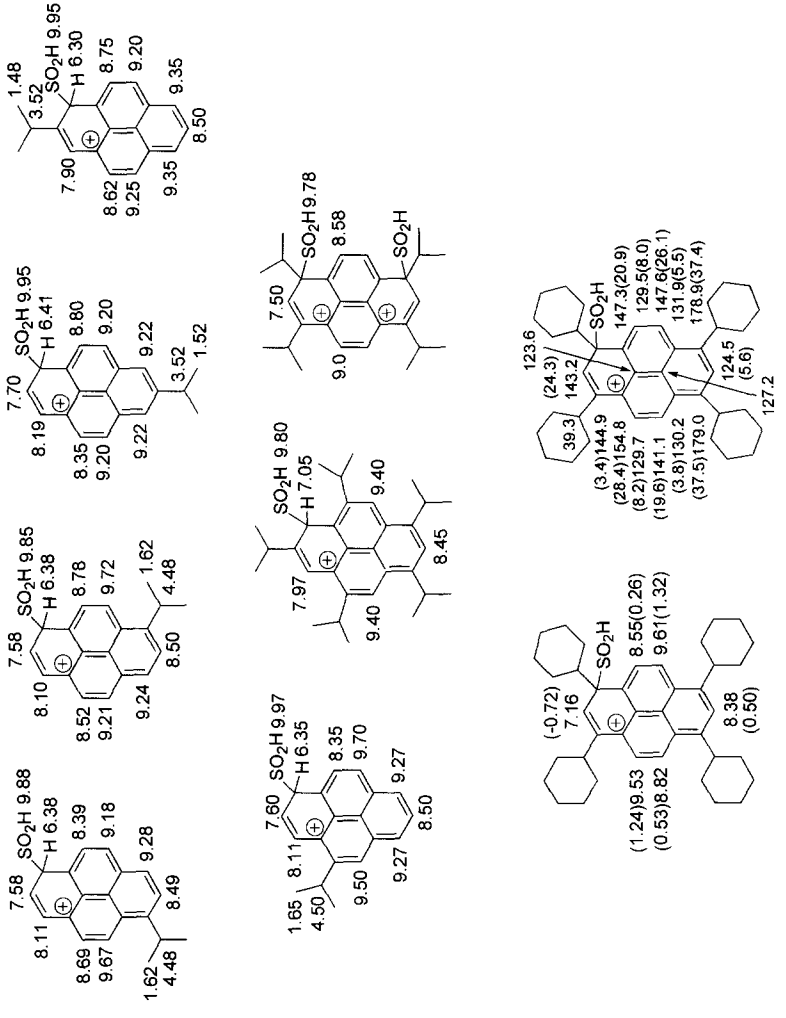

K. K. Laali and P. E. Hansen, *J. Org. Chem.*, 1991, **56**, 6795.

Fig. 18. ^{1}H and ^{13}C NMR chemical shifts for sulfinylated alkyl(cycloalkyl)pyrenium ions (partial $\Delta\delta^{1}H$ and $\Delta\delta^{13}C$ values in parentheses).

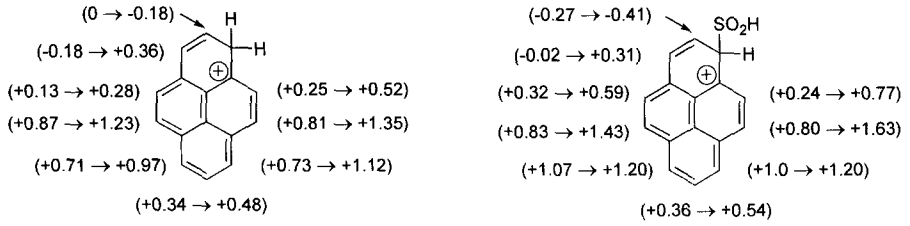

K. K. Laali and P. E. Hansen, *J. Org. Chem.*, 1991, **56**, 6795.

Fig. 19. Comparison of magnitude of $\Delta\delta^1$H values in pyrenium ions of protonation and sulfinylation.

5.6. Benzopyrenium and dibenzopyrenium cations (Figs 35 and 36, pp. 192 and 193)

Figures 35 and 36 summarize the available NMR data for carbocations derived from benzo[a]pyrene (BaP), dibenzo[a,e]pyrene (DBP), and benzo[e]pyrene (BeP).[31] Protonation sites are at α-positions in the pyrene moiety. The C-6 protonated BaP and DBP carbocations exhibit more extensive charge delocalization compared with the BeP cation. Positive charge is primarily delocalized into the pyrene core.

5.7. Benzanthracenium cations and carboxonium ions, and representative α-anthracenium-substituted cations (Figs 37 and 38, pp. 194–197)

The available NMR data for persistent carbocations derived from the benz[a]anthracene (BA) skeleton and for a series of secondary α-substituted carbocations (and related model carbocations) and α-carboxonium ions are gathered in Figs 37 and 38.[32] The *meso* positions (C-7/C-12) in BA are most reactive. The conformation(s) of the carboxonium group was deduced on the basis of NOED experiments. The $\Delta\delta^{13}$C values (Fig. 38) indicate the strong anthrecenium ion character in benz[a]anthrenium and their α-carbocations.

5.8. Dibenzoanthracenium cations (Fig. 39, p. 198)

NMR data for dibenzoanthracenium cations are shown in Fig. 39.[33] Protonation sites are the *meso* positions in the anthracene moiety (C-9/C-14 in dibenz[1,c]anthracene and C-7/C-14 in dibenzo[a,h]anthracene).

5.9. Chrysenium cations and carboxonium ions (Figs 40–43, pp. 199–202)

Unlike dibenzoanthracenium cations for which only limited NMR data are available (Fig. 39),[33] detailed NMR studies on chrysenium (Ch) cations have

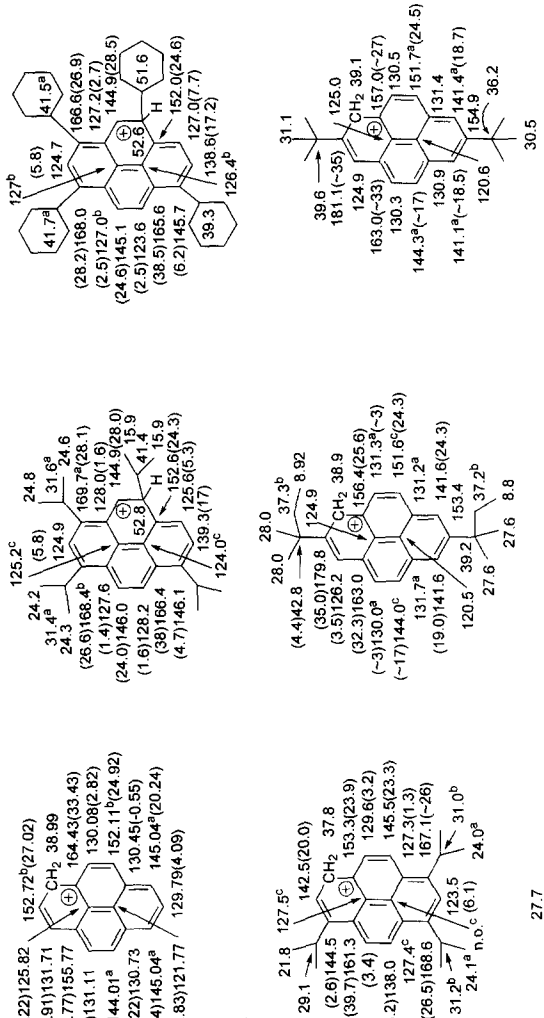

K. K. Laali, *Chem. Rev.*, 1996, **96**, 1873.
K. K. Laali and P. E. Hansen, *J. Chem. Soc., Perkin Trans. II*, 1994, 2249.
K. K. Laali and P. E. Hansen, *Res. Chem. Intermed.*, 1996, **22**, 737.

Fig. 20. ^{13}C NMR chemical shifts for alkyl(cycloalkyl)pyrenium ions ($\Delta\delta^{13}C$ in parentheses).

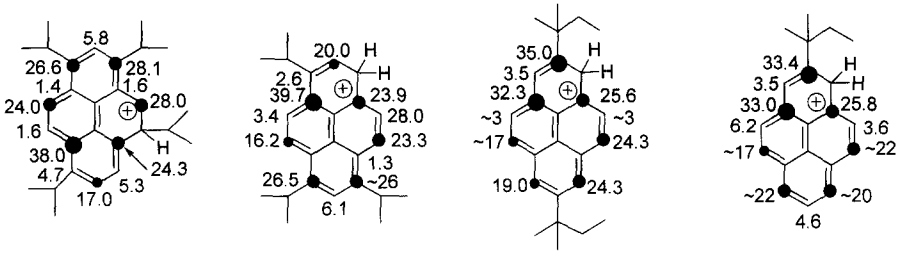

K. K. Laali, *Chem. Rev.*, 1996, **96**, 1873.
K. K. Laali and P. E. Hansen, *J. Chem. Soc., Perkin Trans. II*, 1994, 2249.

Fig. 21. Charge delocalization mode for alkylated pyrenium ions based on the $\Delta\delta^{13}C$ values.

been made (Figs 40–43).[34,35] Carbocations derived from protonation at C-12 (or C-6) are consistently preferred except in the 2-OMe derivatives where attack is primarily directed to C-1. 5-Acetylchrysene gives a carboxonium ion. Relative orientation of the methoxy group in the carbocations and the protonated acetyl in the carboxonium ion were determined by NOE experiments. In the 6-fluorochrysenium cation, fluorine is deshielded by ~57 ppm. The charge delocalization pattern is deduced on the basis of $\Delta\delta^{13}C$ values. This pattern is common for several chrysenium cations with methyl and halogen substituents, except in the 5-methyl derivative (Fig. 41). The methoxy derivatives show limited charge delocalization.

5.10. Benzo[c]phenanthrene and benzo[g]chrysene cations (Figs 44 and 45, pp. 203 and 204)

NMR data are available for the 3-methoxy and 3-hydroxy-substituted benzo[c]-phenanthrene (BcPh) carbocations.[34,35] In the OMe derivatives the resulting carbocations exist in two conformations which are distinct at low temperature. With the OH derivative only a conformationally averaged carbocation was detected. For the benzo[g]chrysene (BgCh) stable ion, NMR data have been obtained for the parent BgCh as well as its OMe, OH, and tetrahydro-1-one derivatives. As with BcPh carbocations, the OMe-substituted carbocations of BgCh exist as two distinct conformers, but the OH derivative exists as a conformationally averaged carbocation. Parent BgCh is protonated at C-10 (K-region). The keto derivative gives a carboxonium cation. Figure 45 summarizes the C-13 data and the $\Delta\delta$ values from which the charge delocalization modes can be deduced and compared. In both cases the methoxy- and hydroxy-substituted carbocations show limited charge delocalization.

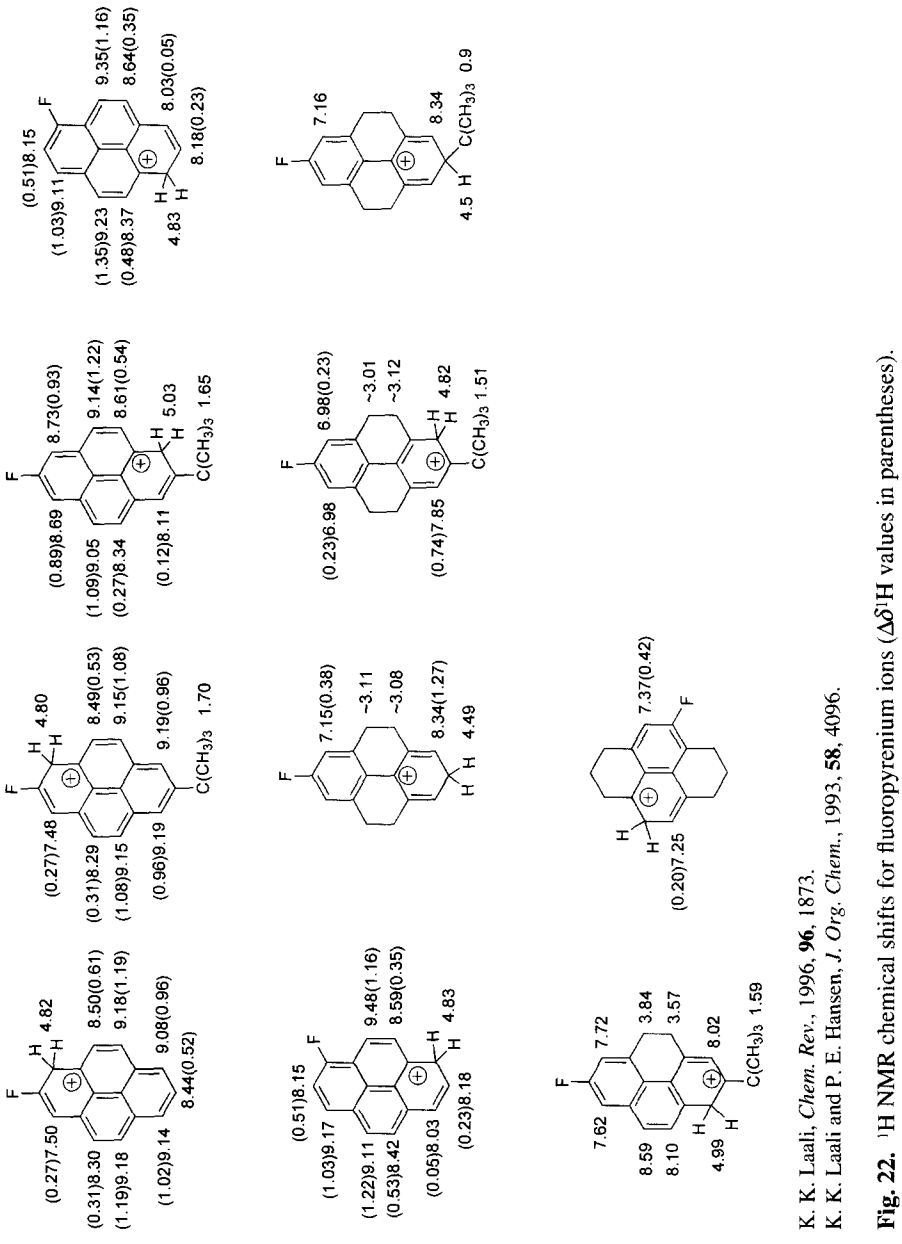

K. K. Laali, *Chem. Rev.*, 1996, **96**, 1873.
K. K. Laali and P. E. Hansen, *J. Org. Chem.*, 1993, **58**, 4096.

Fig. 22. ^{1}H NMR chemical shifts for fluoropyrenium ions ($\Delta\delta^1$H values in parentheses).

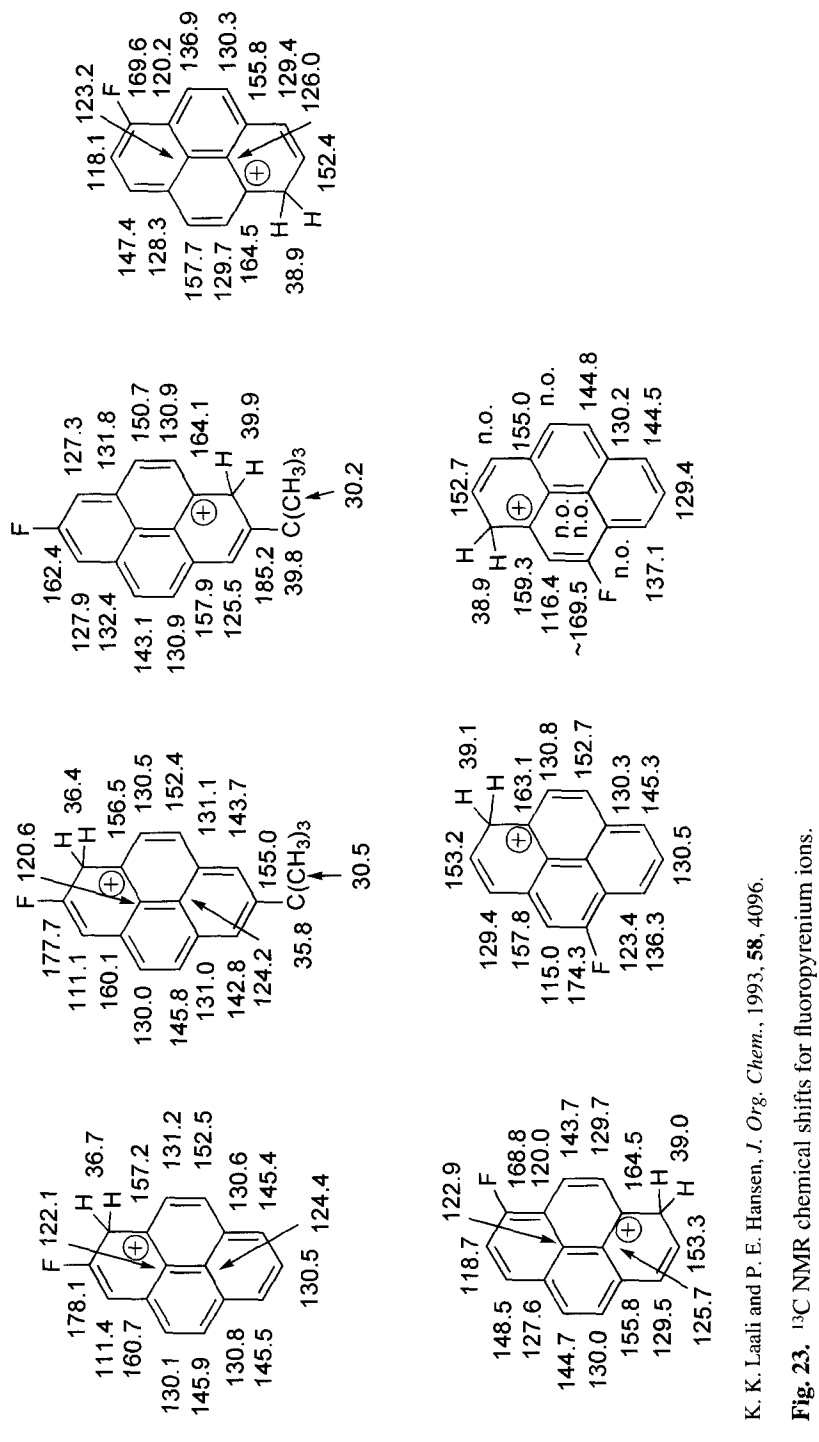

K. K. Laali and P. E. Hansen, *J. Org. Chem.*, 1993, **58**, 4096.

Fig. 23. ^{13}C NMR chemical shifts for fluoropyrenium ions.

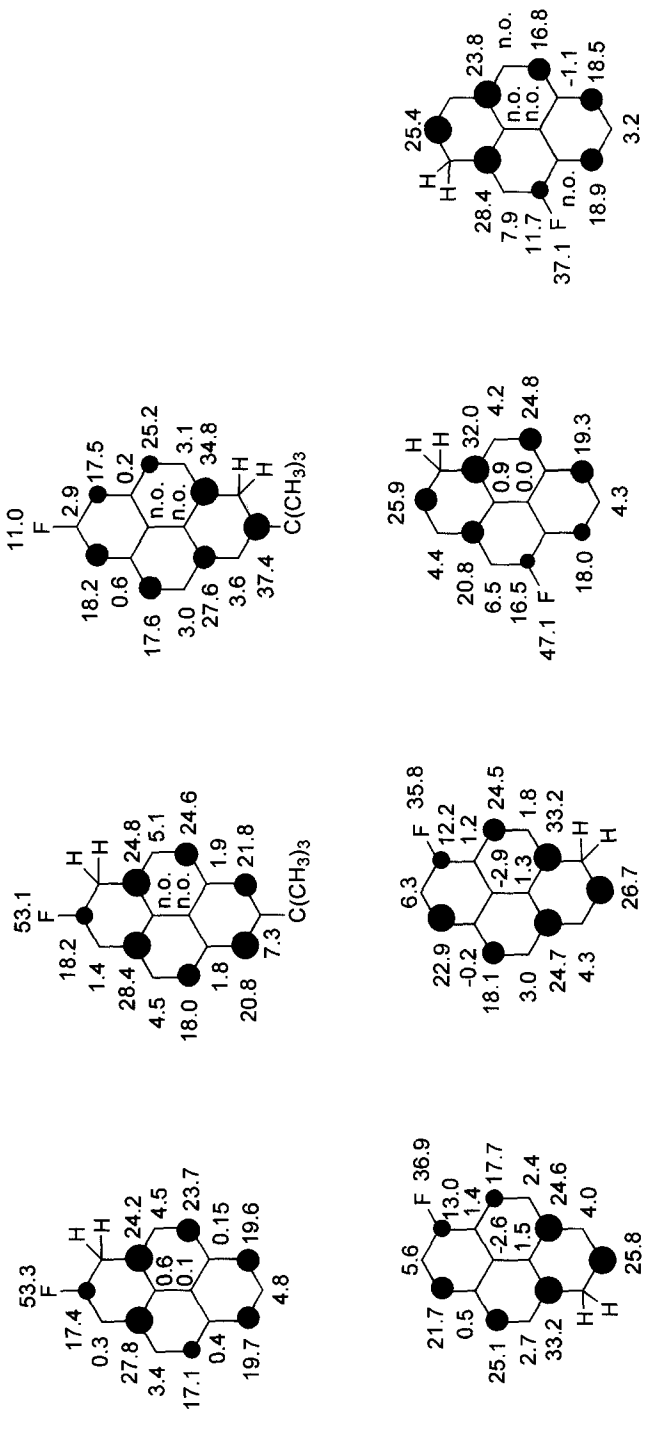

K. K. Laali, *Chem. Rev.*, 1996, **96**, 1873.
K. K. Laali and P. E. Hansen, *J. Org. Chem.*, 1993, **58**, 4096.

Fig. 24. $\Delta\delta^{13}C$ and $\Delta\delta^{19}F$ profiles in fluoropyrenium ions.

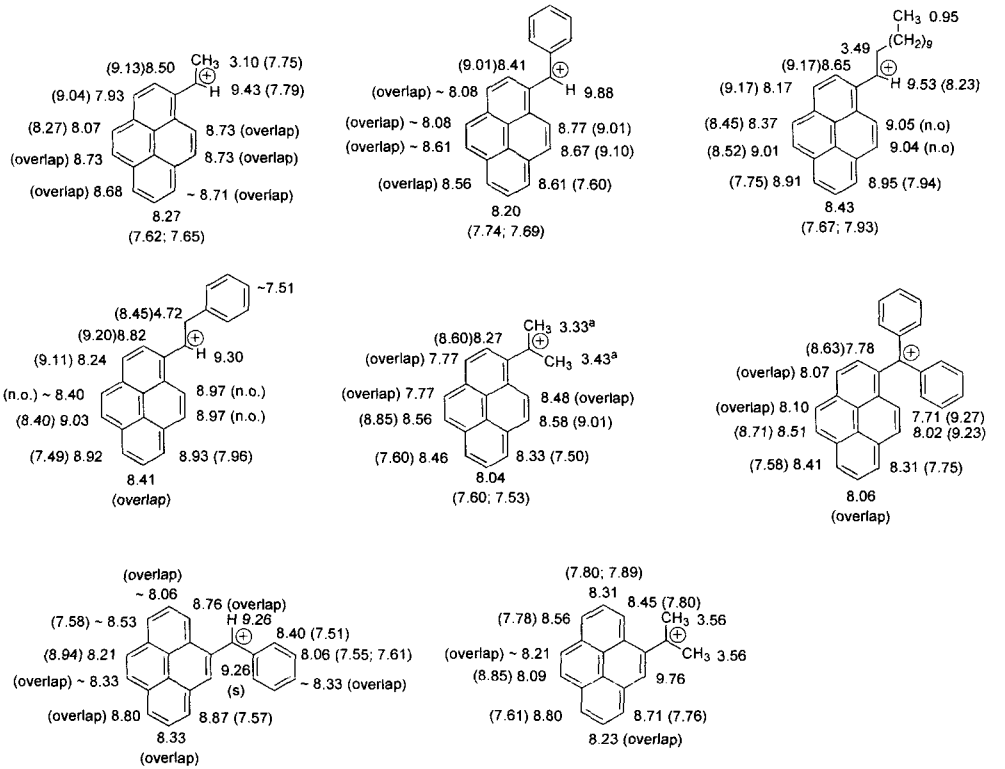

K. K. Laali and P. E. Hansen, *J. Org. Chem.*, 1997, **62**, 5804.

Fig. 25. ^{1}H NMR data for regioisomeric α-pyrene-substituted secondary and tertiary carbocations (δ^1H values for the corresponding neutral pyrenes in parentheses).

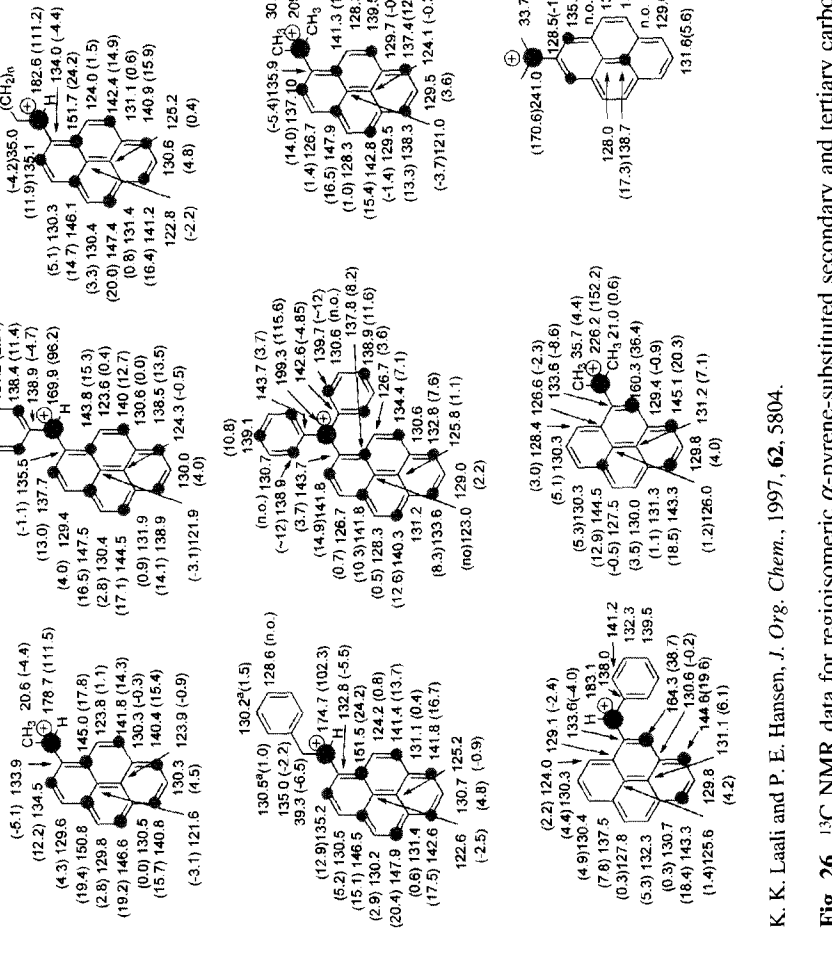

K. K. Laali and P. E. Hansen, *J. Org. Chem.*, 1997, **62**, 5804.

Fig. 26. ^{13}C NMR data for regioisomeric α-pyrene-substituted secondary and tertiary carbocations ($\Delta\delta^{13}C$ in parentheses).

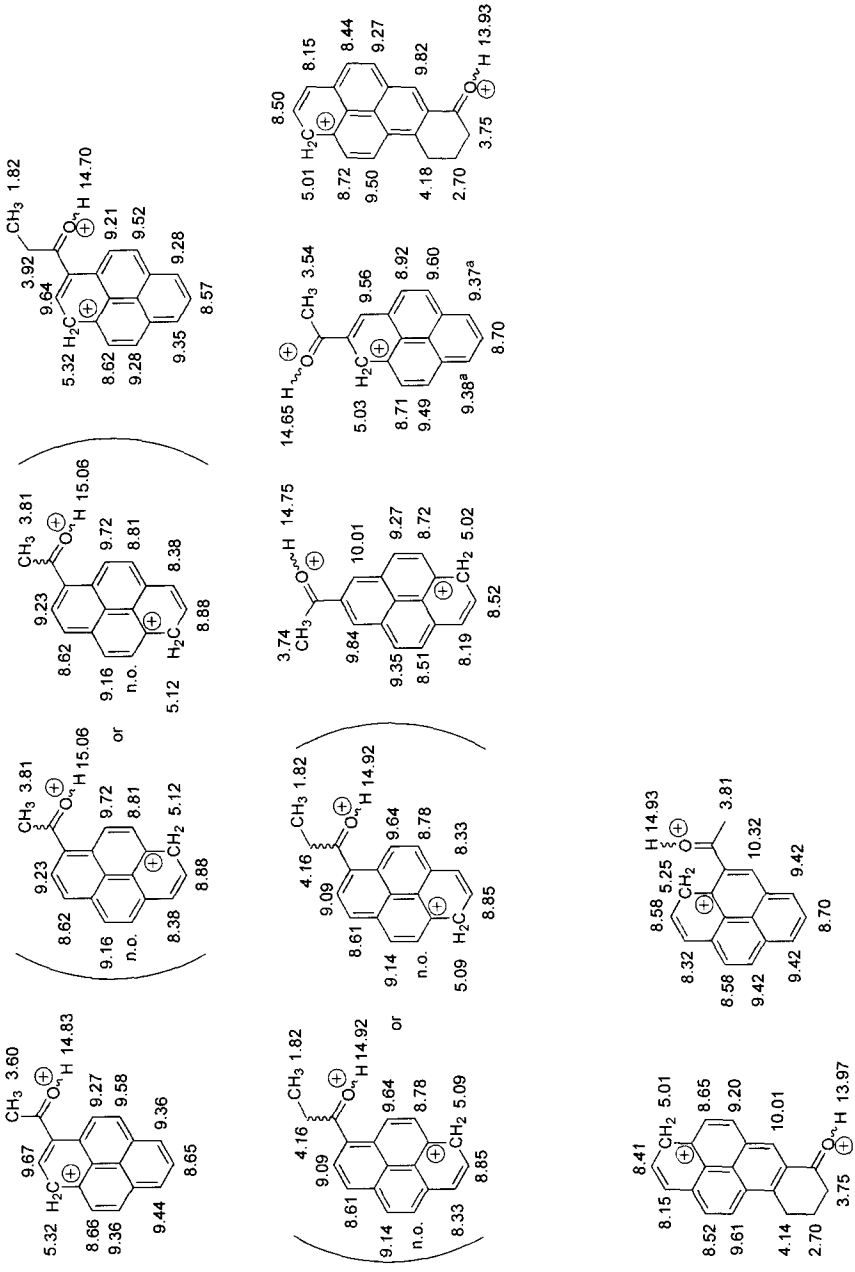

Fig. 27. ^{1}H NMR data for pyrenium–carboxonium dications.

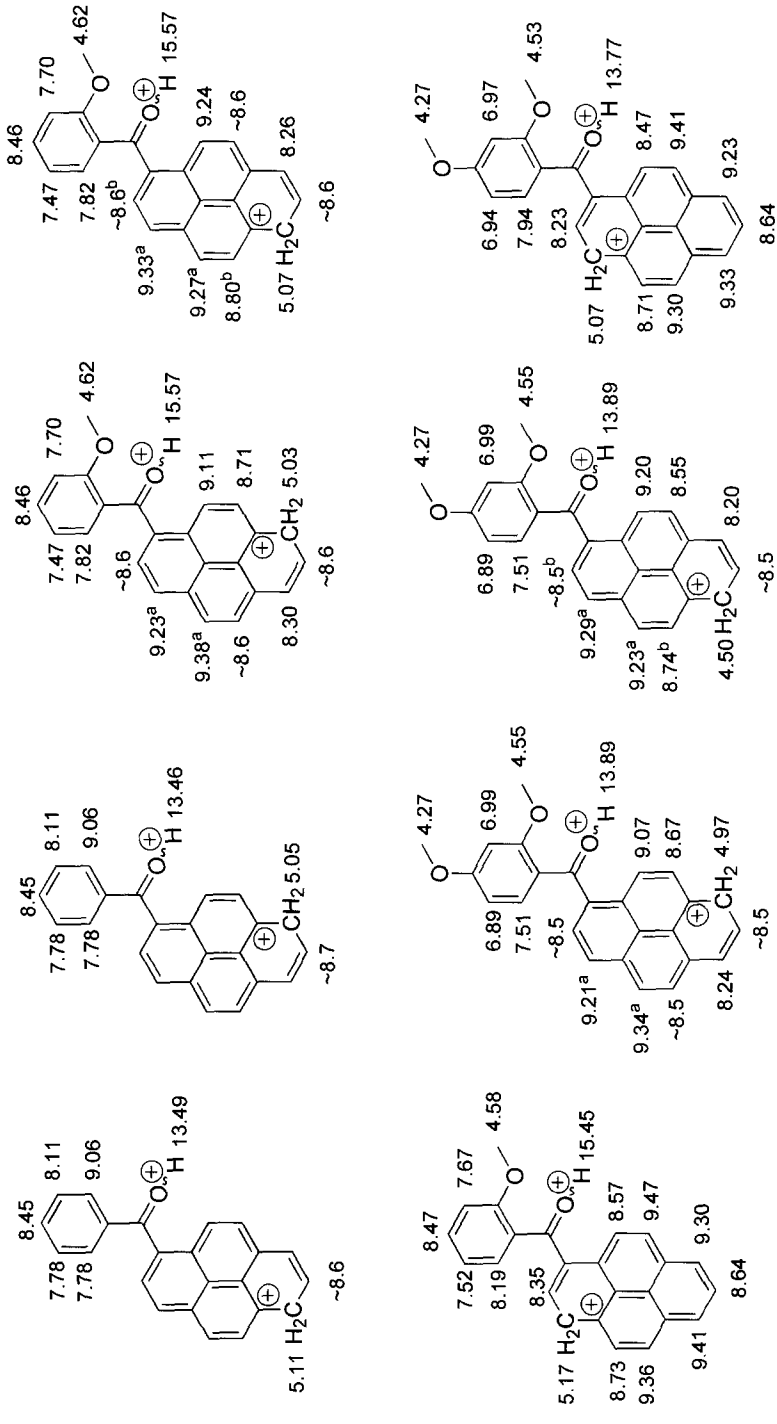

K. K. Laali, T. Okazaki and P. E. Hansen, *J. Org. Chem.*, 2000, **65**, 3816.

Fig. 27. (*continued*).

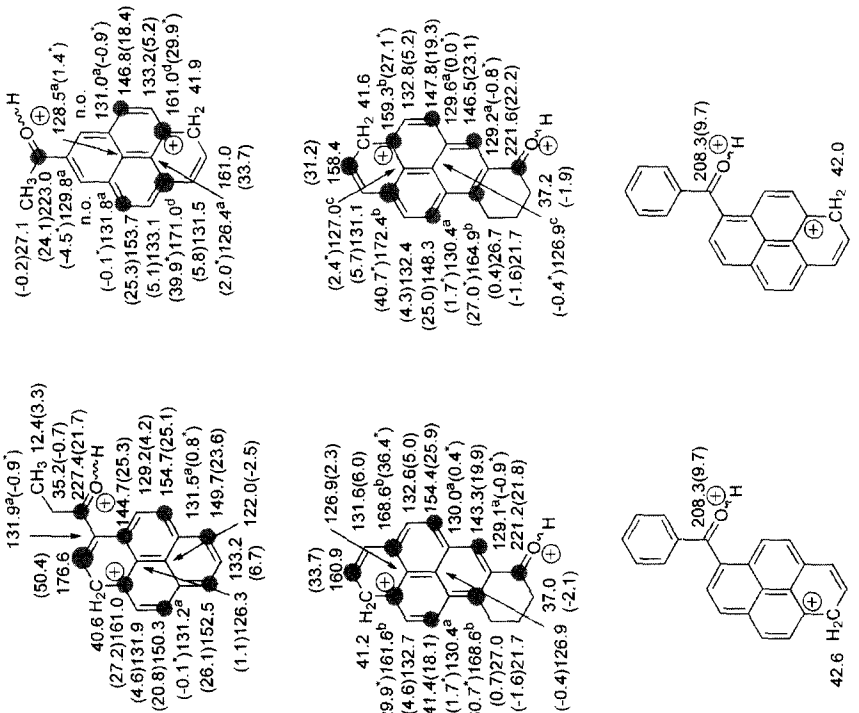

Fig. 28. ^{13}C NMR data for pyrenium–carboxonium dications ($\Delta\delta^{13}C$ in parentheses).

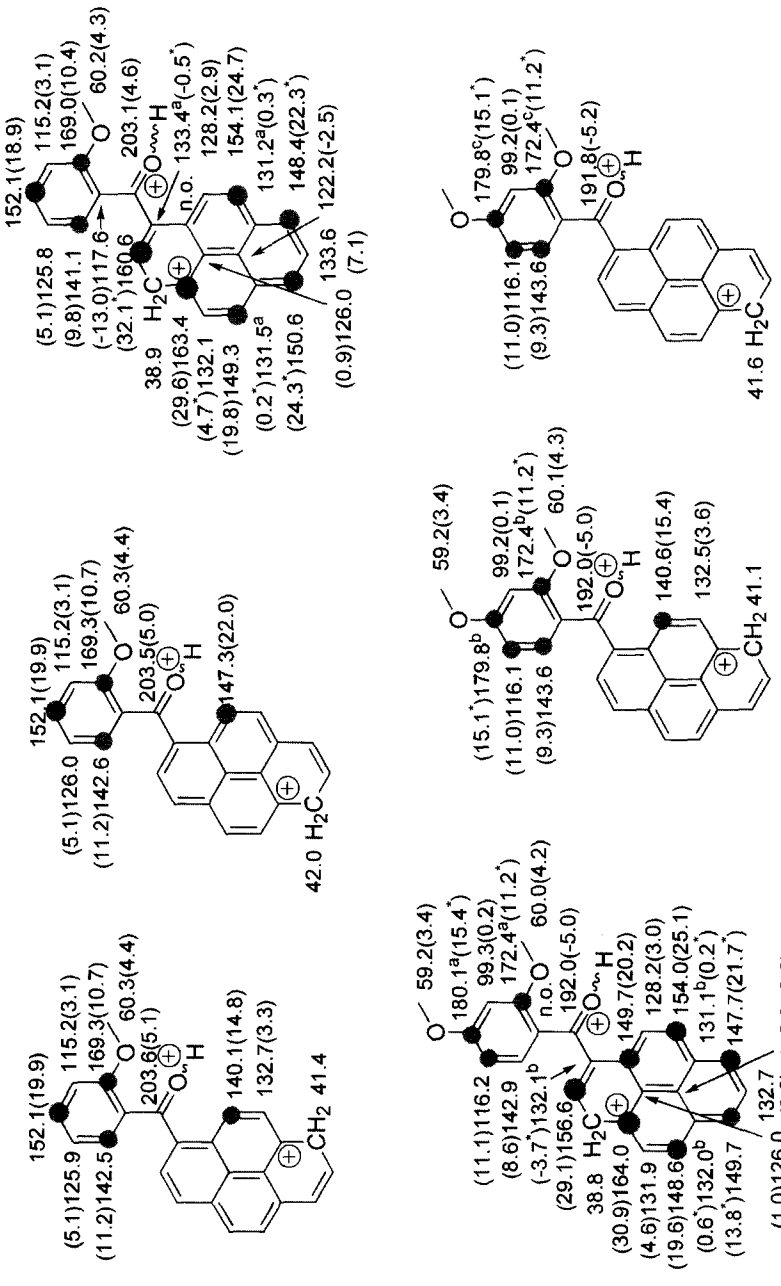

K. K. Laali, T. Okazaki and P. E. Hansen, *J. Org. Chem.*, 2000, **65**, 3816.

Fig. 28. (*continued*).

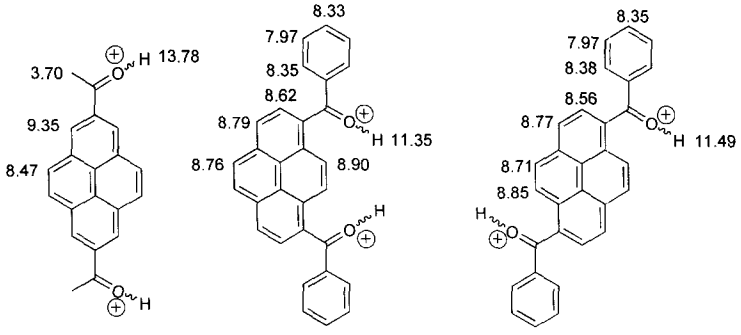

K. K. Laali, T. Okazaki and P. E. Hansen, *J. Org. Chem.*, 2000, **65**, 3816.

Fig. 29. ^{1}H NMR data for pyrene–dicarboxonium dications.

5.11. Hexahelicenium cations (Fig. 46, p. 205)

^{1}H NMR data (and partial ^{13}C NMR data) have been reported for parent hexahelicenium and its 4-methyl derivative.[36] Because of helical chirality, the methylene protons are diasterotopic.

5.12. Carbocations from nitro- and nitroso-PAHs (Figs 47–49, pp. 205–208)

Nitro-PAHs are diprotonated in superacid media and form iminium–arenium dications.[37,38] Figure 47 summarizes the available ^{1}H and ^{15}N NMR data for nitronaphthalenes and a series of sterically crowded nitropyrenes. The nitro group in iminium–pyrenium dications cyclizes on raising temperature. During this process, a methyl singlet grows in, and a new ^{15}N resonance appears. Cyclization is usually complete within minutes. An *ipso*-protonated alkylnitropyrenium cation has also been detected. Positive charge in the iminium–pyrenium dications is highly delocalized throughout the periphery. The ^{13}C data and the $\Delta\delta$ values are summarized in Fig. 48.

Nitrosopyrene and 2,7-di-*tert*-butyl-nitrosopyrene are N,O-diprotonated in superacids to form iminium–pyrenium dications.[37,38] Their NMR data including ^{15}N are gathered in Fig. 49.

5.13. Carbocations from methylene-bridged PAHs (Figs 50–52, pp. 208–211)

Recent protonation studies on methylene-bridged PAHs led to the generation and complete NMR characterization of a series of persistent carbocations.[17,33] Figure 51 summarizes the proton data for these *non-alternant* arenium ions, whereas carbon NMR data and $\Delta\delta$ values are gathered in Fig. 52. The protonation sites

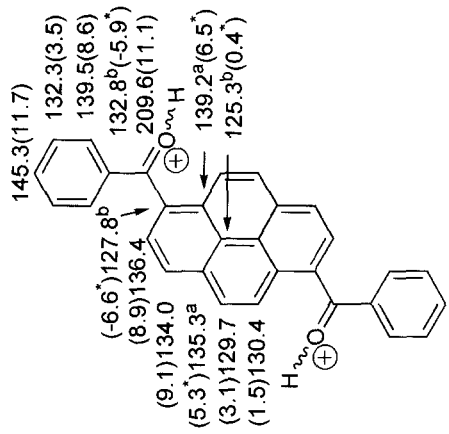

K. K. Laali, T. Okazaki and P. E. Hansen, *J. Org. Chem.*, 2000, **65**, 3816.

Fig. 30. ^{13}C NMR data for pyrene–dicarboxonium dications ($\Delta\delta^{13}C$ in parentheses).

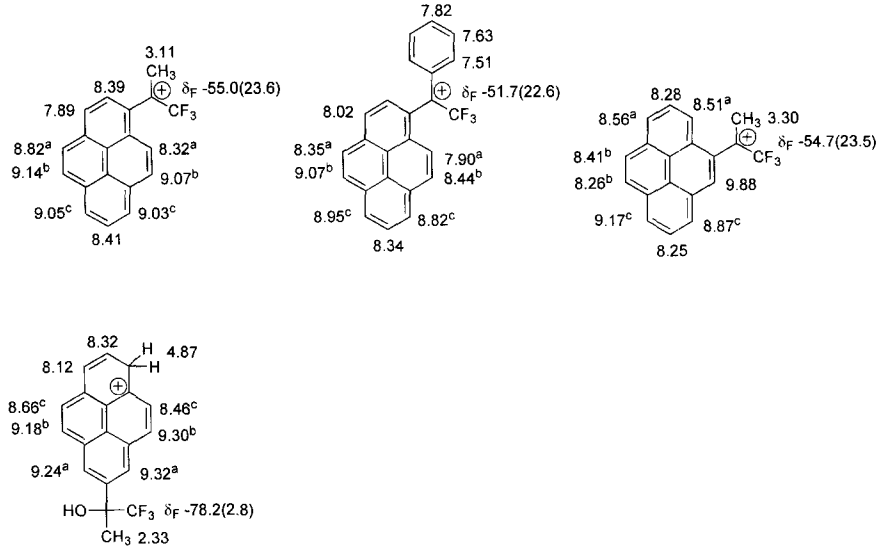

K. K. Laali, M. Tanaka, S. Hollenstein and M. Cheng, *J. Org. Chem.*, 1997, **62**, 7752.

Fig. 31. ^{1}H and ^{19}F NMR chemical shifts for pyrenyl-α-CF_3-substituted carbocations ($\Delta\delta^{19}F$ in parentheses).

are *ortho/para* to the methano bridge, except 1-methyl-4H-cyclopenta[def]phenathrene (*ortho* to methyl) and 4H-benzo[b]cyclopenta[mno]chrysene (*meso* C-6/11).

5.14. Carbocations from fluoranthene PAHs (Fig. 53, p. 212)

A limited number of persistent carbocations from fluoranthene PAHs have been generated.[39] Available NMR data are collected in Fig. 53. The site of attack is the same for parent fluoranthene and benzo[b]fluoranthene. Methoxy substitution directs the attack *ortho* to the substituent. The resulting *non-alternant* carbocations are paratropic, and most proton resonances are shielded relative to their neutral precursors. The ^{13}C NMR assignments and the derived $\Delta\delta$ values are gathered. The uniform charge alternation pattern in the carbocations derived from fluoranthene and benzo[b]fluoranthene breaks down at C-7b. The methoxy derivative exhibits limited charge delocalization.

ACKNOWLEDGEMENTS

We are grateful to the NCI of NIH (R15 CA78235-01A1 and R15 CA63595-01A1) and to NATO (CRG930113) for support of our work on PAH carbocations at Kent State.

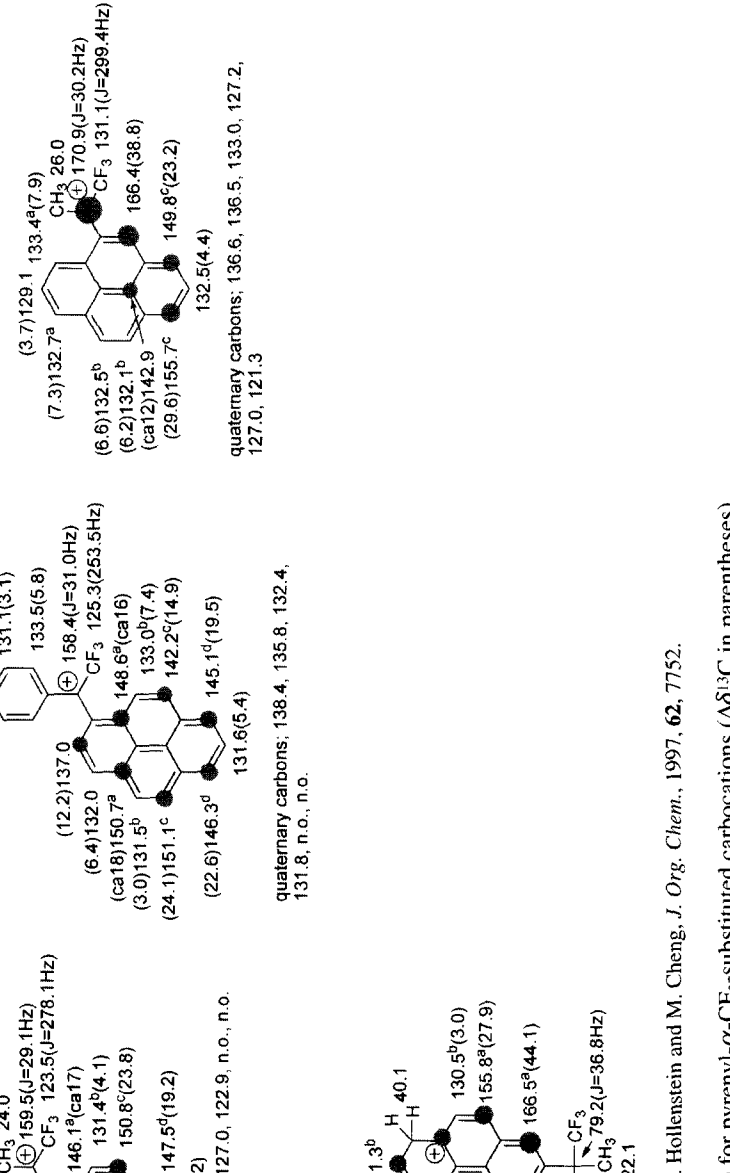

K. K. Laali, M. Tanaka, S. Hollenstein and M. Cheng, *J. Org. Chem.*, 1997, **62**, 7752.

Fig. 32. ^{13}C NMR data for pyrenyl-α-CF_3-substituted carbocations ($\Delta\delta^{13}C$ in parentheses).

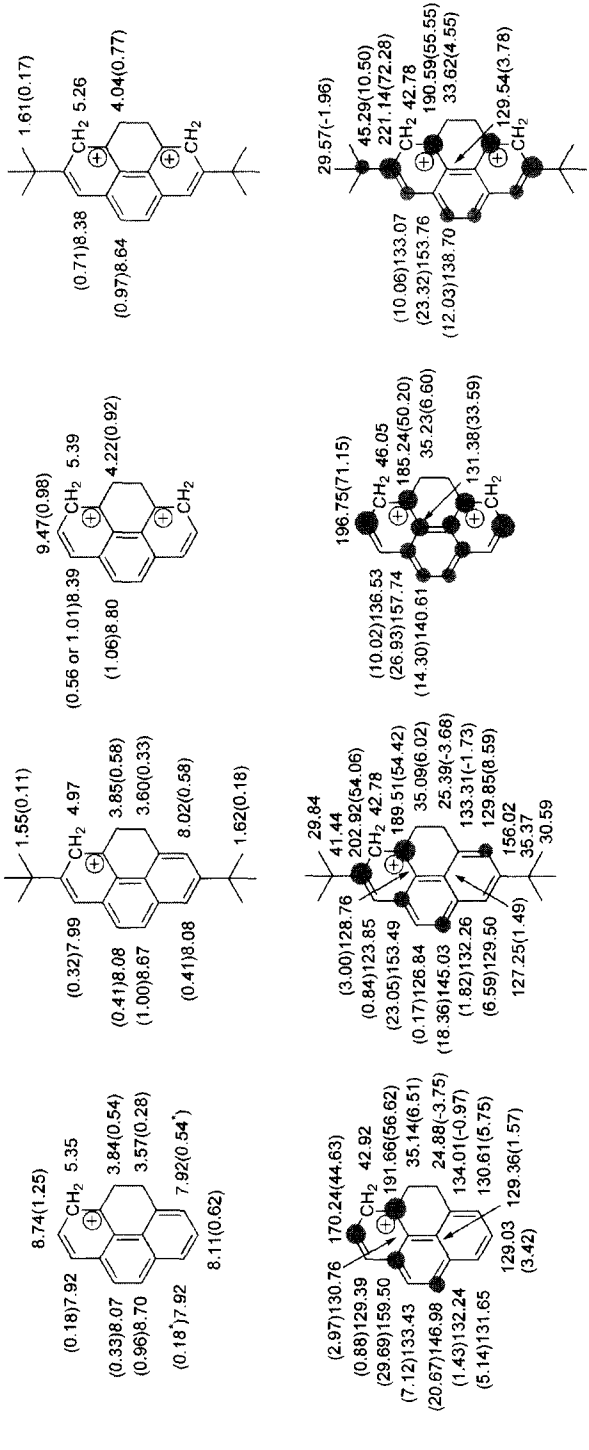

K. K. Laali, *Chem. Rev.*, 1996, **96**, 1873.
K. K. Laali and P. E. Hansen, *Res. Chem. Intermed.*, 1996, **22**, 737.

Fig. 33. ^{1}H and ^{13}C NMR chemical shifts for 4,5-dihydropyrenium mono- and dications ($\Delta\delta^{1}H$ and $\Delta\delta^{13}C$ in parentheses).

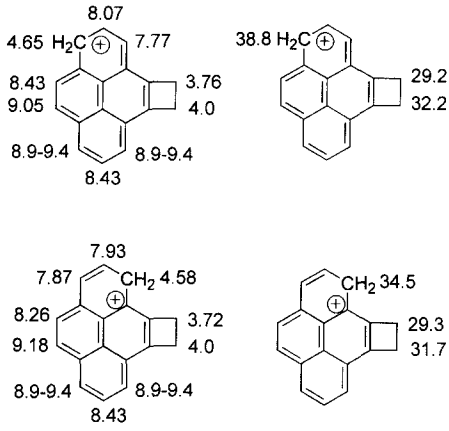

K. K. Laali, S. Hollenstein, S. E. Galembeck and J. Nishimura, *J. Chem. Soc., Perkin Trans. II*, 1999, 2129.

Fig. 34. ^{1}H and ^{13}C NMR chemical shifts for cyclobutene-fused pyrenium cations.

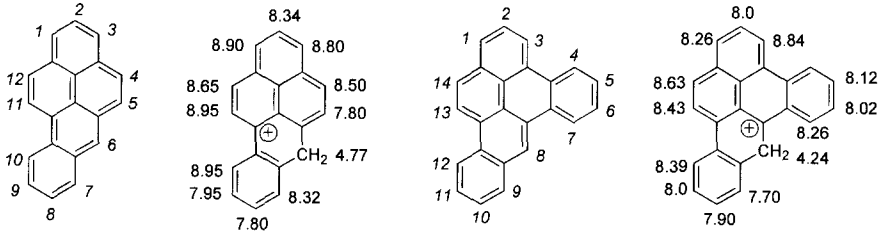

K. K. Laali, P. E. Hansen, J. J. Houser and M. Zander, *J. Chem. Soc., Perkin Trans. II*, 1995, 1781.

Fig. 35. ^{1}H NMR data for carbocations derived from benzo[a]pyrene and dibenzo[a,e]pyrene.

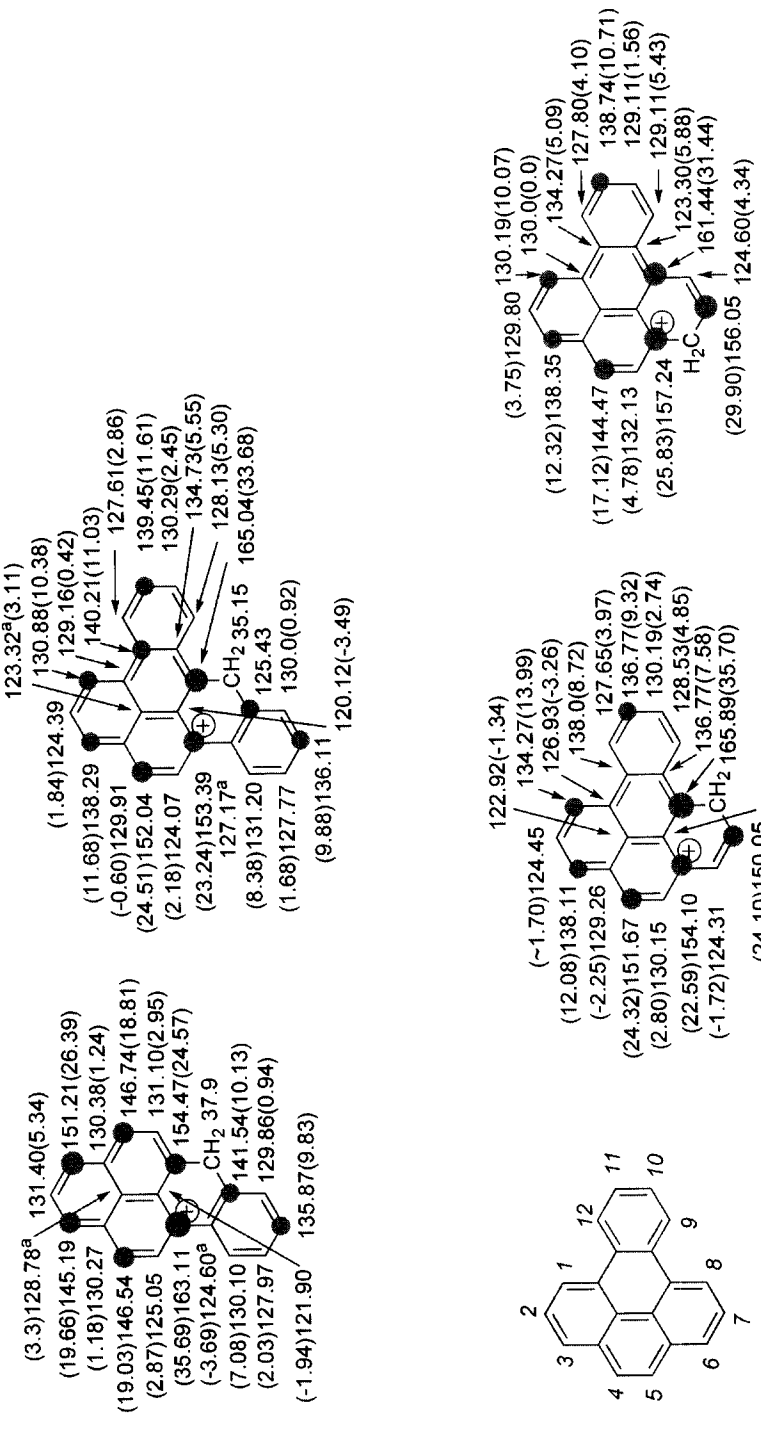

K. K. Laali, P. E. Hansen, J. J. Houser and M. Zander, *J. Chem. Soc., Perkin Trans. II*, 1995, 1781.

Fig. 36. ^{13}C NMR data for carbocations derived from benzo[a]pyrene, dibenzo[a,e]pyrene, and benzo[e]pyrene ($\Delta\delta^{13}C$ in parentheses).

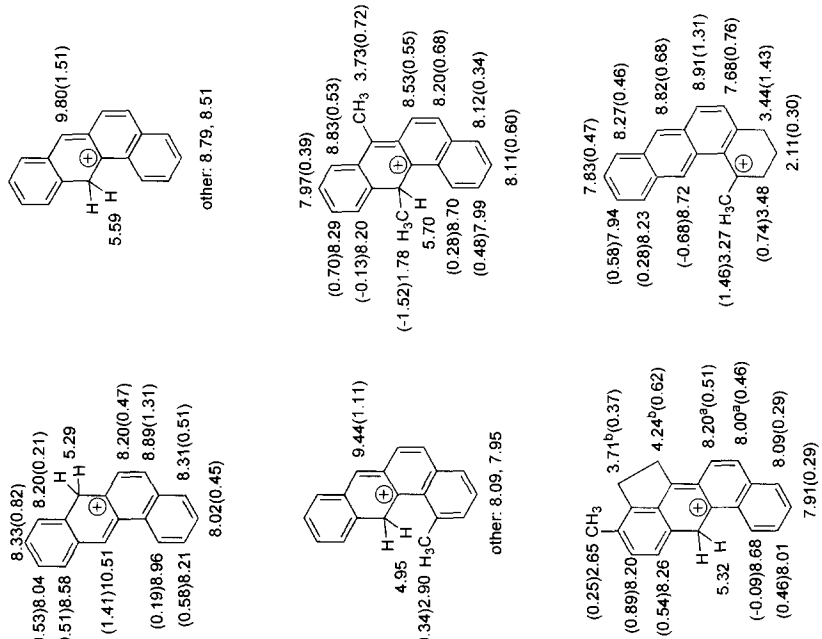

Fig. 37. ^{1}H NMR data for persistent carbocations from the benz[a]anthracene derivatives and for related α-substituted carbocations and α-carboxonium ions ($\Delta\delta^1$H in parentheses).

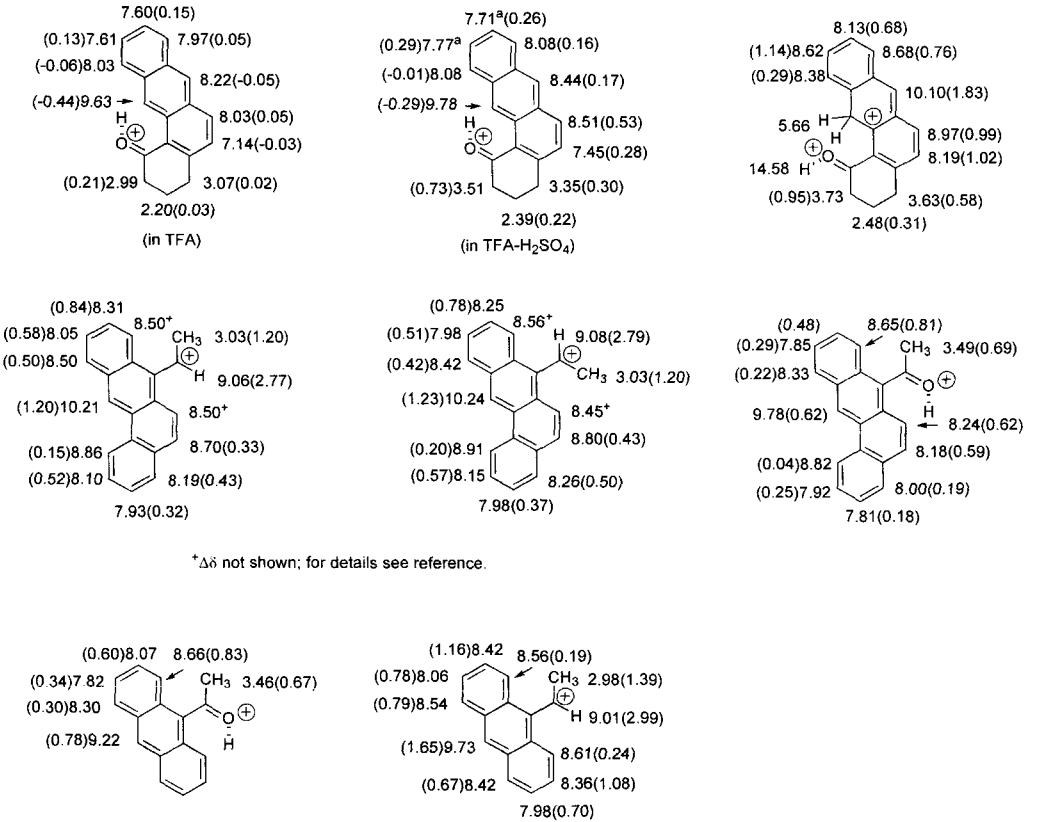

K. K. Laali and M. Tanaka, *J. Org. Chem.*, 1998, **63**, 7280.

Fig. 37. (*continued*).

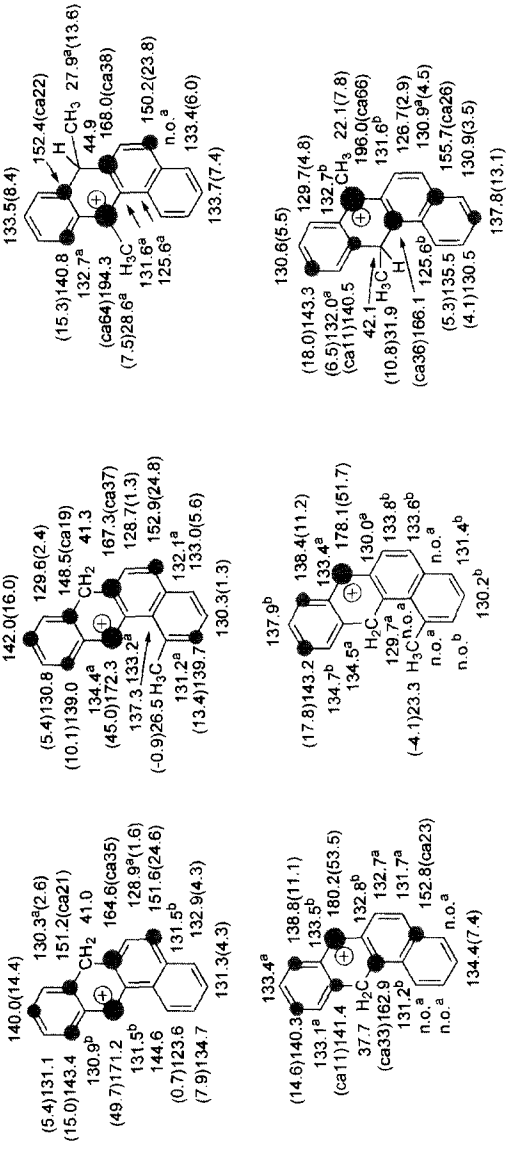

Fig. 38. ^{13}C NMR data for persistent carbocations from the benz[a]anthracene derivatives and for related α-substituted carbocations and α-carboxonium ions ($\Delta\delta^{13}C$ in parentheses).

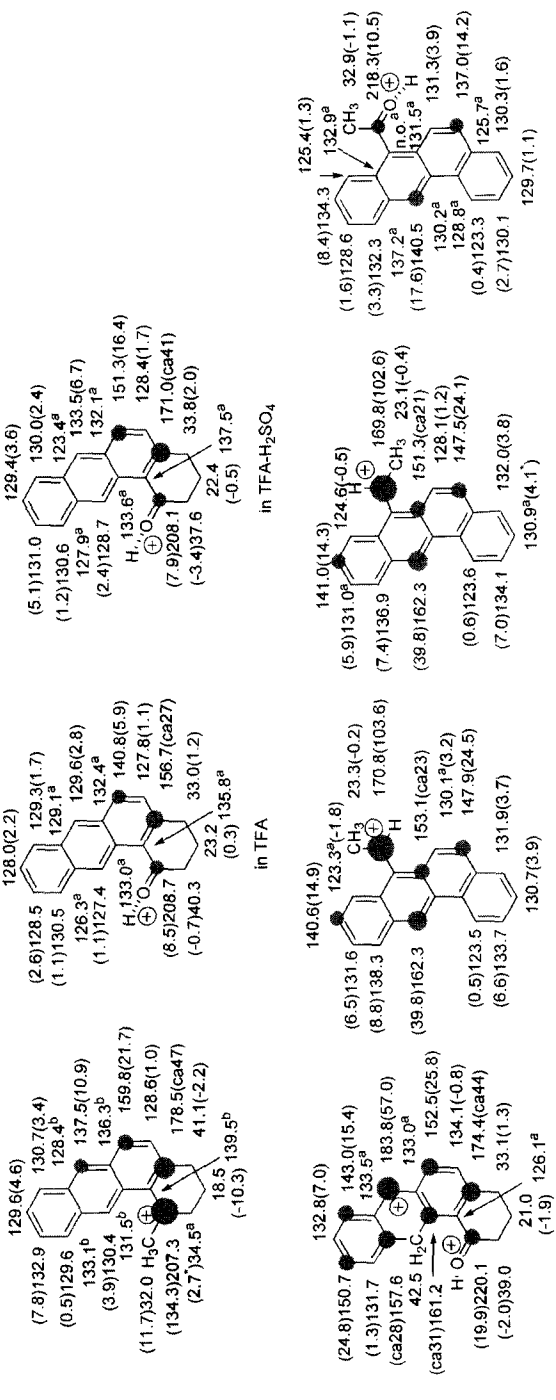

K. K. Laali and M. Tanaka, *J. Org. Chem.*, 1998, **63**, 7280.

Fig. 38. (*continued*).

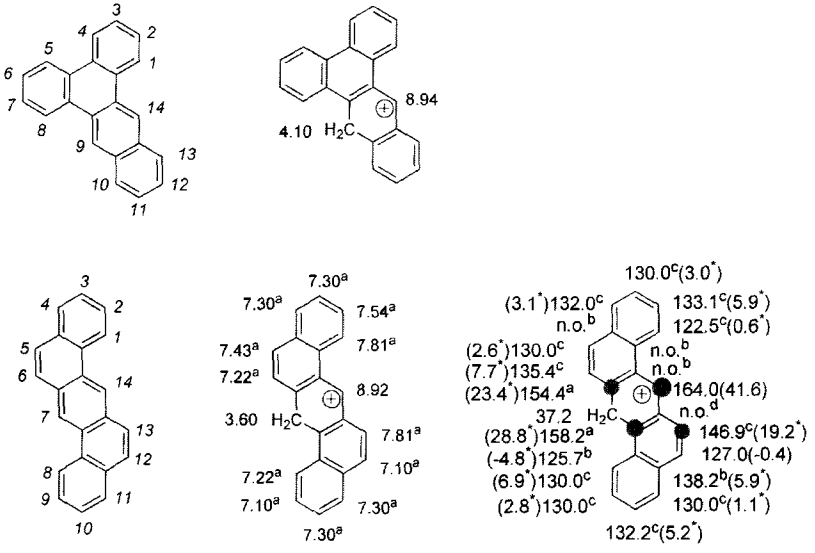

K. K. Laali, T. Okazaki and R. G. Harvey, *J. Org. Chem.*, 2001, **66**, 3977.

Fig. 39. ^{1}H and ^{13}C NMR chemical shifts for dibenzoanthracenium cations ($\Delta\delta^{13}C$ in parentheses).

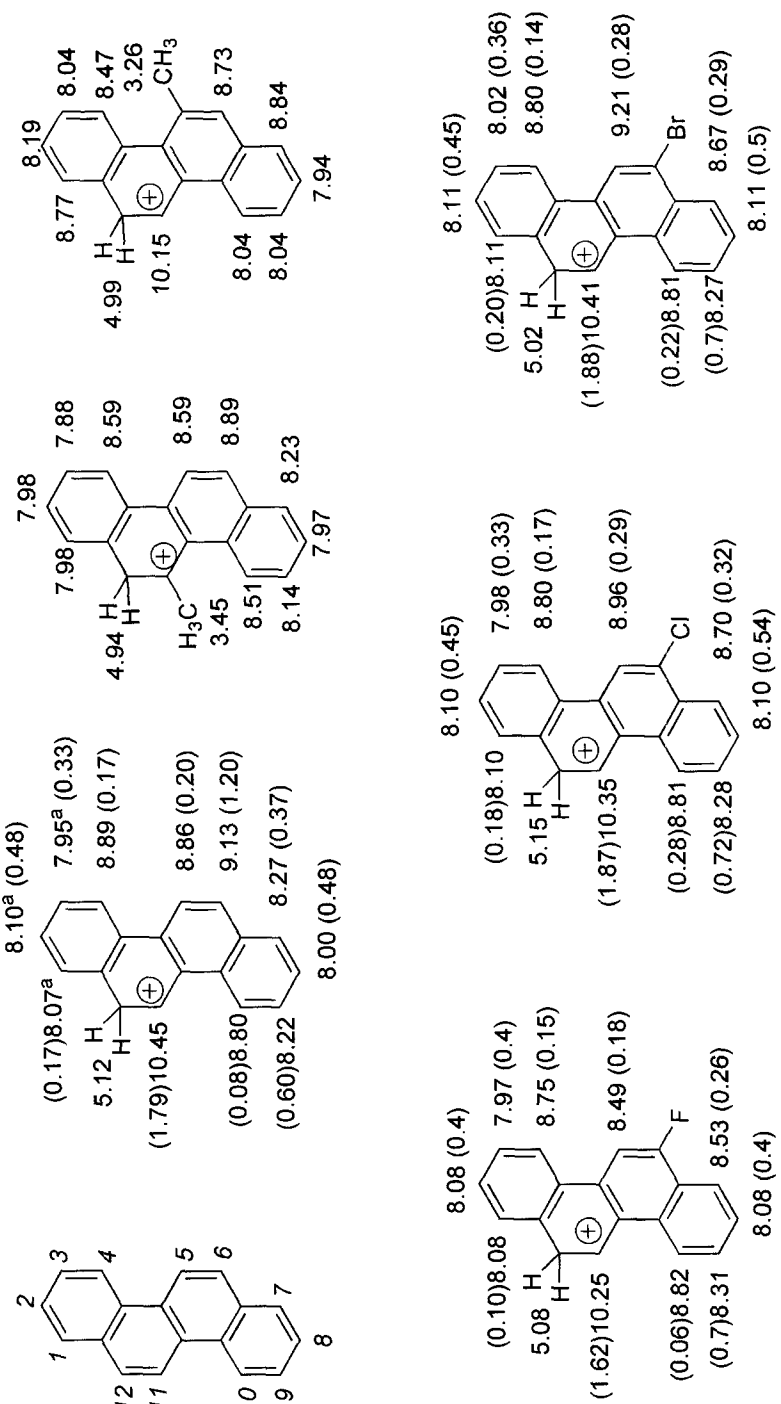

K. K. Laali, S. Hollenstein, P. E. Hansen and P. J. Harvey, *J. Org. Chem.*, 1997, **62**, 4023.

Fig. 40. ^{1}H NMR data for methyl- and 6-halo-chrysenium ions.

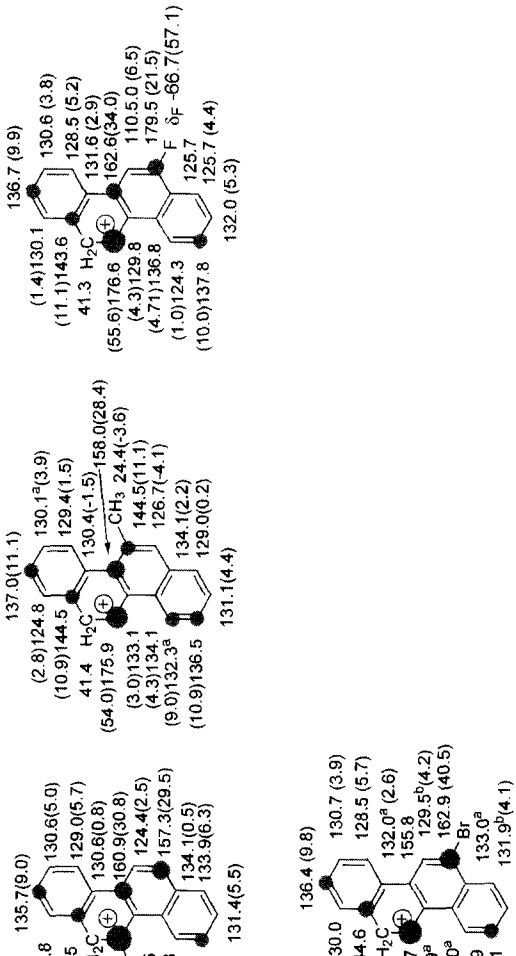

K. K. Laali, S. Hollenstein, P. E. Hansen and P. J. Harvey, *J. Org. Chem.*, 1997, **62**, 4023.

Fig. 41. ^{13}C NMR data for methyl- and 6-halo-chrysenium ions ($\Delta\delta^{13}C$ in parentheses).

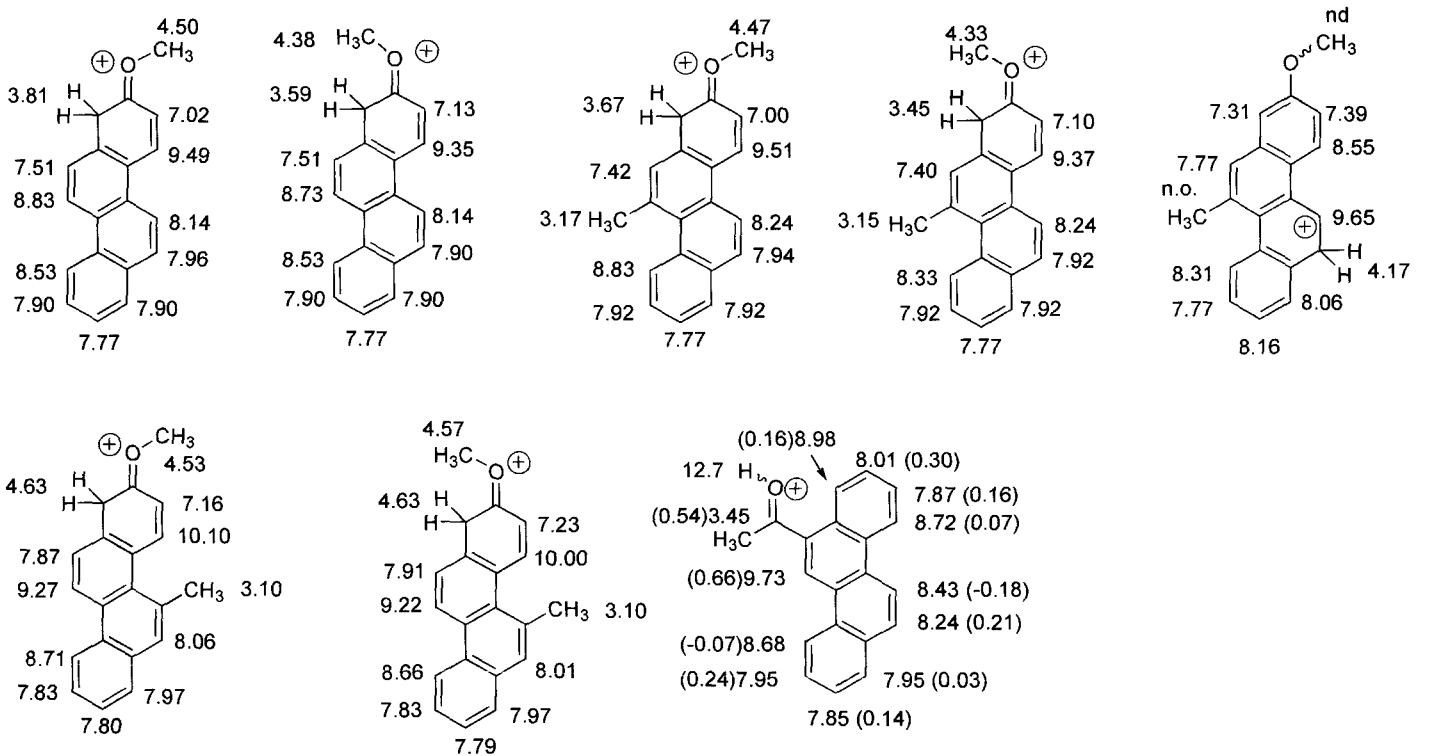

K. K. Laali, S. Hollenstein, P. E. Hansen and P. J. Harvey, *J. Org. Chem.*, 1997, **62**, 4023.
K. K. Laali, T. Okazaki, S. Kumar and S. E. Galembeck, *J. Org. Chem.*, 2001, **66**, 780.

Fig. 42. ^{1}H NMR chemical shifts for carboxonium ions from chrysene derivatives (partial $\Delta\delta^1$H in parentheses).

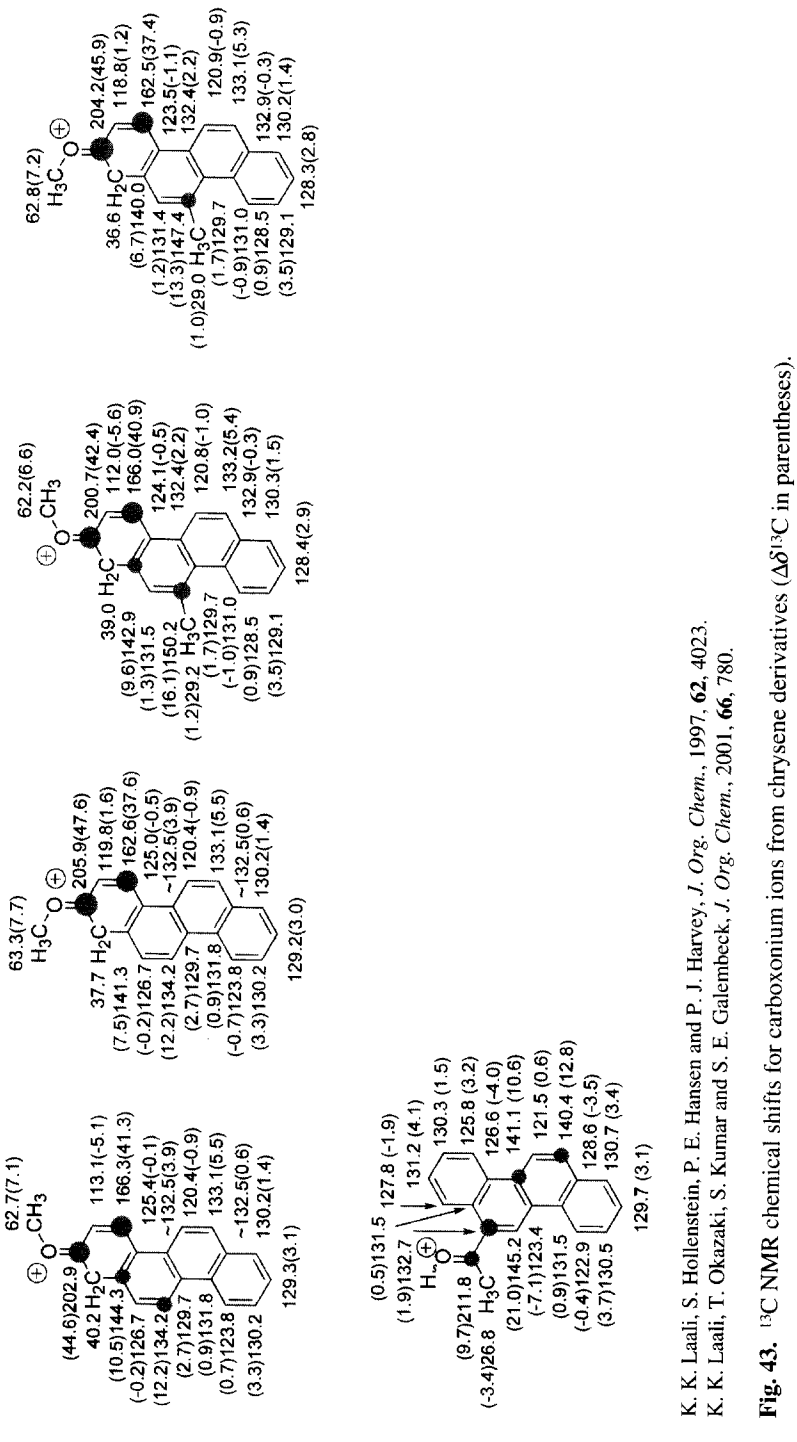

K. K. Laali, S. Hollenstein, P. E. Hansen and P. J. Harvey, *J. Org. Chem.*, 1997, **62**, 4023.
K. K. Laali, T. Okazaki, S. Kumar and S. E. Galembeck, *J. Org. Chem.*, 2001, **66**, 780.

Fig. 43. ^{13}C NMR chemical shifts for carboxonium ions from chrysene derivatives ($\Delta\delta^{13}C$ in parentheses).

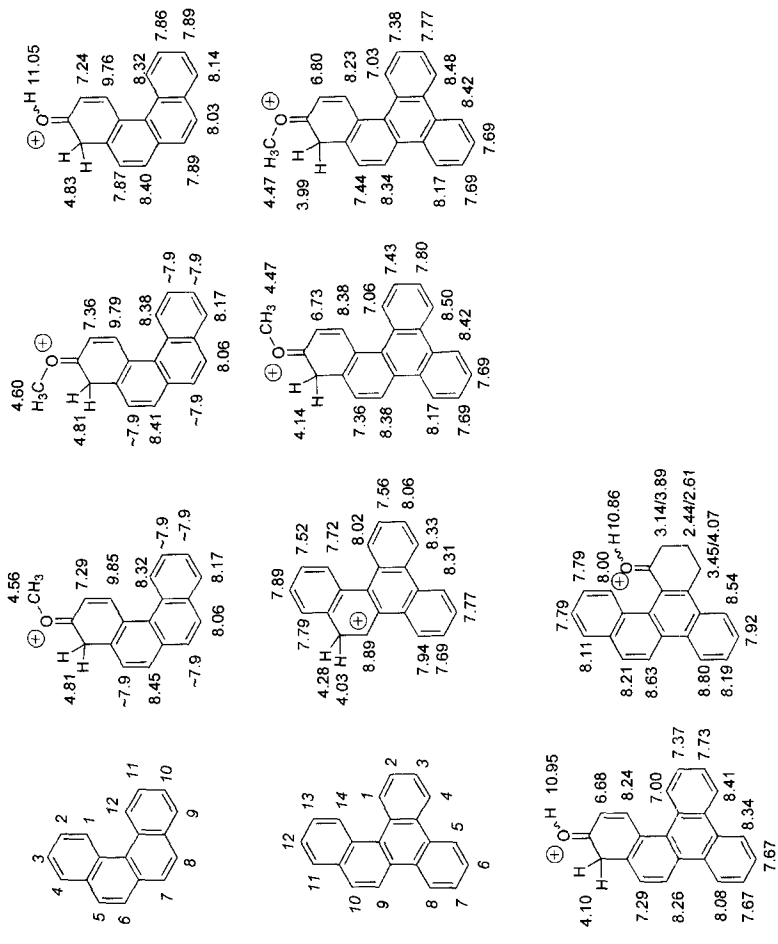

K. K. Laali, T. Okazaki, S. Kumar and S. E. Galembeck, *J. Org. Chem.*, 2001, **66**, 780.

Fig. 44. ^{1}H NMR data for benzo[c]phenanthrenium ions, benzo[g]chrysenium ions, and related carboxonium ions.

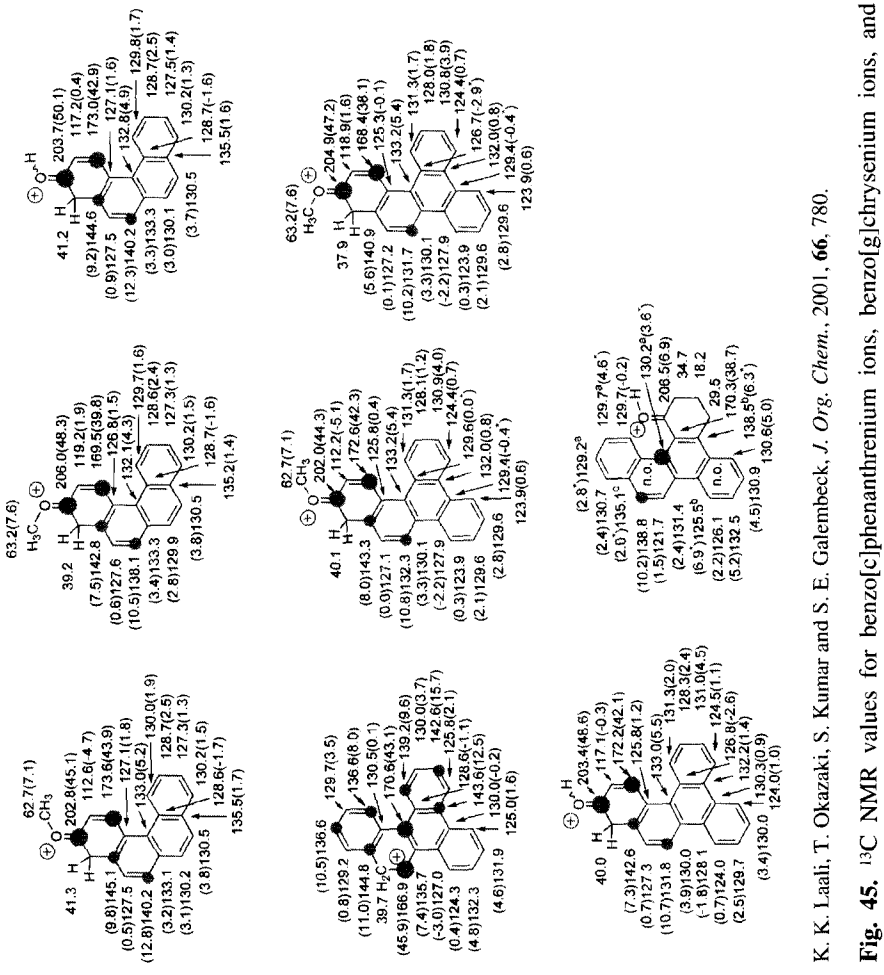

K. K. Laali, T. Okazaki, S. Kumar and S. E. Galembeck, *J. Org. Chem.*, 2001, **66**, 780.

Fig. 45. ^{13}C NMR values for benzo[c]phenanthrenium ions, benzo[g]chrysenium ions, and related carboxonium ions ($\Delta\delta^{13}C$ in parentheses).

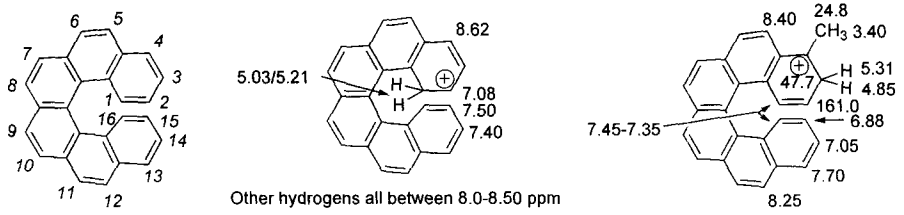

K. K. Laali, *Chem. Rev.*, 1996, **96**, 1873.
K. K. Laali and J. J. Houser, *J. Chem. Soc., Perkin Trans. II*, 1994, 1303.

Fig. 46. Protonation of [6]helicene.

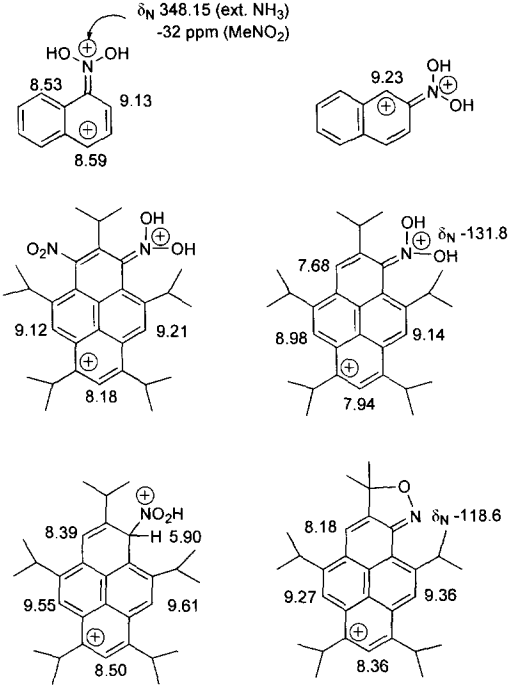

T. Ohta, K. Shudo and T. Okamoto, *Tetrahedron Lett.*, 1984, **25**, 325.
K. K. Laali, S. Bolvig and P. E. Hansen, *J. Chem. Soc., Perkin Trans. II*, 1995, 537.
K. K. Laali, *Chem. Rev.*, 1996, **96**, 1873.
K. K. Laali, *Coordination Chem. Rev.*, 2000, **210**, 47.

Fig. 47. ^{1}H and ^{15}N NMR data for iminium–arenium dications from nitronaphthalene and several nitro- and dinitropyrenes including their nitro-cyclized arenium ions.

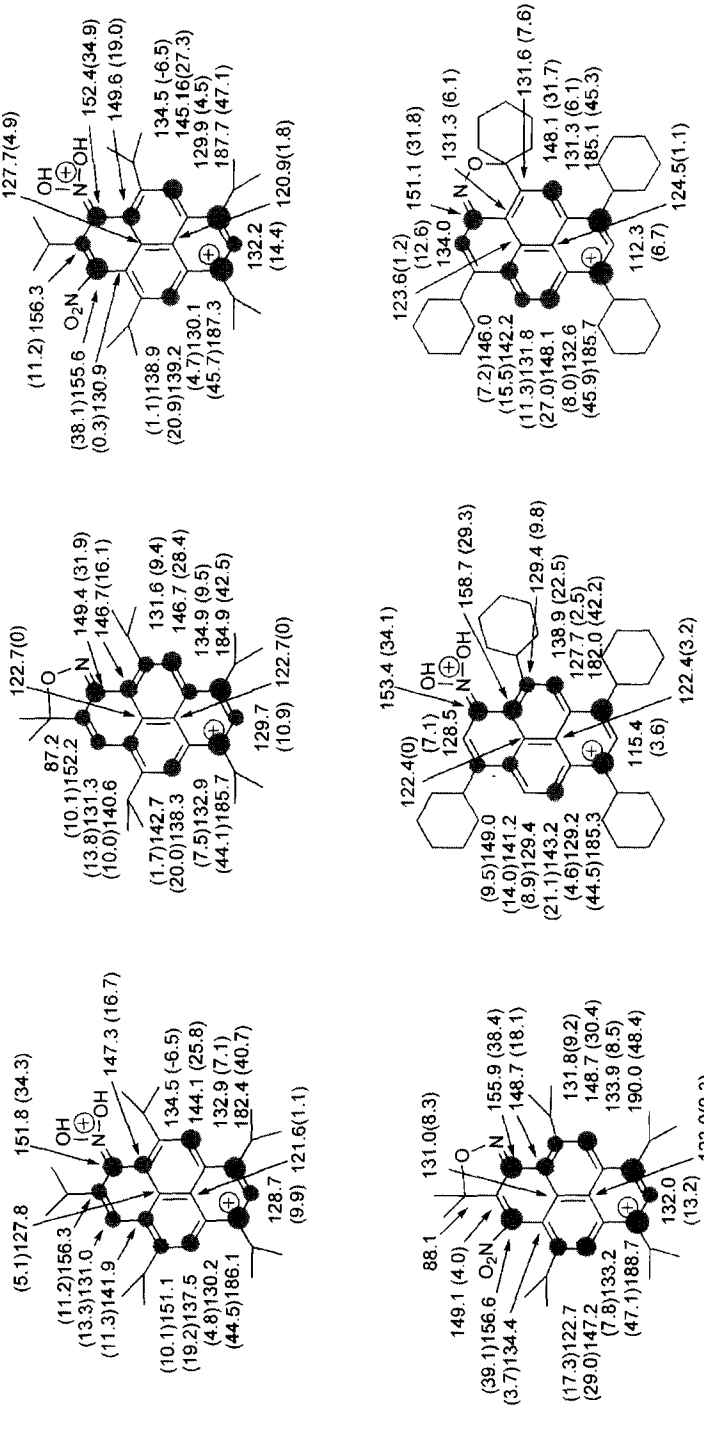

Fig. 48. ^{13}C NMR data for iminium–arenium dications and their nitro-cyclized arenium ions for a series of nitro- and dinitropyrenes ($\Delta\delta^{13}C$ in parentheses).

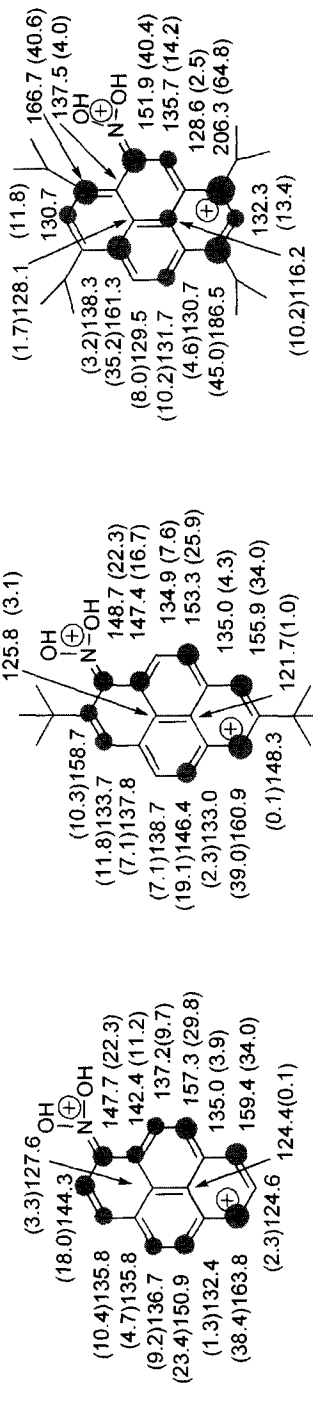

K. K. Laali, *Chem. Rev.*, 1996, **96**, 1873.
K. K. Laali, S. Bolvig and P. E. Hansen, *J. Chem. Soc., Perkin Trans. II*, 1995, 537.
K. K. Laali, *Coordination Chem. Rev.*, 2000, **210**, 47.

Fig. 48. (*continued*).

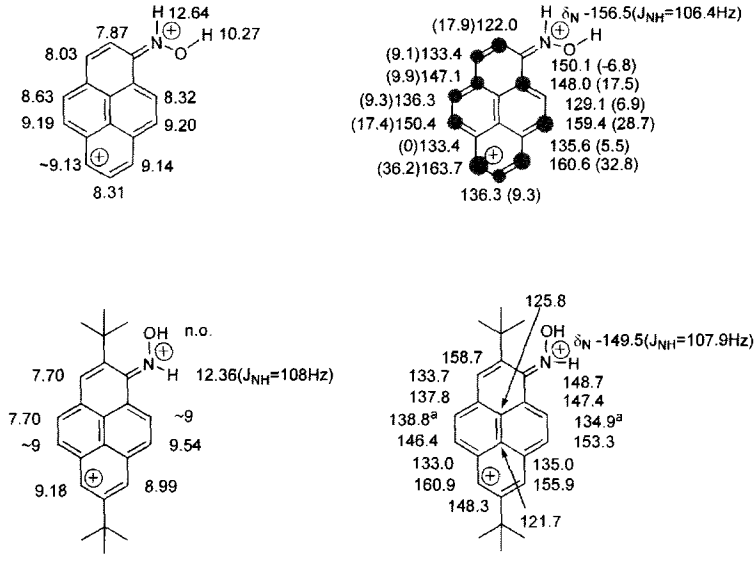

K. K. Laali, *Chem. Rev.*, 1996, **96**, 1873.
K. K. Laali, S. Bolvig and P. E. Hansen, *J. Chem. Soc., Perkin Trans. II*, 1995, 537.
K. K. Laali, *Coordination Chem. Rev.*, 2000, **210**, 47.

Fig. 49. ^{1}H, ^{13}C, and ^{15}N NMR data for iminium–pyrenium dication from nitrosopyrenes ($\Delta\delta^{13}$C in parentheses).

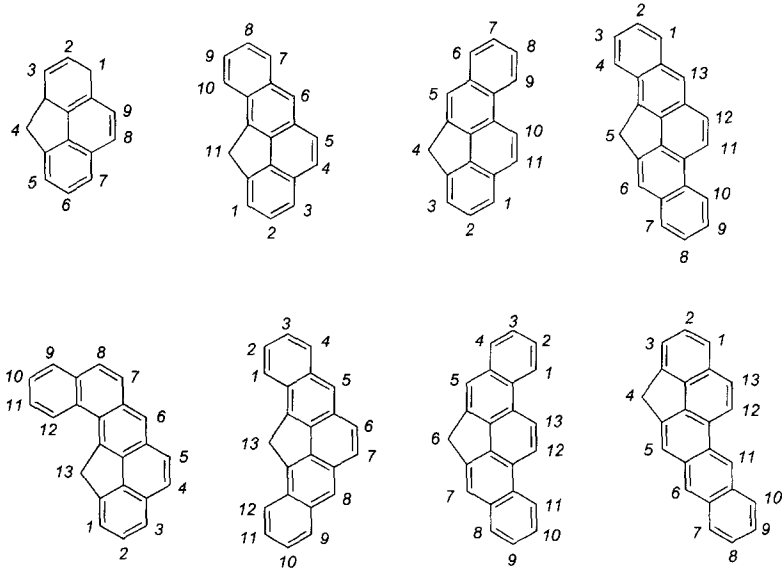

Fig. 50. Numbering of methylene-bridged *non-alternant* polyaromatic hydrocarbon ring systems.

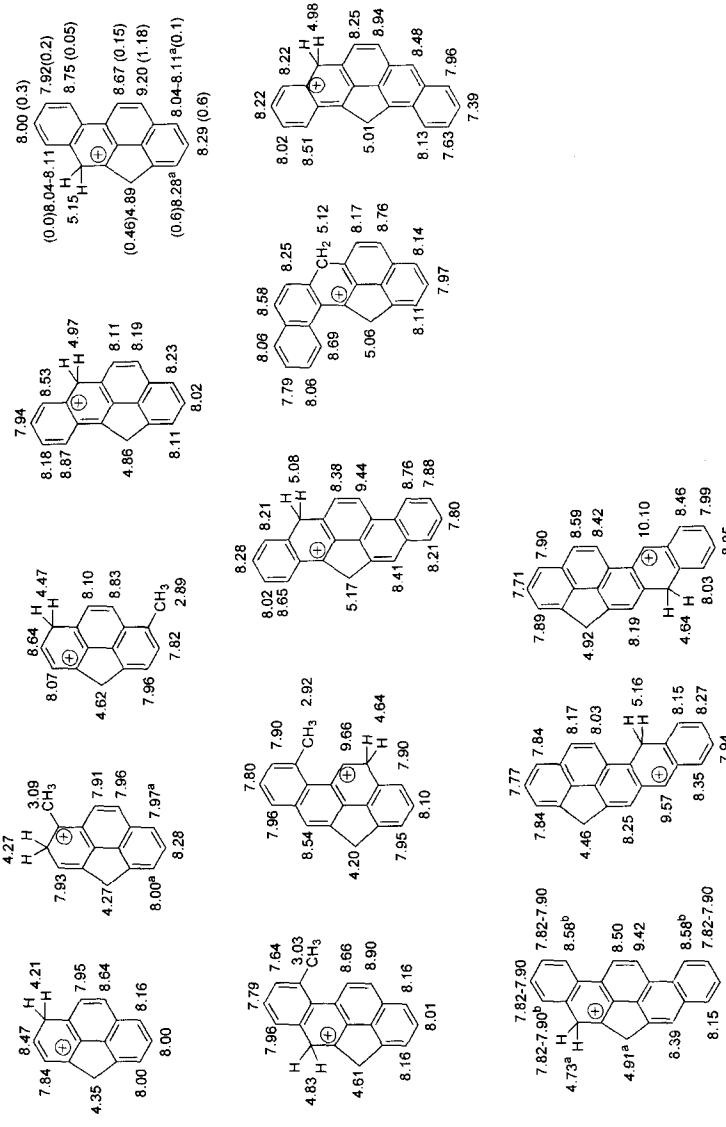

K. K. Laali, S. Hollenstein and P. E. Hansen, *J. Chem. Soc., Perkin Trans. II*, 1997, 2207.
K. K. Laali, T. Okazaki and R. G. Harvey, *J. Org. Chem.*, 2001, **66**, 3977.

Fig. 51. Compilation of ^{1}H NMR data for arenium ions from methylene-bridged *non-alternant* polyaromatic hydrocarbons (partial $\Delta\delta^1$H values in parentheses).

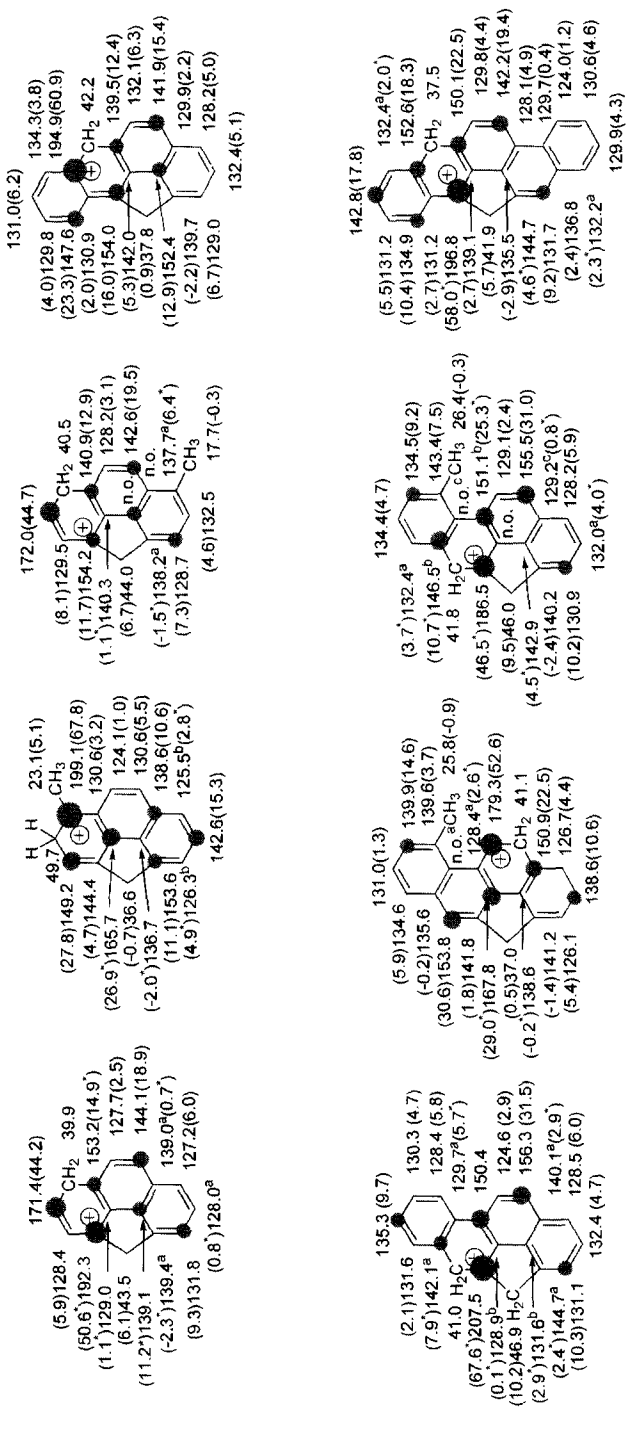

Fig. 52. Compilation of ^{13}C NMR chemical shifts for arenium ions from methylene-bridged *non-alternant* polyaromatic hydrocarbons ($\Delta\delta^{13}C$ values in parentheses).

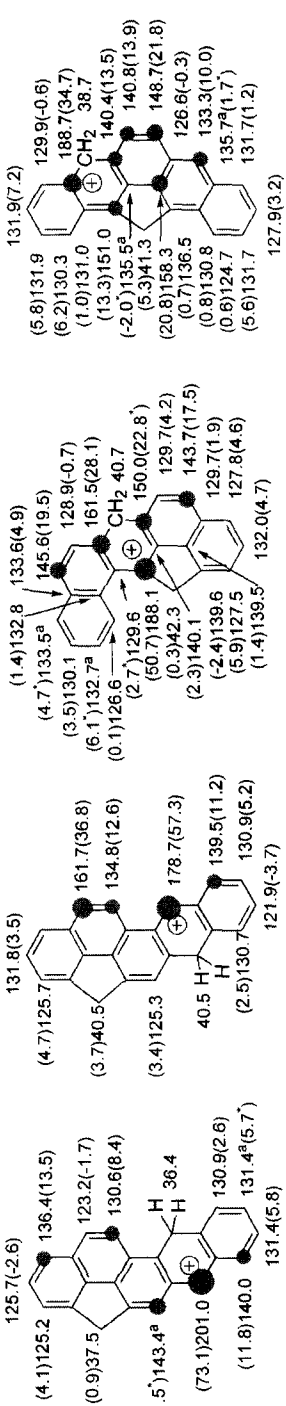

K. K. Laali, S. Hollenstein and P. E. Hansen, *J. Chem. Soc., Perkin Trans. II*, 1997, 2207.
K. K. Laali, T. Okazaki and R. G. Harvey, *J. Org. Chem.*, 2001, **66**, 3977.

Fig. 52. (*continued*).

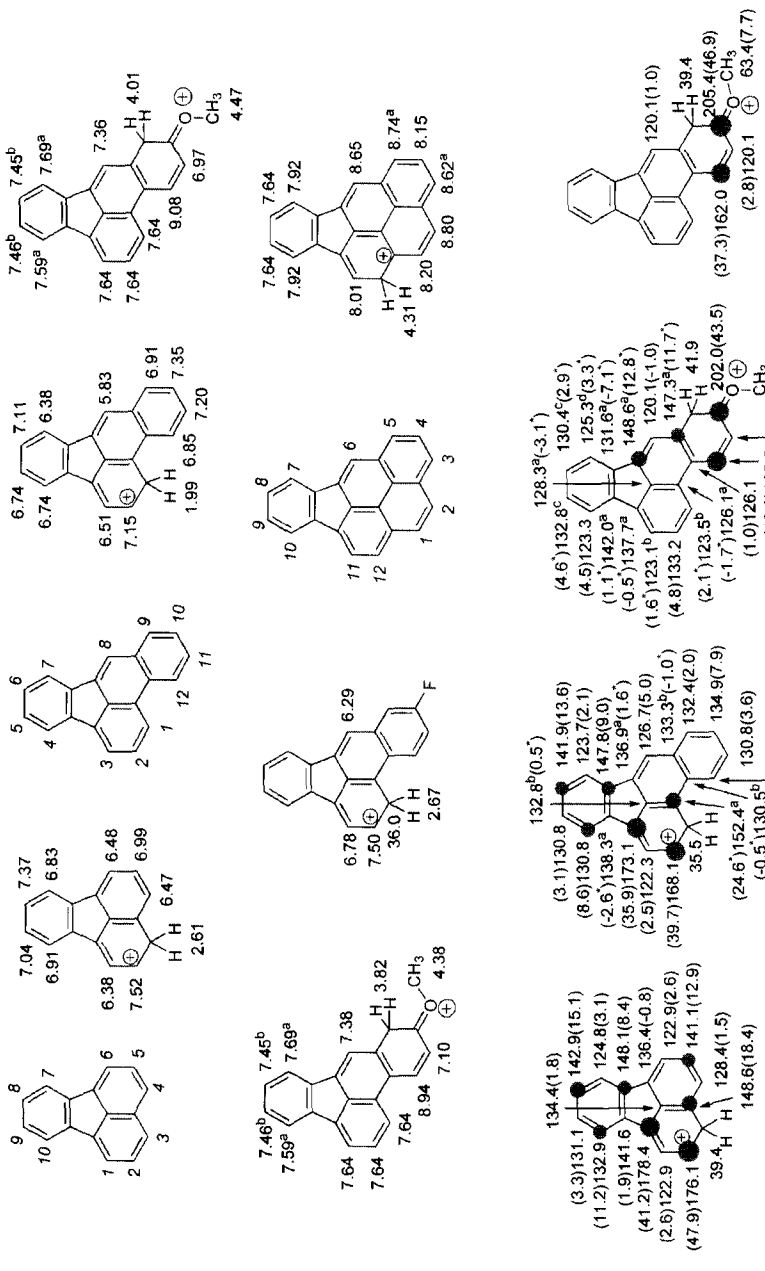

K. K. Laali, T. Okazaki and S. E. Galembeck, *J. Chem. Soc., Perkin Trans. II*, 2002, 621.

Fig. 53. ^{1}H and ^{13}C NMR data for arenium ions from fluoranthene PAHs ($\Delta\delta^{1}$H/$\Delta\delta^{13}$C values in parentheses).

REFERENCES

1. G. A. Olah, *J. Org. Chem.*, 2001, **66**, 5943.
2. G. A. Olah, *Angew. Chem. Int. Edn Engl.*, 1995, **34**, 1393.
3. G. A. Olah, in *Stable Carbocation Chemistry*, (eds G. K. S. Prakash and P. v. R. Schleyer), Wiley, New York, 1997, Ch. 1.
4. Leading Monographs/Reviews: G. A. Olah, G. K. S. Prakash and J. Sommer, *Superacids*, Wiley, New York, 1985; G. A. Olah, K. K. Laali, Q. Wang and G. K. S. Prakash, *Onium Ions*, Wiley, New York, 1998; G. A. Olah, in *Cage Hydrocarbons*, (ed. G. A. Olah), Wiley, New York, 1990; G. K. S. Prakash and P. v. R. Schleyer, *Stable Carbocation Chemistry*, Wiley, New York, 1997; G. A. Olah, V. P. Reddy and G. K. S. Prakash, *Chem. Rev.*, 1992, **92**, 69; M. Saunders and H. A. Jimenez-Vazquez, *Chem. Rev.*, 1991, **91**, 375.
5. K. K. Laali, *Chem. Rev.*, 1996, **96**, 1873.
6. Monograph: R. G. Harvey, *Polycyclic Aromatic Hydrocarbons Chemistry and Carcinogenicity*, Cambridge University Press, Cambridge, 1991.
7. Review: R. G. Harvey and N. E. Geacintov, *Acc. Chem. Res.*, 1988, **21**, 66.
8. Significant Kinetic/Solvolytic/Product Studies: (a) N. T. Nashed, A. Bax, R. J. Loncharich, J. M. Sayer and D. M. Gerina, *J. Am. Chem. Soc.*, 1993, **115**, 1711; (b) N. T. Nashed, J. M. Sayer and D. M. Gerina, *J. Am. Chem. Soc.*, 1993, **115**, 1723; (c) N. T. Nashed, S. K. Balani, R. J. Loncharich, J. M. Sayer, D. Y. Shipley, R. S. Mohan, L. Whalen and D. M. Gerina, *J. Am. Chem. Soc.*, 1991, **113**, 3910.
9. DNA Acidity: G. Lamm and G. R. Pack, *Proc. Natl Acad. Sci. USA*, 1990, **87**, 9033.
10. Representative Computational Studies: (a) G. L. Borosky, *J. Org. Chem.*, 1999, **64**, 7738; (b) J. R. Rabinowitz and S. B. Little, *Chem. Res. Toxicol.*, 1992, **5**, 286; (c) J. P. Lowe and B. D. Silverman, *Acc. Chem. Res.* 1984, **17**, 332; (d) A. F. Lehner, J. Horn and J. W. Flescher, *Theochem.*, 1996, **366**, 203; (e) S. M. Adams and L. S. Kaminsky, *Mol. Pharmacol.*, 1982, **22**, 459; (f) M. T. Poulsen and G. H. Loew, *Cancer. Biochem. Biophys.*, 1981, **5**, 81.
11. G. A. Olah and D. J. Donovan, *J. Am. Chem. Soc.*, 1978, **100**, 5163.
12. G. A. Olah, G. D. Mateescu and Y. K. Mo, *J. Am. Chem. Soc.*, 1973, **95**, 1865.
13. K. Lammertsma and H. Cerfontain, *J. Am. Chem. Soc.*, 1979, **101**, 3618.
14. K. Lammertsma, *J. Am. Chem. Soc.*, 1981, **103**, 2062.
15. F. van de Griendt and H. Cerfontain, *Tetrahedron*, 1979, **34**, 2563.
16. K. K. Laali and H. Cerfontain, *J. Org. Chem.*, 1983, **48**, 1092.
17. K. K. Laali, S. Hollenstein and P. E. Hansen, *J. Chem. Soc., Perkin Trans. II*, 1997, 2207.
18. G. I. Borodkin, M. M. Shakirov and V. G. Shubin, *J. Org. Chem. USSR*, 1990, **26**, 2254.
19. K. K. Laali and S. Hollenstein, *J. Chem. Soc., Perkin Trans. II*, 1998, 897.
20. S. Hollenstein and K. K. Laali, *Chem. Commun.*, 1997, 2145.
21. K. K. Laali, S. Hollenstein, S. E. Galembeck and M. M. Coombs, *J. Chem. Soc., Perkin Trans. II*, 2000, 211.
22. K. K. Laali, T. Okazaki and M. M. Coombs, *J. Org. Chem.*, 2000, **65**, 7399.
23. K. K. Laali and P. E. Hansen, *J. Org. Chem.*, 1991, **56**, 6795.
24. K. K. Laali and P. E. Hansen, *J. Chem. Soc., Perkin Trans. II*, 1994, 2249.
25. K. K. Laali and P. E. Hansen, *Res. Chem. Intermed.*, 1996, **22**, 737.
26. K. K. Laali and P. E. Hansen, *J. Org. Chem.*, 1993, **58**, 4096.
27. K. K. Laali and P. E. Hansen, *J. Org. Chem.*, 1997, **62**, 5804.
28. K. K. Laali, T. Okazaki and P. E. Hansen, *J. Org. Chem.*, 2000, **65**, 3816.
29. K. K. Laali, M. Tanaka, S. Hollenstein and M. Cheng, *J. Org. Chem.*, 1997, **62**, 7752.
30. K. K. Laali, S. Hollenstein, S. E. Galembeck and J. Nishimura, *J. Chem. Soc., Perkin Trans. II*, 1999, 2129.
31. K. K. Laali, P. E. Hansen, J. J. Houser and M. Zander, *J. Chem. Soc., Perkin Trans. II*, 1995, 1781.
32. K. K. Laali and M. Tanaka, *J. Org. Chem.*, 1998, **63**, 7280.
33. K. K. Laali, T. Okazaki and R. G. Harvey, *J. Org. Chem.*, 2001, **66**, 3977.

34. K. K. Laali, S. Hollenstein, P. E. Hansen and P. J. Harvey, *J. Org. Chem.*, 1997, **62**, 4023.
35. K. K. Laali, T. Okazaki, S. Kumar and S. E. Galembeck, *J. Org. Chem.*, 2001, **66**, 780.
36. K. K. Laali and J. J. Houser, *J. Chem. Soc., Perkin Trans. II*, 1994, 1303.
37. K. K. Laali, S. Bolvig and P. E. Hansen, *J. Chem. Soc., Perkin Trans. II*, 1995, 537.
38. K. K. Laali, *Coordination Chem. Rev.*, 2000, **210**, 47.
39. K. K. Laali, T. Okazaki and S. E. Galembeck, *J. Chem. Soc., Perkin Trans. II*, 2002, 621.

Index

Note – Page numbers in *italic* type refer to figures and tables.

Acetylcholine receptor (AchR), 100
Acetylphenanthrenes, 156, *162*
Ala 126 residue, 91, *92*
Alkyl(cycloalkyl)pyrenium ions, *172*, *173*, *175*, *176*
  charge delocalization mode, 159, *177*
  sulfinylated, *174*, *175*
1-alkynyllead compounds, *6*
Allium, 120
Alpha-dextrins, 118
α-helical axis, orientation of, 96–9
Alpha-lactoalbumin, 116
Amino acid residues, notation for, 40
Amylopectin, 117, 118
Amylose, 111, 112, 117, 118
Anions, 16–17
Anthracenium ions, 152, *156*
Apple, 112
Apple juices, 123
Arenium ions, 187, *209*, *210–11*
Arg 82 residue, 91, *92*
ArPbPbAR, 11
Asp 85 residue, 47, 85, 90, 91
Asp 96 residue, 48, 90–2
Atomic force microscopy (AFM), 45–7, 76
Avocados, 130

Bacillas brevis, 99
Bacterio-opsin (bO), 67, 68, *69*, 84, 86
Bacteriorhodopsin (bR), 44–8
  3D structure of, 45, *45*
  assignment of ^{13}C NMR peaks, 52–63
    regiospecific, 51–6
    site-directed mutagenesis, 59–63
  [1-^{13}C]Ala-labeled, 52, 53, *54*
    D85N mutant, 70, *70*, 71, *71*
    W12L mutant, 71–2
    W80L mutant, 71–2
  [1-^{13}C]Ala 14-labeled, 87, 88, *89*
  [1,2,3-$^{13}C_3$]Ala-labeled, 51, *51*
  [2-^{13}C]Ala-labeled, 52, 53–55, *54*
  [3-^{13}C]Ala-labeled, 49, *49*, 52, 53, *82*
    A160G mutant, 79, 84
    Ala 14 signals, 66
    Ala 39 signals, 84, 86, 87
    Ala 51 signals, 60, 84
    Ala 53 signals, 59, 60, 66, 84
    Ala 81 signals, 60–1, *61*
    Ala 84 signals, 60, 66
    Ala 103 signals, 77, 84
    Ala 126 signals, 59, *60*, 61
    Ala 139 signals, 66
    Ala 160 signals, 77, 84, 87
    Ala 184 signals, 60, 66
    Ala 196 signals, 59, *60*, 61–3, *62*, 84, 90
    Ala 215 signals, 60, *61*, 84
    Ala 228 signals, 63, 66
    Ala 233 signals, 63, 66
    Ala 245–248 signals, 63
    assigned signals, *64*
    C-2 fragment, 86, *87*
    D85N mutant, 61, *62*, 84, 92
    D85N/D96N mutant, 92
    D85N/R82Q mutant, 91, *91*
    R82Q mutant, 91
    temperature-dependent change in, 80, *80*
  [1-^{13}C]Pro-labeled, 56
  [1-^{13}C]Val-labeled, 55, *55*, 59, *85*
    assigned signals, *64*
    D85N mutant, 70, *70*, 85, *85*
    D85N/D96N mutant, 85, *85*
    D85N/V49A mutant, 86
    Val 34 signals, 56
    Val 49 signals, 56, 59, 85–6
    Val 69 signals, 55, *55*, 56, 63
    Val 101 signals, 56
    Val 130 signals, 56
    Val 199 signals, 55, *55*, 59, 90
    Val 213 signals, *55*, 85, *85*
  dynamics-dependent suppression of ^{13}C NMR peaks, 67–72, 101
  dynamics of, 79–81, 83–6
  hydration behavior of, 81–6, *82*
  as ideal model system, 43–4, 101
  proton translocation of, 83
  secondary structure of, 45, *46*

Bacteriorhodopsin (bR) – *continued*
surface structure of, 76–8, 81
transmembrane peptides as a component of, 86–90
Barley, 114, 115, *131*
Beef, 129
Beef gravy, 127
Beer, 135, *136*
Benzaldehyde, 123
Benzanthracenium cations, 175, *194–5*, *196–7*
Benzo[b]fluoranthene, 189
Benzo[c]phenanthrenium cations, 177, *203*, *204*
Benzo[g]chrysenium cations, 177, *203*, *204*
Benzopyrenium cations, 175, *192*, *193*
Bicelle, 96
Biopolymers, 113–21
Bis(amino)plumbylenes, *8*, 11, 12
Bis(pentamethylcyclopentadienyl)metallo-cenes, 13
Bitters, aromatic, 127
Black beans, 127
Bloembergen–Purcell–Pound (BPP) model, 132
Blue berries, 127
Blue membrane, 80
Brassicas, 135
Breads, 112, 117, 118, 128, 130
$^{t}Bu_3Pb$ derivatives, 24, *26*

^{13}C chemical shifts
conformation-dependent, 52, 56, *57*, *58*, 59, 64
dynamics dependent, 52, 59, 63–7
C terminal α-helix, 66–7, *73*, 74, 76–8, *78*, 92
C terminal end, 67, 74, 76, 92
Cakes, 118
Calcium pectate gels, 119
Canola seeds, 127
Carbene adducts, 12
Carbon spin–lattice relaxation times (T_1C), 67, 72, *73*, *75*
Carbon spin–spin relaxation times (T_2C), 72, *73*, 74, *75*
Carbonyl carbon, 96
Carboxonium ions, 156, *162*
Carboxylates, 81
κ-carrageenan, 116, 137
Carrots, *130*
Caseins, 112, 115–16
β-casein, 116
κ-casein peptides, 116
caseinomacropeptides, 116
Cations, effect on bR of, *79*, 79–81
Cellulose, 119, 120, 121
Chalcogen–lead bonds, 18
Charge delocalization modes, 151
Chemical shift anisotropy (CSA), 2, 5, 74, 75, 96
Chemical shifts
fixed frequency for, 3, *3*
see also ^{13}C chemical shifts; ^{207}Pb chemical shifts
Chestnuts, 118
Chickens, 129
Chinese water chestnuts, 121
Chocolate, 130, *130*, *131*
C-hordein, 114, 115
Chromatography, 135
Chrysenium cations, 175, 177, *199*, *200*, *201*, *202*
Citrus mesocarp, 120
^{13}C-labeled chromophores, 93
^{13}C-labeled proteins and peptides, 48–52
large-scale preparation, 48–50
multiple ^{13}C labeling, 50–2
$^{13}C{=}O$ chemical shift tensor, 97, *98*
Cod, 128
Cod liver oil, 126
Coffee, 123, *131*
Colicin Ia channel domain, 52
Collagen, 56, 72, 116
Composite pulse decoupling (CPD), 4
Coordination number, 9–17
Corn-starch gel, 117
Cosolvents, 151
Coupling constants, 23–31
long-range, 31
one-bond couplings, 23–30
three-bond (vicinal) couplings, 31
two-bond (geminal) couplings, 30
CPMG sequence, 128
Crabmeat, snow, 128
Crackers, 118
Crayfish, 128
Cryoelectron microscopy, 76
Crystalline peptides, 72
CSA relaxation, 6, 8
Cutin, 112, 121
Cyclopenta[a]phenanthrene ions, 156, *164–5*, *166–7*, *168*, *169*, *170*, *171*
Cysteine, 81
Cytoplasmic surfaces, 48, 76, 78, 81, 92

D-α-galacturonic acid monohydrate, 119
DATEM esters, 130
D/H ratios, 122, 123
Diarylplumbylenes, 11, 12
Dibenzoanthracenium cations, 175, *198*
Dibenzopyrenium cations, 175, *192*, *193*

Diffusion, Fickian, 111
Diffusion, type II, 111
Dihydropyrenium cations, 168, *191*
Diorganolead (bis)amides, 18
Diorganolead diamides, 28
Diorganoplumbylenes, 11, 12
Diorganotin diamides, 28
Diplumbanes, 19
Dipolar correlation spectroscopy, 50–1
Disulphide bonds, 114
DMPC bilayers, 86, *87*, 87, *89*, 96, 99
Doughs, 112, 114, 127, 130, 135, 136
DREAM, 50
Durian fruit, 129
Dynorphin, 87, 96

E. coli, 49, 50
Egg white, 137
Enkephalins, 72
Ethanol, 122
Eukaryotes, 93
Extracellular surfaces, 76

Fast field cycling NMR, 132–4
Fe–Pb bonds, 20, *21*
Fibrous proteins, 72
Fish, 128
Fish canning, 126, 128
Fish oils, 126
Fluoranthene PAHs, 189, *212*
Fluorescence, 76
Fluoronaphthalenium ions, 152
Fluoropyrenium ions, 159, *178–80*
Food freezing, 112, 113
Food packaging, 116, 127
Food science, applications of NMR to, 110–37
  fish quality, 128
  food authentication, 122–7
  fruit and vegetable quality, 129–30
  meat quality, 129
  new methods, 132–7
  plant cell walls, 119–21
  polysaccharides, 116–19
  proteins, 114–16
  review lists, *110*, *112*, *120*, *125*, *130–1*
  textural measurements, 128
  water in foods, 111–13, 128
Fruit juices, 112, 122, 123
Fruits, 127, 135

Gelatin, 116
Gelatinization, 116–17
Gellan gum, 112, 119
Gellan/Mn(II) complex, 119
Genetically modified (GM) products, 126, 135
Germylplumbanes, 19
Glass transition, 115, 117, 118, 130
ω-gliadin, 114
Glu 194 residue, 47, 90, 91
Glu 204 residue, 47, 90, 91
Glutamine residues, 114
Gluten, 112, 114, 115, 137
Glycerol, 122
Glycolysis, 127
GPCRs, 44, 93, 102
Grains, cooking of, 111
Gramicidin A, 90
Grape pomace, 127

^{1}H NMR, 5
Haddock, 128
Halobacterium salinarum, 44
  strain L-33, 50
  strain S-9, 48
Halogen–lead bonds, 18
Harp seal oil, 126
Hazelnut oil, 125
Heavy atom labeling, 76
HEED extended pulse sequences, 23
Hemicellulose, 119, 120
Heteroplumbocenes, 14
Hexaalkyldiblumbanes, 27
Hexahelicenium cations, 187, *205*
Hexahydropyrenium dications, 152
High-resolution NMR spectroscopy, 123–7
Histidines, 95
Honeys, 127
Hop acids, 135
HR-MAS NMR, 135–6
Hydration, 112

iminium–arenium dications, 187, *205*, *206–7*, *208*
INEPT pulse sequence, *4*, 5
Influenza A virus, 99
Inulin gels, 119
Isotope labeling, 102

$^{1}J(^{207}Pb,^{13}C)$, 23–4, *24*, *25*, *26*, *32*
$^{2}J(^{207}Pb,^{13}C)$, *32*
$^{2}J(^{207}Pb,^{1}H)$, 30
$^{3}J(^{207}Pb,^{1}H)$, 24, *26*
$^{4}J(^{207}Pb,^{1}H)$, 31, *32*
$^{1}J(^{207}Pb, M)$, 29
$^{1}J(^{207}Pb, ^{15}N)$, 28
$^{1}J(^{207}Pb, ^{31}P)$, 28–9
$^{1}J(^{207}Pb, ^{207}Pb)$, 27, *27*
$^{1}J(^{207}Pb, ^{77}Se)$, 29

$^{1}J(^{207}Pb, ^{125}Te)$, 29
$^{1}J(^{207}Pb,X)$, 23–30
$^{2}J(^{207}Pb,X)$, 30
$^{3}J(^{207}Pb,X)$, 31
$^{n}J(^{207}Pb,X)$, 31
$^{1}J(^{119}Sn,^{13}C)$, 23
$^{2}J(^{119}Sn,^{1}H)$, 30

Kiwi fruit, 129
$^{1}K(^{207}Pb, ^{207}Pb)$, 27
$^{1}K(^{207}Pb,^{29}Si)$, 24
$^{1}K(^{207}Pb,^{119}Sn)$, 24

Lactobacillus, 113
Lactococcus lactis, 127
β-lactoglobulin, 116
Lactose, 115
Lactose–lysine mixture, 118
LC-NMR, 126, 134-5
LC-NMR-MS, 135
Lead(I) compounds, 22
Lead(II) compounds, 9, 10, 22
Lead(IV) compounds, 9, 15–16, 22
Lead hydrides, 22
Leeks, 127
Legume proteins, 115
Lemon juices, 122
LH1 complex, 95
LH2 complex, 95
Lignin, 121
Lime oils, 127
Linolenic acid, 125
Lipid bilayers
  magnetically oriented, 96, *100*
  mechanically aligned, 96–7
Lipid–protein interactions, *79*, 80, 102
Lipids, NMR studies on, 124–6, *125*
Locust bean gum, 112
Loops, 114
Lyophilization, 43, 82, 95
Lysine, 118
Lysis, 99, *100*
Lysozyme, 116

M2 protein, 99–101
Mackerel, 126, 128
Magnetic relaxation dispersion (MRD), 83
Maillard reactions, 118
Maize, 118, 130
  waxy, 117, 118
Maltodextrin, 117, 119
Mango pulp, 136
Maple syrup, 123
Margarines, *131*
Mass spectrometry, 134–5
Meat quality, 129, *130*
Melittin, 96, 98, 99, *100*
Membrane proteins
  NMR characteristics of, 42–4
  real picture of, 102
  roles of, 41
Me_4Pb, 2, 3
Mesityllead bromides, 18
Methyl ester, 119
Methyl groups, 80, 81
Methylene-bridged PAHs, 187, 189, *208*, *209*, *210–11*
Methyllead compounds, 30
Methylnaphthalenium cations, 152
Methylphenanthrenium dications, 156, *160*, *161*
Methylphenanthrenium ions, 152, *157*, *158*
Methyltin compounds, 30
Microbiological systems, 112–13
Microwave heatng, 114
Milk, 115, *130–1*
Mn^{2+} ions, 60
Mn–Pb bonds, 20
Monomeric plumbylenes, 10
Mo–Pb bonds, 20
M–Pb bonds, 20
Muscle proteins, 116
Mustard oil, 123
Mycoplasma genitalium, 41
Myofibrillar protein solutions, 116

Naphthalenium ions, 152, *153*, *154*
Nectarines, 129
^{15}N–^{1}H dipolar interaction, 97
NIR methods, 130
Nitronaphthalenes, 187, *205*
Nitropyrenes, 187, *205*, *206–7*
Nitrosopyrenes, 187, *208*
NMDAR, 100
NMR solvents, 151
n-octyl-β-D-glucoside (OG), 83, *84*, 84
Nuclear shielding, 9

Oligosaccharides, 127
Olive oils, 122, 123, 124–5
Olives, 129
Onions, 120, *121*
Orange juices, 122, 123, *124*
Orange peel, 120, 127
Oregano, 127
Organolead cations, 16
Organolead–nitrogen compounds, 18
Organolead–phosphorus compounds, 19
Ovalbumin solutions, 116

Oxidation, *125*, 125, 126

PAH carbocations
  compilation of NMR data on, 150–1
  significance of, 151
Pasta, 111
^{207}Pb chemical shifts, 9–23
  isotope-induced, 22–3
  referencing, 2–4
^{207}Pb CP MAS spectra, 5, *6*
^{207}Pb NMR
  observation techniques, 4–5
  solid-state, 5, 32
^{207}Pb nuclear spin relaxation, 6–8
Pb–B bonds, 28
^{207}Pb–^{11}B spin–spin coupling, 7, *7*
^{207}Pb{^{1}H} NMR spectra, 5, *5*, *8*
Pb–N bonds, 20
^{207}Pb–^{14}N scalar spin–spin coupling, *8*
^{207}Pb–X spin–spin coupling, 7, 8
δ^{207}Pb, 2–4
  see also ^{207}Pb chemical shifts
Peas, 115, 118
Pectins, 112, 119, 120
  deuterium-labelled, 119
Pepper, 127
Peptides, 116, 127
Persimmon fruit, 129
$(Ph_5C_5)_2Pb$, 13
Phenanthrenium cations, 152, *153*, 156
  α-phenanthrene-substituted carbocations, 156, *162*
Phloretin, 135
Phlorin, 127
Phosphanyl derivatives, 24
Phosphatidylcholine bilayers, 96
Phospholipids, 81
Phosphorus, 116
Phosphoserine, 116
Photo-CIDNP experiment, 95
Pigs, 129, *131*
PISA wheel, 97
PISEMA experiment, 97
Plant cell walls, 119–21
Plasticized corn zein films, 116
Plumbocenes, 9
Plumbylenes, *8*, 10–12, 32
Polyphenols, 120
Polysaccharides, 116–21, *120*
Pork brining, 129
Porous systems, 113
Potatoes, 117, 118, 121, 128
Proline effect, 56
PROMEGA, 50
Protein tumbling, 83
Proteins, 119
Proton decoupling, 67
Proton-driven spin diffusion (PDSD), 50
Proton release complex (PRC), 47, 90
Proton spin–lattice relaxation times ($T_{1\rho}$H), 72
Prunes, 129
Purple membrane (PM), 43–5, 80
  dehydration/rehydration behavior of, 82–3
Pyrenium cations, 159, 168, *172–92*
  α-pyrene-substituted carbocations, 159, 168, *181*, *182*
  cyclobutene-fused, 168, *192*
  pyrene–dicarboxonium dications, 168, *187*, *188*
  pyrenium–carboxonium dications, 168, *183–4*, *185–6*
  pyrenyl-α-CF_3-substituted carbocations, 168, *189*, *190*

Quadrupolar decoupling, 8
Quadrupolar nuclei, NMR properties of, *3*
Quadrupolar spin relaxation, 7
Quercetin, 135

Radio-frequency-driven dipolar recoupling (RFDR), 50
Radish, 127
Random coil conformations, *58*, 59, 66, 67, 86
Rb spaeroides, 94
Reaction centres (RCs), 94
Receptivity, 2, *3*
REDOR, 66, 88–90, *88*, *89*, *90*, 95
Relaxation mechanisms, 6
  see also CSA relaxation; scalar relaxation
Relaxation parameters, 72–6, 83, *84*, 102
Relaxation time measurements in food analysis, 132
Repetitive domains, 114
Resveratrol monomers, 127
Retinal, photoisomerization of, 44–5, *44*, 47, 48
Retrogradation, 116, 117
Rheological NMR (rheo-NMR), 137
Rhodobacter sphaeroides, 51
Rhodopsin, 93–4
Rice, 111, 113, 117, 128
  cup-cake, 117
Rps. acidophilia, 95
Rps. viridis, 94

Sage, 127
Salmon, Atlantic, 126
Scalar relaxation, 6, 8
Schiff base, protonated, 45, 47–8, *47*, 90

Schiff base counterion distance, 94
Seeds, examination of, 130
Selectivity, 42, 48
Sensitivity, 42, 48, 49
Shear, 137
Sheep rumen fluid, 119
δ^{29}Si, 13
Silk fibroin, 56
Silylplumbanes, 19, 24
^{119}Sn NMR, 5
δ^{119}Sn, 13
(SNIF)-NMR, 122–3
Solid-state NMR in study of complex foods, 127
Soup, 127
Soy, 115, 119
Soya 7S proteins, 133–4, *133*
SPECIFIC-CP transfer, 50
Spectral density function, 132, 134
Spin-1/2 nuclei, NMR properties of, *3*
Spin-labeling, 76
Spore germination, 113
Stable isotope ratio determination, 122–3
Staling, 117, 130
Stannocenes, 9
Stannylplumbanes, 19, 24
Staphylococcus aureus, 113
Starch, 112–14, 116–18
  A-type, 117, 118
  B-type, 117, 118
  C-type, 118
Starch–glucose–lysine mixture, 118
Starch–sorbitol films, 118
Starch/water interactions, *112*
STRAFI, 111
Strawberries, 120
Substituent effects, 17–21, 151
Sucrose, 115
Sugar beet, 119
Sugars, 112, 117
Superacid media, 151

Tapioca, 118
$T_2^{CSA}(^{207}Pb)$, *8*
Teas, 123, *131*
Terminal domains, 114
Tin(II) compounds, 9, 22
Tin(IV) compounds, 9, 22
Tomato ketchup, 137
Tomatoes, 120–1, 126, 128
Trains, 114
Transition metal–lead complexes, 21
Transmembrane α-helices, *73*, 74, 76, 78, 83–4, 85
Transmembrane peptides, 56, 64, *65*, 66
  as a component of bacteriorhodopsin, 86–90
Transmission electron microscopy (TEM), 119
Triacylglycerol, 116, 130, *131*
Trialkylplumbyl lithium compounds, 30
Trimeric diaryllead sulfides, 18
Triorganolead amides, 18, 28
Triorganoplumbyl lithium compounds, 20
Tri(*tert*-butyl) lead derivatives, 17
T_2^{SC}, 8
$T_2^{SC}(^{207}Pb)$, *8*
Tuna, 126
Tyr 83 residue, 91, *92*

Vanilla flavour, 123
Vinegars, 123
Vinyllead triacetates, 30

Water exchange, 83
Water in foods, 111–13, 128
Wheat, 111, 112, 114, 117, 118
  bran, 121
  durum, 114, 136
  HMW subunits of wheat glutenins, 114, *115*
Whey proteins, 116
Wine, 122, 127
WISE experiments, 119, 120, *121*
W–Pb bonds, 20

X-ray diffraction, 64, 76, 93, 94, 101

Zwitterionic species, 12, 16